New phase selection techniques for single-pole-autoreclosure schemes employing directional comparison protection.

Mahmoud, Mahmoud Mohy El-Din

Award date:
1984

Awarding institution:
University of Bath

NEW PHASE SELECTION TECHNIQUES FOR SINGLE-POLE-AUTORECLOSURE SCHEMES EMPLOYING DIRECTIONAL COMPARISON PROTECTION

Submitted by

Mohamed Mohy El-Din Mahmoud

for the degree of PhD
of the University of Bath

1984

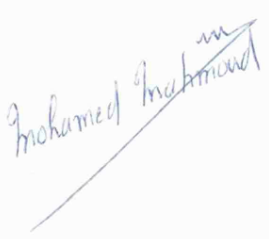

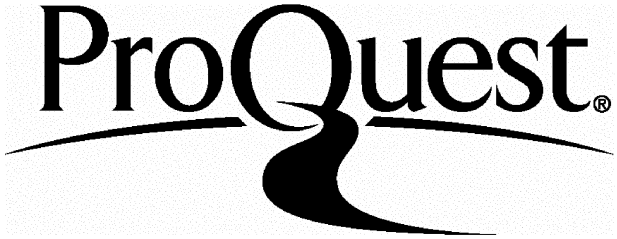

C O N T E N T S

Summary

The success of single pole autoreclosure relies on correct selection of the faulted phase and hence on the ability of the phase selectors to perform this task. In this thesis novel techniques which provide UHS phase selection have been developed.

The lattice method was used to assist with the early development of the algorithm, in order to determine the approximate response of the modal variations of a 3-phase lossless system.

The algorithm, in terms of primary system variations, was then tested using established digital techniques for modelling the faulted response of any arbitrary linear shunt reactor compensated EHV feeder system. The technique was then implemented within secondary simulation programs to indicate any susceptibility to transducers and digital processing errors.

The new phase selector provides satisfactory phase discrimination following very high resistance faults and caters for evolving fault conditions. An evaluation of the performance of the new scheme for different line and source configurations is reported.

The simulation results show the phase selector to have very good selective properties, complemented with very high speed of operation. The scheme, in a typical application such as that considered, has an operating time of 2 to 5ms for most fault conditions.

Some insight is given into the techniques necessary for the opening of only one pole for clearance of both single phase to ground faults and interphase faults clear of ground, and the necessary modifications to the basic phase selector scheme are proposed.

The investigation also presents the results of computer evaluations of the discriminative properties of the new scheme under complete fault clearance sequences. The performance of the phase selection equipment during single pole and three pole autoreclosure sequences is reported.

The thesis concludes by presenting the results of preliminary field tests which go some way towards validating the aforementioned novel phase selection techniques developed.

Acknowledgements

The work presented in this thesis was carried out under the supervision of Dr A T Johns, DSc, PhD, CEng, FIEE, of the School of Electrical Engineering, University of Bath, whose assistance, encouragement and constant guidance are gratefully acknowledged.

Sincere thanks are due to Dr R K Aggarwal and Dr M A Martin for their co-operation and helpful comments.

The author is particularly grateful for discussions and comments regarding practical aspects of the work and the interest shown by engineers at GEC Measurements Ltd, Stafford, England.

Thanks are also due to staff of the University of Bath Computer Centre and programmers at the South West Universities Regional Computer Centre based at Bath, especially Mr T Morrow.

The author also wishes to express his thanks to Diane Milton for typing the manuscript.

LIST OF PRINCIPAL SYMBOLS

p.p.s., z.p.s.	=	Positive and zero phase sequences
j	=	Operator $\sqrt{-1}$
h	=	Operator $1 \angle 120° = -\frac{1}{2} + j\frac{\sqrt{3}}{2}$
$V_s(t)$, $V_f(t)$	=	Time variation of steady-state and superimposed component voltages
$I_s(t)$, $I_f(t)$	=	Time variation of steady-state and superimposed component currents
L	=	Length of faulted line section
X_F	=	Distance to fault from sending end
R_F	=	Fault resistance to earth or between phases
t	=	Time after fault
ω_0	=	Nominal system angular frequency, rad/s
ω	=	Angular frequency, rad/s
ϕ	=	Angle between voltage and current phases (power factor angle)
τ	=	Surge travelling time between sending or receiving end substation (S or R) and fault location F
$Z0^{(k)}$	=	Mode-K, surge impedance, where K = 1,2,3
$R0^{(k)}$	=	Mode-K, surge replica impedance, where K = 1,2,3
$S^{(k)}$	=	Mode-K, composite relaying signals used for purpose of phase selection, K = 1,2,3
D_a, D_b, D_c	=	Phase to earth discriminant signals
D_{ab}, D_{bc}, D_{ca}	=	Interphase discriminant signals

Vrms	=	r.m.s. prefault voltage (line to line)
Q, S	=	Modal transformation matrices
h(t)	=	Unit step function
h(t-T)	=	Delayed unit step function 0, t < T 1, t > T
s.c.l.	=	Short-circuit level
Z, Y	=	Series-impedance and shunt admittance matrices per unit length of line
Zs, Ys	=	Average sum of all conductor self-impedances and admittances at any frequency
Zm, Ym	=	Average sum of all conductor mutual impedances and admittances at any frequency
ZL0, ZL1	=	z.p.s. and p.p.s. line impedances
ZS0, ZS1	=	z.p.s. and p.p.s. source impedances
C1, C0	=	p.p.s. and z.p.s. shunt capacitance
h1, h0	=	degree of p.p.s. and z.p.s. shunt compensation
BL1, BL0	=	magnitude of p.p.s. and z.p.s. inductive susceptance of shunt reactor bank at nominal system frequency
BC1, BC0	=	Magnitude of p.p.s. and z.p.s. capacitive susceptance of any line section at nominal system frequency
Z0, Y0	=	Polyphase surge impedance and admittance matrix
Z_{SS}, Z_{SR}	=	Sending and receiving end source impedance
Zp, Zn	=	Phase and neutral impedances at shunt reactor bank
Lp, Ln	=	Phase and neutral inductance of shunt reactor bank

Rp, Rn	=	Phase and neutral resistance of shunt reactor bank
E_{base}	=	Base voltage
I_{base}	=	Normal positive-sequence charging current ($j\omega_0 C1 E_{base}$)
Isec	=	Residual (secondary) current of phase to ground fault
Isec(p.u.)	=	Normalised secondary arc current ($Isec/I_{base}$)
γ	=	Modal propagation constant matrix
$\Delta\omega$	=	Frequency sampling interval
Tob	=	Observation time
Ω	=	Truncation frequency
σ	=	Sigma factor
α	=	Frequency shift
S1, S2	=	Relaying signals
L_a, L_b, L_c	=	Dynamic threshold levels, of discriminant signals D_a, D_b, D_c respectively
EC_a, EC_b, EC_c	=	Event counters associated with phases "a", "b" and "c" respectively
CDC	=	Common Decision Counter

List of Principal Symbols (continued)

Subscripts

S, R, F	=	Ends S, R and fault point F
a, b, c	=	Phases a, b and c
i, r, t	=	Incident, reflected and transmitted components
α, β, 0	=	Clarke components
N	=	Neutral

Superscript

(k)	=	1, 2, 3 modal components

Suffices

0, 1, 2	=	Zero, positive and negative phase sequence components

CHAPTER ONE

INTRODUCTION

The vast majority of faults affecting EHV networks are of a transitory nature and involve only one phase and earth. From the viewpoint of minimising subsequent system disturbances, especially loss of synchronism caused by such faults, it is desirable to clear them by opening the breaker poles of the faulted phase and subsequently reclose them. In such cases, single pole autoreclosure (SPA) techniques can be used to advantage[1]. The effectiveness of SPA is largely determined by the speed with which the secondary arc is extinguished, thus allowing autoreclosure to be achieved. The emergence of suitable means of extinguishing secondary arcs following single pole opening on EHV transmission lines and the reduction in dead times[2], together with the savings in capital investment made possible by employing single rather than double circuit lines[3], undoubtedly accounts for the increasing interest in the use of SPA. By restricting opening and reclosing to the single faulted phase, system stability can be significantly improved, because the energised sound phases continue carrying power during the period of interruption. Furthermore, single phase faults followed by 3-phase tripping have been known to cause instability problems[4,5]. The success of SPA is heavily dependent upon reliable selection of the faulted phase, this being the main objective of the work in this thesis.

In recent years, however, there has been an increased interest in phase selectors to provide an accurate identification of the faulted phase or phases for all types of fault. By using such a selector in a segregated tripping scheme, any type of fault could be cleared by the opening and reclosing of the minimum number of poles. This is a distinct improvement over the one or all approach of conventional SPA schemes in terms of increased system stability. Some work was therefore carried out to determine the possibility of producing a reliable multi-pole phase selector to form the basis of a segregated tripping protection scheme.

1.1 Classification of Phase Selectors

Phase selectors are indispensable accessories of protective schemes designed for selective pole autoreclosure, the four main applications being:

1.1.1 Single phase tripping

Selectors are used in conjunction with protection relays which do not have phase selection properties to obtain a single phase tripping output for use with SPA. A relay protection scheme that provides for single pole tripping and reclosing will only trip the faulted phase for a single line to ground fault (SLG) or all three phases for all multiphase faults[6]. In such schemes (single, or very occasionally, multi-shot) automatic reclosing is employed.

1.1.2 Segregated tripping

This is a more sophisticated protection scheme in which the selectors provide multiphase discrimination to enable fault clearance

by using single, double and three pole tripping with reclosing as necessary. Hence, the basic SPA requirements of the selector must be extended to include an indication of all the faulted phases in a multiphase fault situation.

1.1.3 Switched scheme

To greatly reduce the number of individual relay measurands required to satisfactorily protect a section of a transmission line, a selector can be used to switch the measuring unit to the appropriate faulted phase(s). In such cases the selectors act as the starting unit of a switched scheme and have similar requirements to single phase tripping.

1.1.4 Fault indicator

In such applications, the selectors are merely used to indicate which is the faulted phase(s) without taking further action.

1.2 Operational Requirements for Phase Selectors

After phase selector classification it is necessary to determine the basic requirements of discrimination, emphasising the essential requirements within each group. The following requirements have been the standards set for schemes employing distance type protection[7,8]. The new phase selector scheme proposed in this thesis, however, is developed using a novel technique and is designed as an integral part of a directional wave comparison protection equipment. Since, at the present time, there is no knowledge of the performance requirements of phase selectors of this class, a basic evaluation of its capability can be gained by a comparison with conventional selector requirements.

1.2.1 Requirements for the operation of phase selectors

(a) During fault conditions, the phase selector operation must ideally be:

(1) Independent of the configuration of the network on both sides of the fault and especially of the location of the points where the neutral of the network is earthed.

(2) Independent of the prefault load and the sound phase currents.

(3) Independent of power swings between the generating stations feeding the network.

(4) Independent of the operation of the protective system and of the phase selector situated at the opposite end of the line.

(5) Independent of the fault location and of its resistance.

(6) Fast enough in operation to ensure that no further delay is introduced in the clearance of the faults. In the case of selectors used for switched distance schemes, the selectors should not introduce an excessive delay in the overall protection time. This is an important requirement, since the selector must not slow down the switching of the measuring unit of the faulted phase(s), because the selectors and the measuring units operate in sequence.

(7) Selective even in the case of evolving faults. In the case of single phase tripping application, the phase selectors must

identify the faulted phase without delay and if the fault condition changes must be able to re-select accordingly by taking appropriate action.

(b) After the clearance of the fault and during the reclosing cycle the phase selector must:

(1) Discontinue selection with breakers poles open, ie. must be insensitive to the position of the poles of the breakers at remote ends of the line.

(2) Provide correct selection for evolving faults occuring with the initial faulted phase or phases open.

(3) Remain inoperative on circuit breaker closing, with fault cleared.

Depending upon the application in which the selector is to be used, the above basic requirements can be categorised into essential and desirable groups. For any phase selector to be considered, it must at least satisfy the essential requirements summarised below:

(1) Operating time less than 1 cycle.

(2) No operation on load current.

(3) For evolving faults, correct selection for first fault, and re-selection for evolved fault.

(4) Correct operation on breaker closing, reselect persistent fault.

(5) Operation when fault current is less than pre-fault load current.

(6) For SPA schemes, provide selected outputs for phase-earth faults and for all other fault types, give three phase trip indication.

(7) For segregated schemes, provide selected outputs for single phase and multiphase faults as necessary.

Any phase selector scheme which fulfils some or all of the following desirable requirements would be regarded as a more attractive proposition:

(1) Earth fault reach not less than phase fault reach.

(2) Operating time less than 5ms.

(3) High resistance fault coverage (eg. 10 to 200 ohms).

(4) Selection for second fault, with one pole open.

(5) Selection for second fault with two poles open.

(6) Selector recovery within the dead time.

(7) Independent of power swings.

(8) Must not operate with load changes below full load.

(9) Correct selection on long lines (> 150 km).

1.3 Pre-Requisitesof System Protection Equipment Employing UHS Phase Selectors

Ultra high speed fault clearance represents an effective method of improving the transient stability and increasing power transfer of a transmission line system. Overall fault clearance times depend on both circuit breaker and relay operating times. The use of faster protection rather than significantly faster circuit breakers represents an attractive solution from an economic point of view.

In order to achieve approximately one cycle breaker clearance time, the protective relay and associated phase selector must operate within 4.7ms and 8ms for 60Hz and 50Hz systems respectively, since a faster relay operating time would produce the same breaker clearing time[9]. (Assuming 12ms breaker operation.)

SPA schemes require the provision of appropriate line relaying and circuit breakers[10]. The main relays must be capable of detecting all types of faults, and must disregard any phase selector action for faults exterior to the protected line.

In long line applications, successful reclosure is achieved by using shunt reactors to allow arc extinction within the dead time[11]. By a suitable connection arrangement, these reactors can be made to serve the additional purpose of voltage control.

1.4 Recent Developments of UHS Protection Schemes Incorporating Phase Selection Equipment

Protective schemes which rely for their operation on the travelling wave set up on transmission lines by system faults are attractive because they offer the possibility of rapid fault detection and clearance. Particular interest has been focussed upon new techniques of UHS transmission line protection of the directional wave comparison type. Most of these techniques are based on the so-called "Invariant properties of the transmission line".

The d'Alembert relay by Takagi[12,13] derives the travelling waves at the local and remote ends then uses their difference to detect an internal fault. Faulted phase selection is then achieved by comparing various transforms of the phase currents with a pre-determined reference table. Dommel[14] computes a fault discriminant which is independent of both fault inception angle and line termination.

The scheme developed by Chamia and Liberman[15] employs directional wave detectors which operate according to the relative difference in the travelling wave components of voltage and current impressed on a system by the occurrence of a fault. This principle is then extended to provide phase selection for the purpose of single phase tripping[16].

A technique by Johns[17,18] makes use of the sequence in which the derived forward and reverse signals exceed given thresholds to determine the direction to the fault. Since the definitive publication, exhaustive research in conjunction with a series of modifications

and refinements, has led to the successful implementation of the above described scheme[19-24]. For such a relaying scheme to be used in a UHS SPA scheme for long line applications, a complementary phase selector with comparable speed and reliability has been developed. When compared with stand alone phase selectors, the novel scheme proposed therefore reduces the interface requirements of the overall SPA scheme.

The implementation of the new phase selector is microprocessor based and relies for its operation on modal quantities derived from the actual fault induced superimposed components of phase voltage and current. The use of modal rather than phase quantities allows a reduction in the minimum number of relaying signals required to reliably select the faulted phase. The result is a considerable saving in terms of processor hardware and software implementation. Furthermore, the use of aerial modes enables the independent relaying of both circuits in double circuit applications, due to the de-coupled nature of the modal signals.

Although the phase selection methods developed are specific to the wave directional comparison detector, they might nevertheless be usefully extended to provide improved discrimination in other digitally based schemes requiring single phase tripping.

1.5 Objectives of the Thesis

The phase selector was primarily designed to be used in conjunction with the above-mentioned UHS wave detector and to provide a single phase tripping output for SPA applications. For direct compatibility with the main relay hardware, the phase selector proposed here was developed using a combination of the readily available modal relaying signals.

The new scheme was specially designed for comprehensive, ultra high speed protection of most practical HV and EHV power transmission systems. In all of the typical applications considered in the thesis, the selector achieved UHS operating times in the range of 2 to 7ms for a 50Hz system.

A variety of existing phase selector limitations include: fault-load current discrimination, incorrect selector particularly with phase to earth faults, load encroachments and excessive operating times. The phase selector is designed to overcome these limitations and to meet the essential requirements detailed in Section 1.2.1.

1.6 Scope of the Thesis

A survey of currently available selectors is presented in Chapter 2, in which the advantages and disadvantages of existing schemes are discussed.

Chapter 3 details the new phase selector theory and its principle of operation when used in conjunction with several types of autoreclosure

schemes. A description of the lattice method used to assist with the early development of the algorithm is given, upon which the phase selector theory is based. In conclusion, the results achieved with the approximate lattice method are compared with those of an accurate digital simulation, employing Fourier Transform techniques.

Chapter 4 presents the implementation of the phase selector within a secondary simulation program to indicate any susceptibility to transducer and digital implementation errors. Software implementation techniques are then discussed.

The configurations of the systems studied are detailed in Chapter 5. Details of line construction and line, source and shunt reactor scheme parameters are discussed.

In Chapter 6, the algorithm is tested using digital techniques for modelling the faulted response of any arbitrary linear shunt reactor compensated EHV feeder system. The effect of transposition and untransposition is discussed, and results of a wide range of system studies are presented.

In Chapter 7, the behaviour of the phase selector and its operation when subjected to abnormal operational conditions are considered. The effect of very high resistance faults, special source configurations and evolving faults are studied.

Chapter 8 presents the results of some computer evaluations of

the overall performance of the new scheme under complete fault clearance sequences. In addition, the performance of the phase selection scheme during single and three pole autoreclosure sequences is reported.

Preliminary field test results are presented in Chapter 9, whereby the phase selector is subjected to actual system data, derived from a transmission network within the UK.

General conclusions, drawn from the work presented herein, are detailed in Chapter 10, with complementary suggestions for relevant future research.

CHAPTER TWO

LITERATURE REVIEW OF EXISTING PHASE SELECTORS

In the past there has been little reported work concerning the development of phase selectors. However, recent publications (post-1976) have revealed increased interest in a new generation of phase selectors based upon superimposed components. In the course of this survey, conventional phase selectors are briefly discussed, with a more detailed consideration of existing UHS travelling wave schemes.

Various types of phase selectors, based upon different operating principles, are currently implemented in electric power systems and these include the following group:

(a) overcurrent selectors;

(b) undervoltage selectors;

(c) impedance selectors;

(d) change in current magnitude selectors;

(e) change in voltage and current magnitude selectors;

(f) travelling wave based selectors.

2.1 Overcurrent Selectors

Overcurrent selectors are applicable to short lines connected to high fault level busbars, where there is no difficulty in discriminating between fault and load current. For double circuit line

applications, the overcurrent setting must be greater than twice the normal load current, to prevent sound circuit operation when a fault is cleared in the other circuit. This setting also caters for the event of a parallel line being switched out. For the particular case of phase to ground faults and for certain source configurations in which only zero sequence current flows, discrimination between the sound and faulted phase currents is not possible, since they are approximately the same in magnitude. An overcurrent setting suitable for such conditions cannot therefore be achieved. In general, overcurrent settings are limited by the source ot line impedance ratios of the system and by the high resistances associated with certain earth faults.

2.2 Undervoltage Selectors

The pre-requisite of a minimum reduction in system voltage excludes undervoltage selectors from application to systems having a low source to line ratio, and limits their capability to cover long lines and high resistance faults.

For interphase connected undervoltage elements, it is possible that a phase to earth fault activates two units, resulting in incorrect selection. This problem is alleviated by using a zero sequence current detector to switch the element connections over to phase to neutral arrangement. The detection of zero sequence currents and subsequent element switching directly increases the selector operating times. Furthermore, undervoltage selectors can operate during de-energisation cycles and so must be interlocked with local breaker

control circuitry.

Undervoltage selectors are commonly employed as a complementary device to other selection schemes, typically overcurrent selectors.

2.3 Impedance Type Selectors

Modern impedance type relays employ some form of characteristic restriction in order to overcome the well known problems[25] associated with conventional earth fault relays and six unit distance protection schemes[26]. The major problem concerning such schemes is incorrect selection when interphase relay elements are excited during phase to earth fault conditions, resulting in the unnecessary tripping of all phases. In addition, it is possible for earth fault relays to over-reach during double phase to earth faults, thus initiating tripping for out of zone faults.

The above problems can be satisfactorily overcome, as stated above by polar characteristic restriction, which obviously reduces the relay faults coverage capability, particularly on unearthed systems. An alternative solution is to employ phase selectors for the purpose of switching the appropriate signals to a measuring unit[27], a technique that is used in some modern protection schemes.

2.4 Change of Current Magnitude Selectors

The maximum level of sound phase current change determines the

minimum change for operation and hence the maximum line length which can be covered. The occurrence of a fault may therefore be detected by monitoring this change of current magnitude.

For systems with high source fault levels and long line lengths, a fault at the end of the line can give rise to a fault current which is less than the maximum load currents, making selection impossible.

Generally speaking, the problems encountered in setting this selector are similar to those of overcurrent selectors, but with reduced restrictions on load current settings.

2.4.1 Fault current phase selector

A phase selector has been proposed by GE of America[28], which is based upon the fault current component, extracted from the total current variation. The phase selector is is implemented digitally and is based upon a fault analysis algorithm, derived using the concept of Clark components[29]. This is a real transformation which enables an instantaneous fault transient analysis.

Taking the a-phase as a reference the following modal relationships are found:

a-phase to ground fault	$I_\alpha = 2I_0$ and $I_\beta = 0$
b-c to ground fault	$I_\alpha = -I_0$
b-c phase fault	$I_\alpha = 0$ and $I_0 = 0$
3-phase fault	$I_\alpha = 0$

where I_α, I_β, I_0 are the Clark transformed current components. The inverse Clarke Transformation allows the corresponding phase relationships to be expressed as:

For

$$I_{neutral} = 0 \quad \text{(faults involving ground)}$$

$$I_b - I_c = 0 \quad \text{for a-earth fault}$$

$$2I_a - I_b - I_c + I_{neutral} = 0 \quad \text{for b-c-earth fault}$$

For

$$I_{neutral} \neq 0 \quad \text{(faults clear of ground)}$$

$$2I_a - I_b - I_c = 0 \quad \text{for b-c fault clear of ground}$$

The neutral current is used to differentiate between faults involving ground and faults clear of ground. For phase faults clear of ground there are three current relationships and if all are non-zero it is assumed that there is a 3-phase fault. For the ground faults the neutral current is not zero and there are six relationships which can distinguish between the three single line to ground faults and the three double line to ground faults.

By taking b and c as reference phases respectively, similar expressions for the other fault types can be derived. These derived relationships for the different faults apply to the actual fault currents.

In practice the above equations cannot be equated to zero due to the physically unbalanced line constructions and therefore limiting values must be taken. By considering these equations it is found that for each phase-phase discriminant, extra signals which are unnecessary have been used, thus complicating the selector processing. In the particular case of b-c faults, the discriminant $2I_a - I_b - I_c$ can be reduced to $-I_b - I_c$, since I_a is always a redundant component.

For cases of faults occurring on line terminated in delta wound transformer selection by such a scheme is not possible, since no neutral current can flow. Furthermore, it is not clear how the derived fault point relationships are related to the relay location and hence source termination.

The above limitations therefore restrict the range of practical systems to which the proposed selector can be applied.

2.5 Change in Voltage and Current Magnitude Selectors

2.5.1 Analogue selectors for switched scheme application

A new approach to high speed phase selection by GEC Measurements Ltd has been proposed[30]. The superimposed quantities of voltage and current (v' and i') are used to identify the type of fault and the phase(s) concerned. The selector is then used for switched distance relays to feed the required signals to the relay comparator. A selection time of a quarter of a cycle (5ms) after fault inception has been reported, which indicates that the selector will operate

well before any CT saturation occurs. The whole selection process is in analogue form, and the identifiable relationships between superimposed quantifies at the relaying end, for the four conventional faults (3ϕ, a-g, a-b-g, a-b) are as given below:

Phase to ground faults

Identification of 'a' to ground fault is achieved when:

$$i'_b - i'_c = 0 \qquad \ldots (2.1)$$

and

$$v'_b - v'_c = 0 \qquad \ldots (2.2)$$

Phase to phase faults

Similarly, another two relations are given for the identification of 'a-b' faults:

$$i'_a + i'_b = 0 \qquad \ldots (2.3)$$

and

$$v'_{bc} = -v'_{ac} \qquad \ldots (2.4)$$

Three phase solid faults

This type is identified using the relationships:

$$v'_a + v'_b + v'_c = 0 \qquad \ldots (2.5)$$

and

$$i'_a + i'_b + i'_c = 0 \qquad \ldots (2.6)$$

Two and three phase to ground faults

Successful identification of these faults depends upon the fault location and the line and/or the ratio of the source to line impedances of the opposite end. The loss of discrimination between these two

types of fault is very common and is mainly due to the neutral current produced by the unbalanced 3-phase fault impedances. The authors then suggest a method of elimination to overcome this problem, whereby the magnitude and phase of the neutral current is compared in turn with the sum of every two phase currents, the nearest sum being selected as the faulted phase pair. If the above comparison fails to produce a difference in magnitude and phase within a predefined limit, the fault is assumed 3-phase with unbalanced fault impedances.

A particular problem caused by neutral earthing is that selector discrimination is sometimes lost at load ends when co-phasal currents are produced. The proposed selector operates upon current and voltage components and so will maintain discrimination for the cases described above. Furthermore, the use of polarised current components permits the use of this scheme in applications where a large range of source capacity is encountered. Eqn (2.1) and (2.2) for an a-g fault are combined as follows:

$$(v'_b - v'_c) + R(i'_b - i'_c) = 0$$

where R is defined as any resistance quantity suitable for the application. In many cases, the resistance associated with current transactor circuit is sufficient. Similarly, the discriminant for phase to phase faults is obtained from (2.3) and (2.4) for a-b faults:

$$(v'_{bc} - v'_{ca}) + R(i'_a + i'_b) = 0$$

The remaining discriminant signals are obtained in a similar manner.

The new technique under development seems to be attractive for single phase tripping applications, although the method for selecting double and three phase faults needs more consideration. Regarding high resistance faults performance, the scheme offers a distinct advantage over distance type selectors, since the discriminant signal relationships remain valid under conditions of either no superimposed voltage or current.

2.6 Travelling Wave Based Phase Selectors

2.6.1 Current differential carrier relaying system

An idea proposed by Takagi et al[12] describes the use of Bergerons' equation[31] as part of a modal analysis method to determine an invariant pattern for the purpose of faulted phase selection. By forming a truthtable based upon each pattern for all types of internal faults, phase selection is achieved by a simple look-up process. The phase selector scheme is essentially travelling wave based, which utilises discriminant signals of the form:

$$\eta^{(k)}(t) = I_F{}^{(k)}(t-\tau^{(k)})$$

where $I_F{}^{(k)}(t)$ is the mode-k fault current, $\tau^{(k)}$ is the mode-k surge transit time between the fault and relay location, where mode-k = 0,1,2. The modal transformation is such that during normal conditions $\eta^{(1)}$, $\eta^{(2)}$ and $\eta^{(0)}$ equal zero, but for any internal fault one or all of these discriminants become finite.

The basic method is then extended to enable faulted phase selection by the use of three transforms each being referenced to the a,-b

and -c phases respectively. Three modal components are associated with each transform, and hence there are nine discriminant signals in total available for the selection of each type of fault.

For an a-earth fault condition the modal and actual fault currents are related by the Karrenbauer transformation by:

$$\begin{bmatrix} I_F^{(0)} \\ I_F^{(1)} \\ I_F^{(2)} \end{bmatrix} = [S^{-1}] \begin{bmatrix} I_{Fa} \\ 0 \\ 0 \end{bmatrix} = \begin{bmatrix} 1/3 & I_{Fa} \\ 1/3 & I_{Fa} \\ 1/3 & I_{Fa} \end{bmatrix}$$

Where $[S^{-1}]$ is the matrix of orthogonal system eigenvectors:

$$[S^{-1}] = 1/3 \begin{bmatrix} 1 & 1 & 1 \\ 1 & -1 & 0 \\ 1 & 0 & -1 \end{bmatrix}$$

It is clearly seen that each modal current in this case is finite, but by changing the reference phase from a to -b, the modal current vector then becomes:

$$\begin{bmatrix} I_F^{(0)} \\ I_F^{(1)} \\ I_F^{(2)} \end{bmatrix} = \begin{bmatrix} 1/3 & I_{Fa} \\ 0 & \\ 1/3 & I_{Fa} \end{bmatrix}$$

Here the mode-1, $\eta^{(1)}$, discriminant is seen to be zero whilst the two others are finite. The final modal relationship is then obtained by taking the -c phase as reference, which results in the following:

$$\begin{bmatrix} I_F^{(0)} \\ I_F^{(1)} \\ I_F^{(2)} \end{bmatrix} = \begin{bmatrix} 1/3 \; I_{Fa} \\ 1/3 \; I_{Fa} \\ 0 \end{bmatrix}$$

In this case the mode-2 component, $\eta^{(2)}$ is equal to zero whilst the other modes are finite.

The nine signals obtained above then form the discriminant pattern for the confirmation of the a-phase to earth fault type. This analysis is extended to all types of fault, which enables a truth table to be formed containing predefined patterns for all fault types.

The method described above is not restricted to the use of one modal transformation. Taking the Karrenbauer transform, Table 2.1 shows how phase selection is limited to SLG faults. However, if the Clarke transformation is considered, Table 2.2 indicates how selection is extended to include double and three phase faults.

There are two possible problem areas associated with this scheme, the first one being due to errors in travelling times, giving rise to non-zero values for the difference current under external fault conditions. The major drawback, however, is due to the independent processing requirement of the modal signals. Since their respective surge velocities are different, this necessitates the use of a complex operating algorithm which increases the minimum operating times and also makes the likely processing hardware very complex.

2.6.2 Wave directional fault discriminant

Dommel[14] describes a method by which a fault discriminant signal is derived for a specified time span equal to twice the modal transit time.

The modal component relationships, derived using the Clark Transformation, are given below.

$$V_0(t) - I_0(t)Z0 = 2V_{F0}(t-\tau_0)$$

$$V_\alpha(t) - I_\alpha(t)Z1 = 2V_F\ (t-\tau_\alpha) \qquad \ldots (2.5)$$

$$V_\beta(t) - I_\beta(t)Z1 = 2V_F\ (t-\tau_\beta)$$

where $V_{0,\alpha,\beta}$ and $I_{0,\alpha,\beta}$ are the modal voltage and current components $0,\alpha,\beta$ at the relay location, $V_{F0,\alpha,\beta}$ are the corresponding fault point components, and Z0, Z1 are the zero and positive line surge impedance respectively.

For a period equal to twice the transit time between the fault and relay locations, each modal signal is equal to twice the respective superimposed modal voltage at the fault point and is independent of the source termination.

The voltage and current changes produced by a line to ground fault in phase "a" is obtained by connecting a voltage source,

$$V_{Fa}(t) = -Vrms\ .\ \sqrt{2/3}\ \sin(\omega t + \phi) \qquad \ldots (2.6)$$

to the fault location F. The Clark de-composition then gives:

$$V_{F\alpha}(t) + V_{F0}(t) = V_{Fa}(t)$$

$$I_{F\alpha}(t) = 2I_{F0}(t) \qquad \ldots (2.7)$$

$$I_{F\beta}(t) = 0$$

The current and voltage at the fault location are related independently for each mode by:

$$I_{F0} = 1/Z0\ V_{F0},\ I_{F\alpha} = 1/Z1\ V_{F\alpha} \text{ and } I_{F\beta} = 1/Z1\ V_{F\beta} \qquad \ldots (2.8)$$

From eqns (2.7) and (2.8) the initial modal variations in terms of the actual superimposed faulted phase voltage at the fault location are obtained:

$$V_{F0}(t) = Z0/(Z0 + 2Z1)\ V_{Fa}(t)$$

$$V_{F\alpha}(t) = 2Z1/(Z0 + 2Z1)\ V_{Fa}(t) \qquad \ldots (2.9)$$

and

$$V_{F\beta}(t) = 0$$

The composite modal expression for the different modal components are independent of the termination but does depend on the angle of fault inception. As shown in eqn (2.10) these are obtained by substituting for eqns (2.9) and (2.6) in eqn (2.5).

$$V_0(t) - I_0(t)Z0 = -2\ \sqrt{2}/\sqrt{3}\ Vrms(Z0/(Z0+2Z1))\sin(\omega t + \phi)$$

$$V_\alpha(t) - I_\alpha(t)Z1 = -4\ \sqrt{2}/\sqrt{3}\ Vrms(Z1/(Z0+2Z1))\sin(\omega t + \phi)$$

$$V_\beta(t) - F_\beta(t)Z1 = 0 \qquad \ldots (2.10)$$

The discriminant signals are formed by combining the modal signals of eqn (2.10) with their respective derivatives as follows:

$$D_0(t) = (V_0(t)-I_0(t)Z0)^2 + 1/\omega^2(dV_0(t)/dt-dI_0(t)/dt\ Z0)^2$$

$$D_\alpha(t) = (V_\alpha(t)-I_\alpha(t)Z1)^2 + 1/\omega^2(dV_\alpha(t)/dt-dI_\alpha(t)/dt\ Z1)^2$$

$$D_\beta(t) = (V_\beta(t)-I_\beta(t)Z1)^2 + 1/\omega^2(dV_\beta(t)/dt-dI_\beta(t)/dt\ Z1)^2 \quad \ldots (2.11)$$

By appropriate substitution, the discriminant signals above become independent of fault inception angle, as shown in eqn (2.12).

$$D_0(t) = 8/3 \quad (Z0/(Z0 + 2Z1))^2 \quad V^2_{rms}$$

$$D_\alpha(t) = 32/3 \quad (Z1/(Z0 + 2Z1))^2 \quad V^2_{rms} \quad \ldots (2.12)$$

$$D_\beta(t) = 0$$

The analysis is extended to produce discriminant signals for all types of fault, thus permitting faulted phase(s) selection under all fault conditions.

Theoretically, the proposed scheme is attractive because it is independent of source termination and fault inception angle, for up to twice the transit time. In practice where faults occur near to the relay location, transit times of the order of less than 1ms are involved, which would suggest that a very high sampling rate is required for correct and reliable selection. The differentiation process within the scheme assumes only power frequency sinusoidal components which require the use of digital filtering, thus extending the overall delay of operation of the selector. Operating times of less than 5ms are quoted by the authors but it is envisaged that there will be delays

in forming the necessary signals which would exclude its use where short operating times are required. On these grounds, it does not appear that this scheme could be successfully implemented in practice for UHS applications.

2.7 Limitations of Existing Phase Selectors

The sections above describe the various drawbacks of the operating principles upon which modern phase selectors are based and emphasises the need for a reliable phase selector to cover all operating conditions.

In general, current operated schemes are limited by system configurations and particular source connections. Undervoltage selectors are restricted by the system source to line impedance ratios and have proven unsatisfactory when operating independently.

The problems encountered with impedance selectors include maloperation of sound phase elements under certain earth fault conditions. In addition, impedance characteristics, which restrict the range of earth fault resistance coverage, are governed by prefault load current. In some cases, the actual relaying equipment employed in the above schemes is of the electromechanical type, which although reliable, is inherently slow. Also, the theory upon which impedance schemes are based assumes steady state fault conditions which is not strictly valid in the fault transient period.

The superimposed component based schemes appear to have overcome some of the foregoing conventional selector problems. Although distinct advantages can be visualised, the practical implementation of the proposed schemes seems rather complex at this stage.

The above limitations have been known for many years and are undoubtedly partially responsible for the rather slow development of selective pole autoreclosure.

Fault discriminant		11-g a b c	21-g a-b	21-g b-c	21-g c-a	21-s a-b	21-s b-c	21-s c-a	31s	31g
	$\eta^{(0)}$	1 1 1	1	1	1	0	0	0	1	0
(a)	$\eta^{(1)}$	1 1 0	1	1	1	1	1	1	1	1
	$\eta^{(2)}$	1 0 1	1	1	1	1	1	1	1	1
	$\eta^{(0)}$	1 1 1	1	1	1	0	0	0	1	0
(b)	$\eta^{(1)}$	0 1 1	1	1	1	1	1	1	1	1
	$\eta^{(2)}$	1 1 0	1	1	1	1	1	1	1	1
	$\eta^{(0)}$	1 1 1	1	1	1	0	0	0	1	0
(c)	$\eta^{(1)}$	1 0 1	1	1	1	1	1	1	1	1
	$\eta^{(2)}$	0 1 1	1	1	1	1	1	1	1	1

Table 2.1 Truth table on $\eta^{(0)}$, $\eta^{(1)}$ and $\eta^{(2)}$ using Karrenbauer transformation (1 means $\eta^{(k)} \neq 0$, 0 means $\eta^{(k)} = 0$)

Fault discriminant		11-g a b c	21-g a-b	21-g b-c	21-g c-a	21-s a-b	21-s b-c	21-s c-a	31s	31g
	$\eta^{(0)}$	1 1 1	1	1	1	0	0	0	1	0
(a)	$\eta^{(1)}$	1 1 1	1	1	1	1	0	1	1	1
	$\eta^{(2)}$	0 1 1	1	1	1	1	1	1	1	1
	$\eta^{(0)}$	1 1 1	1	1	1	0	0	0	1	0
(b)	$\eta^{(1)}$	1 1 1	1	1	1	1	1	0	1	1
	$\eta^{(2)}$	1 0 1	1	1	1	1	1	1	1	1
	$\eta^{(0)}$	1 1 1	1	1	1	0	0	0	1	0
(c)	$\eta^{(1)}$	1 1 1	1	1	1	0	1	1	1	1
	$\eta^{(2)}$	1 1 0	1	1	1	1	1	1	1	1

Table 2.2 Truth table on $\eta^{(0)}$, $\eta^{(1)}$ and $\eta^{(2)}$ using Clarke transformation. (1 means $\eta^{(k)} \neq 0$, 0 means $\eta^{(k)} = 0$)

CHAPTER THREE

THEORY OF THE DIRECTIONAL WAVE COMPARISON PHASE SELECTION SCHEME

3.1 Faulted EHV Transmission Line Response Analysis using Bewley Lattice Methods

In order to assist in the development of the new phase selector, a computer model of a transmission system was required. In the early stages of the project, it was decided to develop a test program based on the lattice diagram method[32], since the implementation of simplified analytical studies can be very useful for determining approximate fault transient waveforms, before more accurate digital studies are performed. The objective of the lattice program was to determine the fault induced superimposed voltages and currents at the point of interest as functions of time, which could possibly lead to the formation of reliable discriminant signals, for the purpose of phase selection.

The occurrence of a fault is equivalent to suddenly superimposing a voltage (V_{fF}) at the fault point, which is equal and opposite to the prefault steady-state fault point voltage (V_{sF}) at the instant of fault inception ϕ, as shown in Fig 3.1[33]. A fault transient solution is obtained by applying V_{fF} to the de-energised network, ie. all source voltages are short circuited.

The application of the voltage V_{fF} sets up a series of travelling wave components of voltage and current, which propagate away from the point of fault. These components may be described in terms of

natural modes of propagation[34], that is, the actual phase voltage and current components can be transformed into modal voltages and currents. The theory of natural modes can be simplified by assuming a lossless, ideally transposed balanced transmission line, such that the transformation matrices [S] and [Q][17] become equal and frequency invariant of the form given by equation (3.1).

$$[S] = [Q] = \begin{bmatrix} 1 & 1 & 1 \\ 1 & 0 & -2 \\ 1 & -1 & 1 \end{bmatrix} \quad \ldots (3.1)$$

The effect of suddenly applying the voltage V_{fF} at the fault point can now be analysed in terms of modal components.

The modal waves propagate along the line being continually attenuated and distorted until they die out. At a discontinuity, a part of the wave is reflected back along the line and the rest is transmitted to other sections of the transmission system. The lattice method relies on a knowledge of the reflection and refraction coefficients, at each point of discontinuity, within the system. The coefficients associated with the fault point are dependent upon the type of fault; ie. each type of fault produces a different reflection and refraction behaviour. The type of fault also controls the magnitude of each suddenly applied modal voltage at the instant of fault inception.

The reflection and refraction coefficient and initial modal voltage and current variations (jumps) at the fault point, for each

type of fault, can be obtained from different interconnected modal networks as described in Appendix A1 (see Figs 3.2-3.13). For any point of interest and for any fault type, the lattice method can then be used to determine the time variation of the fault induced superimposed modal voltages and currents.

The single phase lattice diagram of Fig 3.14 is representative of the initial variations of the superimposed modal voltage for the case of an a-e interconnected network shown in Fig 3.2(b). It will be recalled from Appendix A1 that the series combination of mode-2 and 3 networks have been replaced by an equivalent network, mode-4. Taking predominantly real components of the modal surge impedances, Table 3.1 shows the relationship between the parameters of each mode when an ideally transposed lossless line is considered. The mode 1 and 4 networks are then seen to have equal equivalent impedances, such that the application of a 1 p.u. fault point voltage V_{fFa} at the instant of fault inception causes an equal rise of 0.5 p.u. in each circuit. This instantaneous voltage change initiates travelling waves in each network, which subsequently propagate towards their respective terminating impedances at their particular modal velocity. The lattice diagram enables the travel of these waves to be represented by straight lines in coordinates of time versus distance. Mode-4 waves propagate with the highest velocity, and following the initial jumps, the reflected component associated with this mode is the first to arrive back at the fault point. Any change in a modal voltage caused by the arrival at F of a reflected component, therfore causes changes in the other modal voltages, so that an incident travelling

wave of one mode splits at the point of fault to produce transmitted and reflected components of all modes as explained in Appendix A1. In the absence of attenuation and distortion, voltages at any point on the line will only change in magnitude when a wavefront passes through that point.

The foregoing theory was implemented in a computer program to simulate the response of the ideally transposed line described above, following several types of fault. Figs 3.15 and 3.16 show the superimposed modal and phase voltage waveforms observed at the relay location, for different fault inception instances and fault types. The waveforms clearly illustrate the lattice summating process, since the arrival of each individual wavefront at the observation point causes a visible step change in amplitude.

A numerical analysis of the results has uncovered an interesting property associated with the aerial mode components for the particular fault types involving a single phase to ground and double phase clear of ground. In such cases, a fixed scalar ratio which is independent of fault inception angle, is observed between the mode 2 and mode 3 components, these ratios being summarised in Table 3.2. For all other fault types, a time varying aerial mode ratio is produced that is fault angle dependent and therefore very difficult to define iniquely.

At the fault point in particular, classification features for each fault type can be gained by the use of the algorithm in Appendix A1. The relationship between the initial jumps of each

mode subsequent to fault inception also confirms that a fixed aerial mode ratio exists for the aforementioned fault types. Table 3.3 shows the various relationships between the actual and modal superimposed voltage components at the fault location for all conventional faults.

The relationships between the initial modal variations at the fault point are found to be dependent only upon the type of fault. However, the modal relationships produced at a relay location, close to a source, are very much dependent upon the system and source modal impedances. In practice, it is very difficult to accurately define the ratio of mode-1 to mode-2 impedance for a source, since the source configuration may be constantly changing due to local switching. The ratio of mode-2 to mode-3 impedance, however, for a balanced source termination, remains constant.

A further advantage of the aerial mode property is that for an ideal line, identical parameters such as surge impedance, propagation velocity and refraction coefficients are associated with both mode-2 and mode-3. A consequence of this is that any reflection and refraction of components at all discontinuity points within the system will impose equal percentage changes in each aerial mode. Hence, even if the actual magnitudes of the aerial mode components may change, due to the model wave splitting effects described earlier, the scalar ratio between the two modes is maintained for all time after fault inception.

The foregoing analyses and results clearly imply that a discriminant signal, suitable for phase selector schemes, that is characteristic of only the fault type and not the fault, source or system configurations, can be obtained by using proportions of only aerial mode superimposed components.

3.2 General Phase Selector Discriminant Signal Considerations

The phase selector described in the present work utilises composite signals, which comprise a combination of both superimposed modal voltages and currents, which have the form shown in eqn (3.2).

$$S^{(k)}(t) = V_f^{(k)}(t) - R0^{(k)} I_f^{(k)}(t) \quad \ldots (3.2)$$

where $R0^{(k)}$ is the mode-k [k=1,2,3] replica characteristic resistance which will match $Z0^{(k)}$ for a lossless line. (For a real line the error due to the complex element in $Z0^{(k)}$ is small.

The signals represented by eqn (3.2), known as forward signals, are the same as those used in the directional wave comparison detector. It will be recalled from reference (17) that directional determination is made by the sequence in which the forward and reverse modal signals exceed a predetermined threshold level. The selection algorithm is based on the comparison of a combination of the forward signals described in eqn (3.2), since for forward faults they have the greater rate of rise and for a period equal to twice the transit time, are source independent.

The practical applicability of the phase selector is improved

by utilising discriminant signals comprising voltage and current superimposed components, as this results in greater terminating impedance coverage. For high source capacity terminations, resulting in low levels of superimposed voltage, the selector can operate given a current component alone (vice versa for low source capacity).

Although the equation represents all three modes of propagation, it has been established that some considerable simplification can be achieved by not including the earth mode[19]. This has been possible because there were no cases where an earth mode of propagation is detected without an associated aerial mode. The foregoing phase selector theory has also established the validity of using only aerial mode components for correct discrimination of the specified fault types. The new phase selector would therefore be directly compatible for integration with the UHS directional detection relay in a complete autoreclosure protection scheme.

The resulting general form of the phase selector discriminant signals, based on aerial mode components, is then:

$$D(t) = C1\ S^{(2)}(t) + C2\ S^{(3)}(t) \qquad \ldots (3.3)$$

where C1, C2 are real constants dependent upon the type of fault that the selector is designed to detect.

3.2.1 Particular discriminant signals for single pole autoreclosure

The discriminant signals that will be used to effect phase selection in the case of single pole autoreclosure will have the general form given by:

$$D_{a,b,c}(t) = K1_{a,b,c}S^{(2)}(t) + K2_{a,b,c}S^{(3)}(t) \quad \ldots (3.4)$$

The selector employs three separate measuring signals, the values of the constants K1, K2 being chosen such that the discriminant signal related to the faulted phase will measure zero (theoretically only), while that of the sound phase will have a finite and significant value.

Table 3.2 shows that mode 2 and 3 superimposed voltage and current components have relative proportions which are uniquely definable throughout the line from fault point to relay location, for each particular type of phase to earth fault and for all time after the fault. Assuming that $RO^{(2)}$ is equal to $RO^{(3)}$, manipulation of the general equations (3.2) reveals that these proportions are maintained between the mode 2 and mode 3 composite signals. The values of K1 and K2 required for each phase discriminant signal are then easily evaluated from the general discriminant form (3.4) and are listed in Table 3.5.

By substituting the appropriate values of the constants K1 and K2 in the general equation (3.4), the discriminant signals will take the form:

$$D_a(t) = 3S^{(3)}(t) - S^{(2)}(t)$$

$$D_b(t) = S^{(2)}(t) \qquad \ldots (3.5)$$

$$D_c(t) = 3S^{(3)}(t) + S^{(2)}(t)$$

It is necessary that the phase to earth fault selectors do not operate for all other types of fault and, as shown below, this is an inherent property of the new discrimination technique developed.

The derivation of an expression for the discriminant signal at the relaying point for all types of fault and for all time is a rather difficult task. Instead, the discriminant signal will be derived at the relaying end for only a specified time interval $\tau < t < 3\tau$, as explained below. The modal signals at the relay point are proportional to their respective modal superimposed voltages at the fault location, only for a specified time $\tau < t < 3\tau$. In this respect ref (17) shows that the modal signals at the relay point, for a specified time span of 2τ, are equal to twice the superimposed voltage at the fault point, during which time they are independent of the terminating source. This allows equations (3.2) to be written in the form of eqn (3.6).

$$S^{(k)}(t) = 2V_{fF}{}^{(k)} \; (t - \tau^{(k)}) \qquad \ldots (3.6)$$

It will be recalled that Table 3.3 shows the various relationships between modal and actual superimposed voltage components at the fault location for conventional faults. These relationships can be used in conjunction with the foregoing invariant property to find the corresponding modal signals at the relay location for the specified

time span. The combined expressions for each of the discriminant signals (D_a, D_b, D_c) used for single phase to ground selection can then be obtained for the different types of fault and are as listed in Table 3.6.

Since the ratio between modal signals $S^{(2)}$ and $S^{(3)}$ is constant for all time after the fault (as explained in the previous section), the expressions obtained for the discriminant signals will give a fair indication of their behaviour, for all time after each of the faults considered. Discrimination between single line to ground faults and all other types of fault is achieved using the signals D_a, D_b and D_c. Table 3.6 indicates that for any particular phase to earth fault, the discriminant signal associated with that phase is theoretically zero, whilst for all other faults it has a finite and significant value. The use of three discriminant signals therefore allows reliable phase selection, by distinguishing between a single line to ground fault and any other type of fault. A detailed description of the single pole tripping control is given in Chapter 4.

3.2.2 Particular discriminant signals for segregated schemes

In a more sophisticated scheme, known as segregated tripping, signals are needed for double phase and three phase faults, giving single, double and three pole tripping with reclosing as necessary. Segregated tripping is considered since there is thought to be an improvement in stability compared with a single phase tripping scheme and outputs are required giving the faulted phases for all types of faults. In the latter case total discrimination between all

multiphase faults is necessary to ensure that the minimum number of phases are tripped for each type of fault, ie. single phase tripping for line to ground and possibly double phase clear of ground faults, two phase tripping for double phase fault and three phase tripping for three phase faults.

The tripping of two phases with automatic reclosing did not appear, in the general opinion, to be of interest due to the marginal stability improvements gained for the extra complexity of equipment employed. It is now, therefore, accepted that any considerable fault involving more than one phase, either from its inception or during its elimination, should, perforce, involve the tripping of the three phases.

Although in recent years increasing interest has been focussed on the opening of only one of two faulted phases in the case of double line fault clear of ground, there are hardly any publications in the free literature, covering that area. Two segregated schemes have been suggested in the thesis:

(1) The opening of one pole in the case of single phase to earth faults and double phase faults clear of ground.
(2) The opening of one pole for single phase to earth, two poles opening for double phase faults and three poles opening for three phase faults.

3.2.2.1 Discriminant signals for phase to phase faults clear of ground

An analysis similar to that presented in the previous section for the derivation of single phase to earth discriminant signals reveals, that the for phase to phase faults clear of ground the discriminant signals for such cases will have the general form:

$$D_{ab,bc,ca}(t) = k1_{ab,bc,ca}S^{(2)}(t) + k2_{ab,bc,ca}S^{(3)}(t) \quad . . (3.7)$$

Once again the values of k1 and k2 required to make the interphase discriminant signal zero for that particular interphase fault only are easily evaluated, these values being listed in Table 3.7.

The three possible pure interphase faults will be covered accordingly by three separate signals of the given form:

$$\begin{aligned} D_{ab}(t) &= S^{(2)}(t) - S^{(3)}(t) \\ D_{bc}(t) &= S^{(2)}(t) + S^{(3)}(t) \\ D_{ca}(t) &= S^{(3)}(t) \end{aligned} \quad . . . (3.8)$$

The values of the respective pure interphase discriminant signals when applied to all conventional faults are given in Table 3.8.

As with the case of single phase discriminants associated with single line to ground faults, only the faulted interphase discriminant signal is found to be zero, for that particular pure interphase fault. The result is that for any pure interphase fault, the discriminant

will only select the two phases involved. If the first segregated scheme is to be considered, then six discriminant signals are required, which have the form:

$$
\begin{aligned}
D_a(t) &= 3S^{(3)}(t) - S^{(2)}(t) \\
D_b(t) &= S^{(2)}(t) \\
D_c(t) &= 3S^{(3)}(t) + S^{(2)}(t) \\
D_{ab}(t) &= S^{(2)}(t) - S^{(3)}(t) \\
D_{bc}(t) &= S^{(2)}(t) + S^{(3)}(t) \\
D_{ca}(t) &= S^{(3)}(t)
\end{aligned}
\qquad \ldots (3.9)
$$

A detailed description of the tripping control of such a scheme is studied in Chapter 4.

3.2.2.2 Discriminant signals for double phase faults involving ground

Although selection schemes capable of discriminating between all types of fault do not, at present, represent a practical solution for stability improvements as mentioned previously, future technological advances may result in a requirement for such schemes. In practice, there are hardly any operational segregated schemes which give reliable selective pole opening for double phase faults, particularly for long line applications. To this end, some feasibility studies were carried out into the possibility of producing such a scheme based upon the same technique as for single phase tripping schemes.

Discriminant signals are required for the selection of double phase to earth faults and in such cases, the mode-2 and mode-3 signals have a non-scalar relationship dependent upon the instant of fault inception. For any type of double phase to ground fault, the mode-2 and mode-3 signals at either end of the line for a specific time $\tau^{(2)} < t < 3\tau^{(2)}$ can be expressed by:

$$S^{(2)}(t) = Vm^{(2)} \sin(\Theta + \psi 2)\, h(t - \tau^{(2)}) \qquad \ldots (3.10)$$

$$S^{(3)}(t) = Vm^{(3)} \sin(\Theta + \psi 3)\, h(t - \tau^{(2)}) \qquad \ldots (3.11)$$

where:

Θ = $\omega_o(t - \tau^{(2)}) + \phi$

ϕ = fault inception angle

$\tau^{(2)}$ = aerial surge travelling time from fault location to either end

$Vm^{(2)}$, $Vm^{(3)}$ = mode-2 and mode-3 arbitrary constant dependent on type of double phase to ground fault

$\psi 2$ & $\psi 3$ = mode-2 and mode-3 phase angle respectively dependent on the type of double phase to ground fault

Mathematical manipulation of (3.10) and (3.11) produces the signal ratio:

$$S^{(2)}(t)/S^{(3)}(t) = Vm^{(3)}/Vm^{(2)}\ (\cos\alpha + \sin\alpha\ /\tan(\Theta + \psi 2)) \qquad \ldots (3.12)$$

where $\alpha = \psi 3 - \psi 2$.

It is clearly seen how the fault inception angle ϕ, which is an independent variable, controls the magnitude of the signal ratio. Therefore, unlike the case of SLG faults (see Table 3.3), a uniquely definable relationship between the aerial mode signals cannot be found using the previously adopted comparison technique.

An alternative method of discriminant signal derivation has been investigated, which includes the use of a mode-1 signal in the comparison process. Since the ratio of earth mode to aerial mode source impedance is difficult to define, particularly in large integrated systems, this method has been found to be practically unsuitable. Other techniques for obtaining reliable discriminant signals for double phase to ground faults are therefore required.

3.3 Initial Results Based on the Lattice Program

Having established a novel technique for achieving phase selection, it remains necessary to verify the validity of the scheme developed. The lattice program which has been developed earlier can serve the purpose of partially testing the new phase selector algorithm, and is sufficiently general to allow variation of reflection coefficients (ks) at both busbar ends ($-1 < ks < 1$) and fault inception angle, for any zero resistance faults located anywhere on the line.

The response of a three phase lossless system to a 1 p.u. sinusoidal voltage injected at the fault point is carefully studied. The results of a series of tests demonstrate that the new algorithm

derived will work satisfactorily with the approximate data generated by the transmission line model.

Some results of the new algorithm tests are presented in Figs 3.17-3.20 and emphasis is given to revealing the discriminative properties of the new phase selectors. Fig 3.17 shows a b-earth fault, with fault resistance of zero ohms. The fault is located at 50km (1/6L) on a 300km ideally transposed line, the phase "a" voltage switching angle at the fault point being 90°. The modal reflection coefficients for both mode-1 and mode-4 at each bus-bar ends are assumed equal and have the values of 0.6 and 0.5 for sending and receiving end respectively. Part (a) illustrates the response of the three single phase to earth discriminant signals (D_a,D_b,D_c) for such a fault. Part (b) represents the response of the three pure interphase discriminant signals (D_{ab}, D_{bc}, D_{ca}) for the same fault conditions. Fig 3.18 shows a "b"-"c" fault clear of ground, located at 50km on the same line considered before. Part (a) and (b) represents the behaviour of both single phase discriminant signals and pure interphase discriminant signals respectively for such a fault. In each case, correct discrimination is achieved, the appropriate discriminant remaining zero for the complete observation period.

Fig 3.19 and 3.20 shows the results for a three phase fault and an "a"-"b"-"e" fault respectively, whereby it is seen that none of the discriminants have a constant zero value, indicating that the fault is neither a single line to ground nor double phase clear of ground type.

3.4 Digital Computer Power System Simulation

The new techniques developed were originally verified by using an ideal transposed lossless, uniformly balanced, circuit. Therefore its feasibility had to be verified when applied to practical systems. In the lattice diagram method, it was assumed that voltage and current waves were subjected to the same attenuation at all frequencies and that the line was distortionless. However, in real systems, attenuation and distortion are present together with the effect of frequency dependent network elements, such as earth conductivity, and non-uniform distribution of ground currents respectively.

Direct validation of the new technique, when applied to real system configurations, is obtained by means of modern digital simulation techniques in which account can be taken of the effect of non-transposition of conductors, wave attenuation and frequency variance of the transmission line and earth parameters. Furthermore, they enable the effect of more realistic source side networks to be investigated. In the present work, a digital computer program using the latest digital simulation techniques for modelling the faulted response of any arbitrary linear shunt reactor compensated EHV feeder system, based on the modified Fast Fourier Transform method, was used to evaluate the primary system variations[35]. The parameters of the system are detailed in Chapter 5.

An initial comparison of results achieved for the same fault types simulated in the previous section reveal that, although the appropriate discriminants have non zero values, they are sufficiently

small with respect to all other signals that by suitable processing it will be possible to successfully implement the phase selector scheme (see Figs 3.21-3.24). An extensive CAD study was then performed to assess the development of the new phase selector scheme, and to gain an overall estimate of its performance.

	mode-1	mode-2	mode-3	mode-4
Surge impedance	600 ohm	300 ohm	300 ohm	600 ohm
Propagation velocity	200 km/ms	300 km/ms	300 km/s	300 km/s

Table 3.1 Modal parameters of ideally transposed line considered

Types of fault	$V_f^{(2)}(t)/V_f^{(3)}(t)$	$I_f^{(2)}(t)/I_f^{(3)}(t)$	Useful relations at relay locations
"a"-e	3	3	$I_{fb} = I_{fc}$ $V_{fb} = V_{fc}$
"b"-e	0	0	$I_{fa} = I_{fc}$ $V_{fa} = V_{fc}$
"c"-e	-3	-3	$I_{fa} = I_{fb}$ $V_{fa} = V_{fb}$
"a"-"b"	1	1	$I_{fa} = -I_{fb}$ $V_{fbc} = V_{fca}$
"b"-"c"	-1	-1	$I_{fb} = -I_{fc}$ $V_{fca} = V_{fab}$
"c"-"a"	∞	∞	$I_{fc} = -I_{fa}$ $V_{fab} = V_{fbc}$

Table 3.2 Fixed scalar proportions between mode-2 and mode-3 quantities at any location on the line after fault

Types of fault	MODAL VOLTAGE AT FAULT POINT (initial jump)		
	MODE (1) $V_{fF}^{(1)}(t),\ \tau^{(1)} \leq t \leq 3\tau^{(1)}$	MODE (2) $V_{fF}^{(2)}(t),\ \tau^{(2)} \leq t \leq 3\tau^{(2)}$	MODE (3) $V_{fF}^{(3)}(t),\ \tau^{(3)} \leq t \leq 3\tau^{(3)}$
"a"-e	$V_{fFa}(t)\ \left\{\frac{Z0^{(1)}}{Z0^{(1)}+2Z0^{(2)}}\right\}$	$\frac{3}{2}\ V_{fFa}(t)\ \left\{\frac{Z0^{(2)}}{Z0^{(1)}+2Z0^{(2)}}\right\}$	$\frac{1}{2}\ V_{fFa}(t)\ \left\{\frac{Z0^{(2)}}{Z0^{(1)}+2Z0^{(2)}}\right\}$
"b"-e	$V_{fFb}(t)\ \left\{\frac{Z0^{(1)}}{Z0^{(1)}+2Z0^{(2)}}\right\}$	0	$-\ V_{fFb}(t)\ \left\{\frac{Z0^{(2)}}{Z0^{(1)}+2Z0^{(2)}}\right\}$
"c"-e	$V_{fFc}(t)\ \left\{\frac{Z0^{(1)}}{Z0^{(1)}+2Z0^{(2)}}\right\}$	$-\ \frac{3}{2}\ V_{fFc}(t)\ \left\{\frac{Z0^{(2)}}{Z0^{(1)}+2Z0^{(2)}}\right\}$	$\frac{1}{2}\ V_{fFc}(t)\ \left\{\frac{Z0^{(2)}}{Z0^{(1)}+2Z0^{(2)}}\right\}$
"a"-"b"	0	$(V_{fFa}(t) - V_{fFb}(t))/4$	$(V_{fFa}(t) - V_{fFb}(t))/4$
"b"-"c"	0	$(V_{fFb}(t) - V_{fFc}(t))/4$	$-(V_{fFb}(t) - V_{fFc}(t))/4$
"c"-"a"	0	$(V_{fFa}(t) - V_{fFc}(t))/2$	0
"a"-"b"-e	$\left\{V_{fFa}(t) + V_{fFb}(t)\right\}\left\{\frac{Z0^{(1)}}{Z0^{(2)}+2Z0^{(1)}}\right\}$	$\frac{1}{2}\left\{V_{fFa}(t)\left\{\frac{2Z0^{(2)}+Z0^{(1)}}{Z0^{(2)}+2Z0^{(1)}}\right\} - V_{fFb}(t)\left\{\frac{Z0^{(1)}-Z0^{(2)}}{Z0^{(2)}+2Z0^{(1)}}\right\}\right\}$	$\frac{1}{2}\left\{V_{fFa}(t)\left\{\frac{Z0^{(1)}}{Z0^{(2)}+2Z0^{(1)}}\right\} - V_{fFb}(t)\left\{\frac{Z0^{(2)}+Z0^{(1)}}{Z0^{(2)}+2Z0^{(1)}}\right\}\right\}$
"b"-"c"-e	$\left\{V_{fFb}(t) + V_{fFc}(t)\right\}\left\{\frac{Z0^{(1)}}{Z0^{(2)}+2Z0^{(1)}}\right\}$	$\frac{1}{2}\left\{V_{fFb}(t)\left\{\frac{Z0^{(1)}-Z0^{(2)}}{2Z0^{(1)}+Z0^{(2)}}\right\} - V_{fFc}(t)\left\{\frac{2Z0^{(2)}+Z0^{(1)}}{2Z0^{(1)}+Z0^{(1)}}\right\}\right\}$	$\frac{1}{2}\left\{V_{fFc}(t)\left\{\frac{Z0^{(1)}}{2Z0^{(1)}+Z0^{(2)}}\right\} - V_{fFb}(t)\left\{\frac{Z0^{(1)}+Z0^{(2)}}{2Z0^{(1)}+Z0^{(2)}}\right\}\right\}$
"c"-"a"-e	$\left\{V_{fFc}(t) + V_{fFa}(t)\right\}\left\{\frac{Z0^{(1)}}{Z0^{(2)}+2Z0^{(1)}}\right\}$	$(V_{fFa}(t) - V_{fFc}(t))/2$	$\left\{V_{fFc}(t) + V_{fFa}(t)\right\}\left\{\frac{Z0^{(2)}}{2(2Z0^{(1)}+Z0^{(2)})}\right\}$
3-ϕ	0	$\frac{1}{2}\ (V_{fFa}(t) - V_{fFc}(t))$	$\frac{1}{2}\ (V_{fFa}(t) + V_{fFc}(t))$

Table 3.3 Relationships between modal and actual superimposed voltage components at fault location F for conventional faults on a TL

Modal voltage at F	Mode-1	Mode-2	Mode-3
Fault Type	$V_{fF}^{(1)}(t)$	$V_{fF}^{(2)}(t)$	$V_{fF}^{(3)}(t)$
"a"-earth	$V_{fFa}(t)/2$	$3V_{fFa}(t)/8$	$V_{fFa}(t)/8$
"b"-earth	$V_{fFb}(t)/2$	0	$-V_{fFb}(t)/4$
"c"-earth	$V_{fFc}(t)/2$	$-3V_{fFc}(t)/8$	$V_{fFc}(t)/8$
"a"-"b"	0	$(V_{fFa}(t) - V_{fFb}(t))/4$	$(V_{fFa}(t) - V_{fFb}(t))/4$
"b"-"c"	0	$(V_{fFb}(t) - V_{fFc}(t))/4$	$(V_{fFc}(t) - V_{fFb}(t))/4$
"c"-"a"	0	$(V_{fFa}(t) - V_{fFc}(t))/2$	0
"a"-"b"-e	$2/5(V_{fFa}(t) + V_{fFb}(t)$	$(2V_{fFa}(t)/5 - V_{fFb}(t))/10$	$(V_{fFa}(t)/5 -3V_{fFb}(t))/10$
"b"-"c"-e	$2/5(V_{fFb}(t) + V_{fFc}(t))$	$(V_{fFb}(t) -4V_{fFc}(t))/10$	$(2V_{fFc}(t) -3V_{fFb}(t))/10$
"c"-"a"-e	$2/5(V_{fFc}(t) + V_{fFa}(t))$	$(V_{fFa}(t) - V_{fFc}(t))/2$	$(V_{fFa}(t) + V_{fFc}(t))/10$
"a"-"b"-"c"	0	$(V_{fFa}(t) - V_{fFc}(t))/2$	$(V_{fFa}(t) + V_{fFc}(t))/2$

Table 3.4 Superimposed modal voltages at fault location F for conventional faults on a transmission line (assuming $Z0^{(1)} \sim 2Z0^{(2)}$).

Type of Fault	$S^{(2)}(t)/S^{(3)}(t)$	k1	k2
"a"-earth	3	-1	3
"b"-earth	0	1	0
"c"-earth	-3	1	3

Table 3.5

Discriminant Signals / Fault Type	$\tau > t > 3\tau$ $D_a(t)$ (phase "a")	$\tau > t > 3\tau$ $D_b(t)$ (phase "b")	$\tau > t > 3\tau$ $D_c(t)$ (phase "c")
"a"-earth	0	$3V_{fFa}(t)/8$	$3V_{fFa}(t)/4$
"b"-earth	$-3V_{fFb}(t)/4$	0	$-3V_{fFb}(t)/4$
"c"-earth	$-3V_{fFc}(t)/4$	$-3V_{fFc}(t)/8$	0
"a"-"b"	$(V_{fFa}(t) - V_{fFb}(t))/2$	$(V_{fFa}(t) - V_{fFb}(t))/4$	$(V_{fFa}(t) - V_{fFb}(t))$
"b"-"c"	$(V_{fFb}(t) - V_{fFc}(t))$	$(V_{fFb}(t) - V_{fFc}(t))/4$	$(V_{fFc}(t) - V_{fFb}(t))$
"c"-"a"	$(V_{fFc}(t) - V_{fFa}(t))/2$	$(V_{fFa}(t) - V_{fFc}(t))/2$	$(V_{fFa}(t) - V_{fFc}(t))/2$
"a"-"b"-e	$(V_{fFa}(t) + 4V_{fFb}(t))/5$	$(2V_{fFa}(t)/5 - V_{fFb}(t)/10)$	$(V_{fFa}(t) - V_{fFb}(t))$
"b"-"c"-e	$-(V_{fFb}(t) - V_{fFc}(t))$	$(V_{fFb}(t)/10 - 2V_{fFc}(t)/5)$	$-(4V_{fFb}(t) - V_{fFc}(t))/5$
"c"-"a"-e	$(4V_{fFc}(t) - V_{fFa}(t))/5$	$(V_{fFa}(t) - V_{fFc}(t))$	$(4V_{fFa}(t) - V_{fFc}(t))/5$
"a"-"b"-"c"	$(V_{fFa}(t) - 2V_{fFc}(t))/5$	$(V_{fFa}(t) - V_{fFc}(t))/2$	$(2V_{fFa}(t) + V_{fFc}(t))/2$

Table 3.6 Relationships between phase to earth discriminant signals and superimposed modal voltages at fault location F for conventional faults on a transmission line at either relay end (assuming $Z0^{(1)} \sim 2Z0^{(2)}$)

Type of Fault	$S^{(3)}(t)/S^{(2)}(t)$	k1	k2
"a"-"b"	1	1	-1
"b"-"c"	-1	1	1
"c"-"a"	0	0	1

Table 3.7

Discriminant signals	$\tau > t > 3\tau$ $D_{ab}(t)$	$\tau > t > 3\tau$ $D_{bc}(t)$	$\tau > t > 3\tau$ $D_{ca}(t)$
Fault type	(phase "ab")	(phase "bc")	(phase "ca")
"a"-earth	$V_{fFa}(t)/4$	$V_{fFa}(t)/2$	$V_{fFa}(t)/8$
"b"-earth	$V_{fFb}(t)/4$	$-V_{fFb}(t)/4$	$-V_{fFb}(t)/4$
"c"-earth	$-V_{fFc}(t)/2$	$-V_{fFc}(t)/4$	$V_{fFc}(t)/8$
"a"-"b"	0	$(V_{fFa}(t) - V_{fFb}(t))/2$	$(V_{fFa}(t) - V_{fFb}(t))/4$
"b"-"c"	$(V_{fFb}(t) - V_{fFc}(t))/2$	0	$(V_{fFc}(t) - V_{fFb}(t))/4$
"c"-"a"	$-(V_{fFc}(t) - V_{fFa}(t)/2$	$(V_{fFa}(t) - V_{fFc}(t))/2$	0
"a"-"b"-e	$(V_{fFa}(t) + V_{fFb}(t))/5$	$(3V_{fFa}(t) - 2V_{fFb}(t))/5$	$(2V_{fFa}(t) - V_{fFb}(t))/10$
"b"-"c"-e	$(2V_{fFb}(t) - 3V_{fFc}(t))/5$	$-(V_{fFb}(t) - V_{fFc}(t))/5$	$-(3V_{fFb}(t) - V_{fFc}(t))/5$
"c"-"a"-e	$(2V_{fFa}(t) - 3V_{fFc}(t))/5$	$(3V_{fFa}(t) - 2V_{fFc}(t))/5$	$(V_{fFa}(t) + V_{fFc}(t))/10$
"a"-"b"-"c"	$-V_{fFc}(t)$	$V_{fFa}(t)$	$(V_{fFa}(t) + V_{fFc}(t))/2$

Table 3.8 Relationships between pure interphase discriminant signals and superimposed modal voltages at fault location F for conventional faults on a transmission line at either relay end (assuming $Z0^{(1)} \sim 2Z0^{(2)}$)

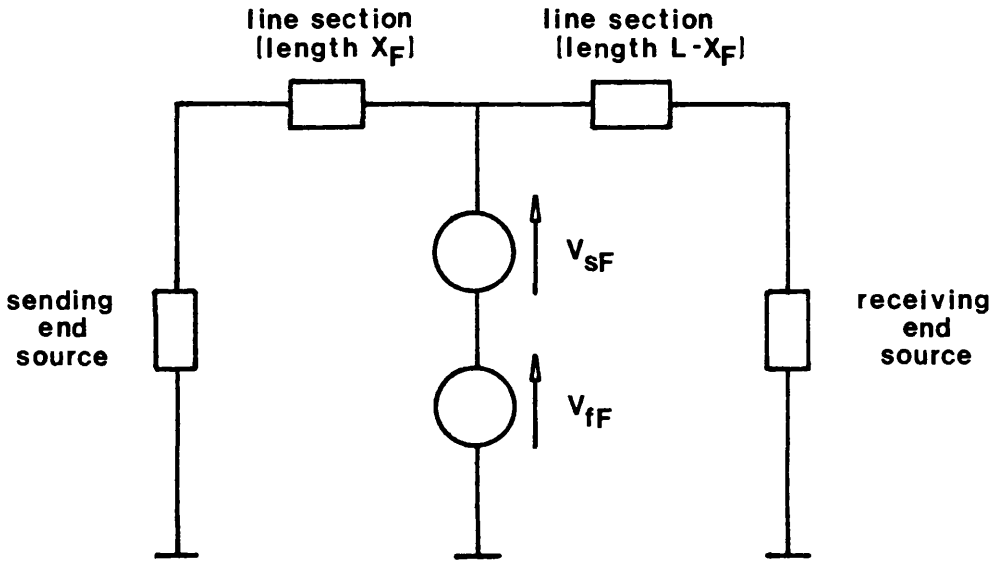

Fig 3.1 Fault transient model using superimposed fault voltage

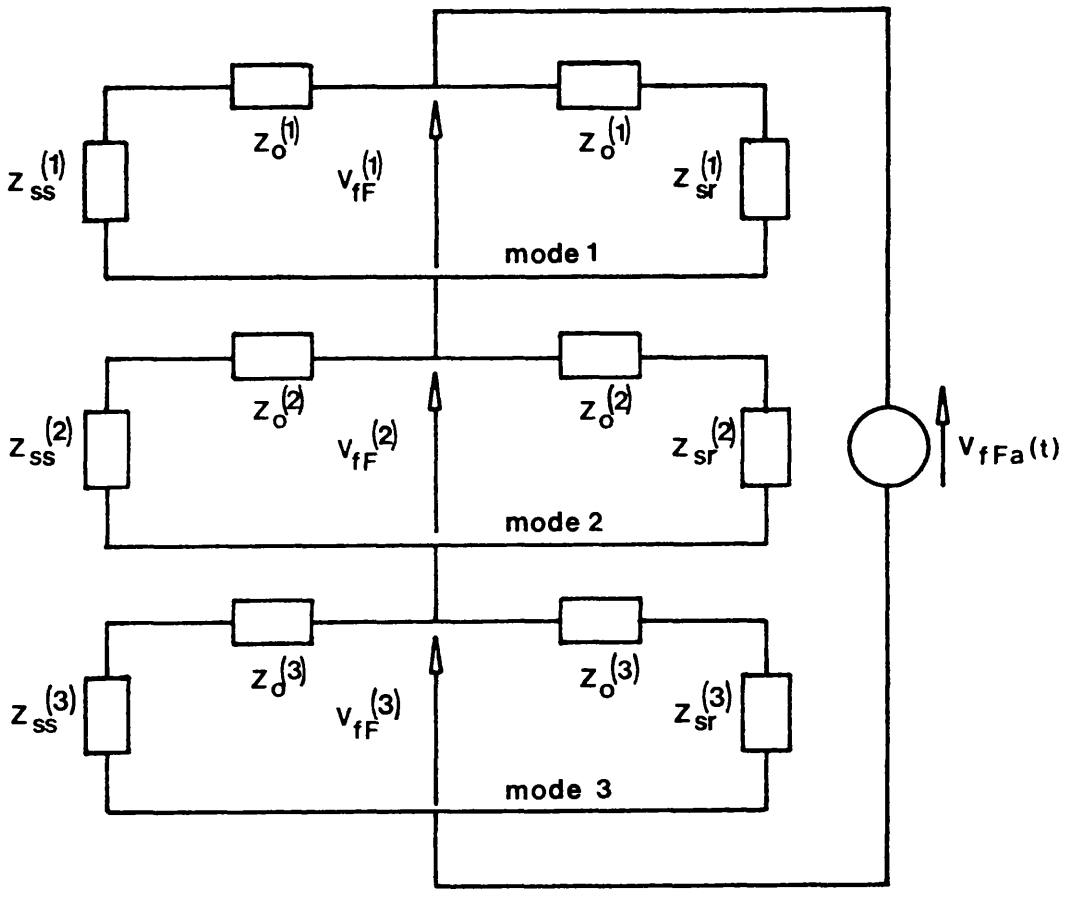

Fig 3.2(a) Interconnection of modal component circuits (solid "a"-e fault)

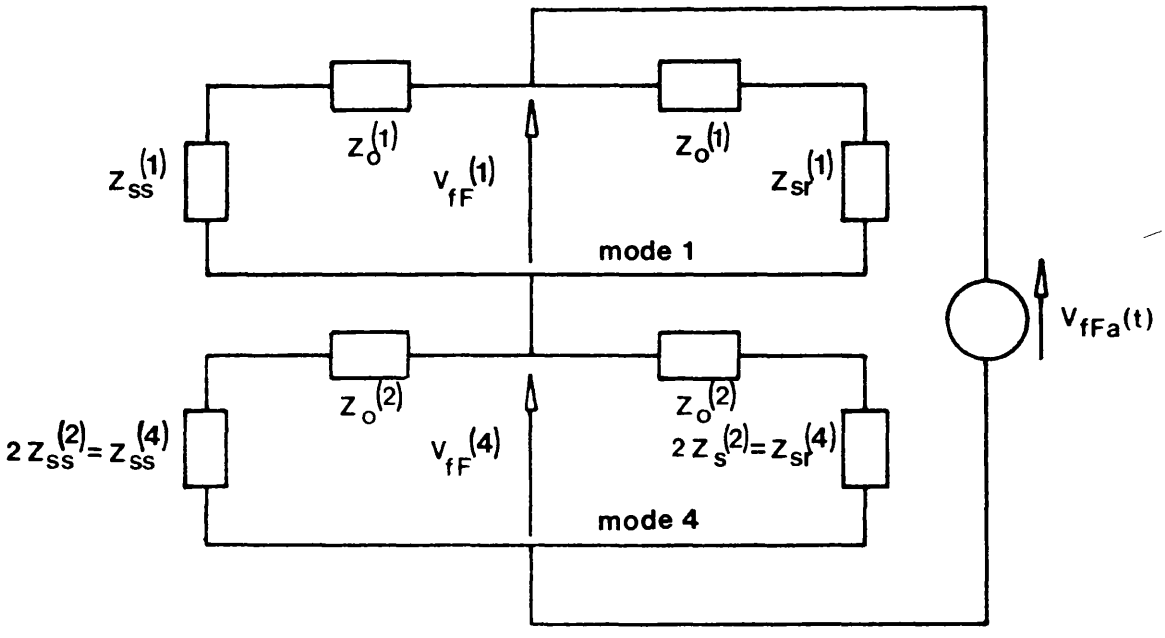

Fig 3.2(b) Simplified modal interconnected circuits (solid "a"-e fault)

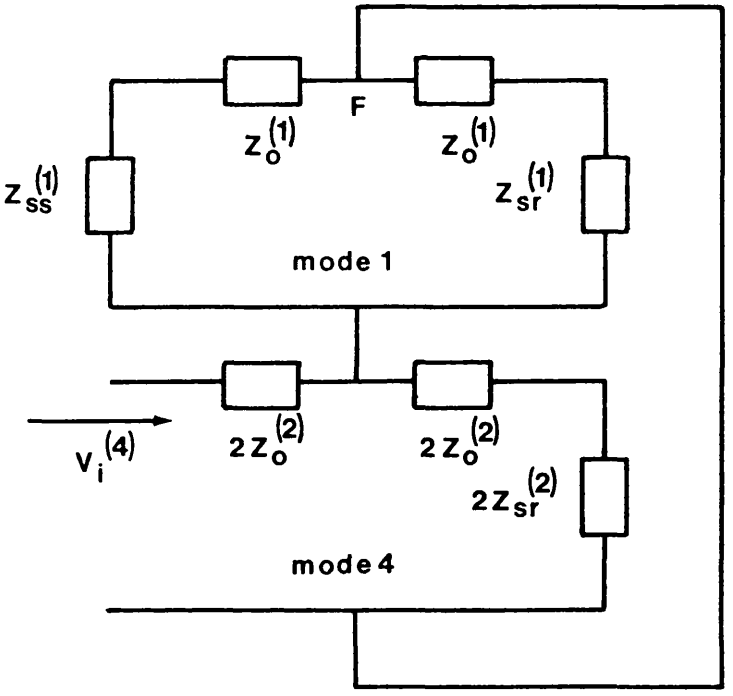

Fig 3.3(a) Equivalent circuit presented to an incident mode-4 voltage wave $(v_i^{(4)})$

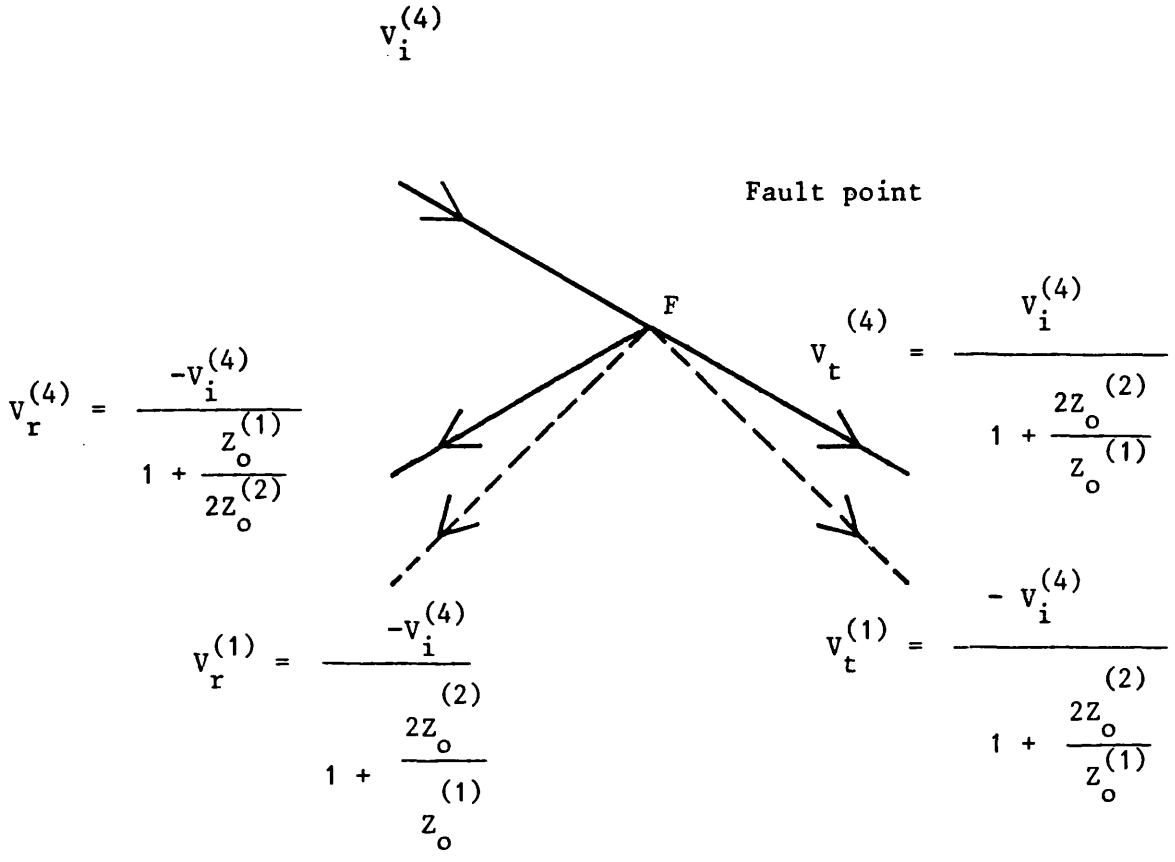

Fig 3.3(b) Reflection and refraction of modal voltages, due to an incident travelling wave of mode-4 voltage at the point of fault for the case of an "a"-e fault

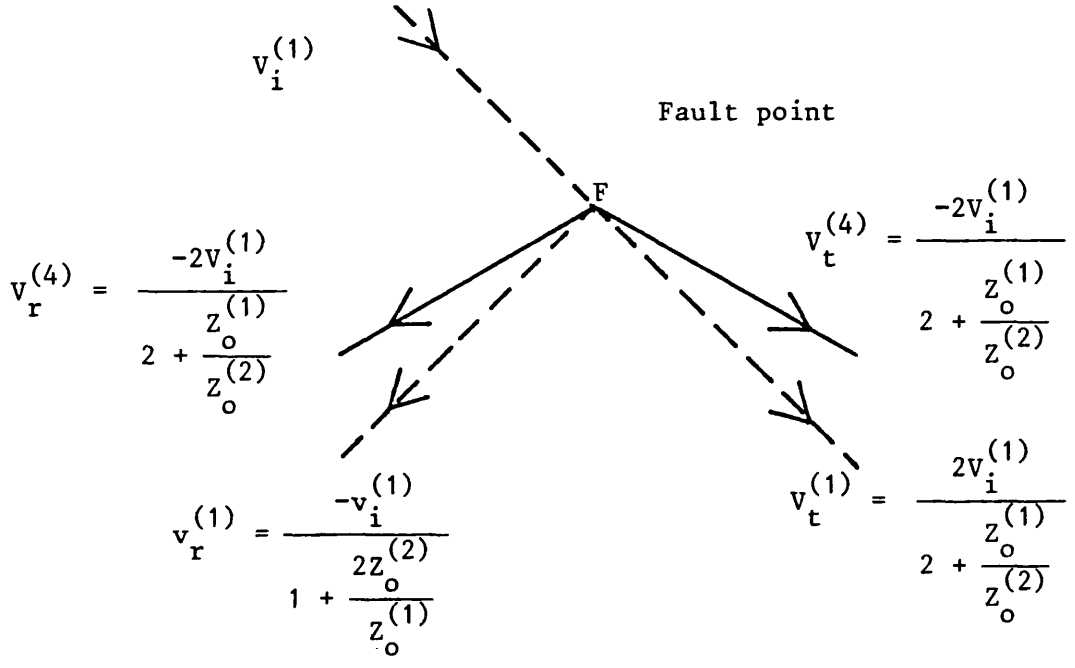

Fig 3.3(c) Reflection and refraction situation at the fault point, for an incident voltage wave of mode-1, for the case of an "a"-e fault

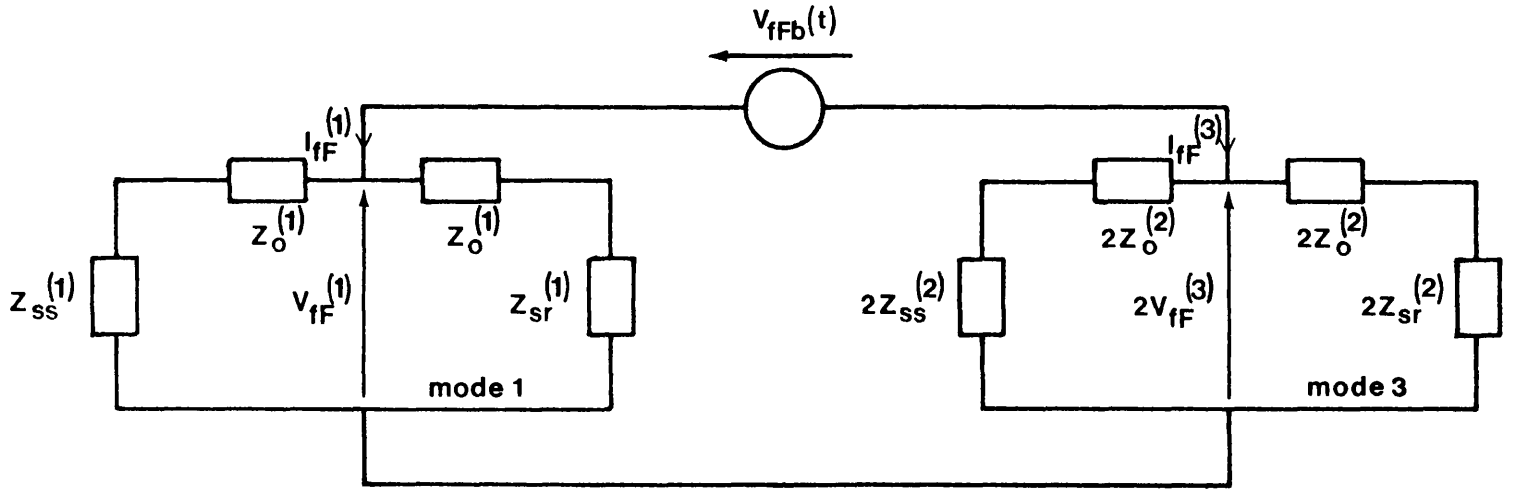

Fig 3.4 Interconnection of modal component circuits (solid "B"-earth faults)

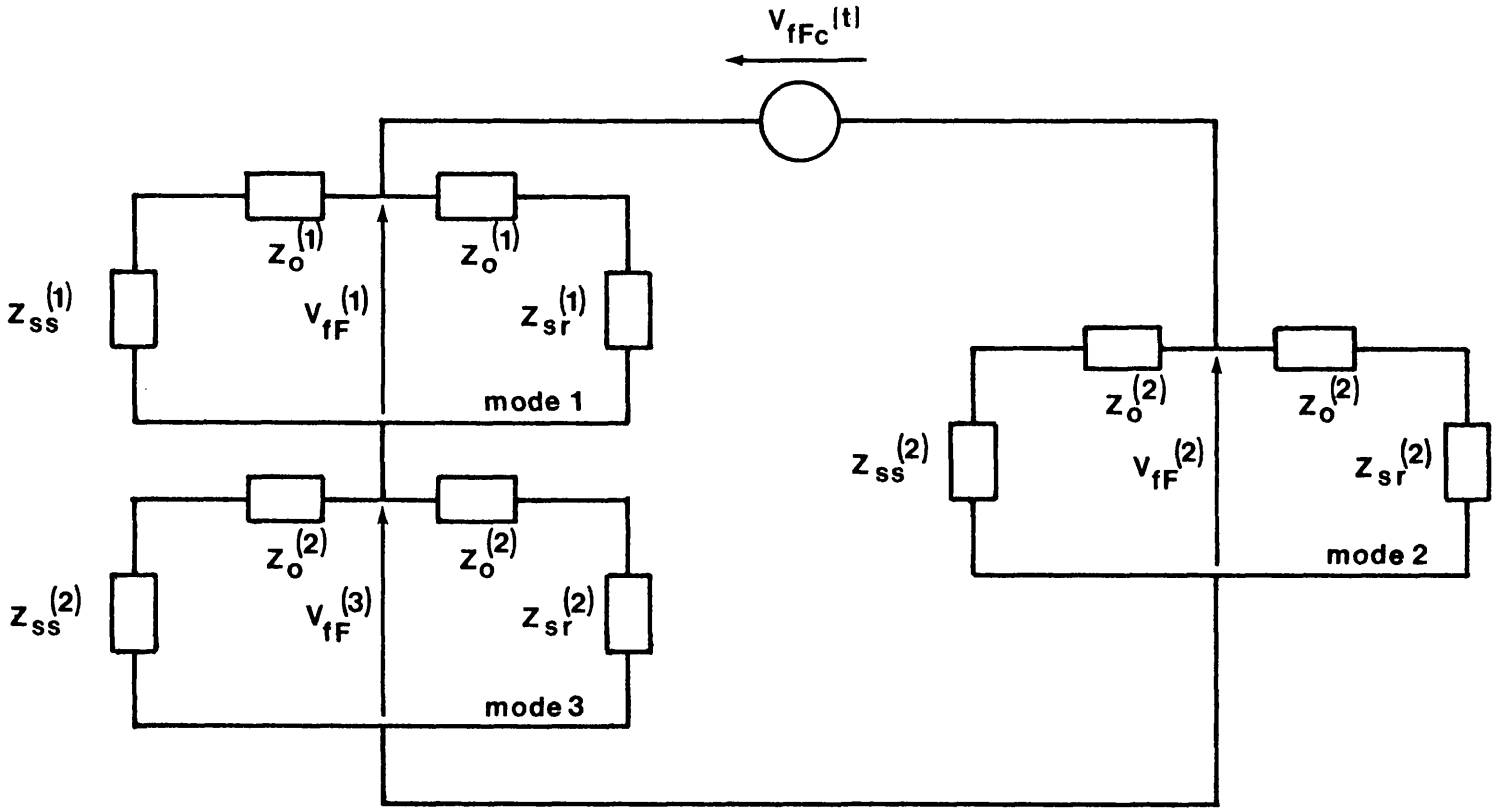

Fig 3.5 Interconnection of modal component circuits (solid "c"-earth fault)

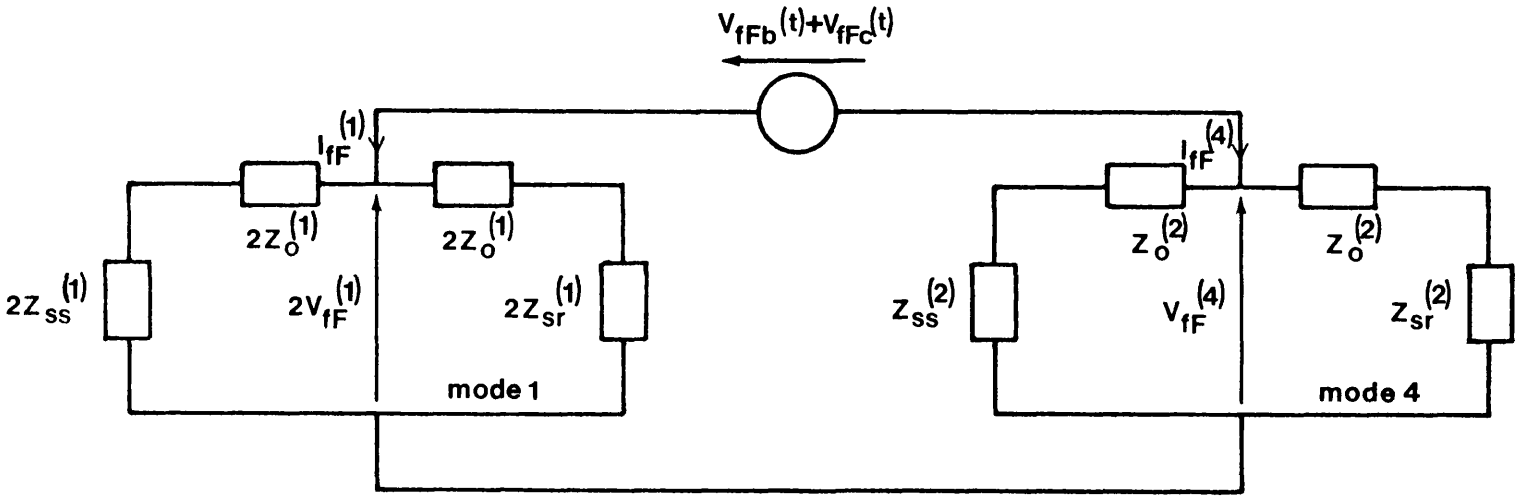

Fig 3.6(a) Equivalent modal interconnected circuits for the case of "b"-"c"-earth fault

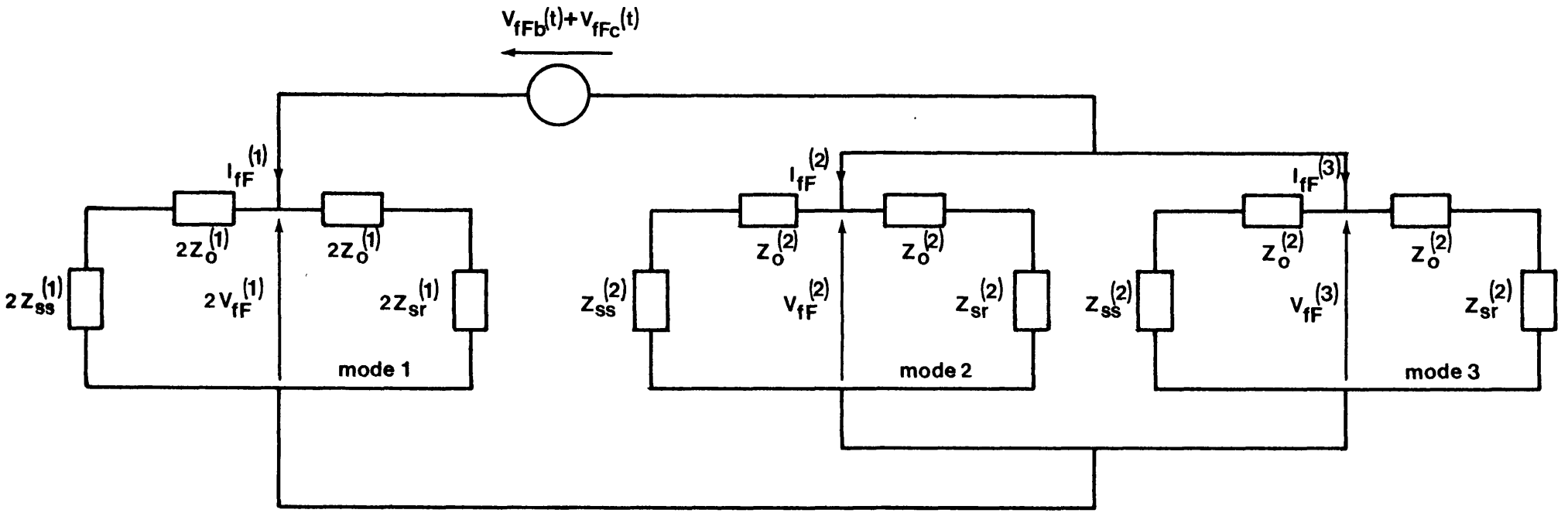

Fig 3.6(b) Interconnection of modal component circuits (case of "b"-"c"-earth fault)

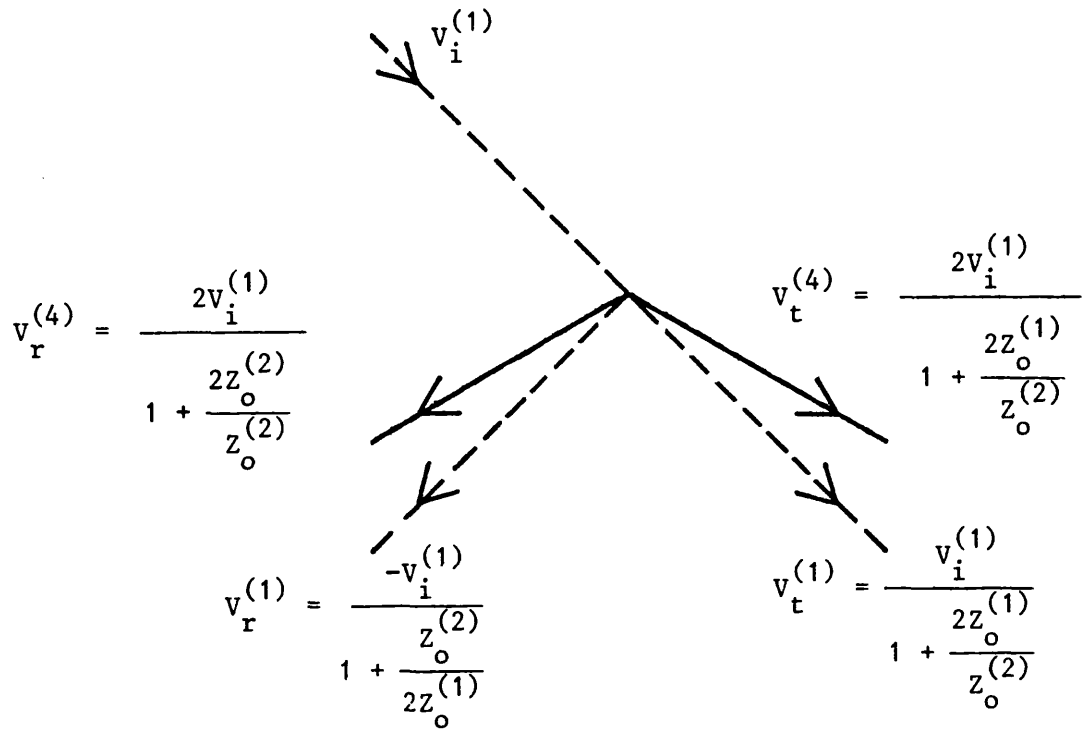

Fig 3.7(a) Reflection and refraction situation at the fault point due to an incident voltage of mode-1, for the case of "b"-"c"-earth fault

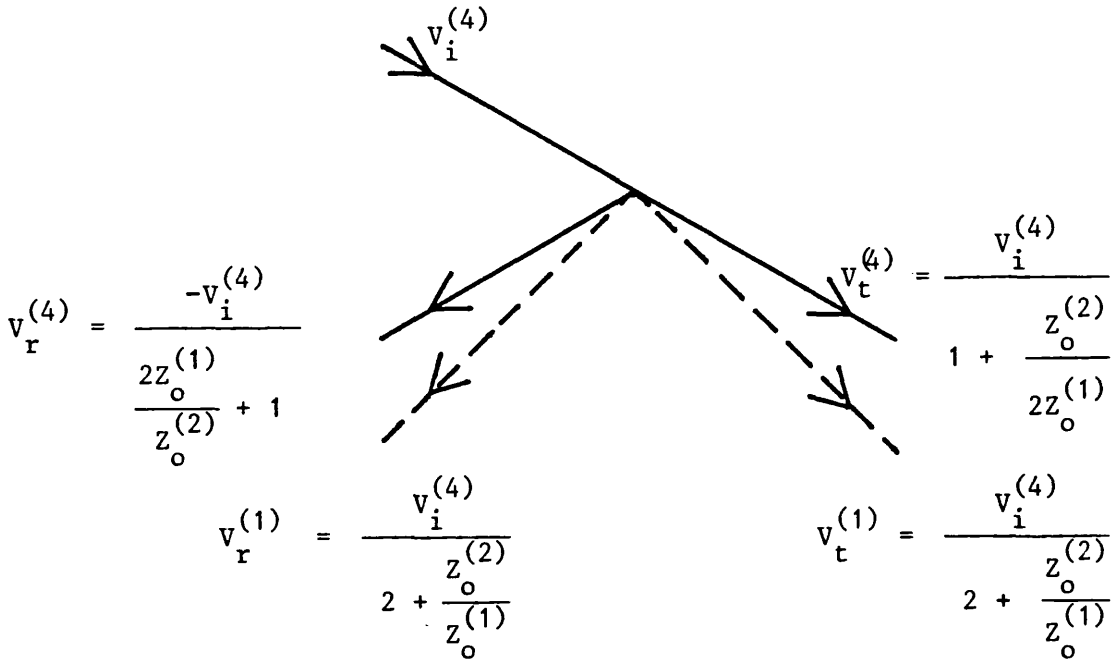

Fig 3.7(b) Reflection and refraction situation at the fault point due to an incident voltage of mode-4, for the case of a "b"-"c"-earth fault

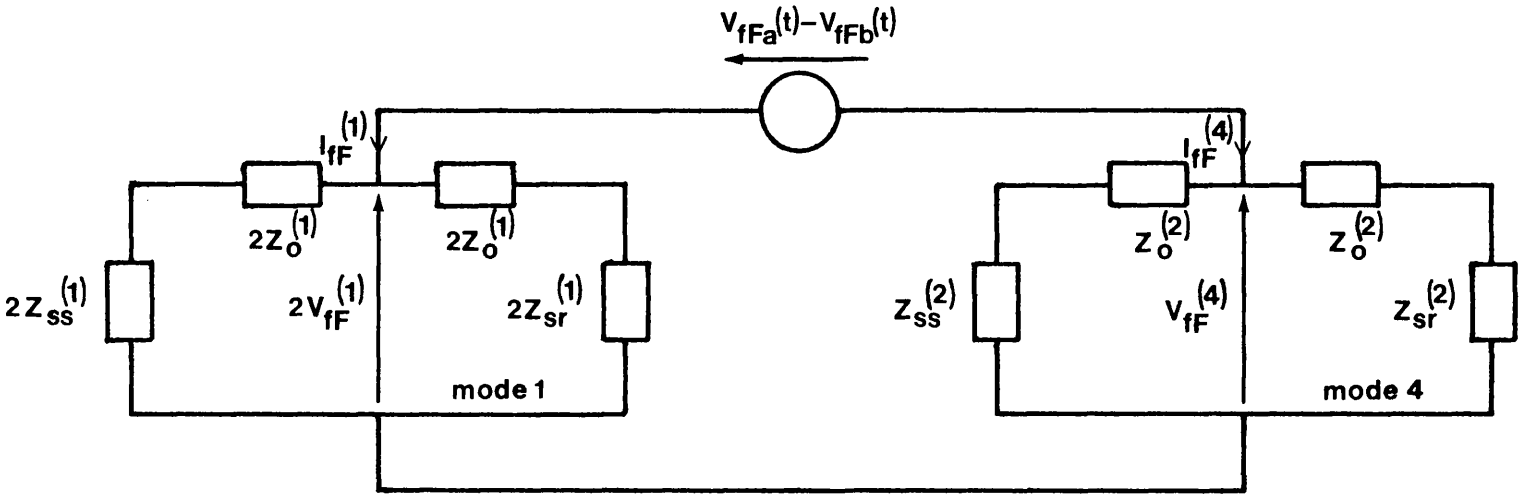

$$V_{fF}^{(2)} - V_{fF}^{(3)} = V_{fF}^{(4)}$$

$$I_{fF}^{(3)} - I_{fF}^{(2)} = I_{fF}^{(4)}$$

Fig 3.8 Equivalent modal circuits interconnection for the case of an "a"-"b"-earth fault

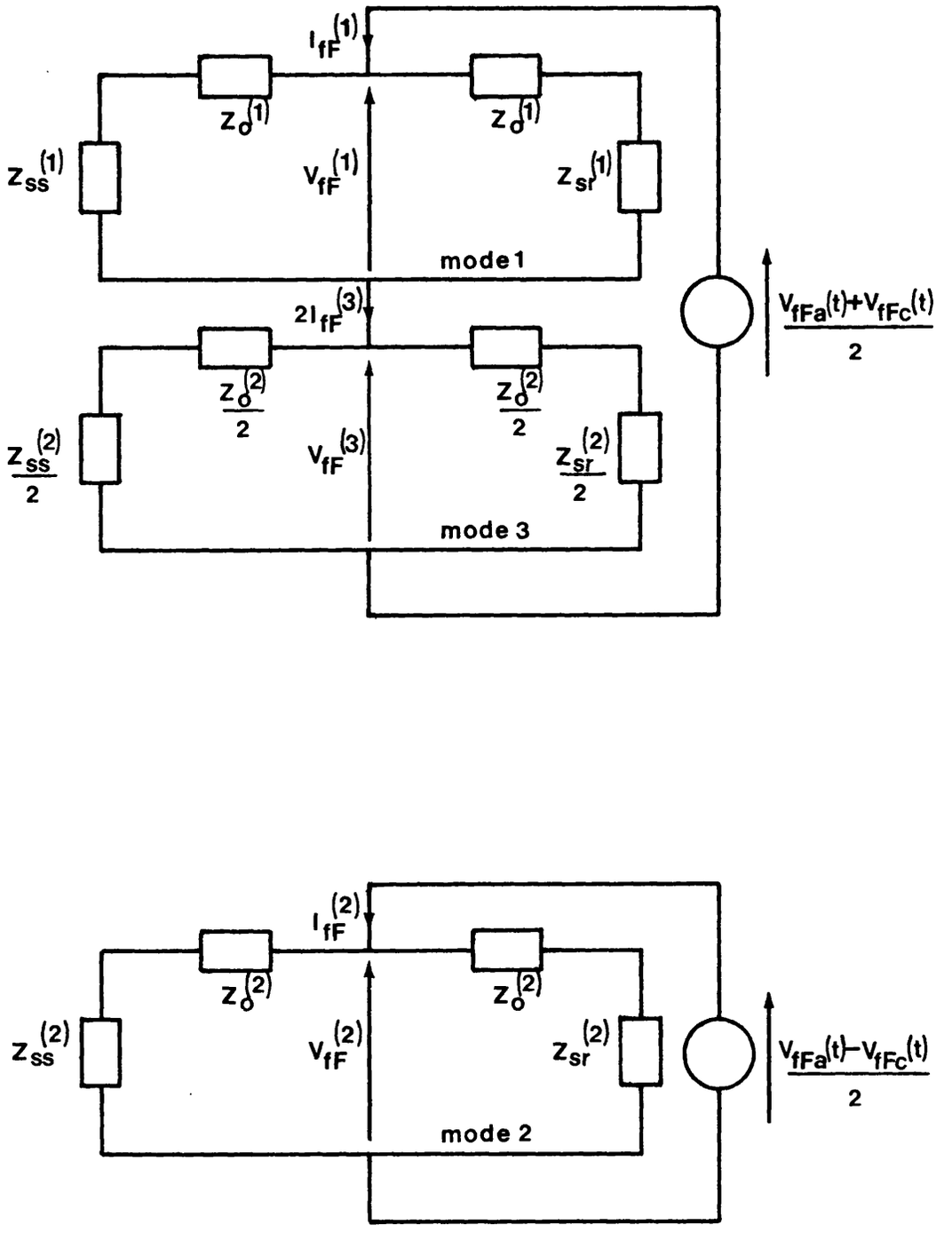

Fig 3.9 The two modal interconnected circuits representative of an "a"-"c"-earth fault condition

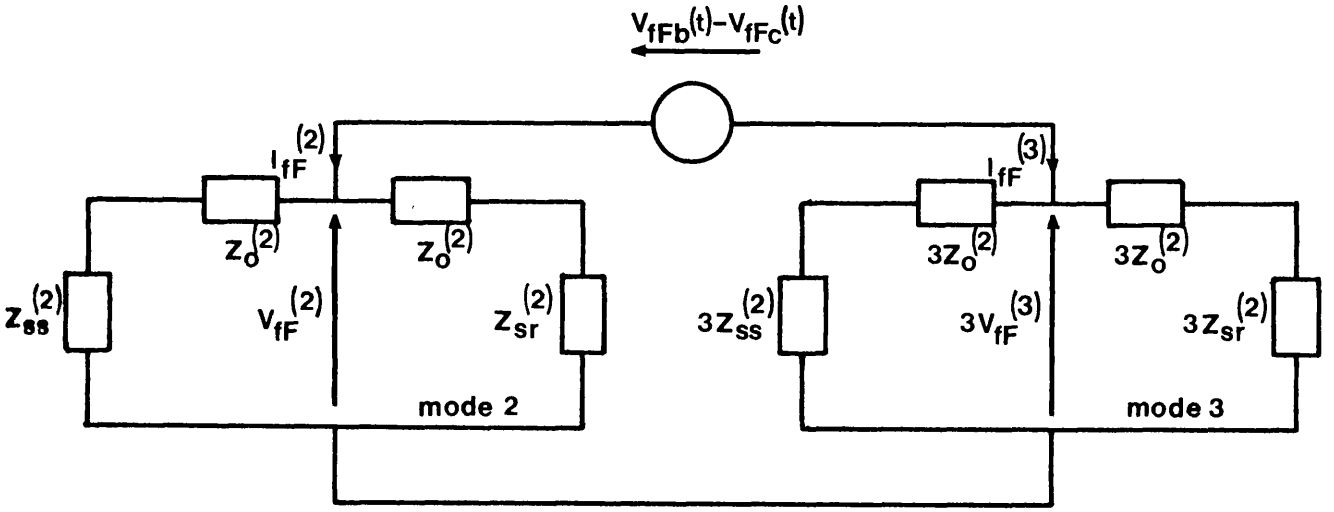

Fig 3.10(a) Interconnection of modal component circuits for the case of "b"-"c" phase fault clear of ground

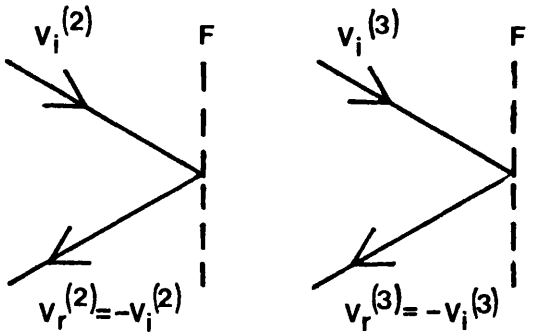

Fig 3.10(b) Reflection coefficient of an incident wave of aerial mode at the fault location for the case of "b"-"c" fault clear of ground

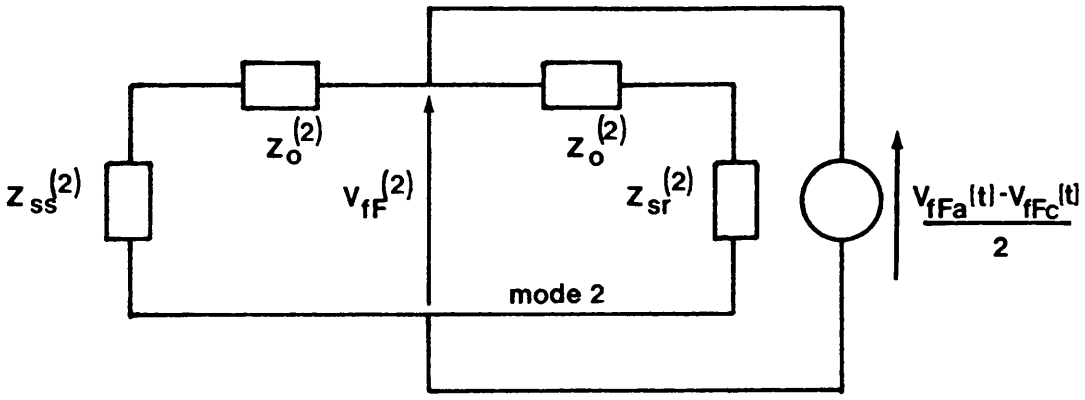

Fig 3.11(a) Equivalent modal circuit for "a"-"c" fault clear of ground

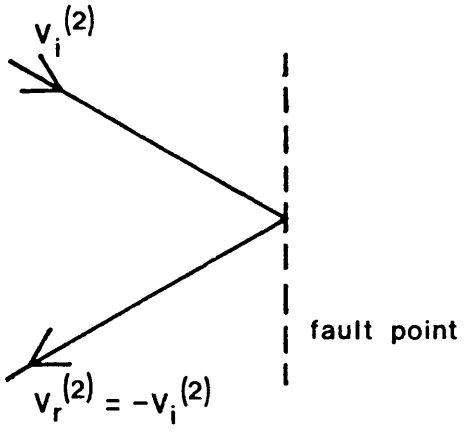

Fig 3.11(b) Reflection and refraction situation at the fault point for the case of "a"-"c" fault clear of ground

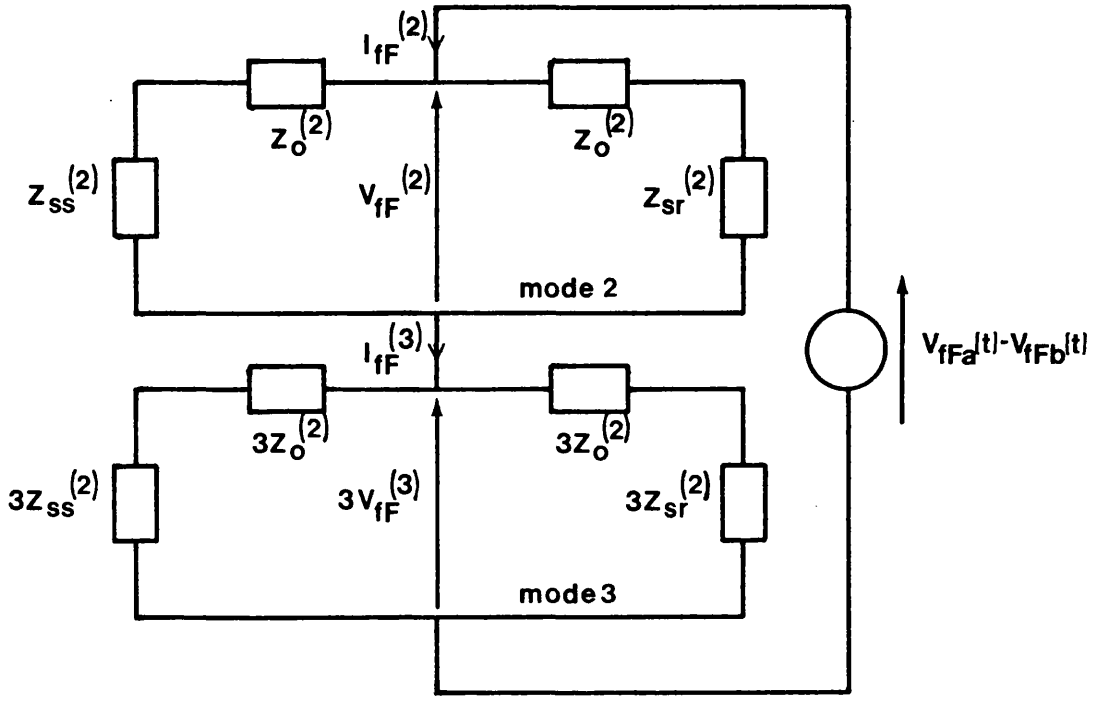

Fig 3.12(a) Interconnection of modal component circuits for the case of an "a"-"b" fault clear of ground

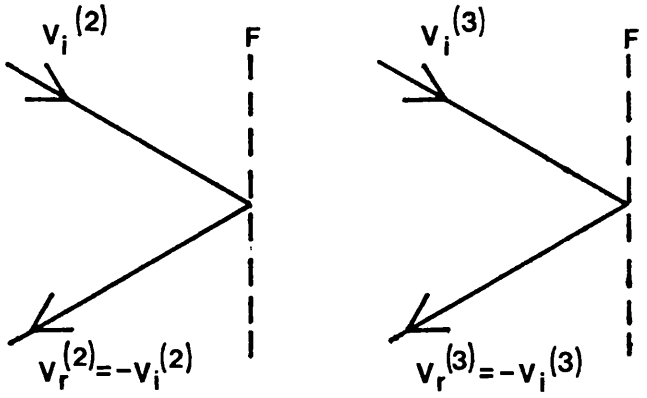

Fig 3.12(b) Reflection and refraction situation at the fault point due to the inception of either of the aerial mode voltage for the case of "a"-"b"-fault clear of ground

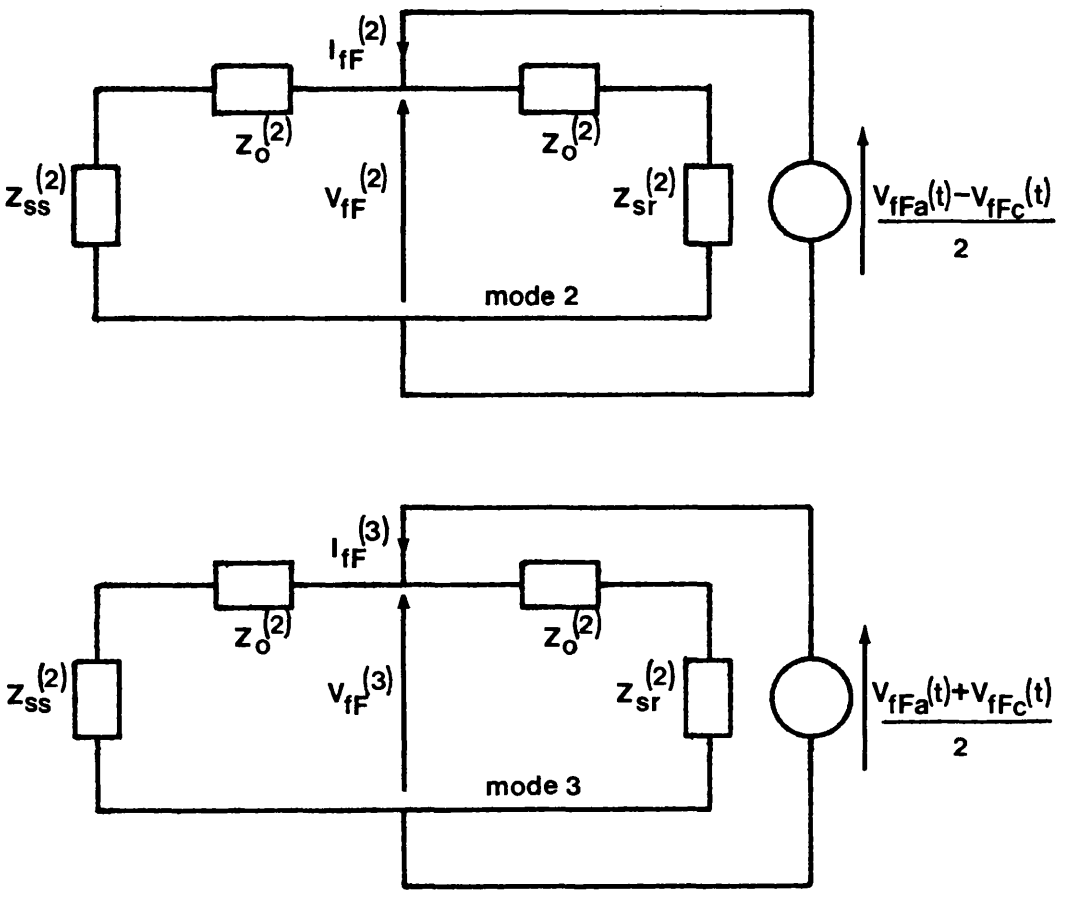

Fig 3.13 Mode-2 and mode-3 independent connection to represent a three phase fault condition

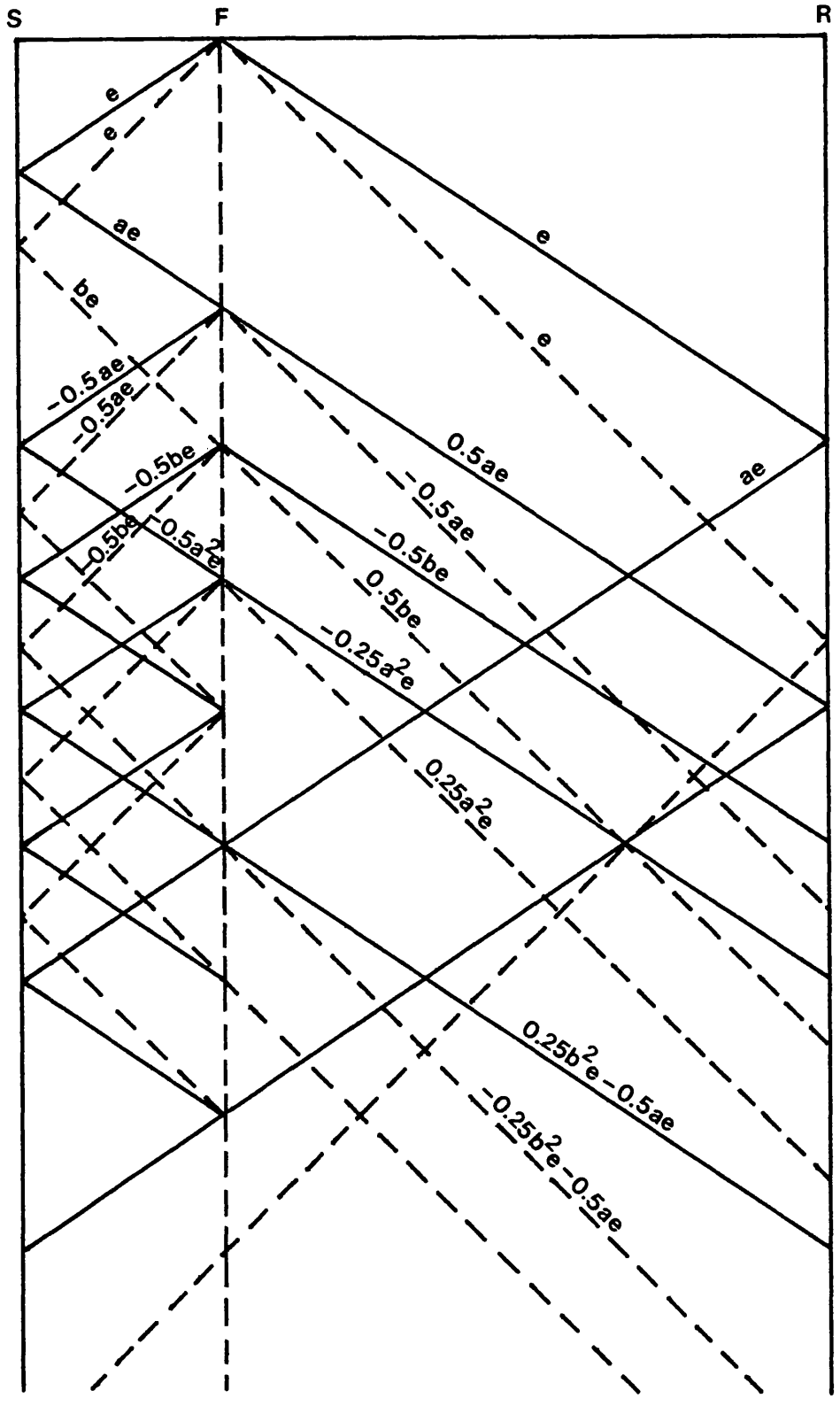

Fig 3.14 Lattice diagram of superimposed voltage surges produced by an a-earth fault, at $x_F = L/4$

Modal reflection coefficients at each end; mode-1 = a; mode-4 = b. Ratio of model wave speeds (mode-1/mode-4 = 2/3. Waves of mode-1 are indicated by dashed lines, and waves of mode-4 by solid lines.

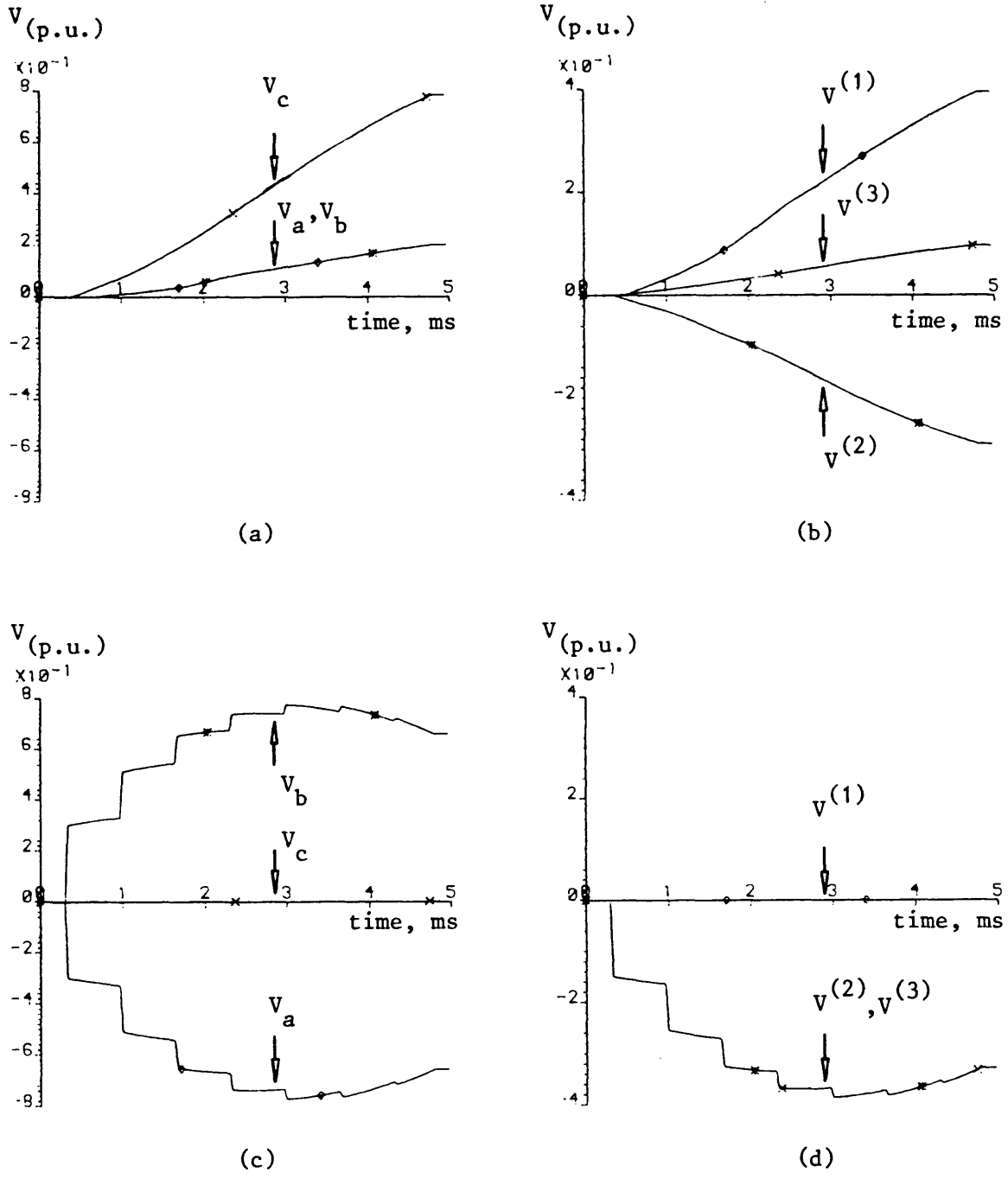

Fig 3.15 Superimposed voltage waveforms at relay location

- for 100km fault distance
- line length = 300km
- R_F = 0.0 ohms; modal reflection coefficients at local and remote ends equal 0.4 and 0.6 respectively.

(a) Phase voltage variations following a "c"-earth fault; inception at zero of prefault "c"-earth voltage.

(b) Modal variations for the same fault conditions as in (a).

(c) Phase voltage variations following "a" to "b" fault; inception at peak of prefault "a" to earth voltage.

(d) Modal voltage variations for the same fault conditions as in (c).

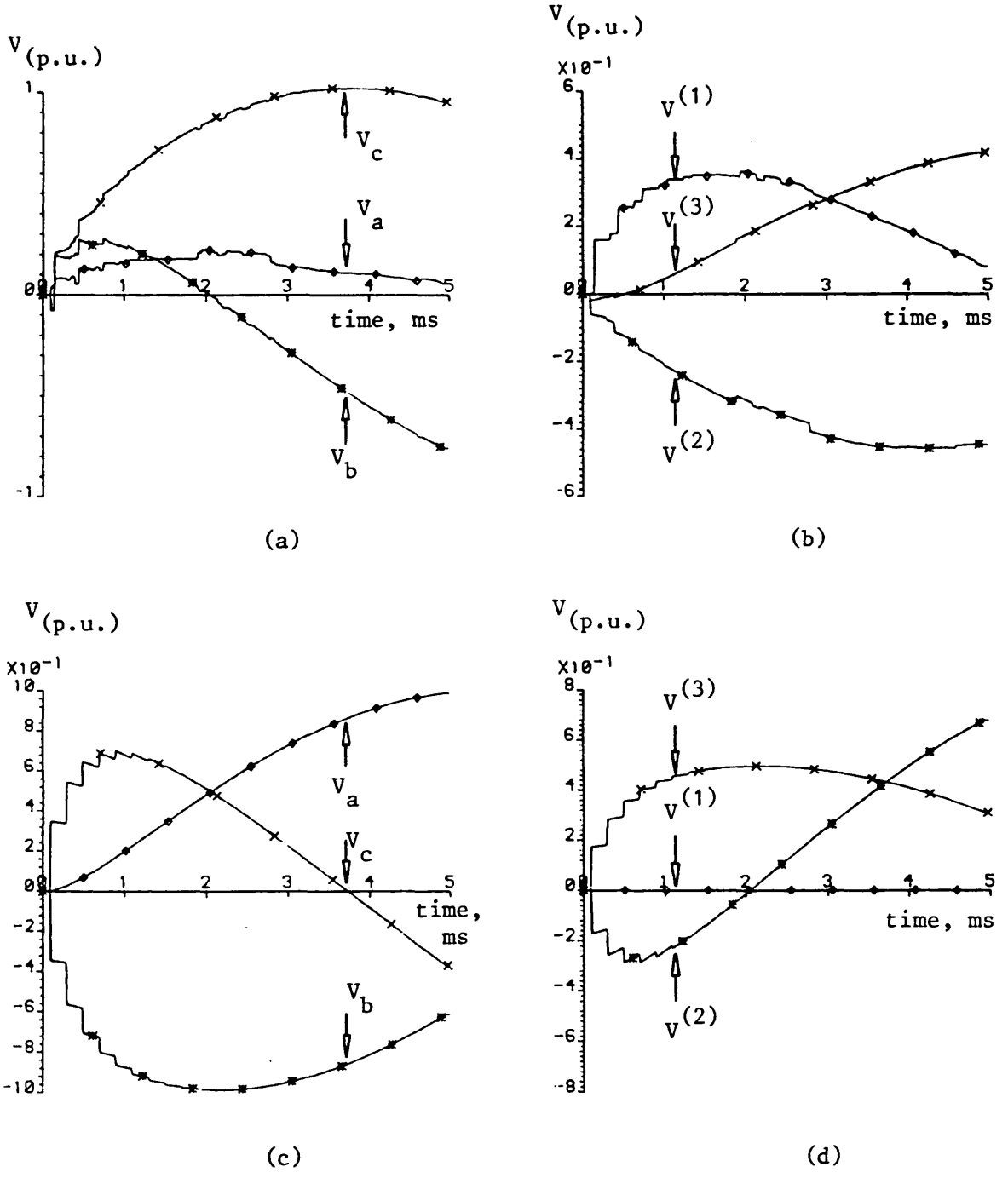

Fig 3.16 Superimposed voltage waveforms at relay location for 100km fault distance

Line length = 300km; R_F = 0.0 ohms; modal reflection coefficients at local and remote ends equal 0.4 and 0.6 respectively.

(a) Phase voltage variations following a "b"-"c"-earth fault; inception at 30° of prefault "a".

(b) Modal variations for the same fault conditions as in (a).

(c) Phase voltage variations following a three phase fault; inception at zero of pre-fault "a"-earth voltage.

(d) Modal voltage variations for the same fault conditions as in (c).

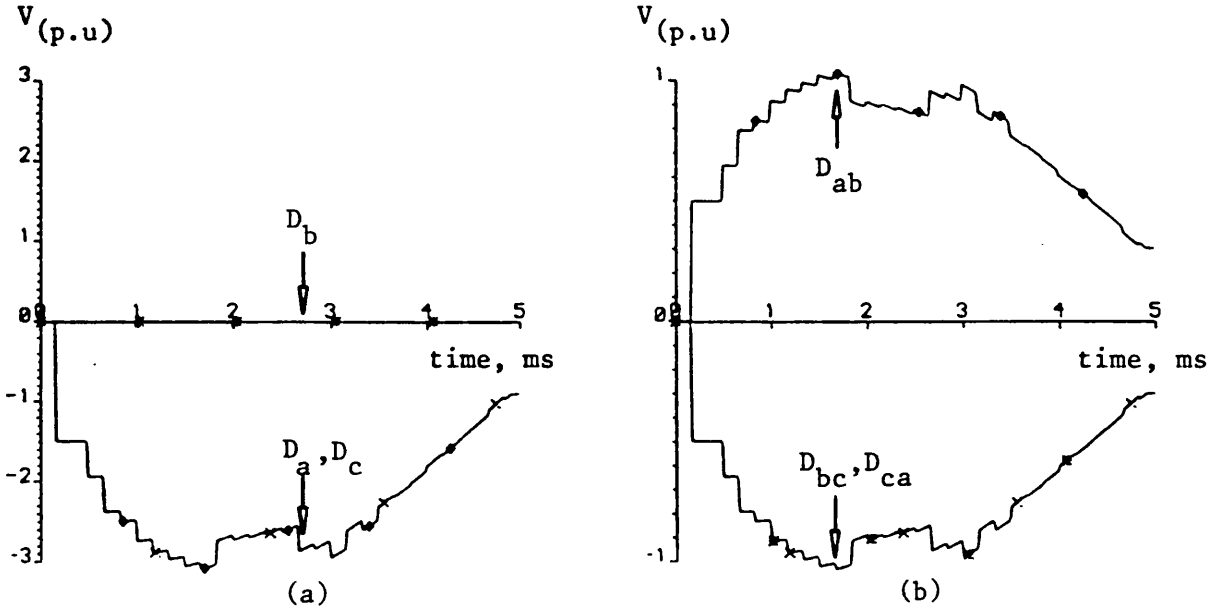

Fig 3.17

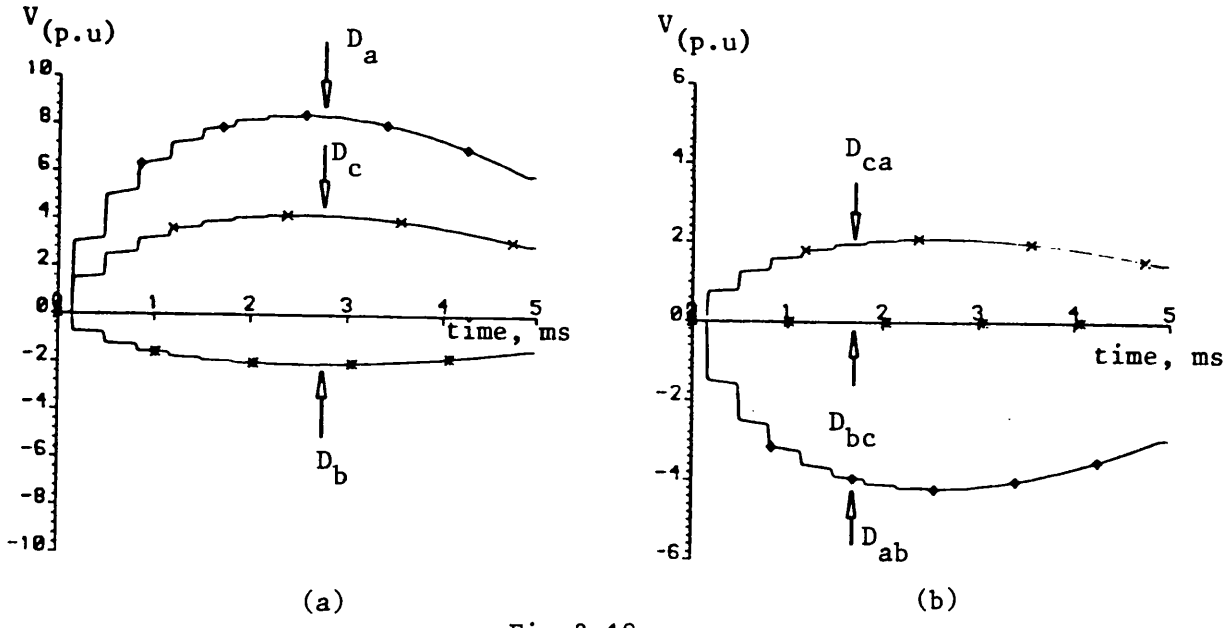

Fig 3.18

Fig 3.17 Discriminant signals for "b"-to earth fault using lattice simulation

- Line length = 300.0km; R_F = 0.0 ohms; X_F = 50 km
- Fault at peak of prefault "b"-earth voltage
- Other conditions are similar to that of Fig 3.15

(a) Responses of phase to earth discriminant signals
(b) Response of pure interphase discriminant signals

Fig 3.18 Discriminant signals for "b"-"c" fault clear of ground using lattice simulation

- Fault conditions are similar to those of Fig 3.17

(a) Response of phase to earth discriminant signals
(b) Response of pure interphase discriminant signals

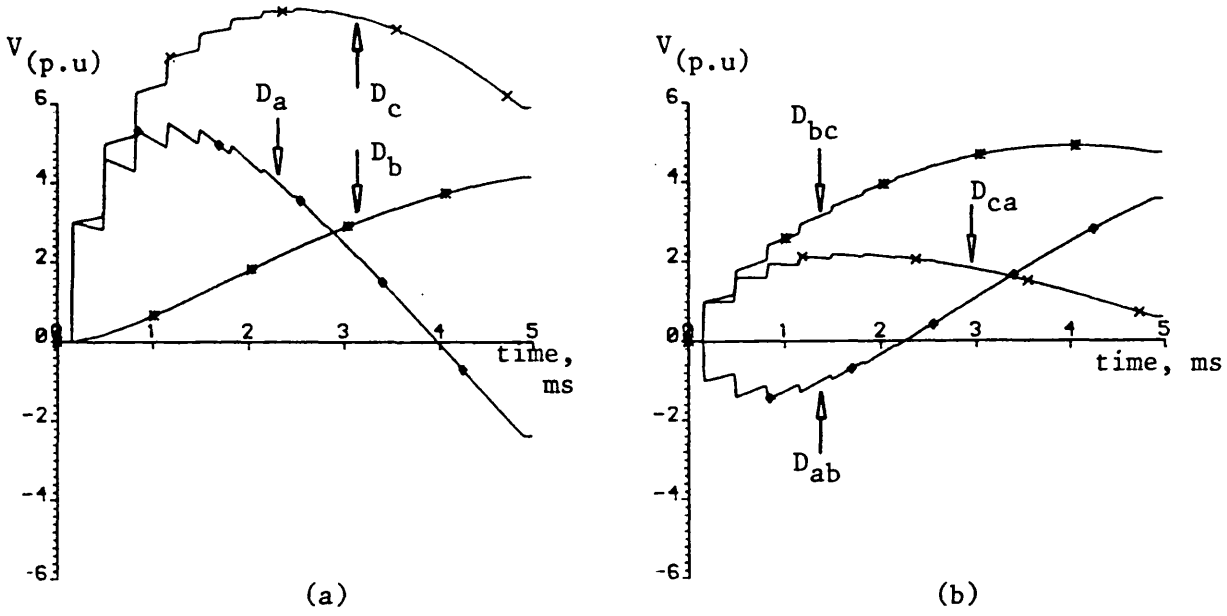

Fig 3.19

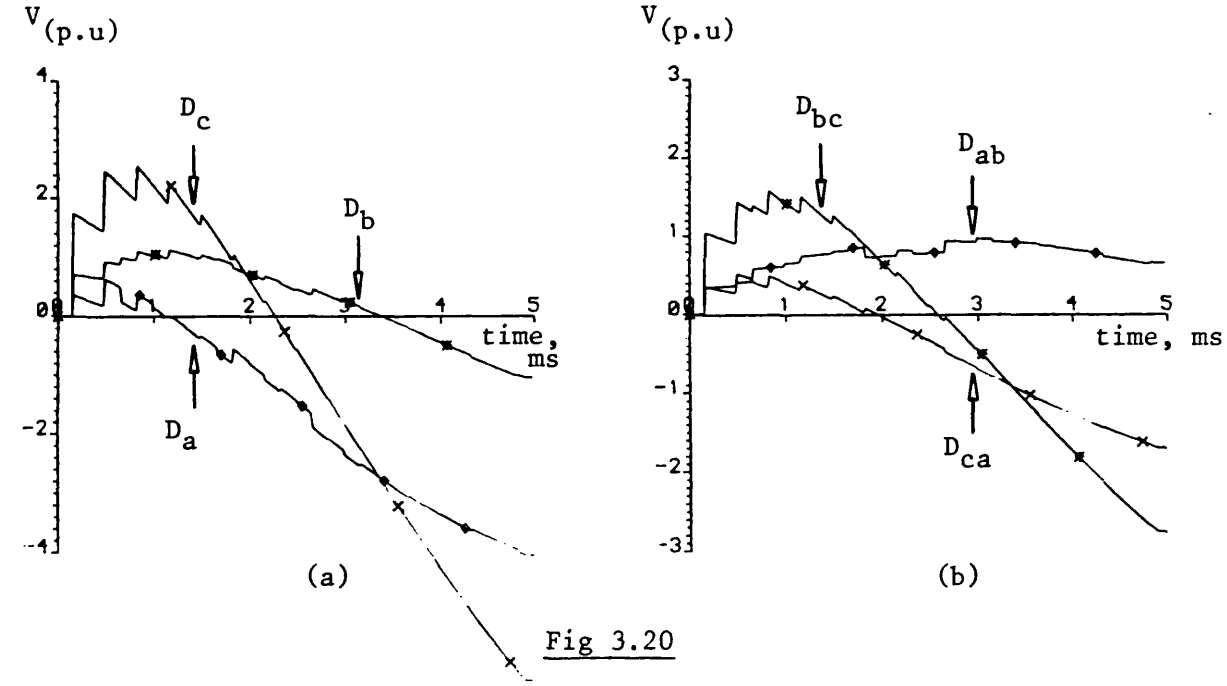

Fig 3.20

Fig 3.19 Discriminant signals for a three phase fault

- X_F = 50km; L = 300km
- Fault at 30° of prefault "a"-earth voltage
- Other fault conditions are similar to those of Fig 3.17

(a) Responses of phase to earth discriminant signals
(b) Responses of pure interphase discriminant signals

Fig 3.20 Discriminant signals during "a"-"b"-earth fault condition

- Fault at zero of prefault "a"-earth voltage
- Other fault conditions are similar to those of Fig 3.19

(a) Responses of phase to earth discriminant signals
(b) Responses of pure interphase discriminant signals

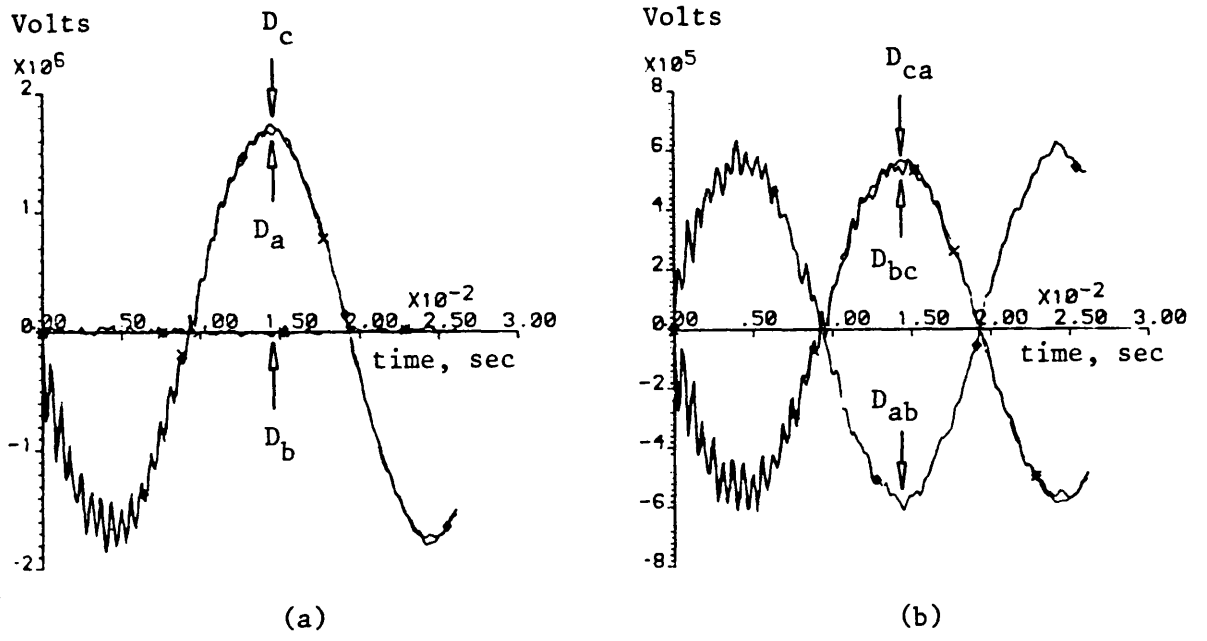

Fig 3.21

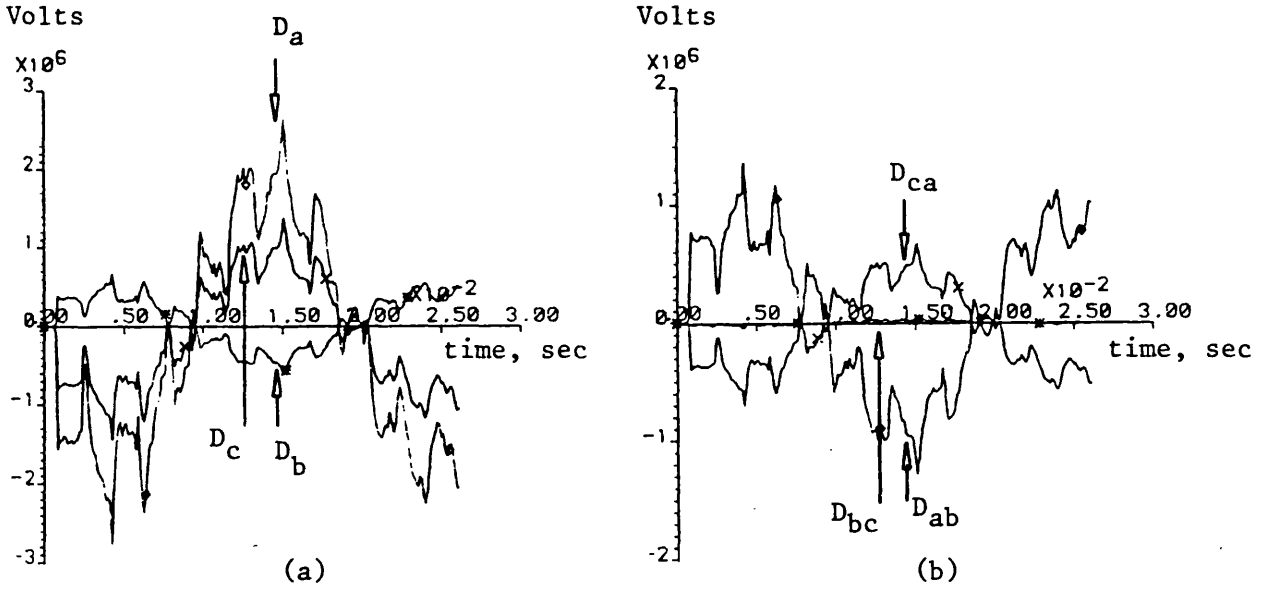

Fig 3.22

Fig 3.21 Discriminant signals obtained during "b" to earth fault condition using digital simulation

- Fault at peak of prefault "b"-earth voltage
- R_F = 0 ohms; X_F = 50km; L = 300km; transposed;
- VS/VR = 1 < 0°; ZSO/ZS1 = 1
- S.E. S.C.1 = 5GVA; R.E. S.C.2 = 5GVA

(a) Responses of phase to earth discriminant signals
(b) Responses of pure interphase discriminant signals

Fig 3.22 Discriminant signals obtained during "b"-"c" fault condition using digital simulation

- Fault at peak of prefault voltage between phases "b" and "c"
- Other conditions are similar to those of Fig 3.21

(a) Responses of phase to earth discriminant signals
(b) Responses of pure interphase discriminant signals

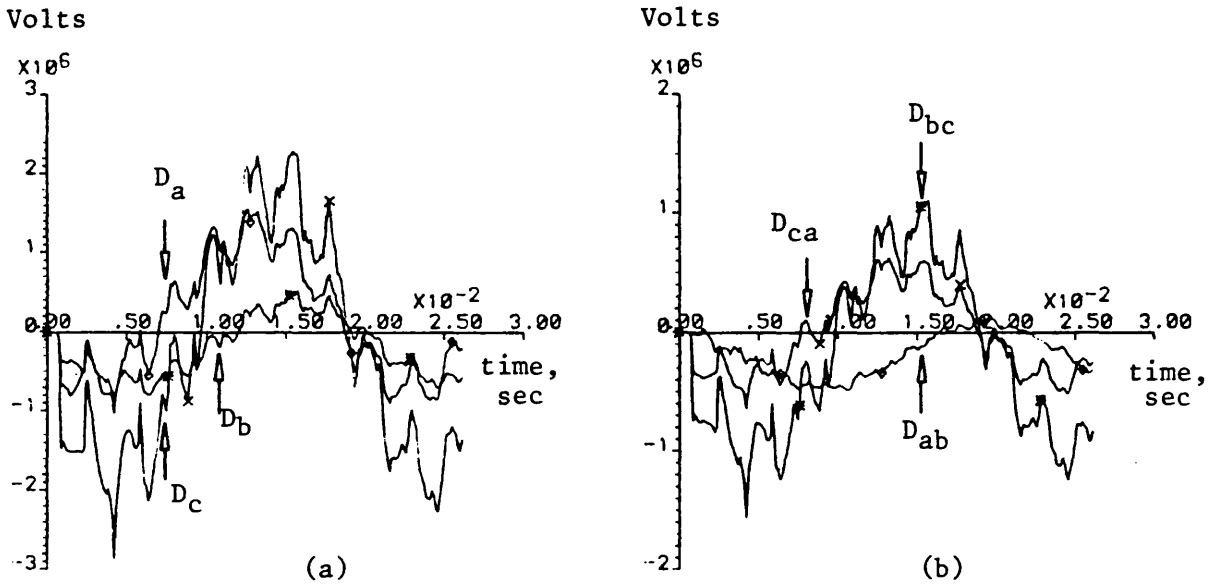

Fig 3.23

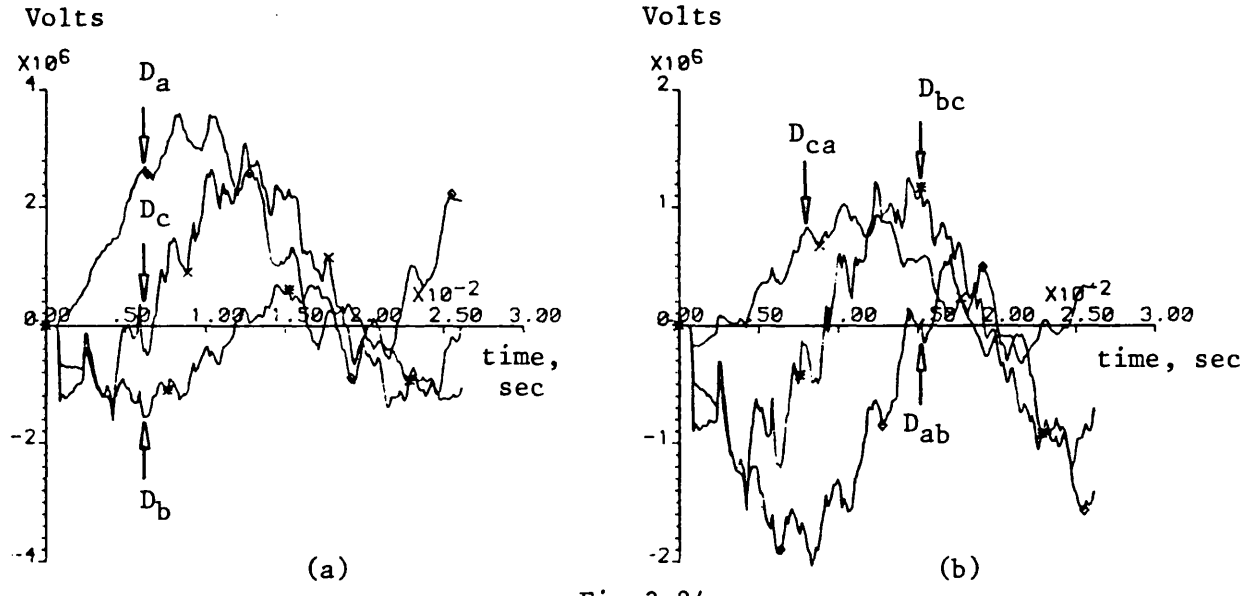

Fig 3.24

Fig 3.23 Discriminant signals obtained during "a"-"b" earth fault using digital simulation

- Fault at peak of prefault voltage between phases "a" and "b"
- Other conditions are similar to those of Fig 3.21

(a) Responses of phase to earth discriminant signals
(b) Responses of pure interphase discriminant signals

Fig 3.24 Discriminant signals obtained during three phase fault condition using digital simulation

- Fault at peak of prefault voltage of "a"-earth voltage
- Other conditions are similar to those of Fig 3.21

(a) Responses of phase to earth discriminant signals
(b) Responses of pure interphase discriminant signals

CHAPTER FOUR

SECONDARY SIMULATION IMPLEMENTATION AND PROCESSING ALGORITHM OF THE NEW PHASE SELECTION TECHNIQUE

The new technique here developed has proven to be satisfactory when applied to primary system data. UHV/EHV protection schemes derive primary system information via transducers, and are thus subjected to transducer errors. Poor transient response of instrument transformers leads to errors in the input signals to the relay and this in turn may affect the operation of the protection scheme. To evaluate the performance of the phase selector, a simulation program has thus been developed to incorporate the effects of CVTs and, as explained in Section 4.1.2, CT modelling was limited to a simple turns ratio.

The design and the performance of current transformers is influenced by a number of factors, particularly the steady state amplitude of the maximum symmetrical short circuit current that, for a given burden, must be faithfully reproduced on the secondary side. The major transient quantity of concern is the exponentially decaying d.c. component of the primary current and its presence is known to be one of the main factors influencing build up of the core flux, which is likely to cause saturation. CT saturation means that incorrect information is fed to the relay at least during part of a cycle. If saturation is caused by the a.c. component of the primary current (steady state saturation), both half cycles will be affected.

However, saturation caused by the d.c. component of the primary current will affect the secondary current on half cycles of one polarity, leaving the halves of opposite polarity almost unaffected.

Besides the risk of ferroresonance, the most troublesome case for relay protection is the transient response of the CVT following large sudden drops in primary voltage. When considering capacitor voltage transformers (CVTs), the transient waveforms generated are dependent upon a number of factors[36]. Two of the more significant factors are the point on wave of fault inception and the nature of the burden applied to the secondary of the CVT.

The foregoing error considerations are normally associated with the performance estimation of distance type protection equipment. Distance and directional comparison schemes operate according to several different measuring principles, and hence are likely to behave differently when errors arise in the measuring quantities because of a poor measuring transformer transient response. A consideration of the new phase selector measuring quantities will therefore enable an estimate to be made of the effect that transducer infidelity has on its overall performance.

The directional wave comparison scheme utilises fundamentally different basic measurands to those of distance protection. The voltage and current signals supplied to the new relay are in fact the quantities superimposed upon the system subsequent to a disturbance. The superimposed component circuit described in Section 4.2.1 is

used to extract the post fault voltage and current information by the suppression of the steady state quantities. An advantage of using superimposed rather than actual voltage variations is that the scheme becomes virtually independent of CVT transient errors, due to the inherent gain (or increase) in signal to noise ratio. (It is technically preferable to provide an accurate voltage measurement whenever possible rather than compensate for CVT errors as in distance protection.) However, since the scheme is not restricted to using a compensated voltage signal as explained, no detrimental effect on the relay operating performance is produced.

The use of superimposed current components in the directional scheme will not, however, alleviate the problem of CT saturation. Also, high speed of operation helps in the prevention of instantaneous saturation. The overall result of using superimposed components is that a higher degree of freedom is possible in optimising the security-dependability aspects of the protection.

4.1 Transducers Simulation

4.1.1 CVT simulation

GEC Measurements have produced a very accurate model of a CVT in order to perform conjunctive testing of relaying equipments. It is the frequency response data provided by this model that is utilised in these particular CAD simulation studies performed. A brief summary of the theory as applied to the CVT simulation is as follows. The impulse response of any system is defined by eqn (4.1).

$$i(t) = 1 / (2.\pi) \int_{-\infty}^{\infty} f(\omega)\, e^{j\omega t}\, d\omega \qquad \ldots (4.1)$$

i(t) is the impulse response of a system having a transfer function $f(\omega)$ in the frequency domain, and this in turn can be defined in terms of a magnitude function $m(\omega)$, and a phase function $p(\omega)$, as described in eqn (4.2).

$$f(\omega) = m(\omega)\, e^{jp(\omega)} \qquad \ldots (4.2)$$

For the CVT model considered, $m(\omega)$ and $p(\omega)$ are shown in Fig 4.1. Function $f(\omega)$ can then be approximated by an equation of the form:

$$f'(\omega) = a_0 + a_1 . \omega + \ldots + a_n.\omega^n \qquad \ldots (4.3)$$

The accuracy of $f'(\omega)$ relative to $f(\omega)$ depends on the number of terms included in the summation. A method described in reference (19) has been used to obtain the impulse response for the CVT considered, the form of which is given by eqn (4.4).

$$i(z) = i_o + i_1.z^{-1} + i_2.z^{-2} + \ldots + i_n.z^{-n} \qquad \ldots (4.4)$$

where $z^{-1} = e^{-j\omega T}$ (the delay operator) and T is the sampling interval. Any primary voltage vp(t) can then be represented by eqn (4.5) and the corresponding secondary voltage at any instant of time tn = nT is shown in eqn (4.6):

$$vp(z) = vp_0 + vp_1.z^{-1} + \ldots + vp_n.z^{-n} \qquad \ldots (4.5)$$

and

$$vs(tn) = \sum_{j=0}^{n} i_j\, vp_k T, \quad \text{where } k = n-j \qquad \ldots (4.6)$$

The simulation studies performed have been taken for a near optimum value of unity power factor burden.

4.1.2 Current transformer simulation

Due to the relatively wide frequency response of CTs, it was decided not to produce a detailed CT simulation covering a wide frequency range in excess of 2kHz. The reason being that any wideband simulation would be effectively swamped by the low pass pre-filters used at the input to the proposed transducer relay. The CT currents may be assumed to be a faithful reproduction of the primary side provided that saturation effects could be avoided, and that the burden to high frequency components is predominantly resistive. The CT is therefore represented by a simple turns ratio.

4.1.3 Analog prefiltering

Prefiltering has been used at the input to new scheme, both for partial noise suppression and for the purpose of balancing the frequency spectra of the voltage and current channels. A second order Butterworth filter characteristic with a cut-off frequency of 2kHz has been developed since the requirement being a minimum of delay to power frequency components. The low pass filter transfer function incorporated in the simulation program is thus of the form:

$$F(s) = \omega_n^2 \; / \; (s^2 + 2.T.\omega_n.s + \omega_n^2) \qquad \ldots (4.7)$$

where $T = 0.707$; $\omega_n = 2.\pi .2000$; $s = j\omega$.

The simulation technique of the prefiltering function is exactly similar in principle to that used for the CVT.

4.2 Simulation of Basic Signal Derivation Circuitry

The block diagram of Fig 4.2 represents the secondary simulation from the primary system data to the input to the superimposed extraction circuits. Primary system data has been computed with a sampling frequency of 8kHz, since a higher sampling rate would be of little practical value because the CVT upper cut off frequency is approximately 600Hz (see Fig 4.1) and the prefilters have a cut off frequency of 2kHz. The maximum speed of operation of the protection scheme is controlled by the sampling rate, which is in turn limited by the hardware processing capability[19].

The practical implementation of the secondary simulation has shown, for the particular equipment used, that the optimum sampling frequency is 4kHz. As stated above, a 2kHz cut off frequency is chosen for the analogue pre-filter which is as high as possible for group delay minimisation, whilst still suppressing any aliasing components due to Nyquist effects.

4.2.1 Superimposed extraction filtering process

The function of the superimposed extraction filter is to extract the steady state component from the total variation of a measurand following a disturbance, in order to obtain the net superimposed quantity.

Essential requirements of superimposed extraction filter:

(1) To reproduce the superimposed quantities for at least a period of time equal to the operating time of the selector.

(2) To have an impulse response duration as short as possible, since this will represent the minimum time before the system can be considered to be de-energised, and the discriminant signals used in the phase selectors can reselect subsequent disturbances.

(3) To provide maximum attenuation of frequency tracking errors generated by normal variations in the system power frequency.

Any extraction filter designed to reject components of a particular frequency, produces a spill output when the input frequency changes by a small amount. Such conditions arise during power swings and changes in load condition. The two types of extraction device considered are as follows:

(a) A full cycle extraction device which employs a 20ms delay and has a frequency transfer function resulting in zero gain at all harmonics of power frequency and at d.c.

(b) A half cycle extraction device employing a 10ms delay with zeros at odd harmonics of power frequency.

From a consideration of harmonic rejection, frequency tracking errors and impulse duration, it has been established that a cascaded combination of the two extraction circuits, referred to as the 10,20 configuration, offers the best compromise[22,23].

4.2.2 Digital filter implementation

In the present work, only the fundamental power frequency component (ω_0) is assumed to exist in the prefault frequency spectrum.

However, postfault relaying quantities contain a large range of frequencies ranging from low frequency exponential components which accompany current waveforms to high frequency components accompanying voltage waveforms. The content of these frequencies in the postfault measurands is mainly dependent upon the fault inception angle, the distance to fault and the configuration of the system considered. Their presence will therefore cause a residual output from the superimposed extraction process that will persist for some time after the impulse duration of 30ms.

Since the main phase selection theory was developed for an assumed de-energised system, a fault occurring within the period where the residual output is of a significant value, might possibly result in incorrect re-selection. In order to cater for such cases, which extend the scheme recycle times, and to reduce the gain of the extraction filter for frequencies up to 50Hz, further filtering after the extraction filter was essential.

(a) Differencing stages

The basic extraction filter cascaded with two differencing stages (for the purpose of low frequency attenuation) each having a delay of 5ms was found to be adequate for the application considered. The impulse response of the filter was then extended to 40ms.

(b) Integral stages

In order to reproduce a similar recovery time for voltage maximum faults, some further modification to the filter function

obtained for voltage zero faults was necessary. The latter was cascaded with two integral stages, each having a moving average of 3.0ms to give adequate performance, for the system studied. The complete schematic representation of the digital filter, together with the superimposed extraction filtering process, is shown in Fig 4.3.

4.3 Control of Source Capacity Coverage

The range of source capacities for which satisfactory fault clearance must be obtained in practice is extremely large. Therefore, the main directional comparison relay was designed so that the range of source coverage can be optimally adjusted in accordance with specific applications. The phase selection scheme was designed to make use of the same modal signals employed by the directional relay, which have the form:

$$S^{(2)}(t) = K\, V_f{}^{(2)}(t) - R0^{(2)}\, I_f{}^{(2)}(t)$$
$$S^{(3)}(t) = K\, V_f{}^{(3)}(t) - R0^{(2)}\, I_f{}^{(3)}(t) \qquad \ldots (4.8)$$

The value of the constant, K, controls the source capacity coverage. In reference (19) it was found that with K = 5 the source capacity coverage extends over the range 1.8 - 35 GVA. If K is reduced below 5, coverage extends below 1.8 GVA, whereas increasing K will provide practical coverage above 35 GVA.

By introducing the source coverage factor, K, into the modal signals, the discriminant signals developed for phase to earth

discrimination remains unchanged. This is because for these particular types of fault, the ratio of mode 2 to mode 3 quantities is a scalar constant, which remains so for all time after the fault, as explained in Chapter 3.

4.4 Determination of Setting Limits

The phase selector hardware incorporates several stages and associated gain constants as shown in the block diagram of Fig 4.4. In many cases, some of these constants are application dependent, but others are merely a function of system voltage and transducer ratios, these being common to a whole range of systems. Appendix A2 outlines the setting procedure for determining each intermediate gain and a brief description of the effects of each stage is given below.

(i) Voltage interface constant, Kv

The constant Kv is used to scale down the input voltage level from 63.5 volts r.m.s. to the maximum internal voltage of 10 volts. In order to maintain the voltage channel within 10 volts peak to peak, it was necessary to compensate for a maximum fault induced overvoltage of 2 p.u. of the peak value, hence:

$$Kv = 10 / (2 \times \sqrt{2} \times 63.5) = 0.0557 \qquad \ldots (4.9)$$

(ii) Current interface constant, Ki

The dynamic range of input current levels produced under various fault conditions is very large. A current interface gain calculated upon the maximum value would therefore render the measurement of small superimposed current components very difficult. In order to maximise

the scheme sensitivity for in-zone faults and to prevent the current channel of clipping for out-of-zone disturbances (for improved recovery performance), a value of I_c is calculated as the maximum possible out of zone fault current level. Then, allowing for a complete offset of fault current as in voltage zero point on wave faults, Ki is found from:

$$Ki = 10 / (2 \times \sqrt{2} \times I_c) \quad \ldots (4.10)$$

(iii) Phase to modal transformation constant, Km

The aerial mode voltage and current are of the form of eqn (4.11):

$$\begin{aligned} Vm2 &= (V_a/2 - V_c/2) \cdot Km2 \\ Vm3 &= (V_a/6 - V_b/3 + V_c/6) \cdot Km3 \end{aligned} \quad \ldots (4.11)$$

The maximum values of Vm2 and Vm3 occur during balanced three phase fault conditions and Km2 and Km3 can be chosen such that the maximum value of both Vm2 and Vm3 are maintained at 10 volts after the transformation. Hence, Km2 and Km3 will be equal to 1.155 and Km3 = 2.0.

Under single phase to earth fault conditions, the selector relies for its operation upon a fixed ratio of mode 2 to mode 3 voltage and current. The effect of scaling the modal quantities will therefore unbalance this aerial mode relationship. To overcome this problem, the mode 2 and 3 signals are scaled by the same constant factor which, to avoid the maximum value of either signal exceeding the maximum value of 10 volts, is taken as 1.155. Hence,

$$Km = Km2 = Km3 = 1.155$$

(iv) RO adjustment constant, Kv2

The secondary aerial mode surge impedance, ROsec, is calculated by using the step down ratio of both CVT and CT, as given by:

$$ROsec = (110/500) \times (1200) \times RO\ primary \quad \ldots (4.12)$$

The constant gain Kv2 is introduced to facilitate fine adjustment of the ROsec setting and is dependent upon the constant clipping current level, Ki. The correct signal scaling, whilst maintaining strong signal levels throughout the voltage channel filter for the purpose of minimising noise, is applied by considering the equality:

$$Kv \cdot Kv2 / 2^n \cdot Ki = 1 / RO \quad \ldots (4.13)$$

The above equation can be rearranged to give the remaining voltage gain, Kv2, in the form:

$$Kv2 / 2^n = Ki / RO / Kv \quad \ldots (4.14)$$

The term 2^n represents an integer power of 2 which simplifies division in the digital process. The correct choice of n is such that the gain Kv2 lies within a limited range $1.0 < Kv2 > 0.5$, so that the errors within the analogue to digital conversion and digital filtering remain small.

(v) Analogue to digital conversion constant, Kc

This gain is representative of the analogue to digital conversion, whereby a signal voltage of +10 volts is converted to a digital two's complement number of 2048. For this purpose, a 12 bit ADC unit was modelled resulting in a signal of ±10 being represented by 4096 quantisation levels.

Hence, $Kc = 2048 / 10$ . . . (4.15)

(vi) Digital filter gain, Kf

This gain is a frequency dependent parameter. However, its magnitude at the power frequency is important because the prefault and postfault signal waveforms are dominated by power frequency components, which in turn determine the peak signal levels achieved within, as well as at the end of the digital filter. From Appendix A2 the digital filter has an overall 50Hz gain of 95.6 and an intermediate gain of 47.8 at the output of the integration stages, making it necessary to scale the signals throughout the filter to avoid overflow. A gain reduction of 1/8 was found to be most suitable, since the digital processing is performed by a 16 bit processor. The gain Kf is then given by:

$$Kf = 95.6 / 8 = 11.95 \quad \ldots (4.16)$$

The scaling down of the signals causes an increase in the quantisation noise in the digital filter which can be reduced by scaling down the signal in two stages, using a factor of 1/4 and 1/2 at the output of the integral stages respectively.

(vii) Digital gain for phase selector

The final mixing of the signals, S_{2sm2} and S_{2sm3} can result in digital overflow occurring within the microprocessor, and to overcome this problem a gain reduction, dependent upon the type of tripping scheme used, is introduced. For the single phase tripping scheme shown in Fig 4.4, a gain reduction of 4 is necessary.

4.5 Formation of Discriminant Signals to Provide Single Phase Tripping

The previous sections describe the hardware employed in the prototype equipment, the components and gains of which are represented by the block diagram of Fig 4.4, which also includes the phase selector. Both modal signals S_{2sm2} and S_{2sm3} are fed into the selector circuitry and these are combined together to give the single phase to earth discriminant signals $D_{a,b,c}$.

4.5.1 Criteria of the decision process

The discriminant signals D_a, D_b and D_c are fed into a decision logic equipment which will determine, within a short period of time consistent with UHS requirements, whether or not the fault is of the single phase to earth type. Further logic circuitry then initiates the appropriate tripping signals in accordance with the type of fault involved.

When a single phase to earth fault occurs, it is necessary to adjust a threshold level such that only the faulted phase discriminant signal lies below that level, in order to retain correct discrimination. It will be recalled from Chapter 3 that under the assumption of an ideally transposed lossless line, the discriminant signal of the faulted phase will measure zero, since the mutual coupling between the sound phases is identical. However, in practice, the faulted phase discriminant signal does not settle to zero but fluctuates around it, and can be considered as noise input to the selector.

The threshold level chosen is a compromise between speed of operation and security. A very low level would increase the sensitivity, and hence the speed of the phase selector, but this obviously increases the possibility of noise components exceeding the threshold, leading possibly to incorrect discrimination.

Some other unwanted components which can be considered as noise input to the selector include frequency tracking errors associated with the superimposed signal extraction process, general system noise and noise introduced into the signals from the relay hardware. Computer studies have been employed to optimise the minimum threshold level setting that is always greater than the total magnitude of the expected noise components. The result is that the best possible security and speed of operation of the phase selector is achieved. The block diagram of the full decision process is shown in Fig 4.5.

The processing of signals D_a, D_b and D_c is identical therefore with reference to the simplified diagram of Fig 4.6; only that for D_a will therefore be described. An event is defined to be when the modulus of the discriminant signal D_a exceeds the preset minimum threshold level. The event counter associated with the "a"-phase discriminant signal is incremented in steps of one after each event, up to a maximum of 25. A memory action is provided by a shift register, in which the previous five values of the event counter are stored. In the absence of a successive event, the status of the register provides the criteria for decrementing or holding the event counter output.

Under certain fault conditions where the discriminant signals are of the same order as the threshold level, or in situations of signal corruption due to noise, a delayed counter decrement is used. For the latter case, a decrement action is vital for maintaining security and correct discrimination for subsequent disturbances. An immediate decrement of the event counter would ultimately decrease the speed of operation, but the knowledge of several previous counter values permits a delay of the decrement rate. Extensive CAD studies have proven that a decrement delay of 5 samples provides the optimum balance between the selector speed and security of operation. Fig 4.7 and the accompanying Table (4.1) provide a better understanding of the operation of the event counter and the associated register.

The digital phase selector event counters provide fault information at discrete intervals of time and any final decision must be based upon a consecutive number of identical fault indications, in order to improve security. The flow diagram of Fig 4.8 describes the operation of a common decision counter which co-ordinates the action of the three event counters. The common decision counter is initiated when any of the event counters reaches a decisive value and is used to delay the final selection by four samples. After reaching a count of four (which is an optimised value gained from experience), the common decision counter then allows the phase selector to make a decision based on the states of the three individual event counters.

The three discriminant signals exceed the present minimum threshold level almost simultaneously for all types of fault except for

double phase to earth and three phase faults. The reason is that the discriminant signals in such cases are largely influenced by the time at which the fault has been initiated. The worst condition encountered is when two of the discriminant signals exceed the threshold almost simultaneously, whilst the third remains below the threshold for some time and then exceeds it. In order to determine this maximum delay time, a large number of fault type simulations were necessary to determine the optimum number of samples required to avoid wrong decisions being rendered. In this respect, it was found that adequate performance is achieved if the decision is held until 4 samples elapse after the decisive count of 4 is first reached. Furthermore, a decision is held if each of the individual event counters does not satisfy the condition of having a value greater than 5 or less than 2, and further individual events are processed until such a situation is met. The output from the selector is either high or low if the event counter associated with that output has a count greater than or equal to 5 or less than 2 respectively. It will be shown later in this section that the selector is designed to always give a three phase tripping indication (fail safe mode), therefore the delayed action mentioned above will not introduce any overall delay in the scheme operating time.

If a fixed threshold level is considered, the reset of the counter after an initial decision being rendered, would restart the initialisation process, because the discriminant signals are still valid for the impulse duration time of the digital filters. In addition, any low frequency components present in the discriminant

signals, which are only partially attenuated by the digital filter, may also cause the counting process to recommence. In order to overcome these problems, a variable threshold level based upon the magnitude sum of the three discriminant signals, was considered. A slight drawback of using a sum of all three signals is that under certain evolving fault conditions, the second fault remains undetected, if it occurs during the insensitive period of the selector. Three variable threshold levels were therefore implemented, each monitoring the discriminant signal of the corresponding phase, which improves the selecting and re-selecting performance of the scheme.

The effect of utilising a variable threshold level is that the selector is desensitised during the initial detection period, which could result in a reduced speed of operation or at worst no fault detection at all. By introducing a delay into the variable level algorithm, the period of maximum selector sensitivity can be increased to improve phase discrimination. However, this extra delay directly increases the minimum period for which the selector is desensitised, following an initial disturbance.

The foregoing requires the use of 3 dynamic threshold levels as functions of time $L_a(t)$, $L_b(t)$ and $L_c(t)$, each monitoring their corresponding discriminant signal. The averaging algorithm developed for calculating these dynamic levels is then:

$$L_{a,b,c}(t) = 1/N \sum_{m=32}^{n=72} [D_{a,b,c}(n-m)] \qquad \ldots (4.17)$$

The effect of each variable level is to produce a delayed summation over a window of information of 10ms, which helps in reducing the rate of rise of L(t) in the initial fault inception period whilst maintaining maximum selector sensitivity and providing a smooth average for components around the fundamental frequency. The delay of the moving average window, together with the window width, dictates the time taken after the impulse duration time of the filter for the full sensitivity to be regained following a disturbance. In order to prevent the immediate increase of the threshold levels $L_{a,b,c}(t)$ with $D_{a,b,c}(t)$ respectively, the averaging window is delayed by 8ms, which in turn enables selection to be accomplished for all point on wave with the preset fixed minimum threshold level being maintained throughout the comparison period.

The discriminant signals are only available for comparison during the impulse response time of the digital filters. Once the selector has made an initial decision, the trip outputs are latched until all of the dynamic thresholds have returned to their minimum levels. During this latched period, the selector decision can only be changed for one particular fault condition, that being a single phase to earth fault evolving into any other type of fault. For this particular case, the event counter of the faulted phase is tracked to determine whether it exceeds the decisive count of 10. If so, the selector decision can then be changed to give a three phase trip, following which selector lock-out takes place.

4.5.2 Tripping logic implementation using tabulation techniques

After the phase selector has reached a decision, the outputs are fed into a trip logic circuitry which initiates appropriate signals compatible with the required single pole auto reclosure. The selector operations, depending upon the nature of the fault, are summarised as follows:

(1) Temporary single phase to ground: The main relay (detector) will be prevented by the phase selector. Only the pole involving the faulted phase is tripped and reclosed.

(2) Permanent single phase to ground: Single pole tripping is the same as above, then three pole tripping following unsuccessful single pole reclosing.

(3) Single phase to ground followed by another fault while one pole is opened. Three pole tripping should be issued.

(4) Three pole tripping is initialised following other than single line to ground faults.

The trip logic circuitry of the new selector is shown in Fig 4.9, with the accompanying truth table describing the various outputs for all possible combinations of input signals D_a, D_b and D_c. This circuit can then be successfully integrated with further scheme logic to enable the selector to satisfy the four above operation requirements.

The overall trip decition (T) from the main relay controls any final tripping from the selector. However, the selector is used to

override the decision in the case of single phase to earth faults, whereby only one tripping signal is given. The selector must be fail safe for cases where the discriminant signals $D_{a,b,c}$ are not related and produce input patterns. The truth table shows that for any faults other than single phase to earth and for any other arbitrary input conditions, the trip logic circuitry of the selector initiates three phase tripping. In the case of unrelated input conditions and when each discriminant signal is zero due to an internal malfunction, the selector has a fail safe mode of operation to improve the security of the scheme. This permits three phase tripping to be initiated, depending upon the main scheme decision alone. The selector cannot differentiate between in-zone and out of zone disturbances and any selector tripping for out of zone faults is inhibited by the main scheme.

The performance of the decision process for a "b" to earth fault is shown in Fig 4.10, in which the time origin is the time of fault inception. Fig 4.10 shows a delay existing due to wave propagation of 0.1666ms after which the counters will operate according to the fault type. It will be recalled from the previous section that any event counter reaching a decisive count of four will enable a common decision counter, which in turn prevents a decision being made until further samples have been processed. This delay after the arrival of the measurands, can be seen from Fig 4.10 and is due to the finite time required for both counters to render the decision, which will be latched until the fault is cleared. Fig 4.10 represents the trip output from the logic circuitry described in Fig 4.9. The final trip decision (T_{Fa}, T_{Fb} and T_{Fc}) is controlled by the main directional

comparison scheme, and only if the fault is inside the protected zone will tripping actually be initiated (see Fig 4.9).

Chapter 8 deals in more detail with the complete auto-reclosure scheme.

4.6 Formation of Discriminant Signals for Particular Segregated Scheme Application

The formulation of the discriminant signals to include the selection of double phase clear of ground faults is described in Chapter 3. A further three interphase discriminants are required and the signal mixing process is shown in the block diagram of Fig 4.11. It is seen that the new set of discriminant signals is divided by a factor of 2 to avoid overflow problems.

The decision criteria for the selection of double phase clear of ground faults is exactly the same as for the single phase to earth case. The segregated scheme merely requires more complex tripping logic circuitry to provide single phase tripping, as shown in Fig 4.12.

For the particular case of an "a"-"b" fault, the discriminant signals shown in Fig 4.13 verify the foregoing algorithm, in that only the discriminant signal concerned with phases "a" and "b", D_{ab}, remains low, whilst all others exceed the threshold level.

The individual event counters then indicate that the fault involves the "a" and "b" phases only. After the 4 sample delay associated with the common decision counter the six event counter states are processed by the tripping logic mentioned above. As seen in Fig 4.14, the overall scheme decision is that the "a"-phase only should be tripped.

Alternative tripping logic could be implemented to provide two pole tripping, ie. both "a" and "b" phases for the above case, depending upon the secondary arc extinction arrangements employed.

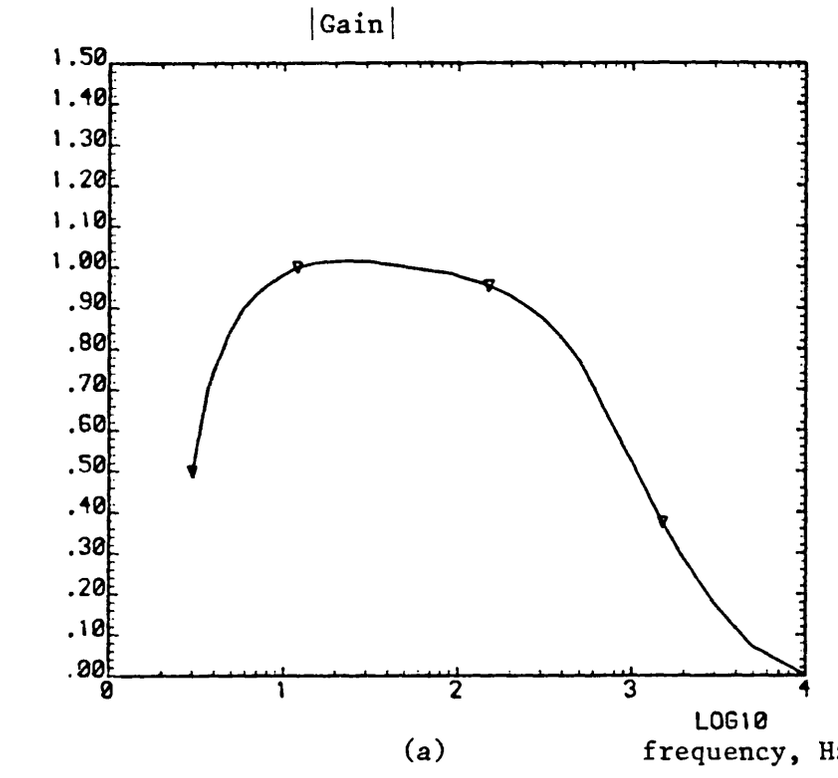

(a)

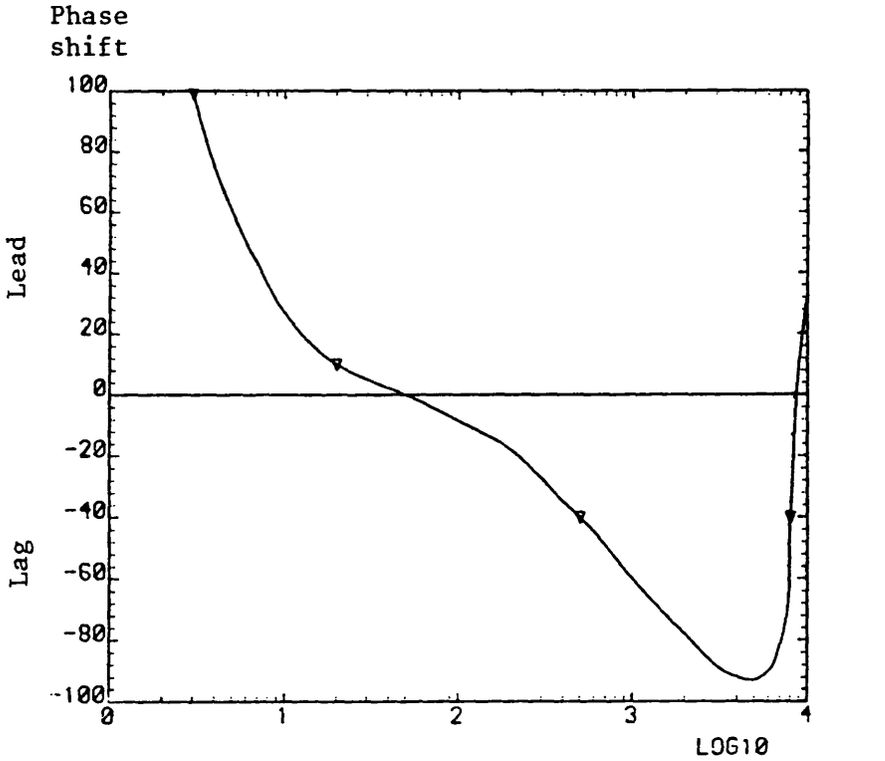

(b)

Figure 4.1 CVT model frequency response

(a) Magnitude

(b) Phase

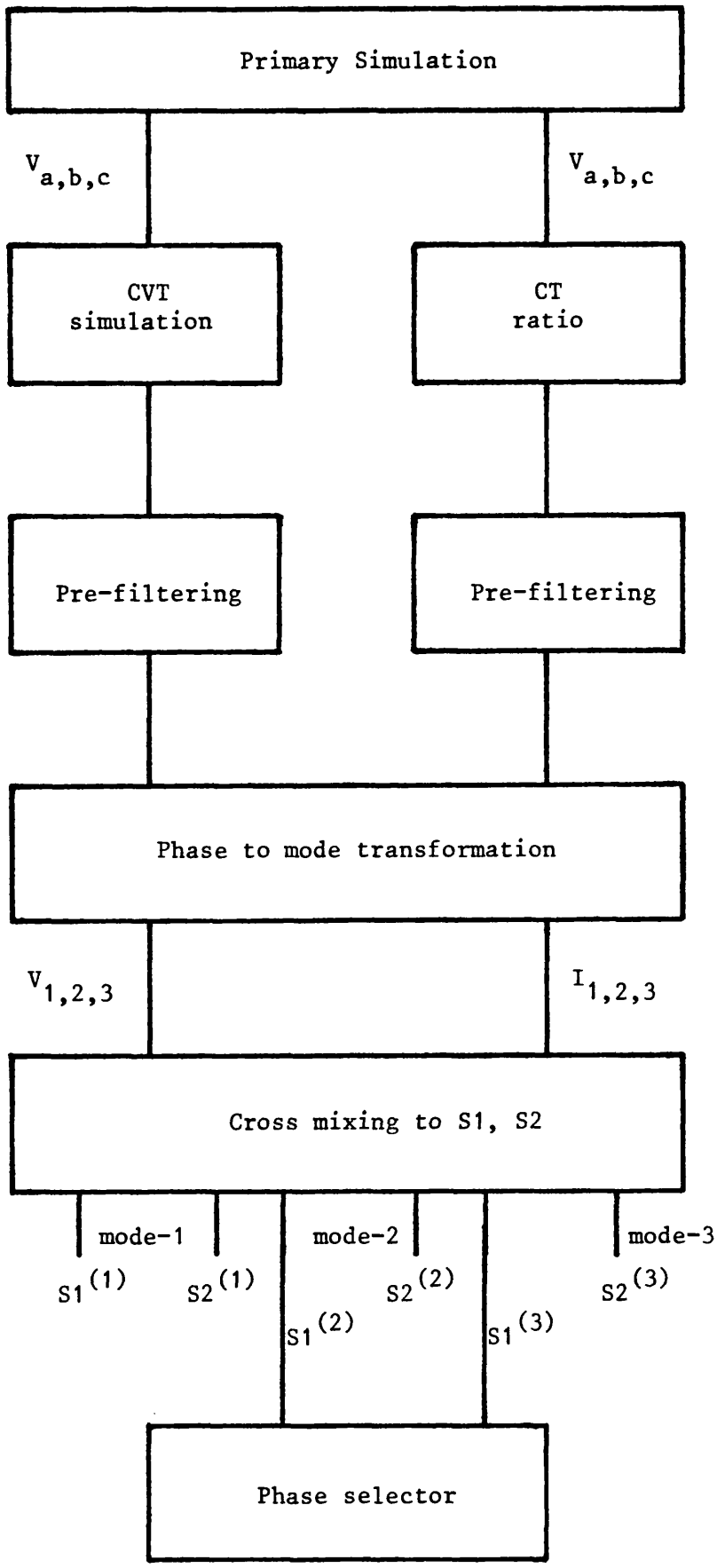

Figure 4.2 Secondary simulation schematic diagram

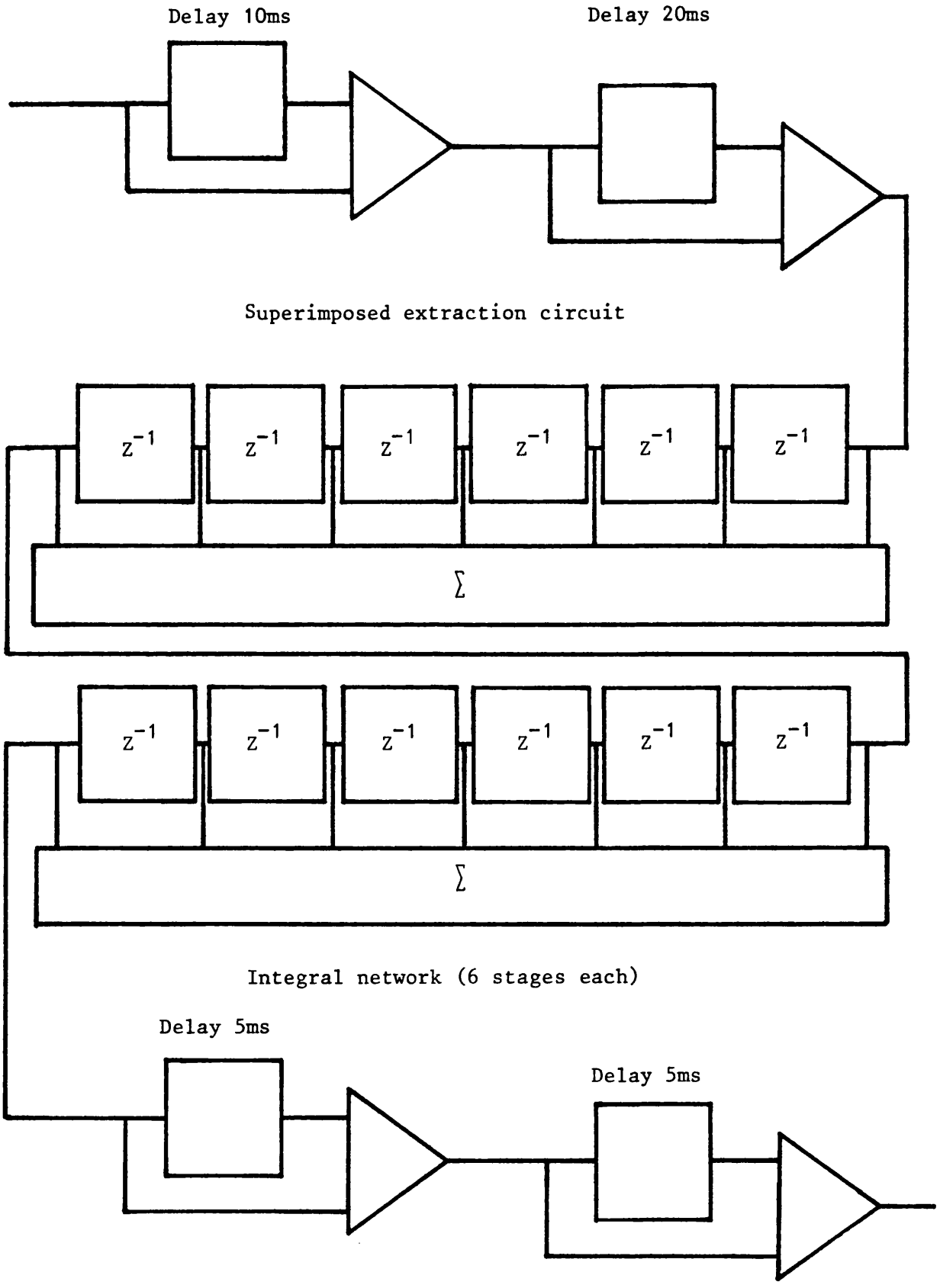

Figure 4.3 Representation of superimposed component digital filter

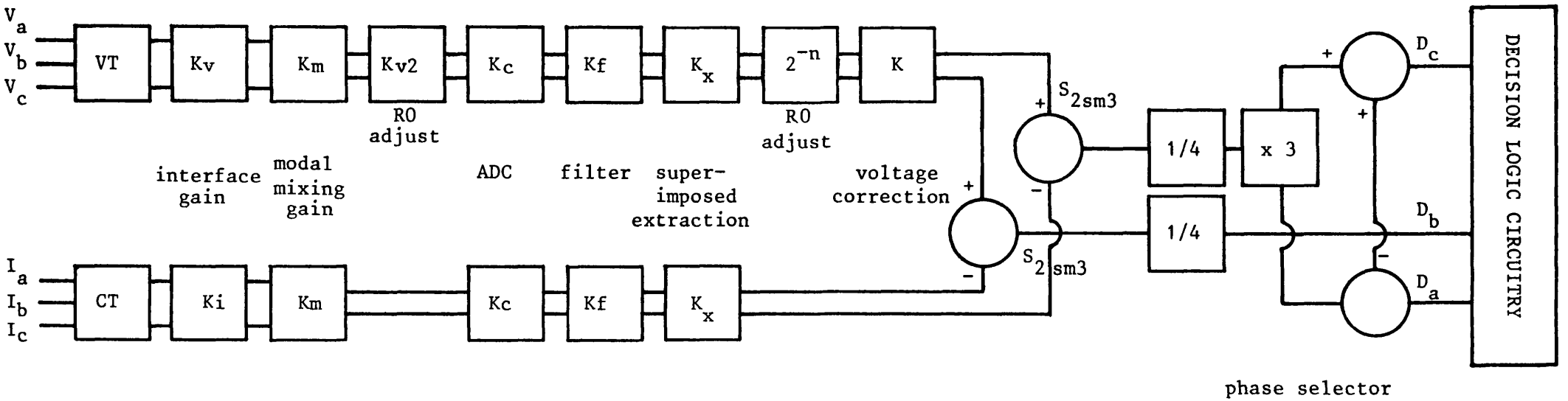

Fig 4.4 Processing Block Diagram

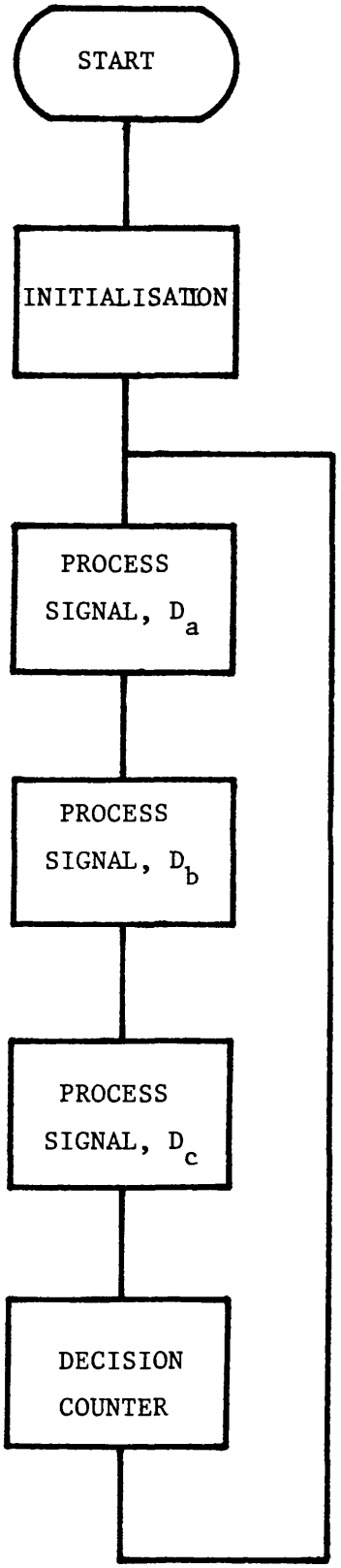

Fig 4.5 Block Diagram of Decision Process

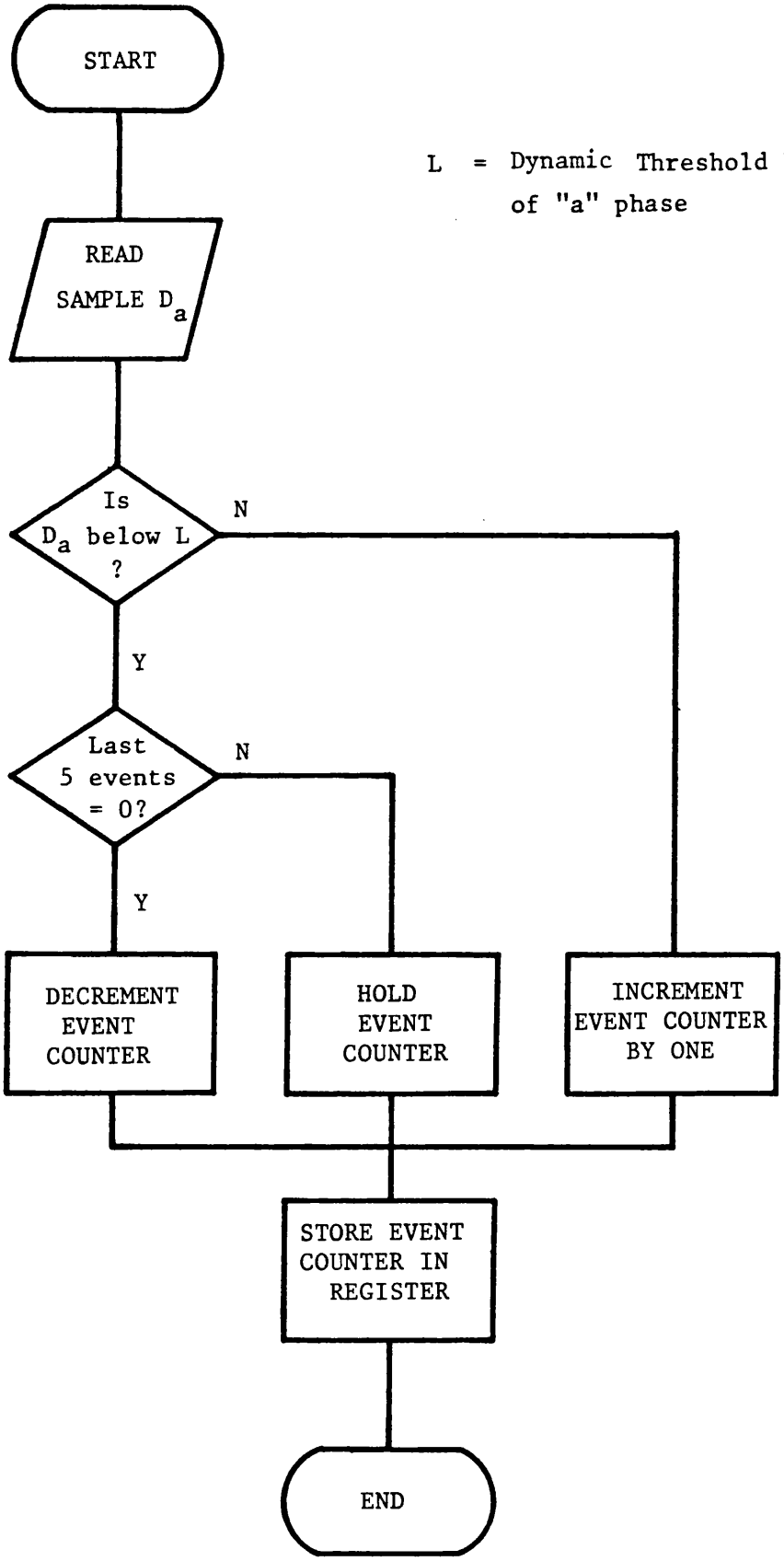

Fig 4.6 Flow Diagram of Processing of D_a

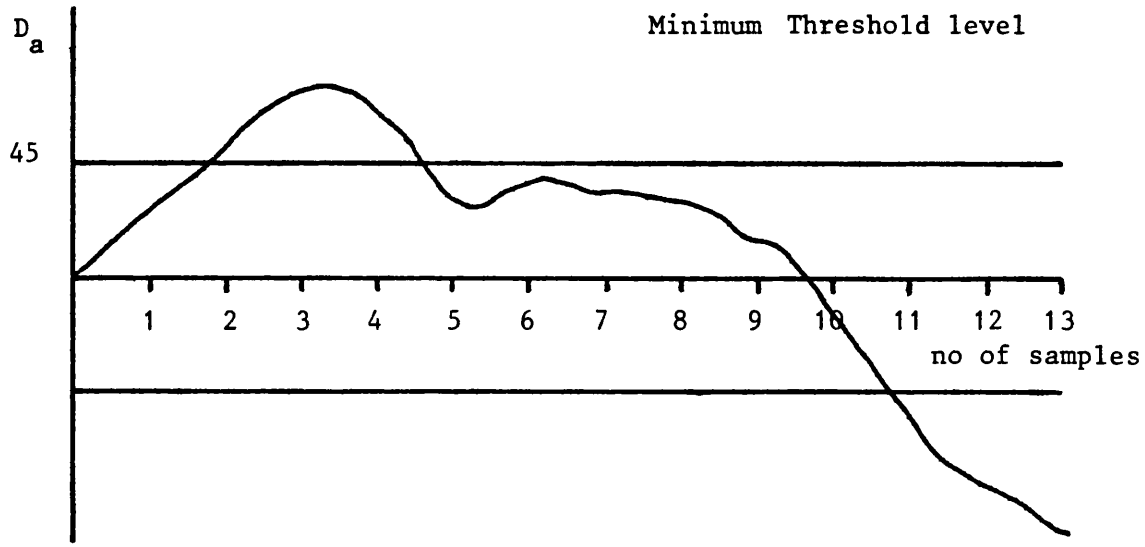

Fig 4.7 Initial variation of discriminant signal D_a

Sample No	Signal Level relative to threshold	Register Status		Counter	
		Before	After	Before	After
1	Below	00000	00000	0	0
2	Above	00000	00001	0	1
3	Above	00001	00011	1	2
4	Above	00011	00111	2	3
5	Below	00111	01110	3	3
6	Below	01110	11100	3	3
7	Below	11100	11000	3	3
8	Below	11000	10000	3	3
9	Below	10000	00000	3	3
10	Below	00000	00000	3	2
11	Above	00000	00001	2	3
12	Above	00001	00011	3	4

Table 4.1 Operation of event counter and associated register

- EC_a, EC_b, EC_c : Event counters for phases a, b and c
- A, B, C : Decision outputs for phases a, b and c
- CDC : Common Decision Counter

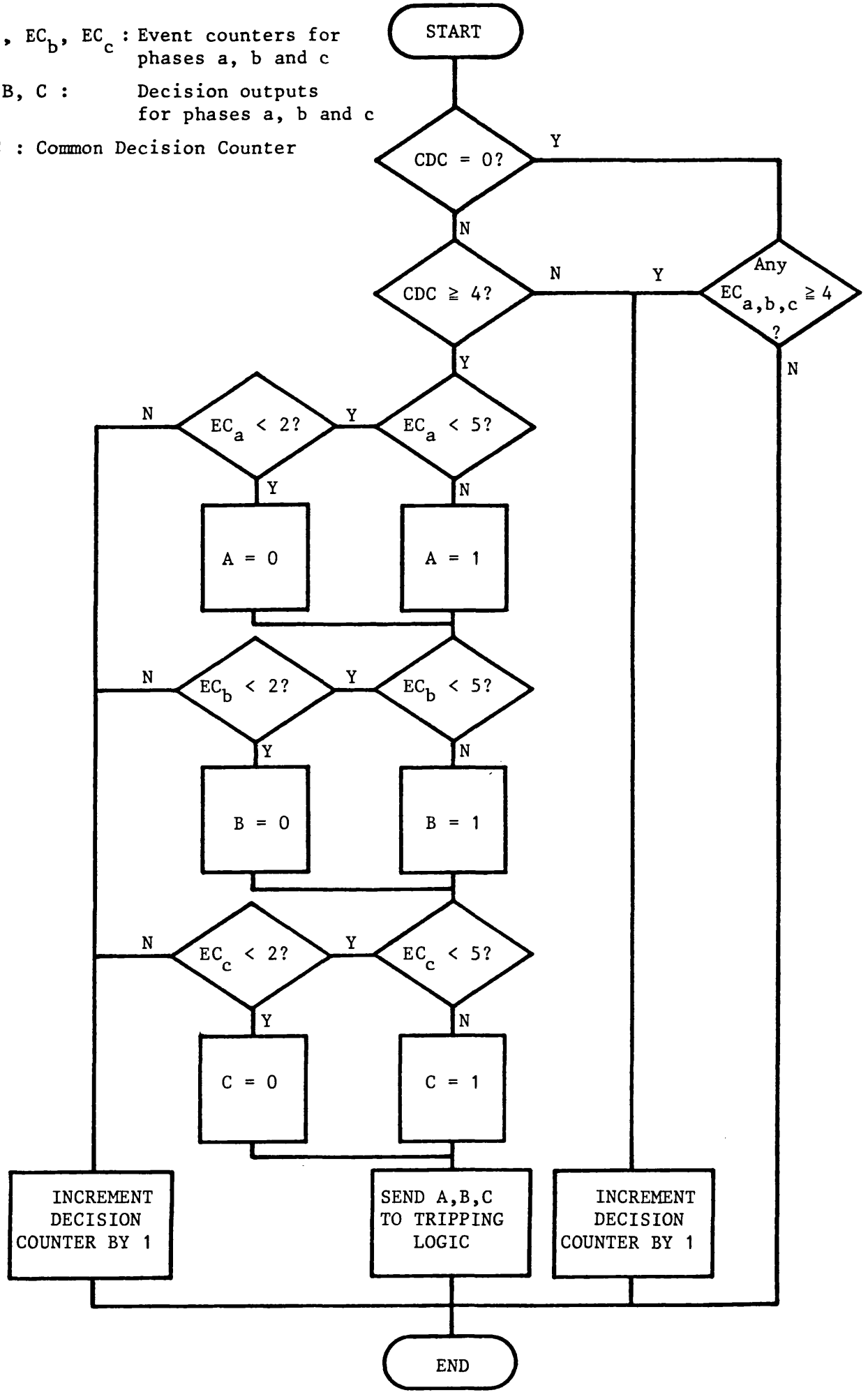

Fig 4.8 Flow diagram of decision counter

TYPES OF FAULT	A	B	C	AB	BC	CA	M	$\overline{AM}$	$\overline{BM}$	$\overline{CM}$	ABC	T_a	T_b	T_c	T_{Fa}	T_{Fb}	T_{Fc}	T_{Fa}	T_{Fb}	T_{Fc}	
															In Zone Fault			Out of Zone Fault			
No fault or mode failure	0	0	0	0	0	0	0	1	1	1	0	1	1	1	1	1	1	0	0	0	*
Mode failure	0	0	1	0	0	0	0	1	1	1	0	1	1	1	1	1	1	0	0	0	*
Mode failure	0	1	0	0	0	0	0	1	1	1	0	1	1	1	1	1	1	0	0	0	*
"a"-earth	0	1	1	0	1	0	1	1	0	0	0	1	0	0	1	0	0	0	0	0	
Mode failure	1	0	0	0	0	0	0	1	1	1	0	1	1	1	1	1	1	0	0	0	*
"b"-earth	1	0	1	0	0	1	1	0	1	0	0	0	1	0	0	1	0	0	0	0	
"c"-earth	1	1	0	1	0	0	1	0	0	1	0	0	0	1	0	0	1	0	0	0	
Faults other than single ϕ to earth	1	1	1	1	1	1	1	0	0	0	1	1	1	1	1	1	1	0	0	0	

* Denotes fail safe operation

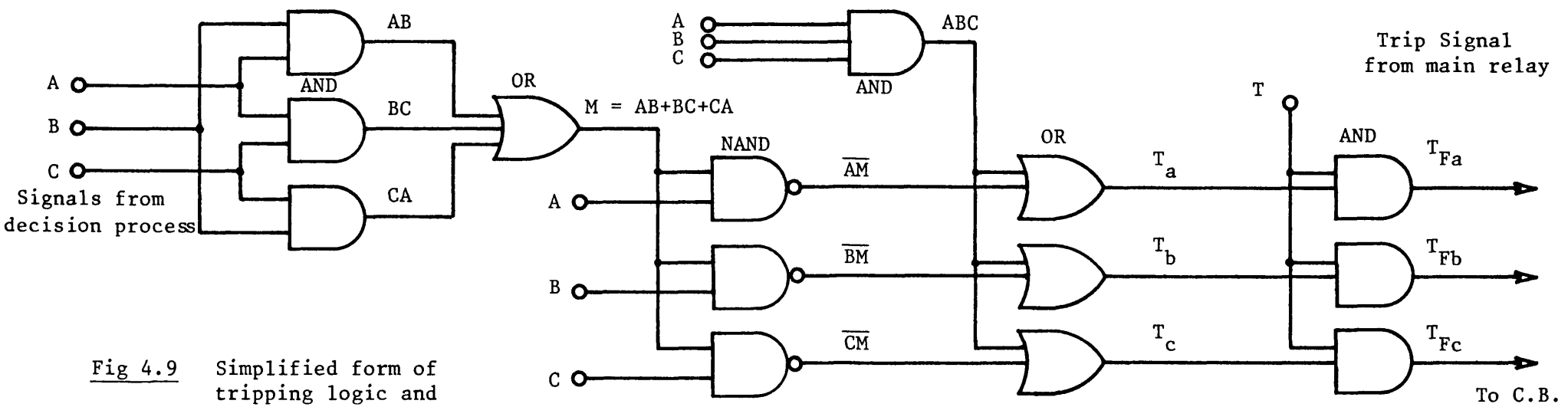

Fig 4.9 Simplified form of tripping logic and associated truth table

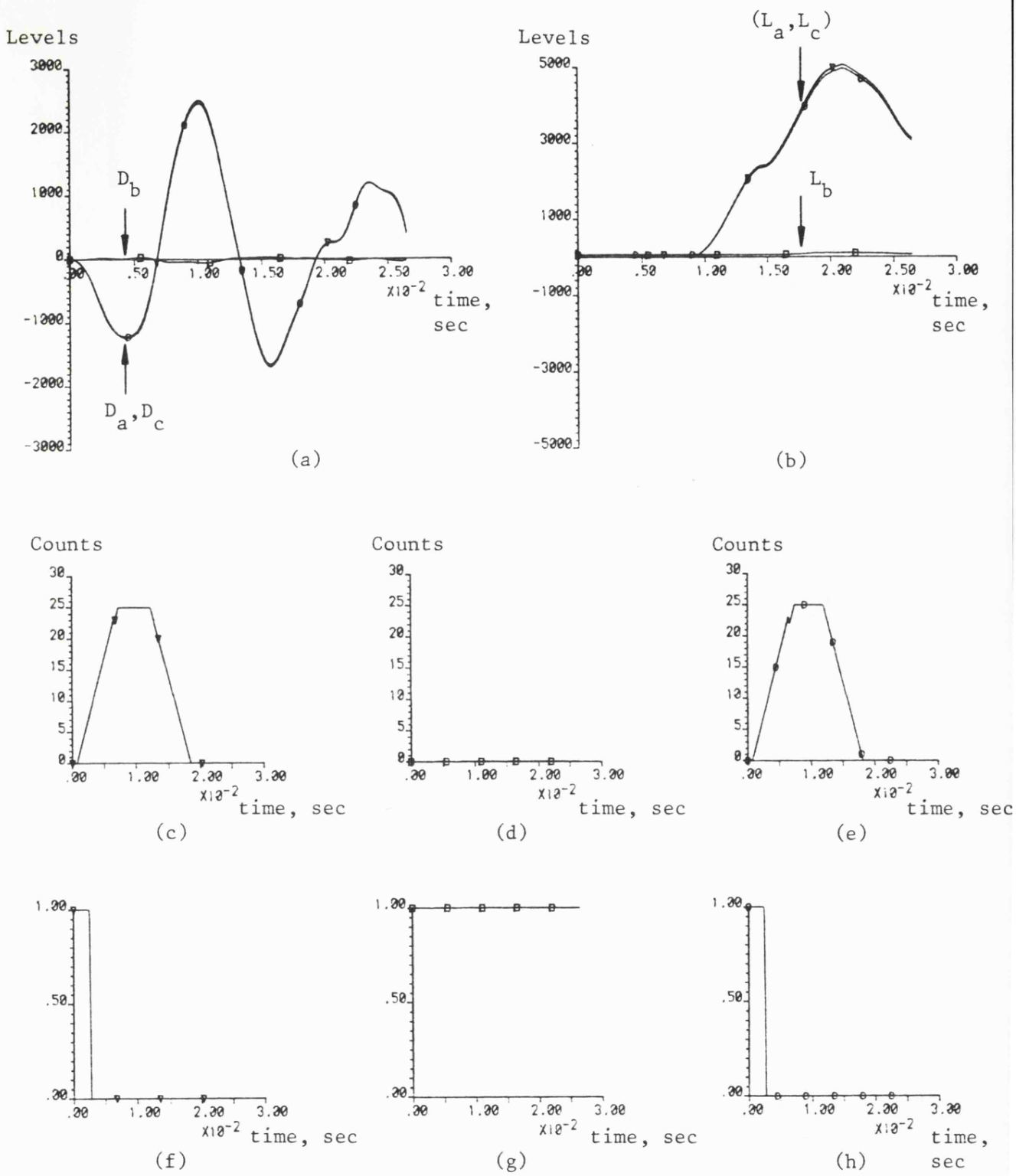

Fig 4.10 Signal variations at different output stages within the phase selection equipment, for the case of single phase to ground fault

- 4-section feeder; shunt compensated; discretely transposed
- Type of fault "b"-e; at peak of prefault "b" to earth voltage; X_F = 50km; R_F = 0.5Ω; Minimum threshold = 45 quantisation levels

(a) Discriminant signal variations (Da, Db, Dc)
(b) Dynamic threshold level response (La, Lb, Lc)
(c),(d),(e) Event counters (ECa, ECb, ECc) of phases "a", "b" and "c" respectively
(f),(g),(h) Output from tripping logic (Ta, Tb, Tc), see Fig 4.9

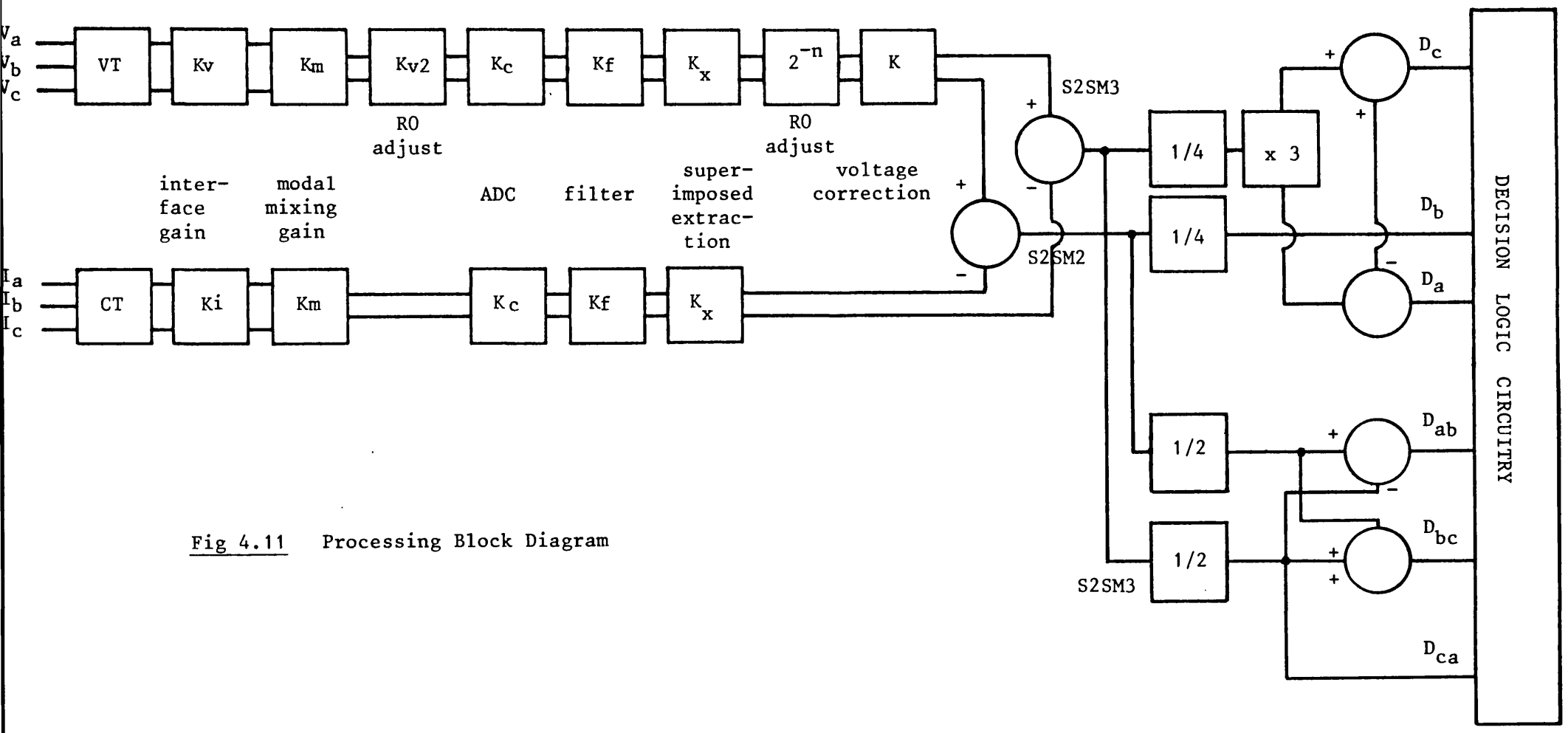

Fig 4.11 Processing Block Diagram

$$T_a = D_a D_{ab}(D_{bc} D_{ca}(D_b \oplus D_c) + D_b D_c(D_{bc} \oplus D_{ca}))$$
$$T_b = D_b D_{bc}(D_{ab} D_{ca}(D_a \oplus D_c) + D_a D_c(D_{ab} \oplus D_{ca}))$$
$$T_c = D_c D_{ca}(D_{ab} D_{bc}(D_a \oplus D_b) + D_a D_b(D_{ab} \oplus D_{bc}))$$

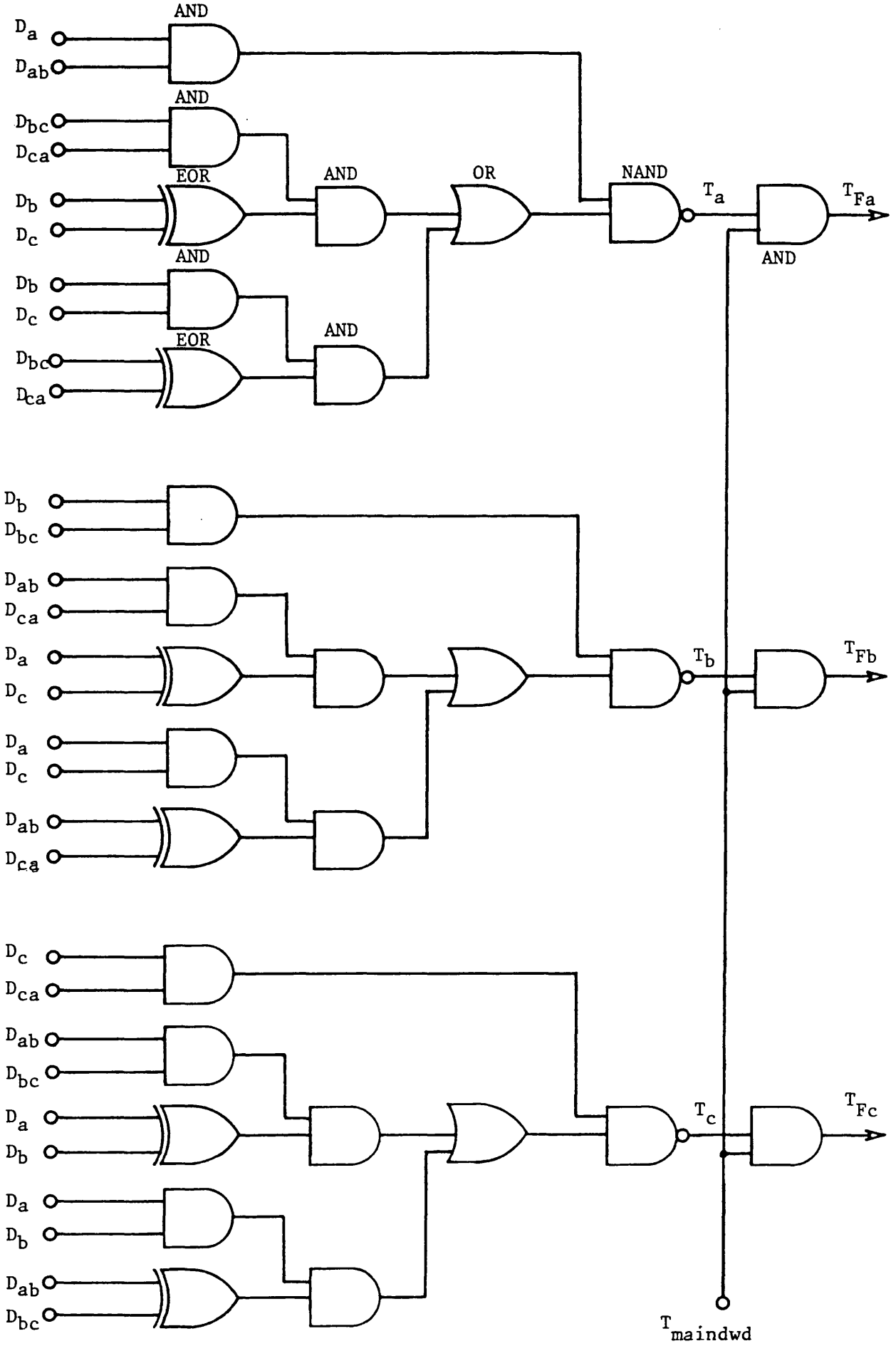

Fig 4.12 Simplified form of tripping logic for single pole opening for double phase clear of ground and for single phase to earth faults

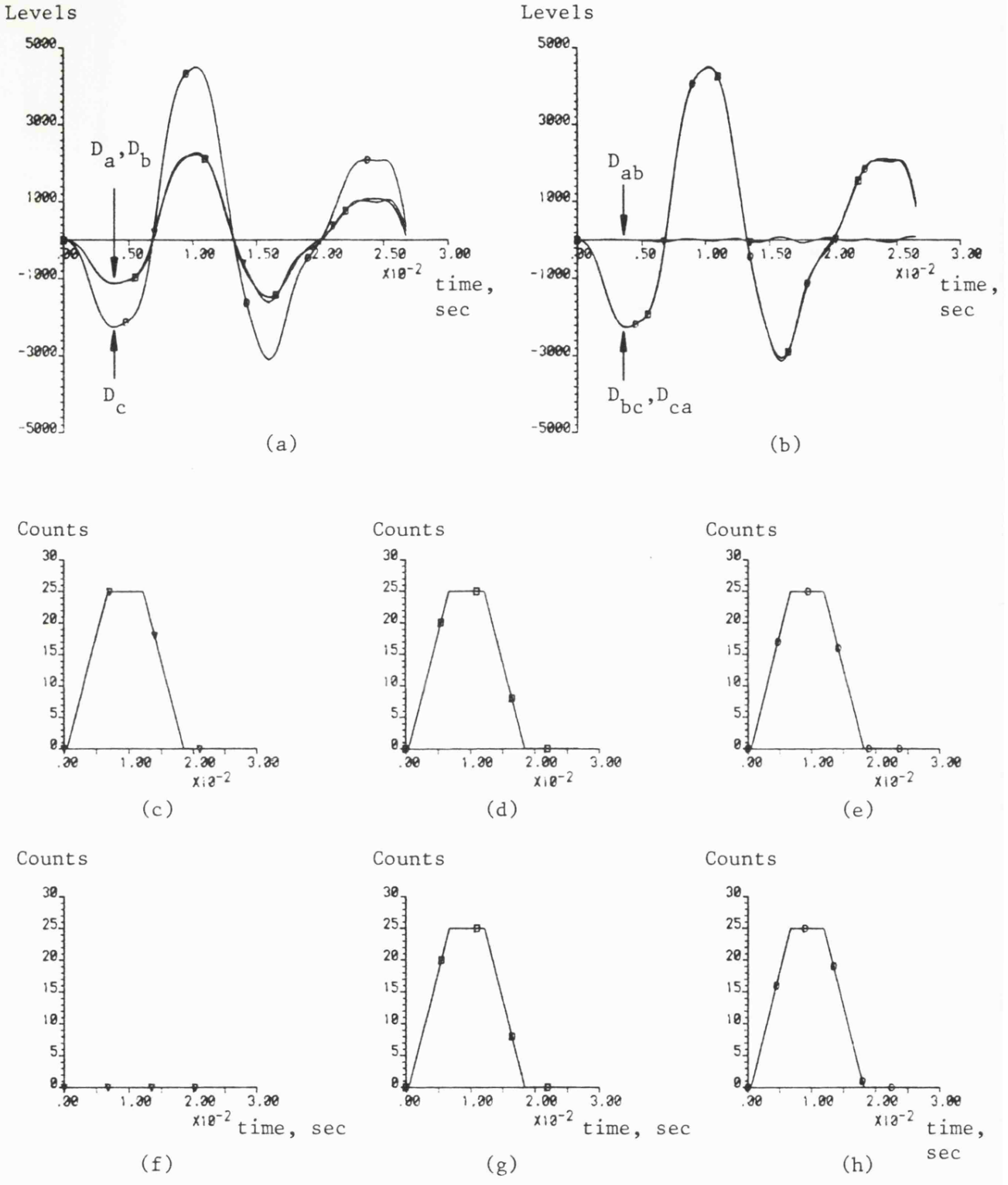

Fig 4.13 Output signals at intermediate processing stages within the phase selection equipment, for the proposed segregated tripping scheme

- 4-section feeder; shunt compensated; discretely transposed
- Type of fault "a"-"b" fault; at peak of prefault voltage between phases "a" and "b"; X_F = 50km; R_F = 0.5Ω

(a) Phase to earth discriminant signals (Da, Db, Dc)
(b) Interphase discriminant signals (Dab, Dbc, Dca)
(c), (d), (e) Event counters (ECa, ECb, ECc)
(f), (g), (h) Event counters (ECab, ECbc, ECca)

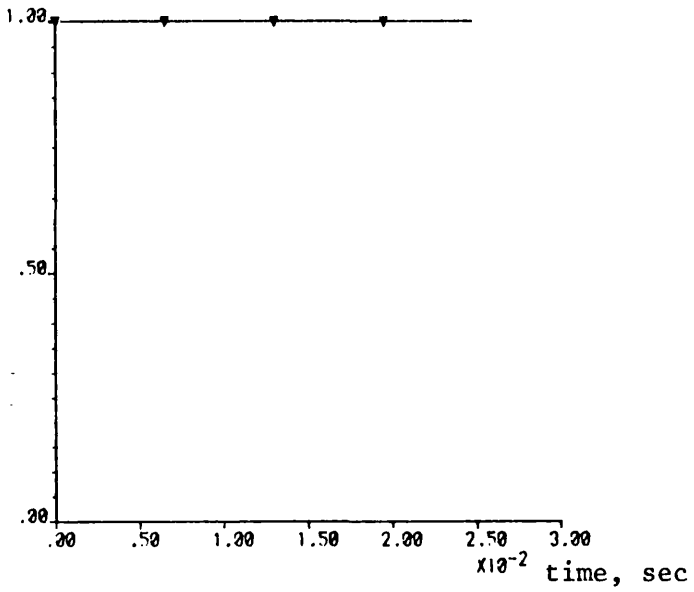

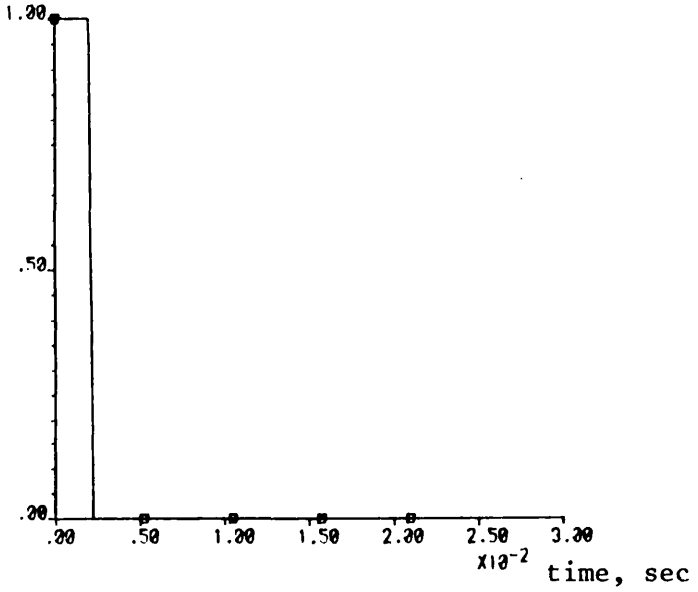

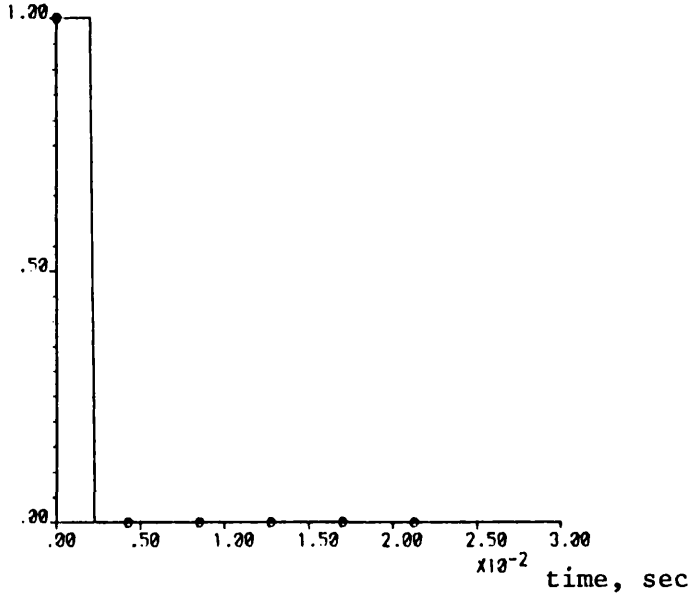

Fig 4.14 Signal outputs from segregated scheme tripping logic based upon the intermediate signals of Fig 4.13

CHAPTER FIVE

PARAMETERS OF SYSTEMS STUDIED

In practice there are a large number of possible system configurations, but feeders which have more than four sections between main generation sources are rarely encountered. Therefore, a general study has been carried out to evaluate the performance of the newly developed phase selector when applied to several different system and source conditions. Two common single circuits of differently constructed lines are considered, these being a horizontal construction with twin shield wires and a vertical construction with a single shield wire.

The basis of the power system simulation is a mathematical program using the Modified Fourier Transform Method. The program calculates the instantaneous values of the voltages and currents at any relay location in a single circuit, three phase transmission line. The realistic primary system simulation techniques developed by Johns and Aggarwal[33,35] are sufficiently flexible to incorporate the frequency variance of all line and earth parameters as well as the effect of discrete conductor transposition, commonly used in long distance transmission.

5.1 Transmission Line Parameters of Horizontal Construction

The general study for such cases has been performed for the two configurations illustrated in Fig 5.1. Each can either be

compensated for the long line application (300 km) by the 4-reactor scheme located at each section end, or uncompensated for short line (120 km). Both lines are regularly transposed through three equal intervals at the termination of each section or at intermediate points thereon, where required.

In the case of the 4-section feeder (Fig 5.1(b)), the faults are simulated on the 300km section shown, and it is fed by the main sources (S.C.1 and S.C.2) at its remote ends as well as from other local source infeeds (S.C.3, S.C.4 and S.C.5).

The single section feeder is fed from the main sources SC1 and SC2 as shown in Fig 5.1(a).

5.1.1 Line construction

Fig 5.2 shows the typical quad conductor 500kV line configuration considered. The positions of the conductors illustrated correspond to the positions over the first one third of the line section from the sending end of any discretely transposed section (Fig 5.3).

The data for the horizontal constructed line is:

(i) Phase conductors 4x 477 MCM Al alloy, 21.5mm overall equivalent, 242mm^2 Al equivalent, 19/4.3 mm stranding.

(ii) Earth shield wires 7/35 mm Alumoweld.

(iii) Earth resistivity 100Ω/m.

(iv) Distance between arcing horns 4.05m.

(v) Conductor resistance, 0.0217512 Ω/km (at 50Hz).

(vi) Conductor reactance, 0.00380647 Ω/km (at 50Hz).

(vii) Earth wire resistance, 1.0916841 Ω/km (at 50Hz).

(viii) Earth wire reactance, 0.3877944 Ω/km (at 50Hz).

(ix) For the two system configurations considered, line lengths are:

(a) for the single section feeder system, L(120-300km);

(b) for the 4-section feeder system line length are 300, 300, 150, 150 km from the sending end to receiving end respectively.

5.1.2 Computed basic parameters

The basic line parameter matrices are the series impedance (Z) and the shunt admittance (Y) matrices which are uniformly distributed along its length. For a multiconductor line, the basic line parameter matrices have been formulated for realistic transient studies, and are reported elsewhere[34,37,38]. Other line parameter matrices such as surge impedance (Z0), surge admittance (Y0), and propagation constant are then derived from these basic parameters. The line series impedance (Z) and shunt admittance (Y) matrices at power frequency (50 Hz) are shown below.

$$Z = \begin{bmatrix} (0.1019157+j0.5011533) & (0.7914845+j0.1856753) & (0.08136367+j0.227285) \\ (0.7914845+j0.1856753) & (0.1019157+j0.5011533) & (0.08136367+j0.227285) \\ (0.08136367+j0.227285) & (0.08136367+j0.227285) & (0.1049047+j0.4979125) \end{bmatrix} \times 10^{-3} \ \Omega/m \qquad \ldots (5.1)$$

$$Y = \begin{bmatrix} (j0.3443485) & -(j0.01972752) & -(j0.0643521) \\ -(j0.01972752) & (j0.3443486) & -(j0.0643521) \\ -(j0.0643521) & -(j0.0643521) & (j0.35866486) \end{bmatrix} \times 10^{-8} \ \mho/m \qquad \ldots (5.2)$$

From equation (5.1) and (5.2) the propagation constant matrix [γ] the surge impedance matrix [ZO] and the corresponding surge admittance matrix [YO] can be calculated.

Modal surge impedances

The general differential equations used to define wave propagation in a multiconductor transmission system have the form:

$$d^2[V]/dx^2 = [P][V],\ d^2[I]/dx^2 = [R][I]$$

where $[P] = [ZY]$

$[R] = [YZ]$

For the purpose of frequency domain analysis, the transformed values of the voltage and current vectors are taken, such that:

$$d^2[V]/dx^2 = [P][V],\ d^2[I]/dx^2 = [R][I] \qquad \ldots (5.3)$$

By using the method developed by Wedepohl[37], the actual voltages and currents are related to some fictional quantities by the following relationships:

$$[V] = [S][Vc]\ ,\quad [I] = [Q][Ic] \qquad \ldots (5.4)$$

Where [S] and [Q] are transformation matrices and [Vc] and [Ic] are modal component vectors, such that:

$$[Vc] = \begin{bmatrix} V_c^{(1)} \\ V_c^{(2)} \\ V_c^{(3)} \end{bmatrix} \quad \text{and} \quad [Ic] = \begin{bmatrix} I_c^{(1)} \\ I_c^{(2)} \\ I_c^{(3)} \end{bmatrix}$$

Substituting (5.4) into equation (5.3) gives:

$$d^2[Vc]/dx^2 = [S^{-1}\ P\ S]\ [Vc]$$
$$d^2[Ic]/dx^2 = [Q^{-1}\ R\ Q]\ [Ic] \qquad \ldots (5.5)$$

There are a number of transformation matrices (Q&S) which can be chosen to diagonalise the product $[Q^{-1}\ P\ Q]$ and $[S^{-1}\ R\ S]$ in equation (5.5). If an ideally transposed single circuit line is considered the form Q=S given in equation (5.4) is particularly useful, in that the modal components of voltage and current are easily derived as linear scalar combinations of the actual phase variations.

$$[Q] = [S] = \begin{bmatrix} 1 & 1 & 1 \\ 1 & 0 & -2 \\ 1 & -1 & 1 \end{bmatrix}$$

The use of the foregoing transformations (Q=S) to diagonalise the modal relationships of eqn (5.5) yields a set of decoupled propagation characteristics described by equation (5.6).

$$\frac{d^2}{dx^2} V_c^{(k)} = (\gamma^{(k)})^2\ V_c^{(k)}\ ,\quad \frac{d^2}{dx^2} I_c^{(k)} = (\gamma^{(k)})^2\ I_c^{(k)} \qquad \ldots (5.6)$$

These equations show that wave propagation in a three phase line can be considered in terms of three separate and independent components, each possessing its own propagation constant (γ) and associated surge impedance [Z0]. Because idealised line transposition is assumed, the surge impedance assoicated with each mode is as given in equations (5.7)[17].

The values $Z0^{(2)} = Z0^{(3)}$ are seen to be dependent on the p.p.s. line parameters and are often referred to as aerial mode surge

impedances. On the other hand, the so-called earth mode surge impedance $Z0^{(1)}$ depends on the zero sequence parameters of the line.

$$Z0^{(1)} = (Zs + 2Zm) / (Ys - 2Ym) = ZL0/YL0$$
$$Z0^{(2)} = Z0^{(3)} = (Zs-Zm) / (Ys+Ym) = ZL1/YL1 \quad \ldots (5.7)$$

The values of the average sum of all conductor self impedances and admittances at power frequency can be found by substituting for the corresponding values of Z and Y obtained in equations (5.1) and (5.2) in equation (5.8) and (5.9) respectively.

$$Zs = (Z(1,1) + Z(2,2) + Z(3,3)) / 3 \quad \ldots (5.8)$$

Hence,

$$Zs = (1.02912 + j5.00073) \times 10^{-4} \ \Omega/m$$

and

$$Ys = (Y(1,1) + Y(2,2) + Y(3,3)) / 3 \quad \ldots (5.9)$$

then

$$Ys = -(j3.491152) \times 10^{-9} \ \mho/m$$

Similarly, the average sum of all conductor mutual impedances and admittances at power frequency are given by:

$$Zm = (Z(1,2) + Z(2,3) + Z(3,1)) / 3 \quad \ldots (5.10)$$
$$= 0.8062525 + j2.134152 \times 10^{-4} \ \Omega/m$$

and

$$Ym = (Y(1,2) + Y(2,3) + Y(3,1)) / 3$$
$$= -(j4.947724) \times 10^{-10} \ \mho/m \quad \ldots (5.11)$$

The values of the zero and positive sequence line impedance and

admittance are then obtained as follows:

$$ZL0 = (Zs+2Zm) = (2.64163+j9.269034) \times 10^{-4} \ \Omega/m$$

$$YL0 = (Ys-2Ym) = (j2.501607) \times 10^{-9} \ \mho/m$$

and

$$ZL1 = (Zs-Zm) = (0.2228675+j2.866578) \times 10^{-4} \ \Omega/m$$

$$YL1 = (Ys+Ym) = (j3.985924) \times 10^{-9} \ \mho/m$$

The earth and aerial mode surge impedances are calculated by substituting in equation (5.7) for the values of the zero and positive line sequence line impedance and admittances.

$$Z0^{(1)} = ZL0/YL0 = (614.735718 - j85.88839)$$

and

$$Z0^{(2)} = Z0^{(3)} = ZL1/YL1 = (268.377 - j10.417)$$

5.1.3 Shunt reactor parameters

Fig 5.4 shows the circuit of the four reactor arrangement considered. The parameters of the reactors are determined assuming ideal transposition of the line section to which the reactor bank is connected.

The parameters of the shunt reactor bank, when arranged to compensate one half of any line section of length 1, are as given in equation (5.12):

$$h1 = BL1/BC1 = 2/(\omega_0^2 \ L1 \ C1 \ 1)$$

$$h0 = BL0/BC0 = 2/(\omega_0^2 \ L0 \ C0 \ 1) \qquad \ldots (5.12)$$

The line shunt capacitances (C1, C0) are calculated by averaging the sum of all conductor self and mutual capacitances per unit length of the line section to be compensated.

Reactor impedances consistent with constant values of Rp, Rn, Lp and Ln, as defined in reference (35) are used in the course of this work and are given below:

$$Zp = Rp + j\omega Lp = 2/\omega_0 h1C11 \{1/Q + j\omega/\omega_0\}$$

$$Zn = Rn + j\omega Ln = 2(h1C1-h0C0)/3\omega_0 h0h1C0C11 \{1/Q + j\omega/\omega_0\} \quad \ldots (5.13)$$

A typical Q-factor of 250 was assumed for the neutral and phase reactors, which allows the relatively small values of Rp and Rn to be neglected. In practice, the normal service loading levels on long compensated feeders are typically between one half and two thirds of the surge impedance power level, and the corresponding level of p.p.s. shunt compensation required (h1) is approximately 0.75.

For the line considered, the sequence capacitance ratio C0/C1 is approximately equal to 0.62761, and the associated level of zero sequence compensation (h0) required to theoretically minimise both secondary arc current and residual voltages is approximately 0.6016635[39,40].

That is, for a value of h1 of 0.75, to produce a value of Isec = 0 pu, the value of h0 required is 0.602. The values of h1

and h0 are then used to calculate the optimum reactor impedances (ignoring the effect of electromagnetic coupling), which for this case are:

Xn = j733 Ω (at 50Hz)

Xp = j22301 Ω (at 50Hz)

and X0/X1 = 1.986

For a 300km line, it was found that to limit the capacitive component of the steady-state secondary arc current to 20A rms, the value of h0 is: h0 = 0.8787121 for h1 = 0.75.

The neutral inductance Xn in such a case will be:

Xn = j267.5 Ω

and X0/X1 = 1.359

The impedances of Xn and Xp are seen to be very much smaller than in the former case, and since the capital cost of reactors is roughly proportional to X^2 which represents a considerable saving in cost.

The majority of the studies were therefore performed with the two latter degrees of compensation, but for studies involving different levels of p.p.s. compensation (h1), h0 is chosen to minimise the secondary arc currents and the recovery voltage.

5.1.4 Source parameters for different sections studied

For the purpose of confirming the digital simulation here described, a general source model based upon arbitrarily defined short circuit levels at the terminating busbars was developed (see Fig 5.5).

The impedance matrix of each local infeed/outfeed has been estimated from a knowledge of the power frequency short circuit levels and the ratio of zero phase sequence to positive phase sequence impedance of the source in question. More complex local source network models can be simulated instead of the normal lumped parameter source network, but in many applications the local infeed during fault conditions is relatively small and the considerable extra computational effort required can be avoided without serious loss of realism.

(a) Single section feeder

Sending end source capacity S.C.1 = (500 - 50000 MVA)

Receiving end source capacity S.C.2 = (500 - 50000 MVA)

Q-factor at nominal power frequency (50Hz),X/R = (30 - 100)

Source ZSO/ZS1 ratio = (0.5 - 1.0)

(b) Four section feeder

The Q-factor at the nominal power frequency of 50Hz was taken as 100 for all p.p.s. and z.p.s. source impedances.

The source ZSO/ZS1 ratio and their capacities starting from sending end are as follows:

S.C.1	=	0.25 GVA	ZSO/ZS1	=	0.4
S.C.2	=	5.0 GVA	ZSO/ZS1	=	1.0
S.C.3	=	5.0 GVA	ZSO/ZS1	=	1.0
S.C.4	=	1.0 GVA	ZSO/ZS1	=	0.5
S.C.5	=	5.0 GVA	ZSO/ZS1	=	0.5

5.1.5 Modified fast Fourier Transform parameters

The occurrence of a fault on the line causes voltage and current components to propagate away from the fault towards each source. A proportion of these components is reflected from the terminating busbars and from within each source network, to form a series of travelling waves which are ultimately damped by the system. Such phenomena represent a wide frequency variation, and it is therefore necessary to evaluate the system equations over the entire frequency spectrum of the disturbance in order to obtain the complete transient response. The Modified Fast Fourier Transform Method (FFT) forms the basis by which the frequency spectrum is used to determine the corresponding time variation of any voltage or current of interest.

In order to implement the FFT digitally, it is necessary to truncate the infinite range of integration. This finite range of integration gives rise to Gibbs oscillations[41,42] which are overcome by the introduction of the σ factor to improve the rate of rise at the integrand discontinuity points. Furthermore, a very small step length is necessary for the numerical evaluation of the inverse integral. This is due to the fact that the poles of the integrand

may be close to the path of integration, which causes the integrand to peak. Hence, to ensure numerical stability when the integral is evaluated digitally, and to move the path of integration away from the poles, so producing smoother integrand and allowing the use of a greater step length, a frequency shift constant alpha (α) is introduced.

The relationships between the sigma factor (σ), frequency shift constant (α) and truncation frequency are the subject of an extensive study by Day et al. The appropriate values for these quantities should be used to guarantee the success of the computational results.

In the present studies, these parameters are taken according to:

(1) Choice of observation time "Tob" : Tob is simply chosen as the time duration of interest in the transient analysis. It should be pointed out that there is a tendency for the time function to break up as t -> Tob when applying the inversion formula, which means that it is necessary to discard results obtained for t > 0.8 Tob. Therefore, Tob is chosen slightly larger than actually required to make allowance for this phenomena. The choice of Tob controls the value of the basic frequency, $\Delta\omega$, according to $\Delta\omega = \pi/Tob$.

(2) Choice of frequency shift constant "α" : An empirical formula is applied which limits the value of alpha to alpha = $2\Delta\omega$. But, since $\Delta\omega$ is fixed by the choice of Tob, α is found directly from

$$\alpha = 2\pi/Tob$$

(3) Choice of number of samples "N" : The choice of N is determined in relation to the bandwidth of f(t), assuming that f(t) represents the response of a physical system. It will generally be possible to assign a value of angular frequency Ω rad/sec, beyond which the frequency spectrum associated with f(t) may be reasonably neglected. A knowledge of the physical system involved will enable an appropriate choice of Ω to be made.

Based upon this value, N can be determined from:

$N = \Omega/2.\Delta\omega$ and since $\Delta\omega = \pi/Tob$, then $N = Tob.\Omega/2/\pi$

It is of interest to note that the above choice of N leads to the following sampling rate in the time domain:

$$\text{Sampling rate} = 1/2.\Delta\omega = 2.N/Tob$$
$$= 2.\Omega/2\pi$$
$$= 2.(\text{bandwidth in Hz})$$

The sampling rate for the studies were carried out at 8kHz. Hence, the above factors are tabulated below:

Sampling Rate (kHz)	Ω (kHz)	Tob (secs)	N	α
8	4	0.032	256	196
8	4	0.064	512	98
8	4	0.128	1024	46
8	4	0.256	2048	23
8	4	0.512	4096	12.25

5.2 Multi-Ended, Plain Feeder with Sequential Fault Capability

A versatile program was developed to simulate the practical system model of Fig 5.6. This program represents a 2-section feeder with relay locations R1, S1 covering line PQ and R2, S2, covering line QR. Faults can be simulated on either of the 2 sections, PQ and/or QR. A fault in section PQ is considered as an in-zone fault for relays R1 and S1, but as out of zone disturbance for relays R2 and S2. This program simulation gives a greater flexibility for examining the performance of the selector equipment under a variety of forward and reverse disturbances. The sequential fault facility enables the simulation of sequential as well as evolving faults on the system allowing the performance of the phase selector to be studied under such conditions.

The sequential capability allows a first fault to occur on either line section followed, after a specified delay, by a second fault on the other section. This facility is not only useful for studying the recovery performance of the digital filter within the process, but also to indicate whether the selector will reselect correctly on the occurrence of a second disturbance on the system.

At each busbar, equivalent source networks can be formed from a combination of local generation and any number of infeeding lines. The measurands presented to all relay locations are then representative of those that would be produced by a system of a much higher degree of complexity.

Most of the modelling techniques and computational algorithms applied to the system described earlier are equally applicable for this multi-ended, vertical construction system, thus simplifying the implementation of the simulation.

Parameters of vertical construction system:

The short line studies apply to a typical quad conductor 400kV line, having the mean spacings given in Fig 5.7.

The data for this line is:

(i) Phase conductors are $4 \times 54/7/0.33$ cm s.c.a. with 0.305 m bundle spacing (bundles = 4).

(ii) Earth wire is 54/7/0.33 cm s.c.a.

(iii) Earth resistivity is 100Ω/m.

(iv) Conductor resistance = 0.2175×10^{-4} Ω/km (at 50Hz).

(v) Conductor reactance = 0.3810×10^{-5} Ω/km (at 50Hz).

(vi) Earth wire resistance = 0.1902×10^{-2} Ω/km (at 50Hz).

(vii) Earth wire reactance = 0.3878×10^{-3} Ω/km (at 50Hz).

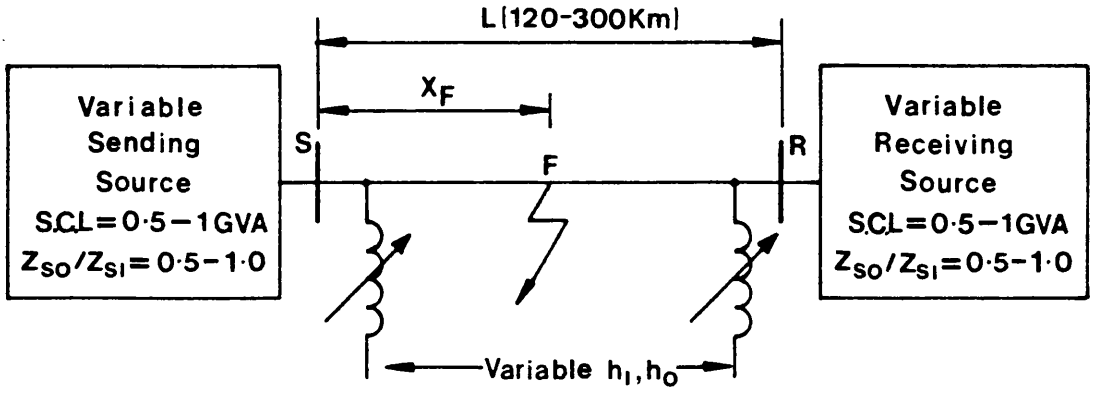

(a)

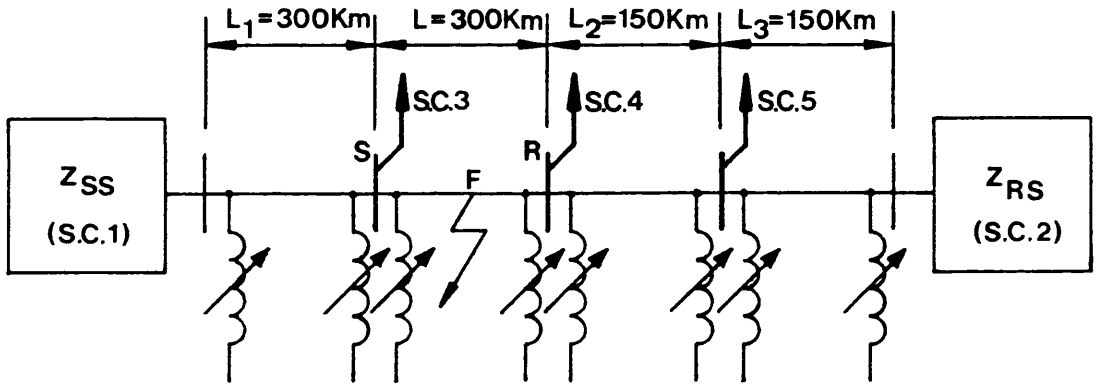

(b)

Fig 5.1 Schematic diagram of the shunt-compensated systems studied

(a) Single-section feeder system

(b) Four-section feeder system

(S.C.1 - S.C.5) as stated in section 5.1.4

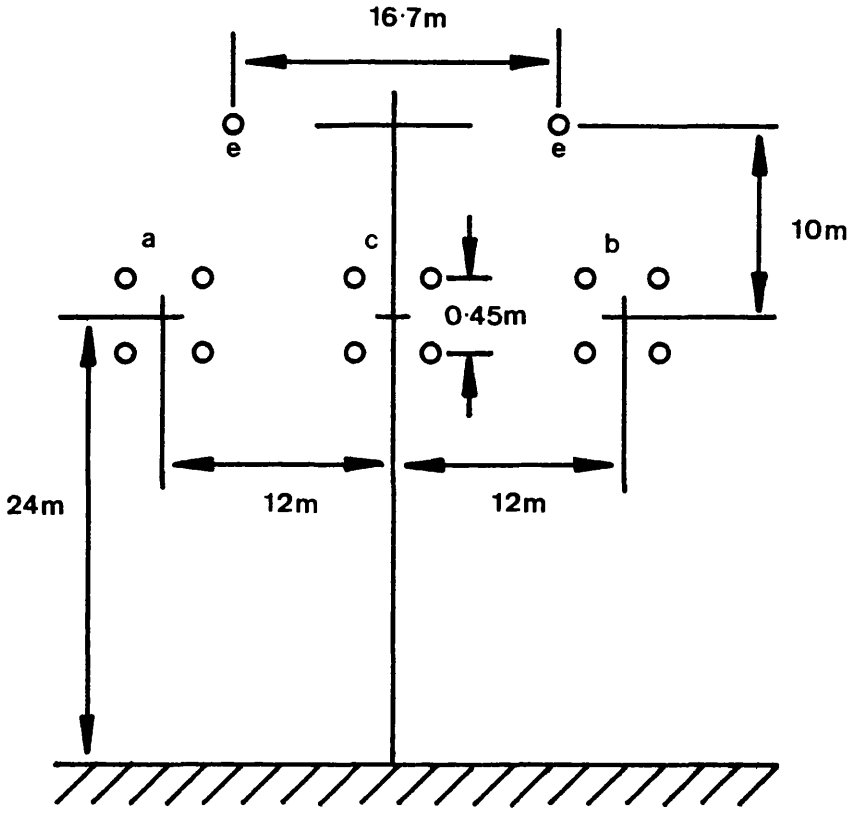

Fig 5.2 500kV line construction simulated

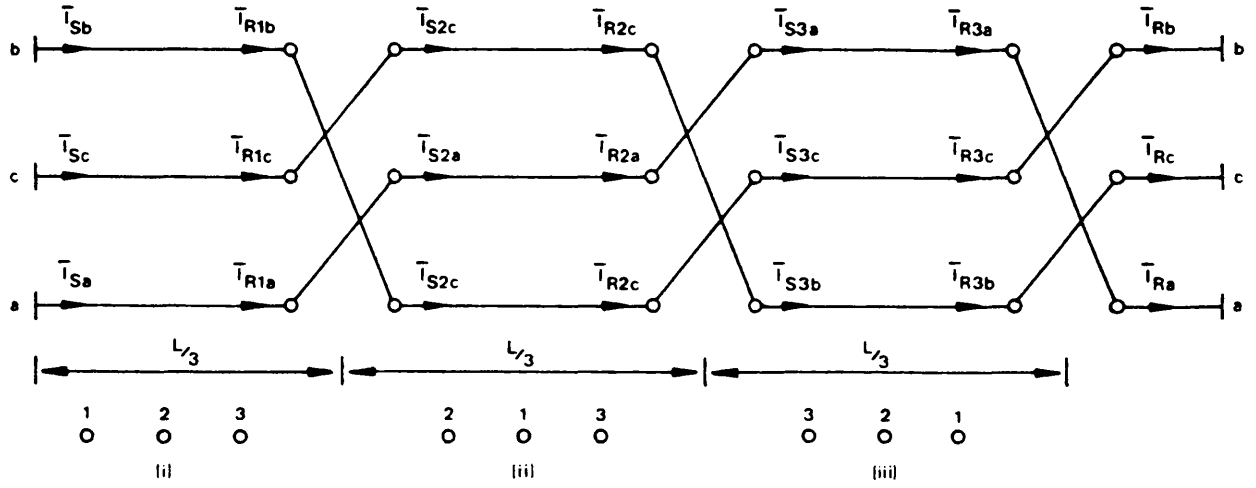

(a)

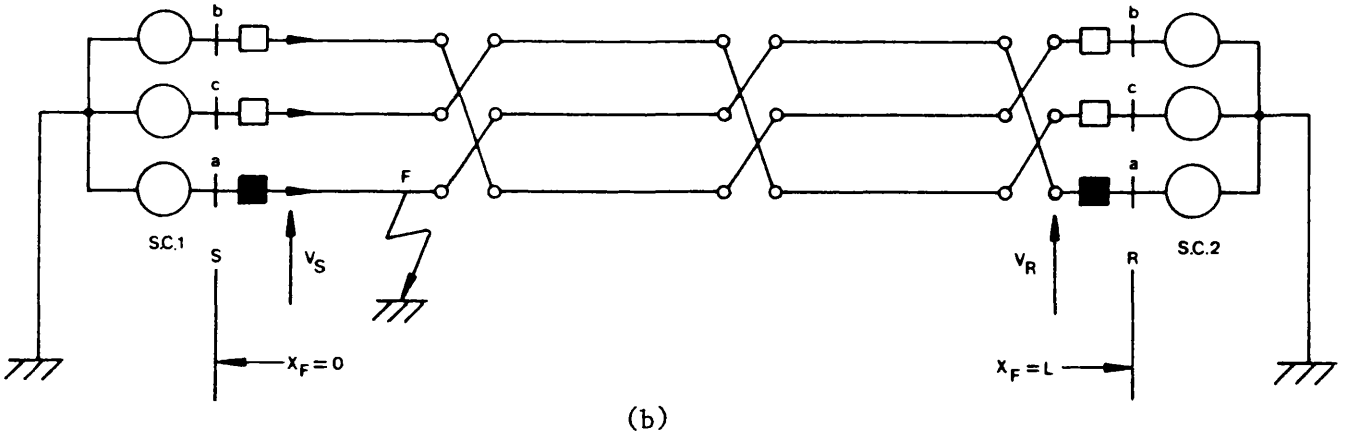

(b)

Fig 5.3 (a) Schematic diagram of transmission line with a complete cycle of transposition

(b) Equivalent system configuration for a discretely line model

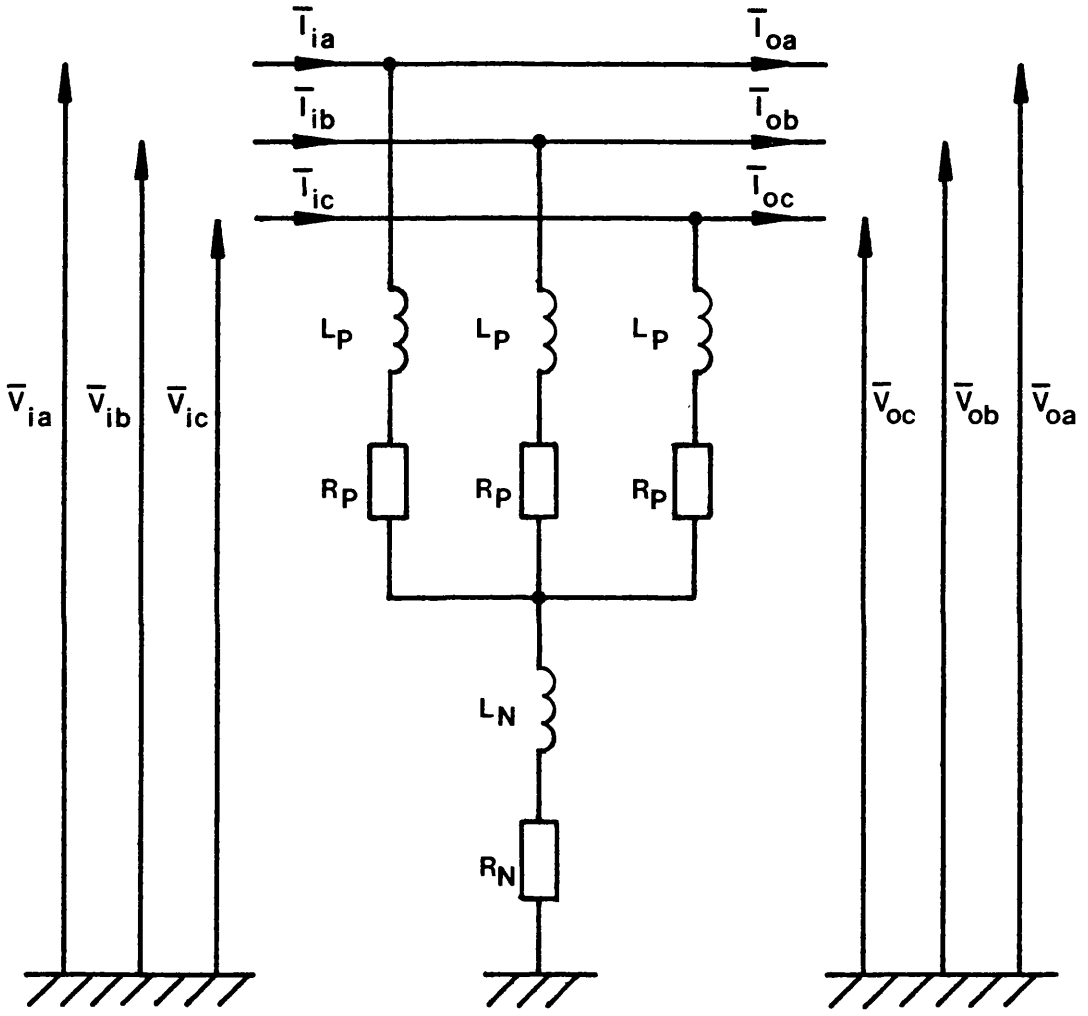

Fig 5.4 Shunt reactor arrangement

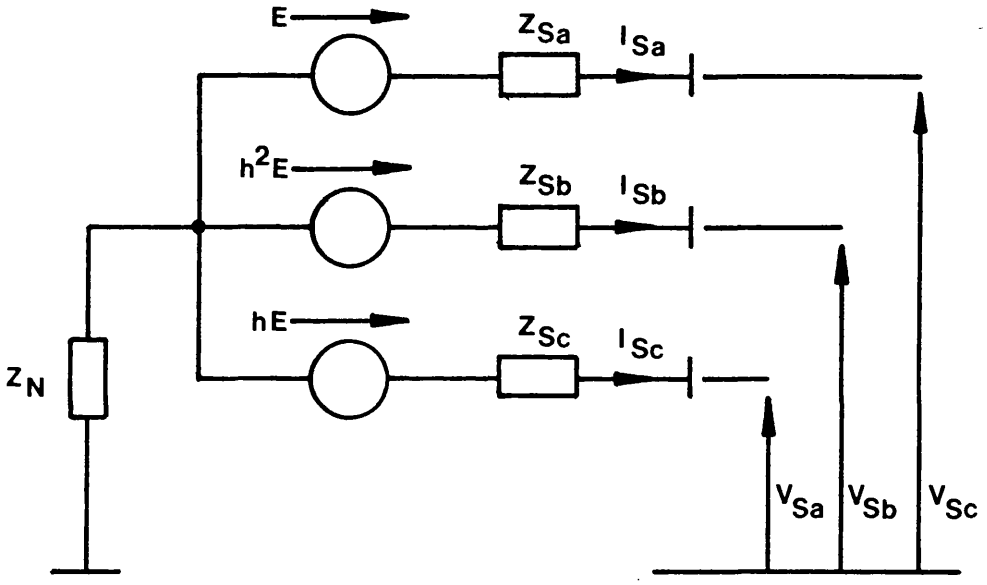

Fig 5.5 Symmetrical source representation

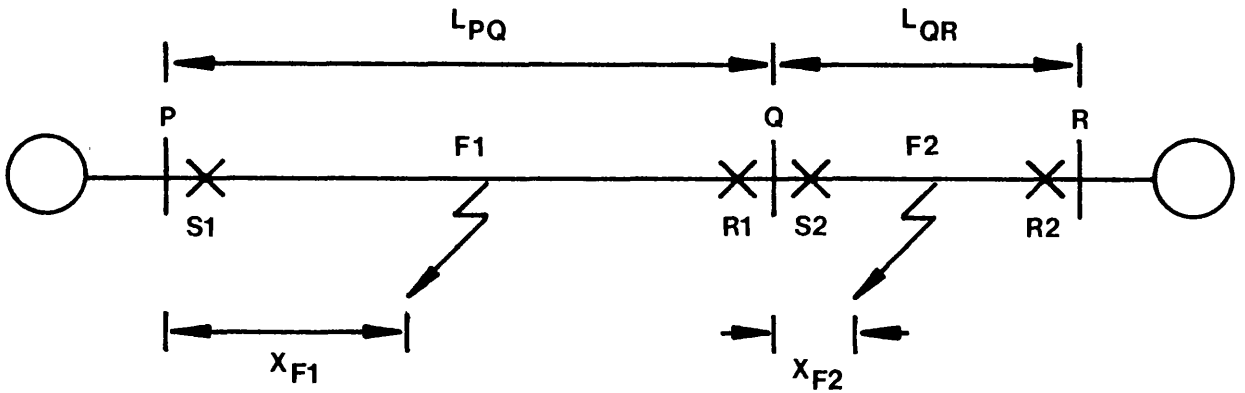

Fig 5.6 Single line representation of model used to simulate sequential faults

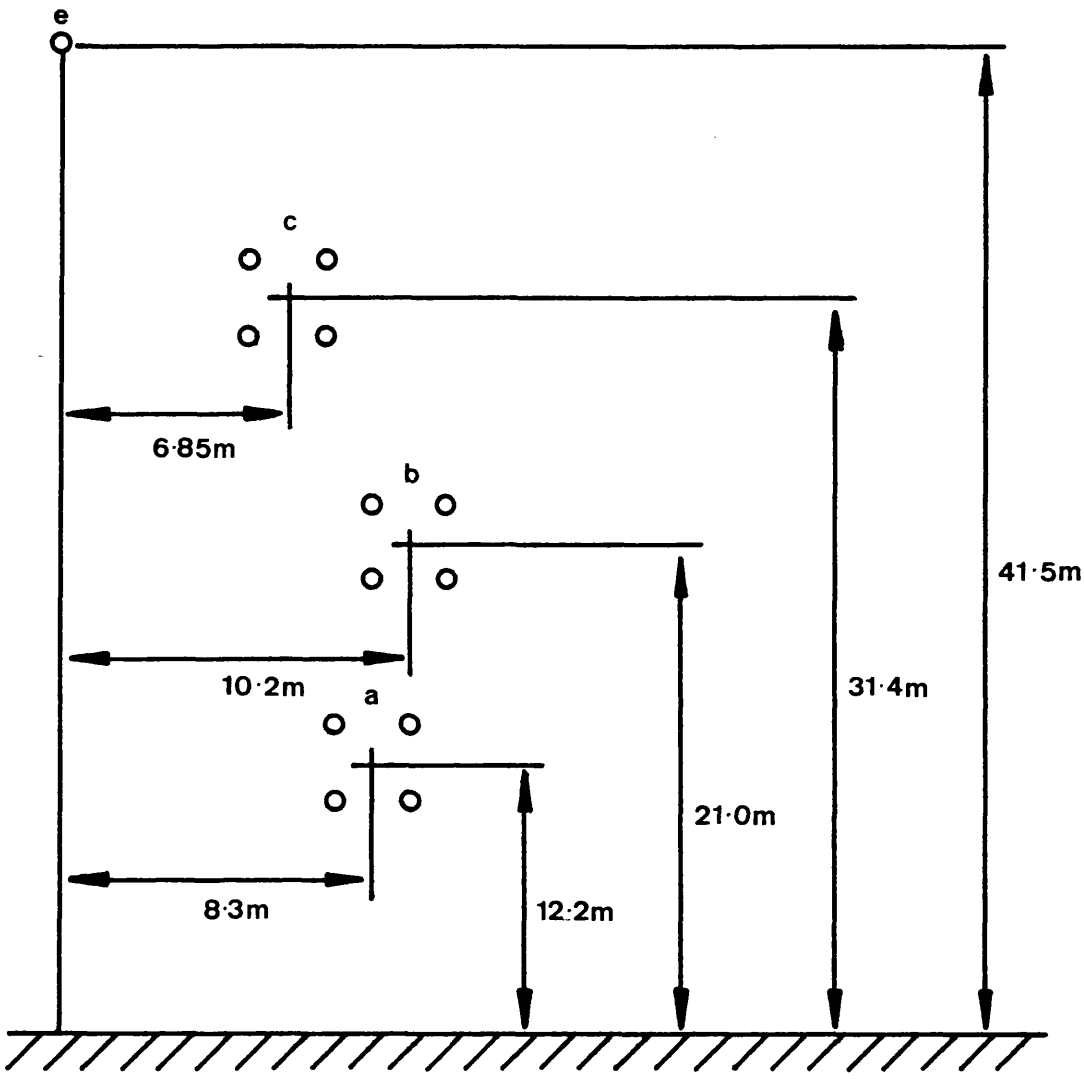

Fig 5.7 400kV line configuration

CHAPTER SIX

VALIDATION OF THE NEW PHASE SELECTOR TECHNIQUE

The new phase selection scheme is primarily designed for the purpose of discriminating between single phase to earth and all other types of fault. Furthermore, the selector must differentiate between the three single phase to earth faults and maintain this capability under different system and source conditions.

The work presented in this chapter includes computational results derived from the digital simulation program described in Chapter 5. The validity of the latter for emulating real system faulted responses has been the subject of many publications[33,35,39], and with recent trends in computer development, frequency domain techniques (hitherto prohibitively time-consuming and expensive) have become the norm in many fields of simulation work. Accurate performance evaluation of the new phase selection scheme, when applied to practical systems, can therefore be gained from primary simulation data generated by the aforementioned digital program.

As with all UHS power system protection devices, the performance factors of interest include the balance between speed and security of operation. It is practically impossible to estimate the selector performance encompassing the infinite number of system conditions, which may prevail at the precise instant of fault inception. Some preliminary investigations were therefore necessary to establish the

worst case conditions, under which the slowest speed of operation of the selector is expected.

6.1 Behaviour of the Phase Selector when applied to Transposed Systems

6.1.1 Effect on fault type

It will be recalled from Chapter 3 that the fundamental requirement for correct phase selection is that for single phase to ground faults, the relevant faulted phase discriminant signal should remain low whilst the other two attain relatively large magnitudes. Furthermore, all other types of fault should not produce a similar discriminant signal pattern which would cause the selector to wrongly indicate a single phase fault.

To illustrate the various stages of signal processing within the phase selector Figs 6.1-6.3 show the signal patterns produced for the three types of single phase to ground fault respectively. It can be seen that the behaviour of the discriminant signals is as predicted theoretically, and that a trip indication is given for the particular discriminant which remains low.

Corresponding results for all other types of fault are illustrated in Figs 6.4 and 6.5, whereby neither case results in a similar discriminant signal relationship to that obtained for any single phase to ground fault.

6.1.2 Effect of fault position

The new scheme is based upon total superimposed components

impressed upon the system by the occurrence of a fault. The time taken for the fault transient components to reach the relaying location is inversely proportional to the distance to fault, which therefore directly influences the speed of operation of the selection equipment.

A series of solid phase to ground faults was simulated at various positions along the line section between busbars S and R of the 4-feeder configuration described in Chapter 5. For selection equipment based at both ends, Fig 6.6 shows the interpolated operating time/fault position characteristic for both 0° and 90° fault inception instances. Clearly seen is the gradual reduction in selection speed observed at either end as the distance to fault increases and over the entire range of fault position correct discrimination was maintained. The characteristics do not display symmetry about the mid point (150 km) which is due to the different effective source/line impedance combination presented to busbars S and R, this effect being further detailed later in this chapter.

6.1.3 Effect of fault inception angle

The point on wave of fault inception controls the initial rate of rise and hence magnitude of the modally derived discriminant signals. The primary effect of this is to degrade the speed of faulted phase selection for some inception angles.

For all values of fault inception angle, the selector must render the correct decision, ie. a single phase trip indication for the case

of single phase to ground faults and a three phase indication for all other fault types. The particular case of a double phase to ground fault produces a discriminant signal pattern, which for some fault point on wave is likely to give a single phase fault indication if the selector is to render a very quick decision. Fig 6.7 shows four fault conditions including different fault inception instances, whereby the latter are seen to directly influence the time delay, t_d, before the third discriminant signal exceeds the threshold level. Moreover, the order in which the individual signals exceed the minimum threshold level is also a function of the fault inception angle. To overcome this problem, a decision delay, described in Chapter 4, prohibits wrong selection being rendered by accounting for the worst possible rise delay encountered in practice. Such a delay does not impair the overall fault clearing capability of the whole protection scheme under any fault conditions requiring the opening of all three phases. This is because the phase selector, as part of a complete protection scheme employing a directional wave comparison relay, is required to operate in a fail safe, three phase, trip mode. In cases where the selector is slow to respond, or indeed where no selection is made, fault clearance is then still possible, as the tripping responsibility lies solely with the main relays.

For single phase to ground faults, however, the delay merely adds to the minimum operating times of the selector. Fig 6.8 shows the interpolated operating time/fault inception characteristics for an "a"-phase to earth fault on the 4 feeder configuration used. For each fault position at 0 and 300 km from end S, a fault point on wave

around voltage minimum (0°, 180°) results in the slowest speed of operation at each end, the fastest times being achieved around voltage maximum (90°). From Fig 6.8 it can be seen that the combination of distance to fault and hence effective system and source impedances, together with point on wave variation, produces different characteristics, but correct UHS selection is retained over the entire range, the response for faults in the third and fourth quadrant being a mirror image.

6.1.4 Effect of source capacity

The effects of source short circuit levels upon fault transient waveforms are well known. For very large source capacities, the voltage waveforms are smooth, since the current components circulating within the low source impedance produce insignificant voltage transients thereby maintaining an almost constant busbar voltage. By comparison, the voltage components generated at high impedance source discontinuities are relatively large, particularly so in the healthy (sound) phases. This phenomena is explained by the fact that the infeed of current from the remote end is greater than that of the local source, inducing unipolar current and hence voltage components in the other phases. The effect of this is cumulative in that current begins to flow etween the two ends, resulting in further voltage waveform distortion after subsequent reflection at discontinuity points within the system. Furthermore, under earth fault conditions, the ratio of zero phase sequence to p.p.s. impedance of the source contributes to the distortion of the superimposed components. The underlying principle of the phase selector is based upon the sound phase quantities being equal under phase to earth fault conditions. As described above, the distortion of the sound phase components, which directly influences

the error content in the selector discriminant signals, is therefore controlled by the effective source impedance. Accordingly, the minimum threshold level associated with the discriminant signals, which is set above all expected error components, is therefore a function of the source capacity.

A particular limitation of existing phase selectors operating upon voltage or current is the restricted range of source capacity coverage. A selector operating upon voltage alone would suffer under high source capacity conditions, and in contrast a current operated scheme would be limited by low source capacities. The new scheme utilises composite signals of voltage and current, with reliable selection being possible in the absence of one of the two components. Furhtermore, the introduction of a voltage channel gain K boosts the superimposed voltage component, which extends the coverage range even further. The proposed selector can therefore be applied to systems with a wider range of source short circuit levels, outside the capability of conventional selectors, making it extremely versatile when compared with the latter.

The operating principle of the phase selector is based upon a fixed modal relationship between aerial mode quantities which is independent of source parameters. However, the rate of rise of the superimposed components is not only a function of the fault point on wave, but is indirectly influenced by the magnitude and hence rate of increase of the discriminant signals.

The above facts lead to the conclusion that the speed of operation of the selector only varies significantly with source capacity when the line section impedance between the local source and point of fault is large enough to limit both voltage and current components. Under boundary conditions where one or both of these components have fallen below the required level, the main relay would fail to respond, whilst the selector remains operational. From this point of view, an evaluation of the selector performance under greatly reduced signal conditions was deemed unnecessary.

To demonstrate the effects of a variation in source capacity, a single section plain feeder simulation was used, with single generators modelled at each end. The receiving end (END R) capacity is fixed at 1 GVA, whilst the corresponding source at the sending end (END S) takes values between 1 and 30 GVA. This range of capacity variation is thought to include the absolute maximum level encountered in most long line applications. For a fault location of 150km from end S, the filtered modal superimposed currents at that end are shown in Fig 6.9. It is seen that as the capacity is increased and therefore as the source impedance decreases, the magnitude of the current rises. A complementary effect is noticed in the voltage components, whereby the magnitude of voltage rises as the source capacity is decreased, as shown in Fig 6.10. At this point it must be noted that the variation of voltage and current with respect to a change in source capacity is exponential in nature. That is, beyond a certain capacity, further changes in the latter do not have such a pronounced effect upon the voltage and current, since the line impedance to fault becomes the

limiting factor. The discriminant signals are formed from composite signals of the aforementioned voltage and current components and the compensating effect of having large current for high source capacities and high voltage levels for low source capacities then produces discriminant signals of fairly constant magnitude, clearly seen in Fig 6.11. However, the variation of source capacity has a negligible effect upon the rate of rise of the discriminant signals and hence the time at which they exceed the threshold level. For this particular system test, the operating time of the selector does not significantly change over the entire source capacity range, even for the worst case of fault inception angle around voltage zero.

The results obtained lead to the conclusion that the UHS performance of the new phase selector, when applied to systems with constantly varying source conditions, remains unaffected.

6.2 Comparison of the Phase Selector Equipment when applied to Transposed and Non-transposed Systems

The results presented in the above section are those obtained from discretely transposed models of practical systems. The transposition of phases reduces the electrostatic and electromagnetic unbalances, since overall each conductor shares an equal position with respect to a horizontal reference. Furthermore, the transposition compensates for conductor bundling, which is known to cause an increase in zero and negative sequence unbalance. Moreover, transposition is found to considerably improve arc extinction times for long lines employing single pole autoreclosure as detailed in ref (40).

From an economic point of view, the transposition of phases on EHV systems at locations distant from the points of generation has proven costly. Consequently, the trend has been towards transposition of conductors at the power station busbars, and in some applications, the transposition is completely omitted.

For non-transposed short line applications the unbalance effects are negligible, but for longer line lengths the unequal mutual impedances between phase become a significant factor. The plain feeder system model described in Chapter 5 was therefore utilised to establish any derogatory effects that non-transposition has upon the phase selector performance. The line length is taken as 300km and direct comparisons are made between the three cases of ideal, discrete and non-transposition, for the shunt compensated system considered.

The total phase current variations under "a" to earth fault conditions are shown in Fig 6.12. The discretely transposed system produces healthy phase currents which are largely similar, Fig 6.12(a), whereas with non-transposition, Fig 6.12(b), the differences in induced currents in the sound phases are more pronounced.

Fig 6.13 shows the discriminant signal waveforms derived from the system in which ideal, discrete and non-transposition is considered in turn. As expected, the discriminant signal associated with the faulted phase remains approximately zero throughout the observation period, for the ideally transposed case, Fig 6.13(a). A comparison

of Fig 6.13(b) and 6.13(c) reveals that discrete transposition reduces the spill output content in the discriminant signals which is caused by system unbalance. This unwanted component is clearly seen in the faulted phase discriminant signal and is considered as a noise factor when setting the minimum threshold levels of the phase selector.

Discrete transposition using three line sections equalises the magnitude of the noise signal produced by a fault involving either phase in either section. However, for the non-transposed system, due to the horizontal line construction, a fault involving the "c"-phase and earth results in spill output magnitude comparable to the ideal case. This effect is clearly seen in Fig 6.14 and is explained by the fact that with respect to the "c"-phase, the healthy phases are equidistant and therefore display similar mutual coupling.

The variation of the discriminant signals during the initial fault period for each transposition case considered is almost identical.

The phase selector designed for use with the discretely transposed system can therefore be equally applied to an untransposed system without loss of UHS phase discrimination. However, the noise content in the discriminant signals is greater for non-transposed systems. Furthermore, the noise amplitude is dependent upon the line lengths and source short circuit levels involved. Hence, when applying the phase selector to non-transposed systems and higher source capacities it may be necessary to slightly increase the minimum threshold levels.

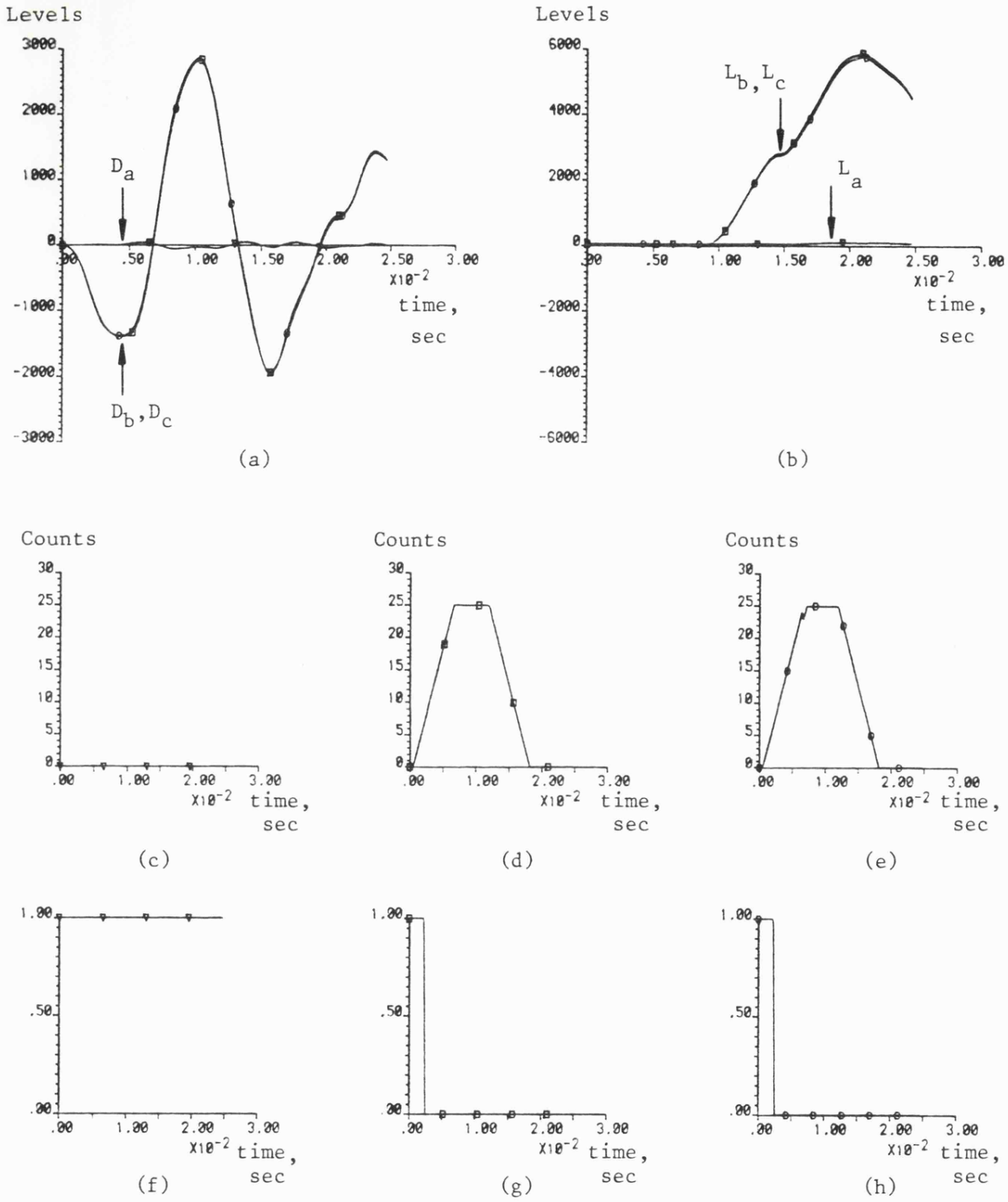

Fig 6.1 Signal variations at various stages within the phase selection process during "a"-earth fault condition

- 4 section feeder, X_F = 10km; R_F = 0.5 ohms
- Shunt compensated; discretely transposed
- Fault at peak of prefault faulted phase voltage

(a) Discriminant signals (b) Dynamic threshold levels

(c), (d), (e) Outputs from event counters (EC_a, EC_b, EC_c)

(f), (g), (h) Outputs from tripping logic (T_a, T_b, T_c)

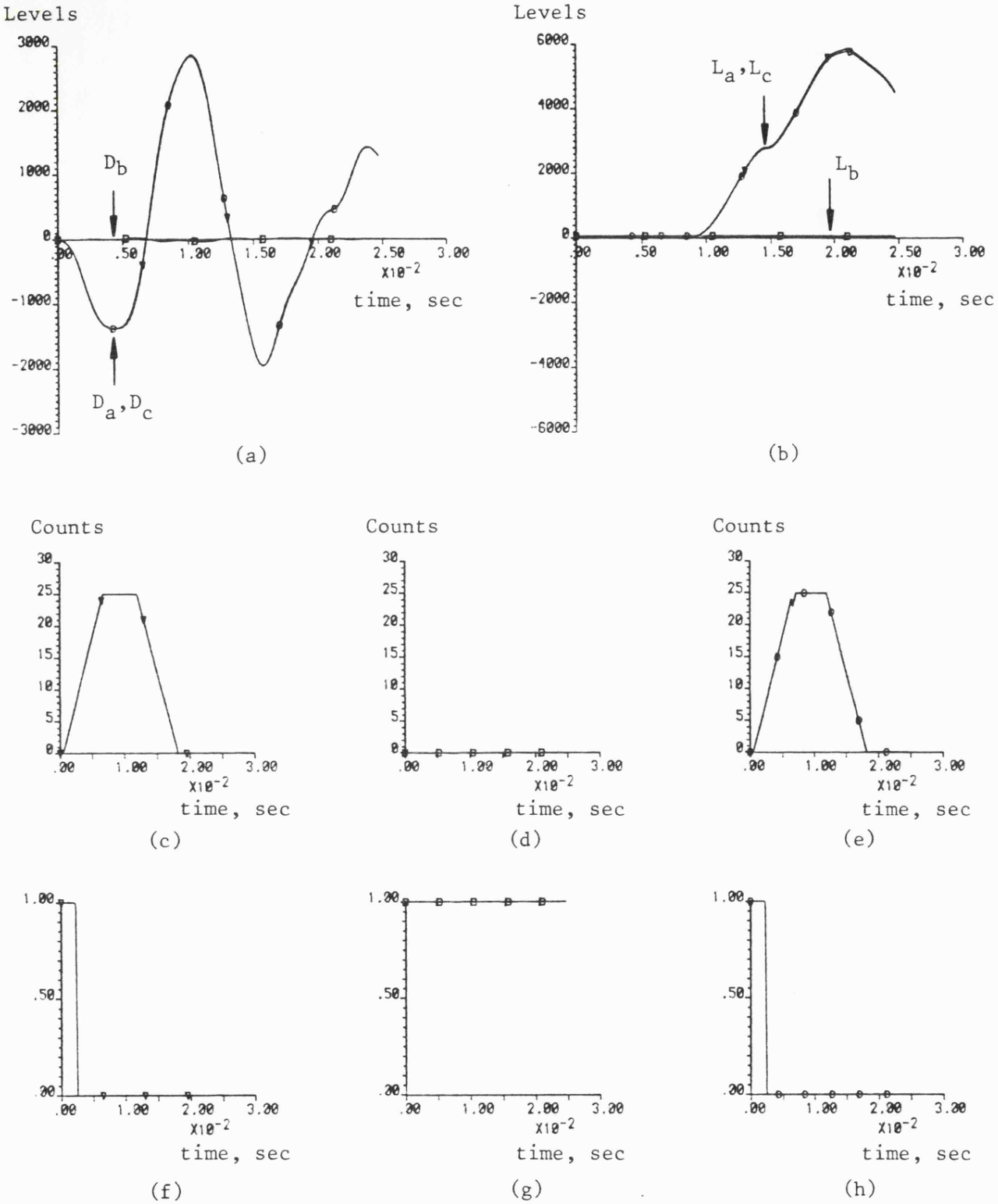

Fig 6.2 Signal variations at various stages within the phase selection process during "b"-earth fault condition

- Fault conditions as stated in Fig 6.1

(a) Discriminant signals (b) Dynamic threshold levels

(c), (d), (e) Outputs from event counters

(f), (g), (h) Outputs from tripping logic

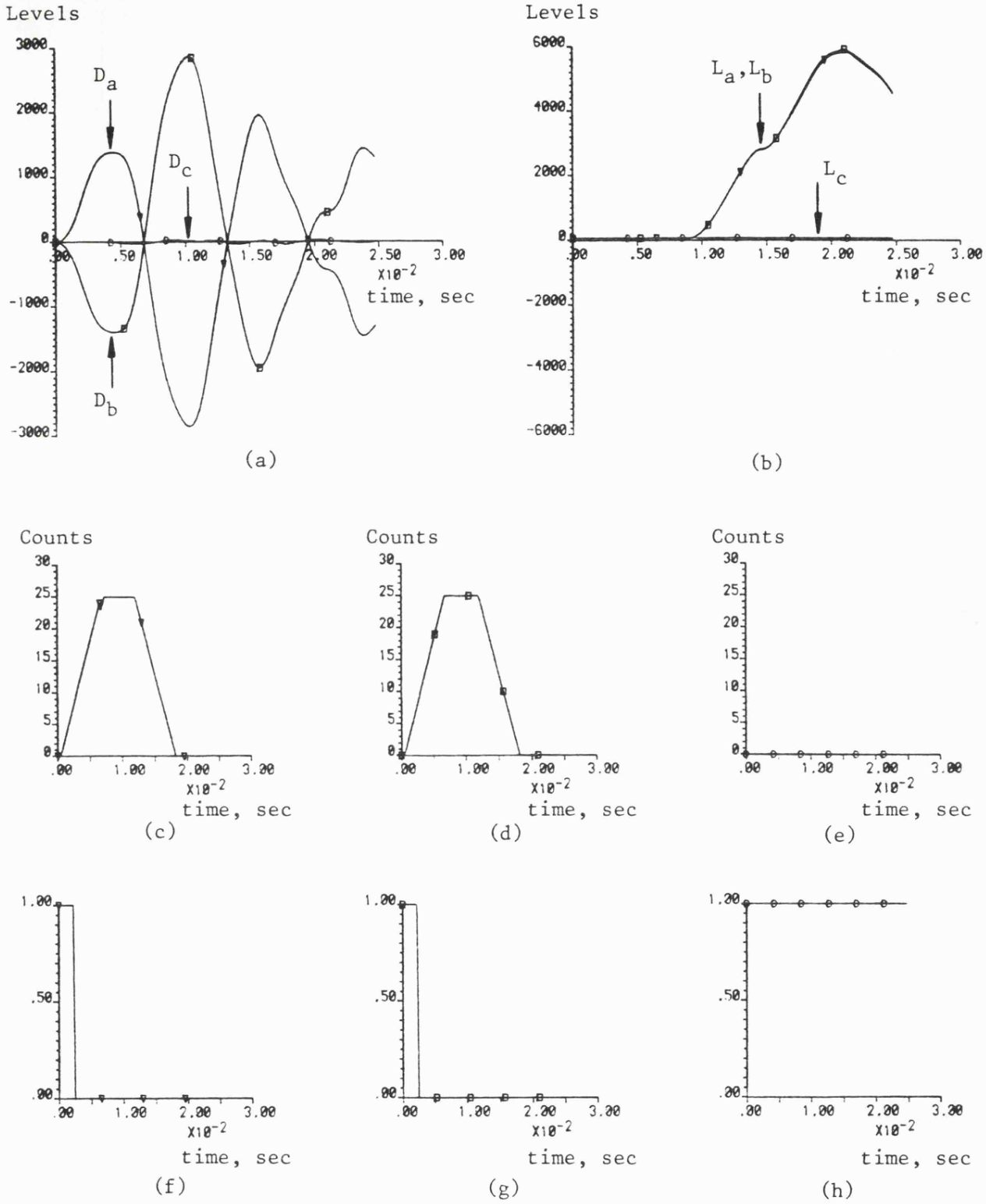

Fig 6.3 Signal variations at various stages within the phase selection process during "c"-earth fault condition

- Fault conditions as stated in Fig 6.1.

(a) Discriminant signals (b) Dynamic threshold levels

(c), (d), (e) Outputs from event counters

(f), (g), (h) Outputs from tripping logic

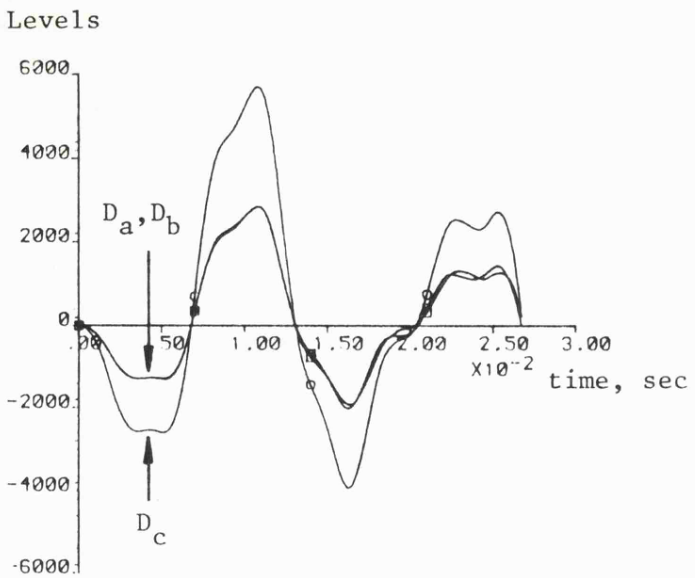

(a)

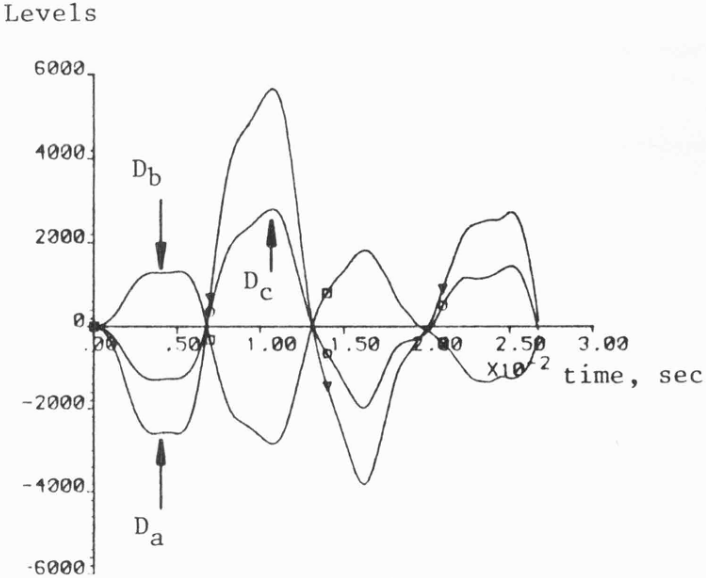

(b)

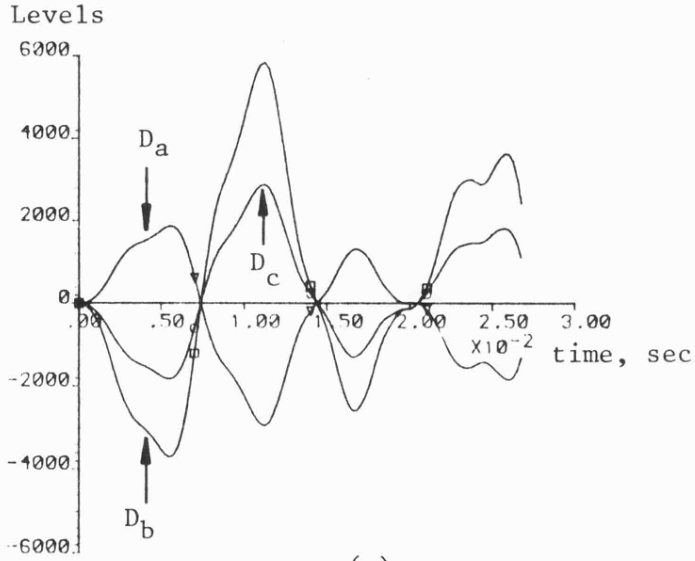

(c)

Fig 6.4 Response of phase to earth discriminant signals during interphase faults

- Same fault conditions as in Fig 6.1
- Fault at peak of prefault interphase voltage

(a) "a"-"b" fault

(b) "b"-"c" fault

(c) "c"-"a" fault

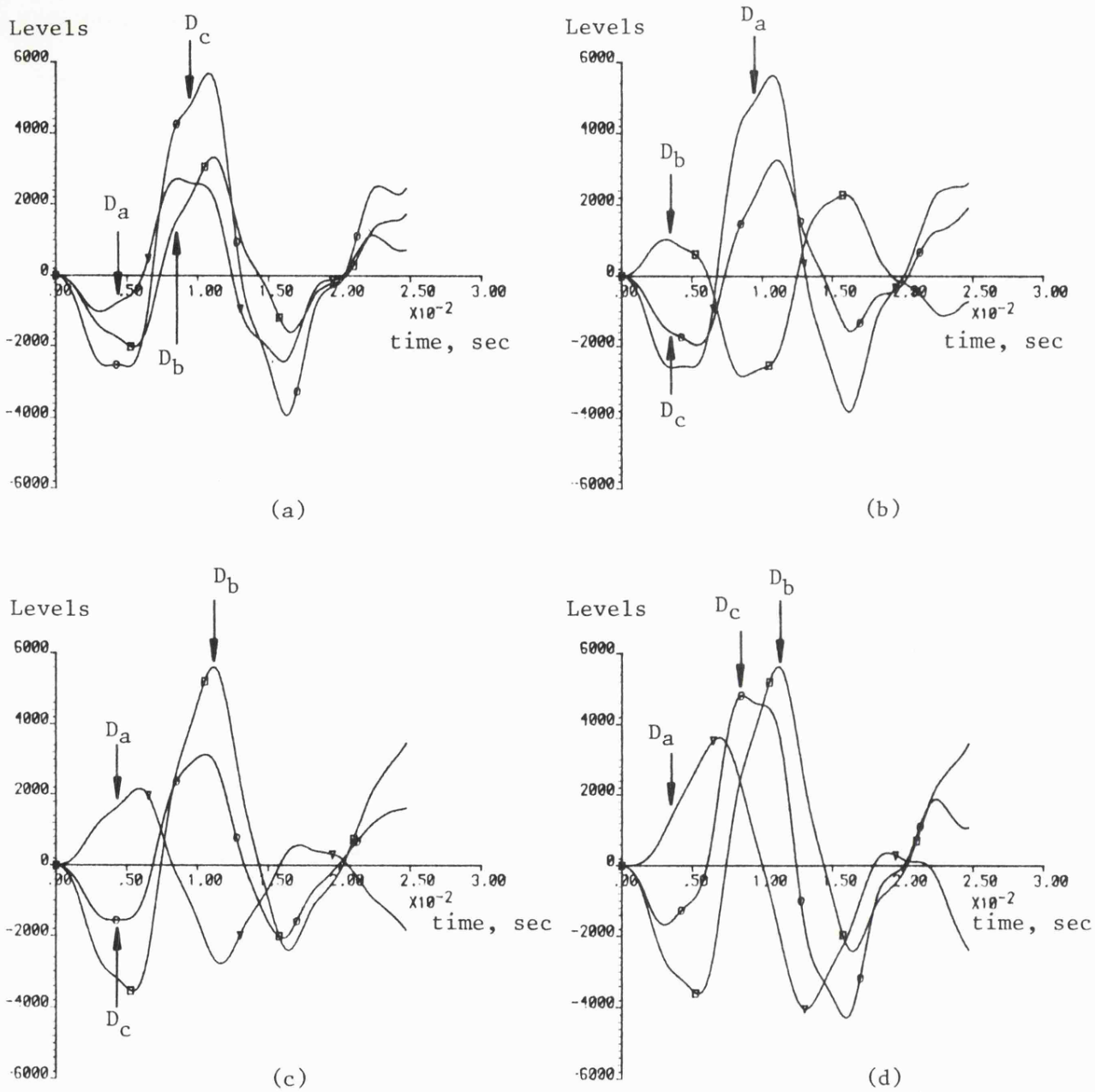

Fig 6.5 Response of phase to earth discriminant signals during phase to earth and three phase faults

- Same fault conditions as in Fig 6.4.

(a) "a"-"b"-e fault

(b) "b"-"c"-e fault

(c) "c"-"a"-e fault

(d) Three phase fault; fault inception at peak of prefault "a"-e voltage.

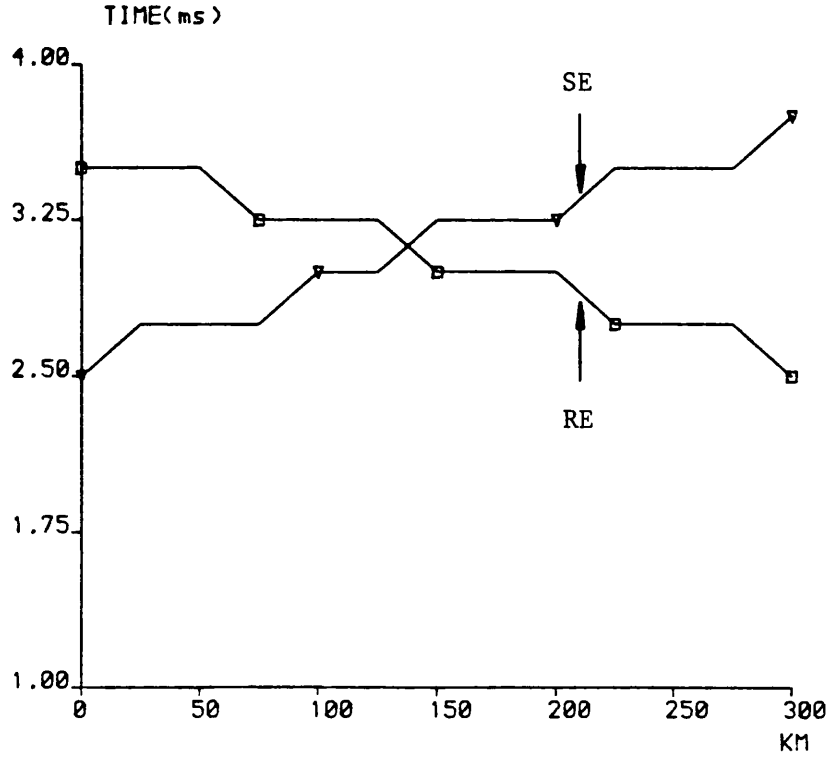

(a)

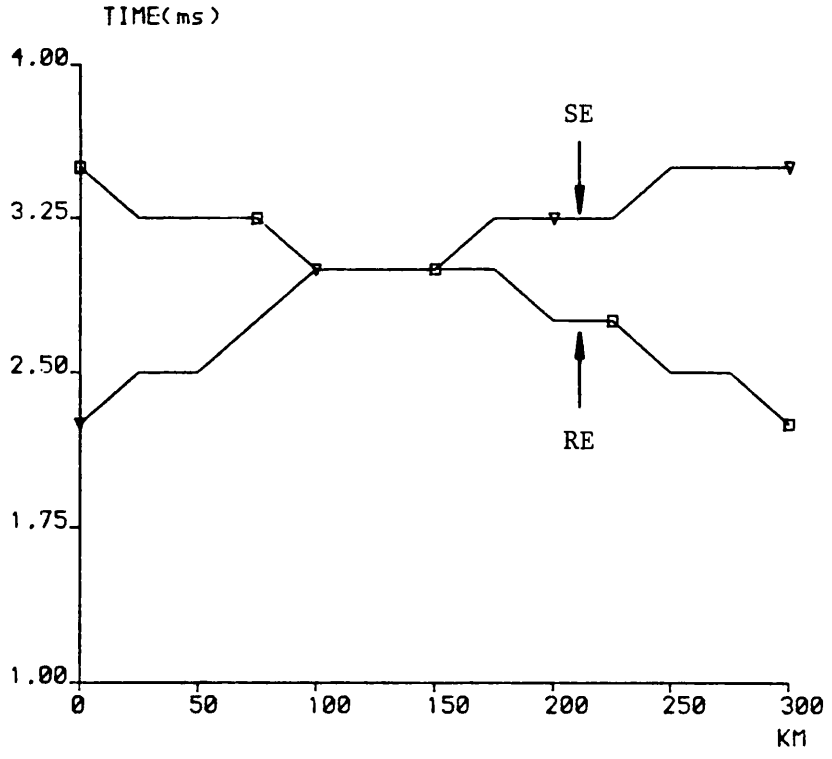

(b)

Fig 6.6 Phase selector operating time, time/fault position characteristic for single phase to ground fault

- 4 section-feeder; shunt compensated; discretely transposed;
- Fault type, "b"-e

(a) Fault inception at zero prefault "b"-earth phase voltage

(b) Fault inception at peak of prefault "b"-earth phase voltage

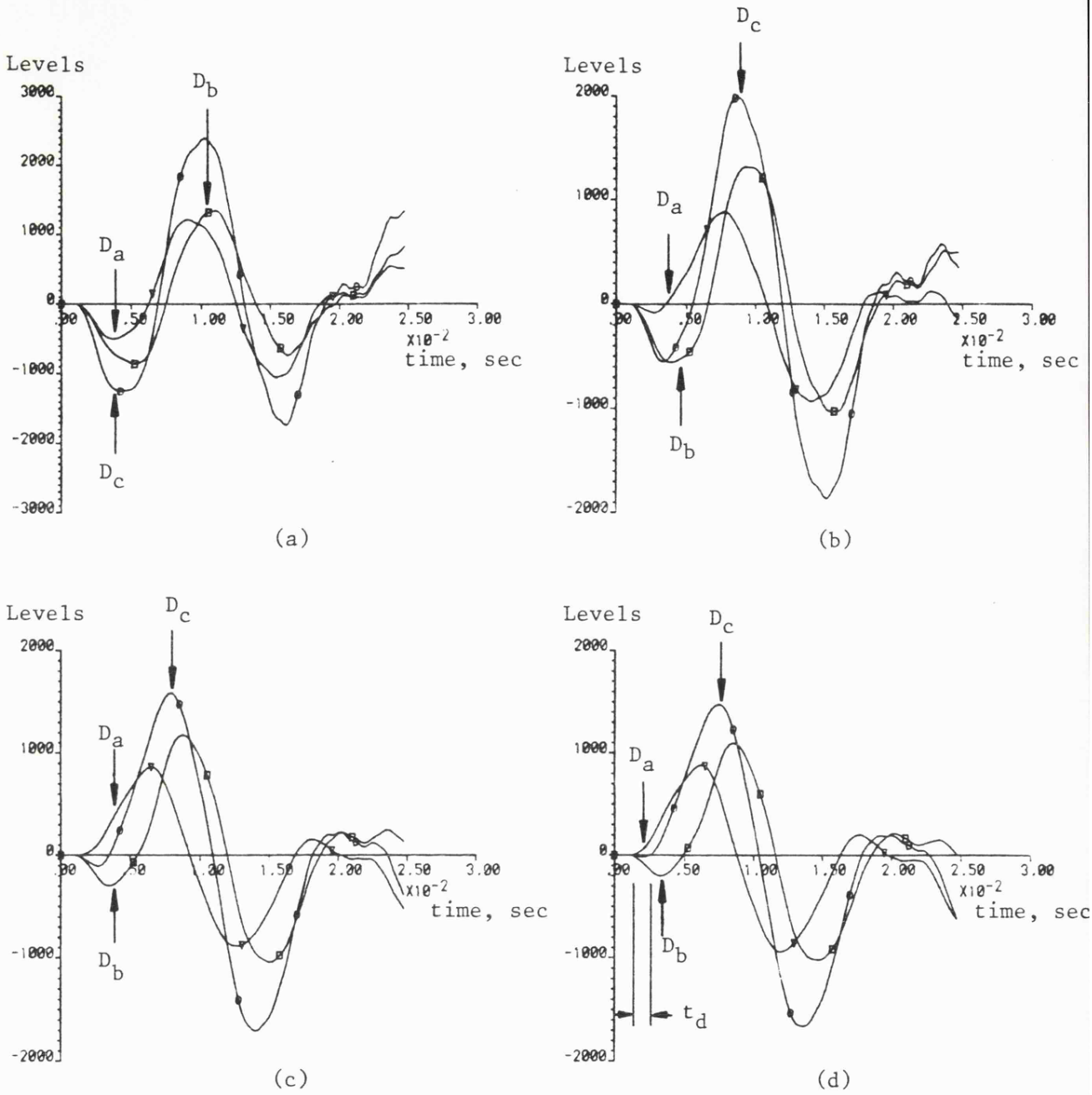

Fig 6.7 Behaviour of phase to earth discriminant signal for different fault inception instances during double phase to earth faults

- 4 section feeder; shunt compensated; discretely transposed
- Fault type "a"-"b"-e; X_F = 300km
- Fault inception instances on prefault voltage between phases "a" and "b"

(a) 90°

(b) 135°

(c) 160°

(d) 170°

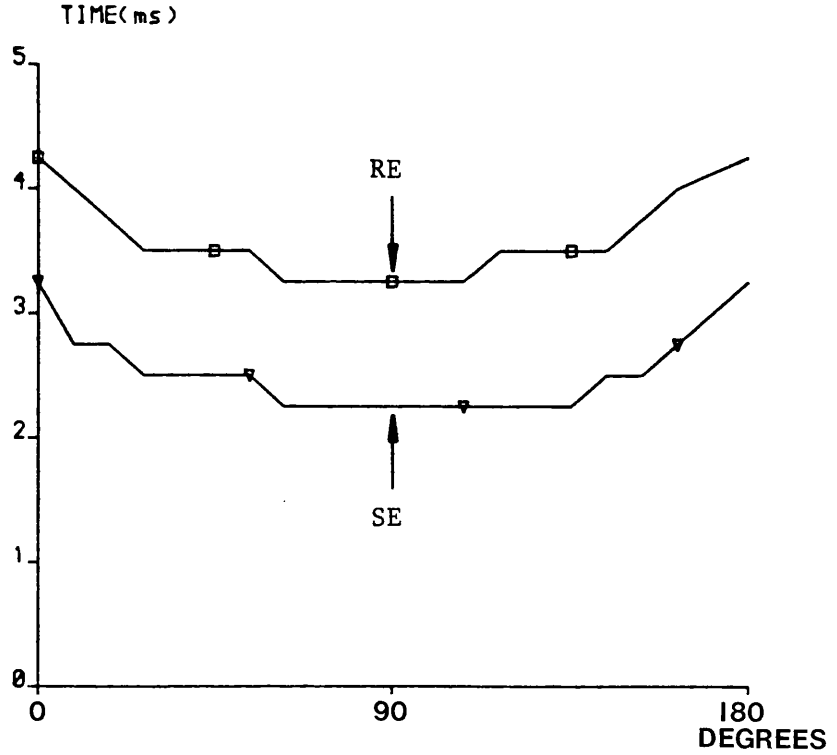

(a)

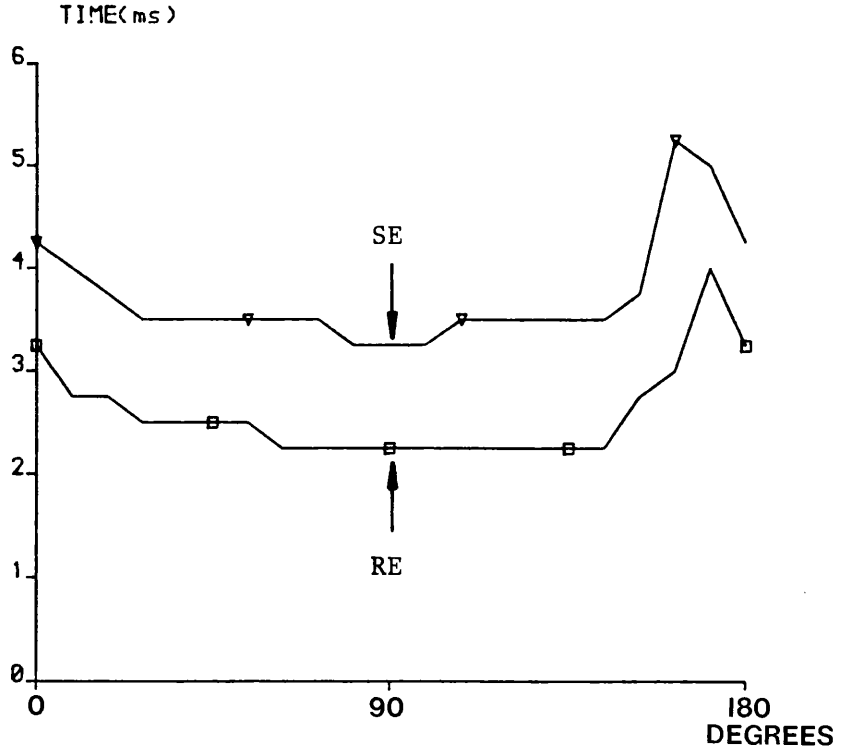

(b)

Fig 6.8 Phase selector operating time-fault inception angle characteristic for single phase to ground faults

- 4-section feeder; shunt compensated; discretely transposed;
- Fault type "a"-e fault

(a) Distance to fault, X_F = 0.0 km

(b) Distance to fault, X_F = 300 km

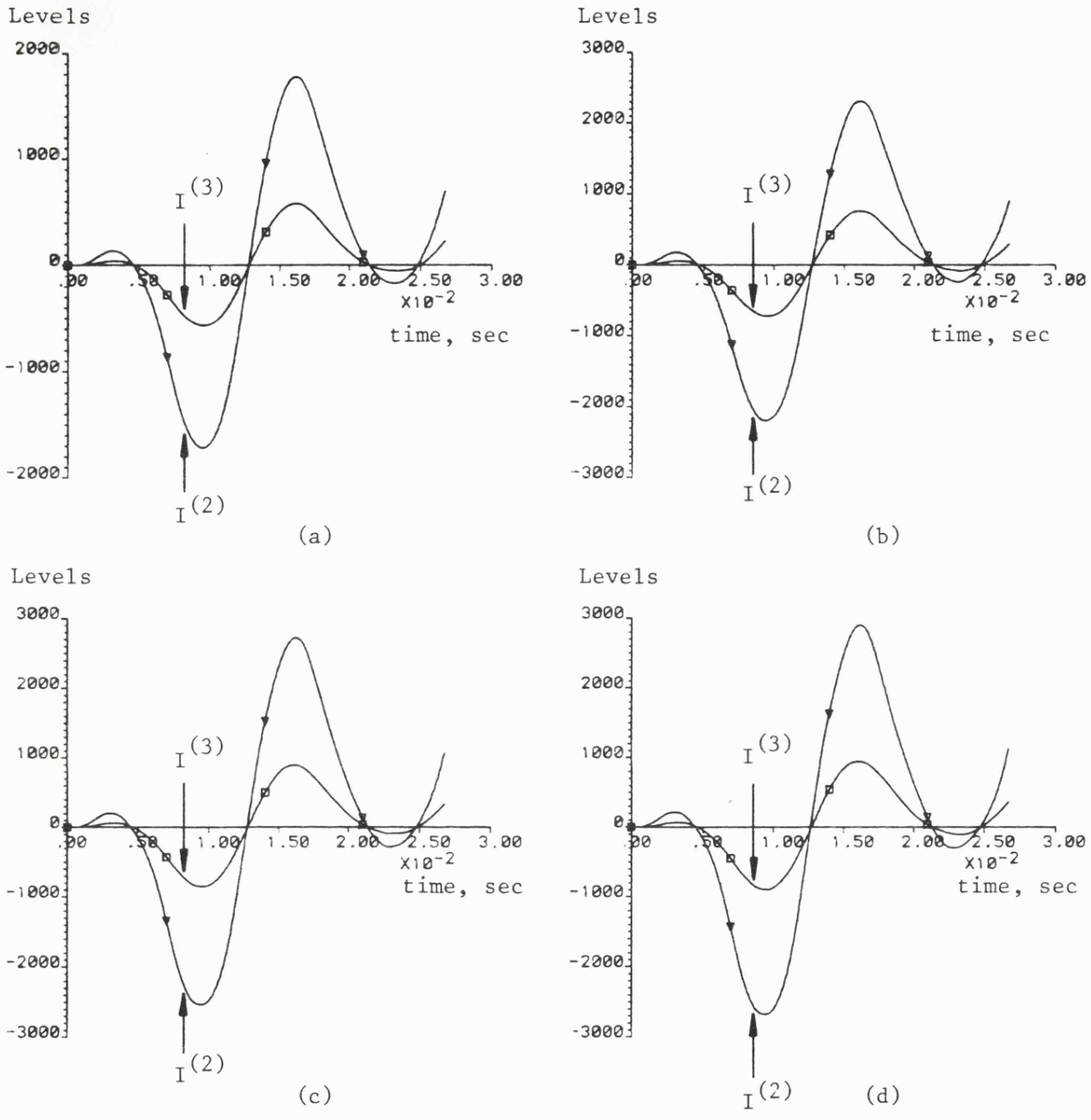

Fig 6.9 Filtered modal superimposed currents

- 1 section feeder; shunt compensated; discretely transposed
- line length, L = 300km; X_F = 150km; ZSO/ZS1 = 1
- fault type "a"-e
- fault inception at 150° of prefault "a"-earth phase voltage
- Receiving end source capacity fixed at 1GVA
- Sending end source capacities

(a) 5GVA (b) 10GVA
(c) 20GVA (d) 30GVA

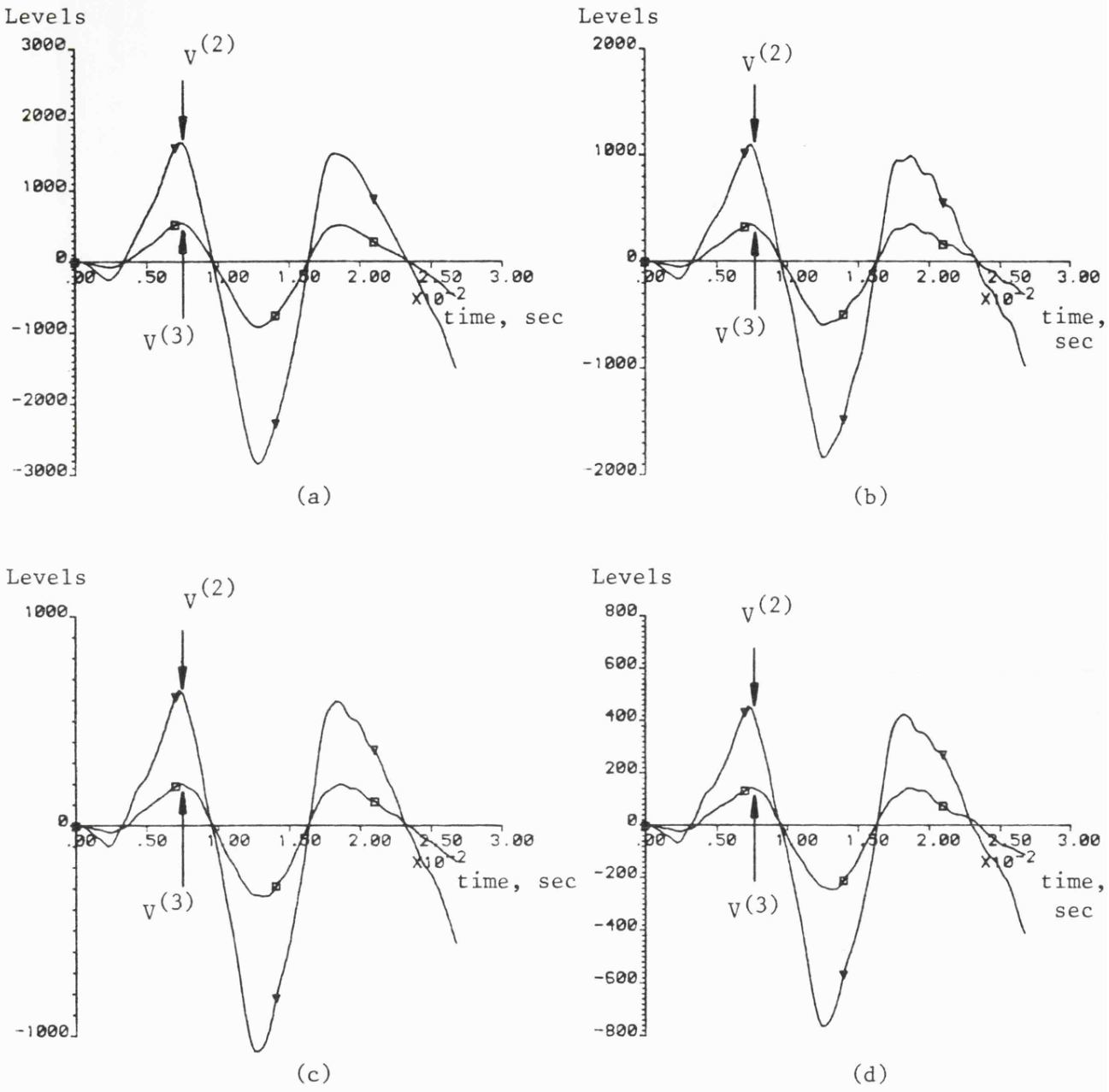

Fig 6.10 Filtered modal superimposed voltages

- Similar fault conditions as in Fig 6.9

(a) 5 GVA

(b) 10 GVA

(c) 20 GVA

(d) 30 GVA

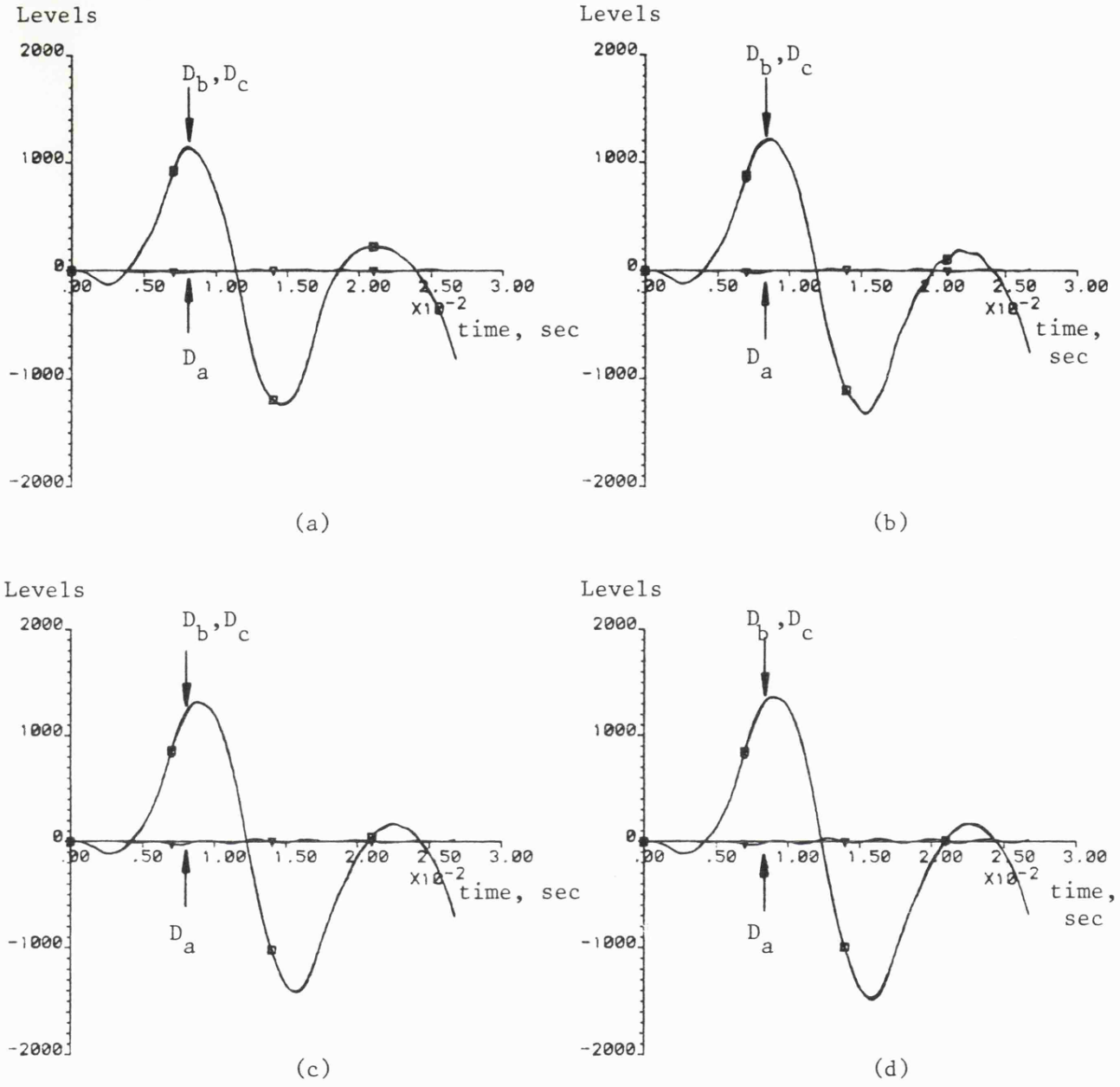

Fig 6.11 Variation of discriminant signals derived from superimposed components of Figs 6.9-6.10

- Similar fault conditions as in Fig 6.9

(a) 5 GVA

(b) 10 GVA

(c) 20 GVA

(d) 30 GVA

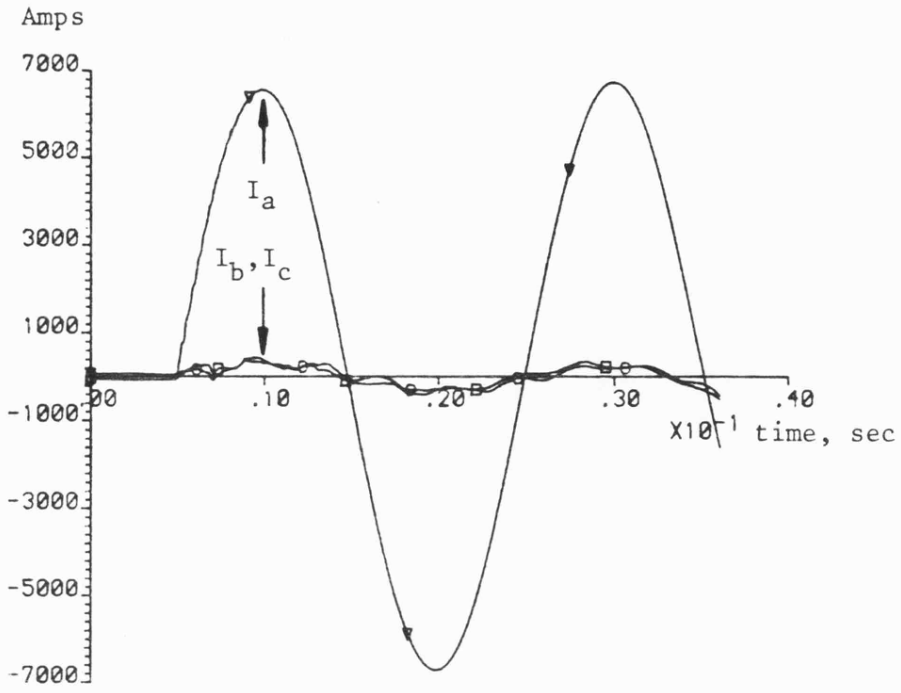

(a)

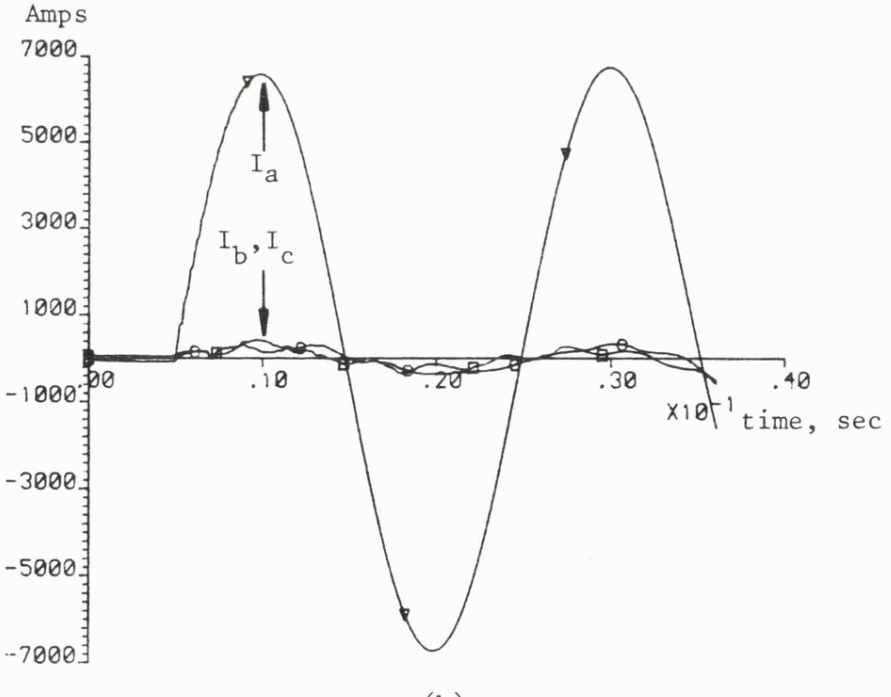

(b)

Fig 6.12 Initial phase current variations under "a"-to earth fault conditions

- 1 section feeder; line length L = 300km; X_F = 25km shunt compensated; source capacities at both ends, 5GVA; ZS0/ZS1 = 1.
- Fault inception angle at peak of prefault "a"-e phase voltage

(a) Discretely transposed

(b) Non-transposed

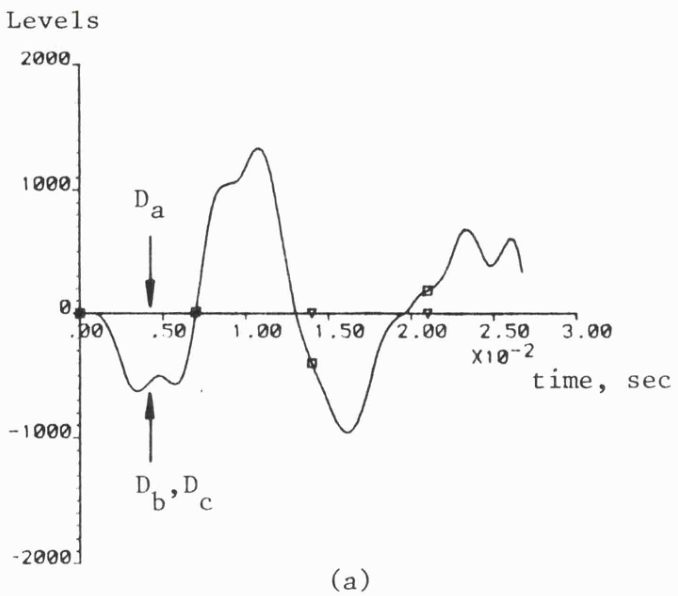

(a)

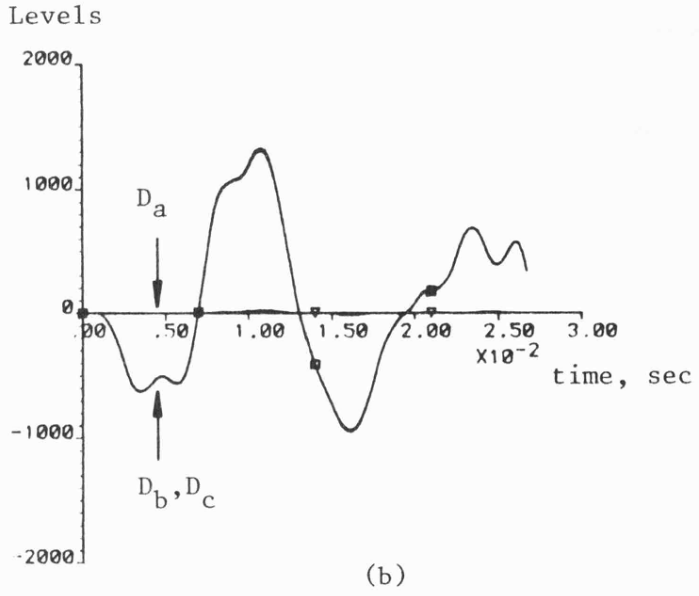

(b)

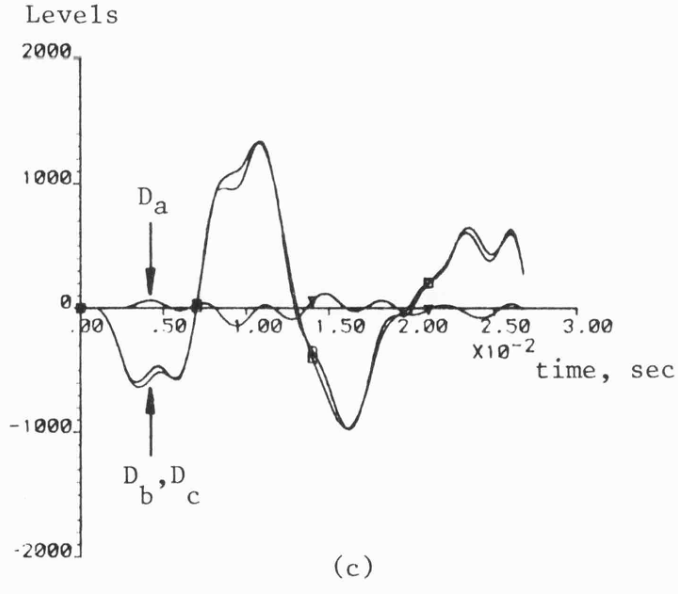

(c)

Fig 6.13 Discriminant signal behaviour during "a"-e fault conditions for the three transposition conditions under consideration

- X_F = 275 km; shunt compensated
- Same fault conditions as in Fig 6.12

(a) Ideally transposed

(b) Discretely transposed

(c) Non-transposed

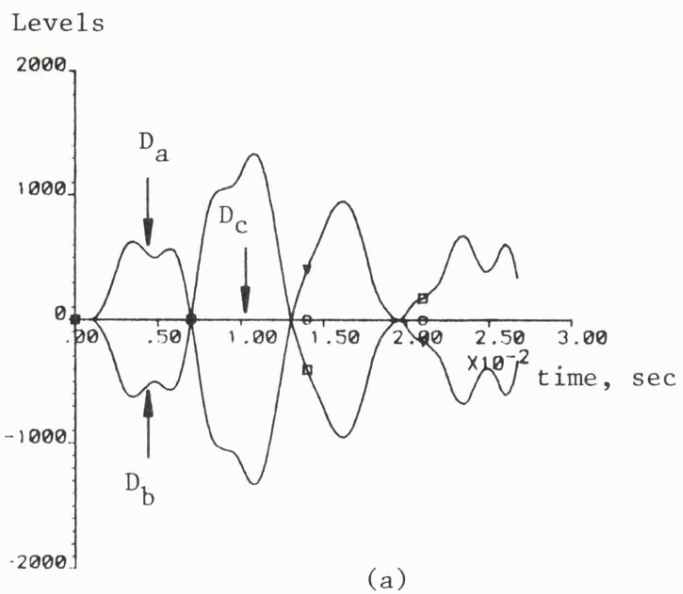

(a)

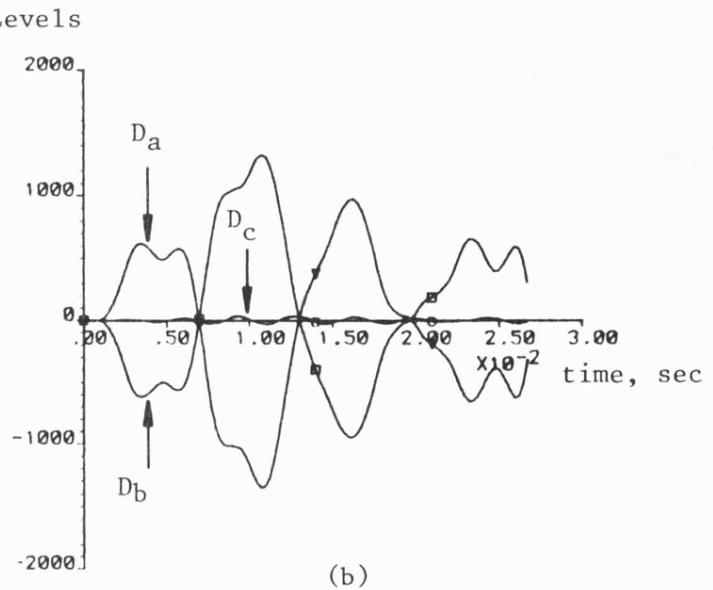

(b)

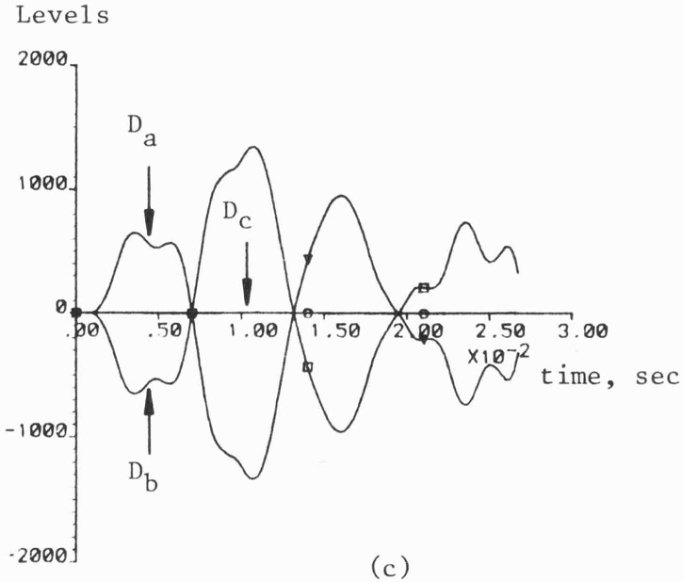

(c)

Fig 6.14 Discriminant signal response during "c"-e fault conditions for the same fault conditions as in Fig 6.13.

(a) Ideally transposed

(b) Discretely transposed

(c) Non-transposed

CHAPTER SEVEN

OPERATION OF THE PHASE SELECTOR UNDER ABNORMAL OPERATING CONDITIONS

7.1 Performance for Very High Resistance Earth Faults involving SPA

Many power transmission networks are routed over geographical locations which encourage high resistance faults, particularly through vegetation. The conventional impedance type selectors discussed in Chapter 2 are limited by the range of impedance that can be measured and hence by the effective fault path resistance. The magnitude of fault induced superimposed components is still somewhat limited by the fault resistance in that components detected at relay locations are greatly reduced. There must therefore be a definable limit on the size of fault resistance that produces detectable superimposed components for relaying purposes.

The main directional wave detector relies for its operation upon the superimposed voltage and current components, each of which must be above a minimum value for reliable operation[23]. This is summarised in the simplistic sensitivity diagram of Fig 7.1.

The phase selector here proposed has a subtle advantage over the main relay, in that its operation is guaranteed even with the absence of either voltage or current. In other words, a minimum level of either the voltage or the current is sufficient to ensure reliable phase selection. With respect to the sensitivity diagram of Fig 7.1,

the only restricted area of operation for the selector is that below V_{min} and I_{min}, namely area A. In terms of fault resistance coverage capability, the phase selector is not only superior to impedance based equipment, but even surpasses the remarkable performance of the main directional wave detector.

7.1.1 Case for phase to earth fault

To establish the performance of the phase selector under very high resistance faults, the specific model of a four section shunt compensated system described in Chapter 5 is used. The faults simulated are internal to the protection equipment and involve resistances up to 600Ω. This is the maximum fault resistance considered, since it was thought to be well above the capability of the main relay.

The variation of the selector discriminant signals as the fault resistance is increased, is shown in Fig 7.2. As expected, the signal magnitudes are greatly reduced due to the very high fault loop impedance. However, as shown in Fig 7.3, UHS operation is maintained over the range of 0 to 600Ω by the selection equipment at either end. Furthermore, the results achieved are for zero point on wave fault inception angles, which are found to cause the slowest operating times for the particular system studied. The discrepancies between operating times at each end are explained by the fact that different effective short circuit level and hence impedances are presented to each relaying point.

For faults applied near busbar S (Fig 7.3(a)), the local selector operates quicker than that of the remote end (R), but as shown in Fig 7.3(b), the situation is reversed for faults near (R). These results show clearly that despite minor variations in operating times, the range of fault resistance coverage is not restricted by the change in fault position nor the change in equivalent source impedance.

For the cases of earth faults involving the "b" and "c" phases respectively, similar operating characteristics are obtained.

7.1.2 Case for double phase clear of ground faults

By comparison with the results obtained in the above tests, the double phase clear of ground faults yield faster operating times over the entire fault resistance range. This is anticipated, since larger modal components are generated by the line voltages involved. Fig 7.4 shows the selector performance at end S and R, with a similar fault resistance/operating time characteristic as for the phase to ground case.

7.1.3 Case for double phase faults involving ground

The selector incorporates some delayed decision logic circuitry to cater for double phase to ground point on wave variation, as described in both Chapters 4 and 6. For such types of fault, one particular discriminant signal can remain below the threshold level for some time and subsequently exceed it. The delay in signal increase is very much dependent upon the fault inception angle and

upon the amount of fault path resistance. For very high resistance faults (greater than 300Ω), this signal can remain low for a period long enough for the selector to initially give an incorrect selection. However, given the appropriate delay mentioned above, correct re-selection is made to trip all three phases as required by this scheme.

Fig 7.5 shows the delays in signal rise for resistances of zero and 300Ω. It can be seen that after a certain amount of time, all of the discriminant signals exceed the threshold and a correct decision is possible. Hence, by introducing extra delay in the decision logic circuitry, it is possible for coverage of high resistance double phase to earth faults to be extended beyond 300Ω. However, a fixed delay of this type will impair the earth fault performance of the selector and for this particular system, coverage of 300Ω fault resistance for double phase to earth faults was considered more than adequate.

Studies have revealed that for any two ended system employing communication links, with channel delays greater than 5ms, the selector will override its initial decision and security of operation is maintained. The only possible flaw of this scheme, for double phase, very high resistance earth faults, is therefore when it is implemented with UHS communication equipment (fibre optics). Fig 7.6 shows the operating characteristics of the selector at each end whereby correct phase selection is made for faults up to 600Ω at the corresponding times.

7.2 Behaviour of the Phase Selector for Evolving Faults

7.2.1 Definition and requirements for evolving faults

An evolving fault can be defined as a changing fault condition which takes place before any circuit breaker reclosing is initiated, and three phase tripping with lockout is required whatever the fault evolves into. Any new fault condition is regarded as a completely separate fault condition if it occurs after a successful reclosure operation. During the dead time of a single phase auto-reclosure cycle, if the fault evolves, ie. another phase is faulted, the remaining two poles must be tripped and all poles locked out.

7.2.2 Case of single phase to earth evolving faults

Statistics show that evolving faults originate as fault between one phase and earth, possibly developing into faults involving one or both of the other phases. If single phase to earth faults can be dealt with quickly, then the development of more extensive faults can be prevented and the damage and disturbances to the system limited.

Under evolving fault conditions, the relaying point quantities will obviously undergo changes which are constantly monitored by the individual dynamic threshold levels of each discriminant signal. For the case of a single phase to earth fault, the relevant discriminant signal indicating the faulted phase remains below the threshold for the whole recovery period of the selector. When an evolving fault condition arises, the discriminant signal which indicated the initial faulted phase then exceeds the threshold level and re-selection is made to trip all three phases.

The majority of evolving faults occur from a single phase to earth fault condition and before any pole is opened. To study the behaviour of the selector under such conditions, the case of an "a" phase to ground followed by a "c" phase to ground fault is considered. The general system model described in Chapter 5 has the versatility of being able to simulate faults at any instant of time, on either line section PQ or QR. For the purpose of simulating an evolving fault condition, particularly with regard to relaying equipment at end P, the line section OR is reduced to a very small length of 0.5km. Looking from P towards Q, an "a"-phase to earth fault on section PQ very close to Q, followed by a "c"-phase to earth fault just beyond Q on section QR, adequately simulates the evolved fault condition required (see Fig 7.7).

The decision logic circuitry permits a minimum selector operating time of 2ms. For an evolving fault condition, with less than 2ms between faults, it is therefore possible that the selector may give a three phase tripping output for the whole observation period. Fig 7.8 shows the results achieved for a fault time difference of 1.8ms. Each discriminant signal is seen to increase almost simultaneously after the first fault inception and the selector accordingly indicates a three phase trip condition. As the fault time stagger is increased to 5ms, it is seen from Fig 7.9 how the selector at first indicates that the "a"-phase is faulted by giving low trip outputs for the "b" and "c" phases. Upon the inception of the "c" phase fault, re-selection to a three phase trip condition is made. To verify that even a greater time stagger between faults does

not cause selector mal-operation, Fig 7.10 shows the results achieved for a 25ms fault time difference. Fig 7.10(a) and 7.10(b) display the actual discriminant signals $D_{a,b,c}$ and the associated dynamic threshold levels respectively. The threshold level which responds to the variation in the discriminant D_a, is seen to remain low until a short time after the instant of second fault inception. As explained in Chapter 4, this delayed action in the initial fault period allows the selector maximum sensitivity for the detection of the evolved "c" phase to earth fault. Therefore, as soon as the second fault occurs, the discriminant D_a exceeds its minimum threshold level and as shown in Figs 7.10(c) and 7.10(d), re-selection is made as in the previous case.

The selector has been proven to operate correctly for evolving fault conditions. In some situations, however, single pole opening for the initial faulted phase is effected before the second fault occurs.

At present, the simulation is limited to the modelling of a single fault condition with associated single pole opening, without any further system disturbances. Therefore, exact evaluation of the performance when subjected to evolving fault conditions described above is not currently possible.

7.3 Phase Selection for Different Types of Fault with Star/Delta Transformer Source Connection

Particular abnormal fault conditions of interest are those which do not give rise to aerial mode current components and which occur for certain system and fault conditions. It is necessary to establish if the phase selector proposed will operate under such conditions since its basic principle of operation involves the use of aerial mode components alone.

Fig 7.11 shows a system fed by a lumped source with its remote end connected to an open circuit star/delta transformer. During fault conditions on the line, the situation described above gives rise to only earth mode current at the load end. This situation is described as a 1,1,1 case whereby the superimposed phase currents produced at the load end are equal in magnitude and co-phasal. Hence the selector at this end will only receive zero sequence current components, equally distributed on the three phases.

For the case of an "a" to earth fault on the line, the modal interconnection diagram of Fig 7.12 permits a better understanding of the behaviour of modal components during the faulted period. The absence of mode-2 and mode-3 current is simulated by the open switches at the load side, but, as seen from Fig 7.12, this does not prevent the generation of aerial mode voltage components at that end.

In practice, several transformer banks may be connected to the load end busbars at any time. A consideration of the effective short circuit level (s.c.l.) of each bank will yield values of zero sequence source impedance (ZSO) necessary for the simulation program. The range of s.c.l. taken for this particular system varies between 1GVA and 5GVA.

Figs 7.13 show the load end relaying point quantities for the case of a "b"-phase to earth fault at near zero prefault "b"-phase voltage. Clearly seen is the similarity in the three line currents giving rise to no aerial mode current components (Fig 7.13(b)). The variation of both mode-2 and mode-3 voltage is shown in Fig 7.13(c), which causes the discriminant signals to behave in the manner indicated by Fig 7.13(d). Correct selection of the faulted "b"-phase is made since the discriminant signal D_b remains low whilst D_a and D_c exceed their corresponding threshold levels. The above results apply to an effective load side s.c.l. of 5GVA and Fig 7.14 displays the corresponding results for a "c"-phase to ground fault involving a reduced load capacity of 1GVA. The signal behaviour is seen to be very similar to the previous case and permits correct selection of the faulted phase to be made as before.

The two cases studied above, further illustrate the versatility of a selector based upon composite signals of aerial mode voltage and current. It is therefore envisaged that a phase selector of the type proposed here can offer high standards of performance for a wide range of system configurations and abnormal fault conditions.

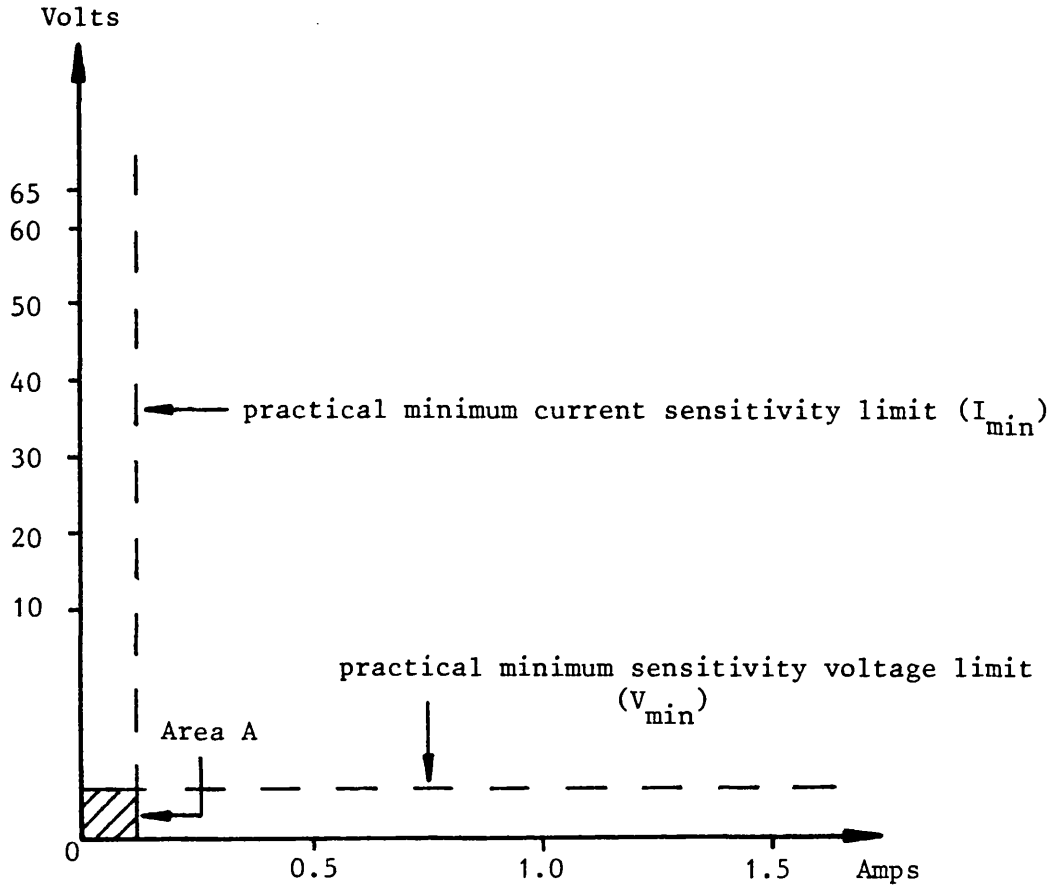

Fig 7.1 Simplistic sensitivity diagram for main directional comparison relay

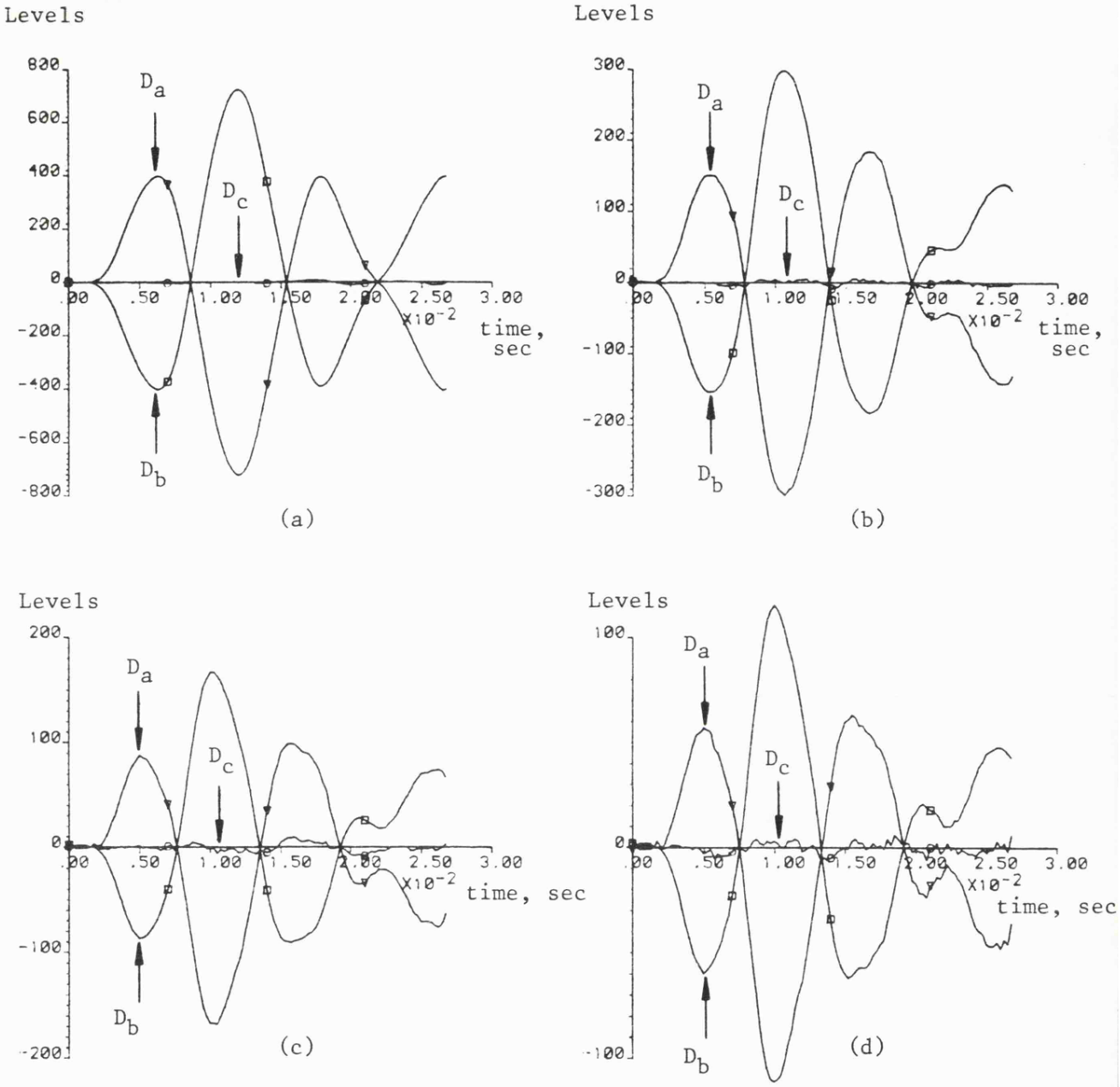

Fig 7.2 Behaviour of phase selector discriminant signals during "c" to e fault conditions involving different values of fault path resistance

- 4 section feeder; shunt compensated; discretely transposed
- X_F = 300km
- Fault inception angle at zero prefault of "c"-earth phase voltage
- Fault resistance values, R_F

(a) 50Ω

(b) 200Ω

(c) 400Ω

(d) 600Ω

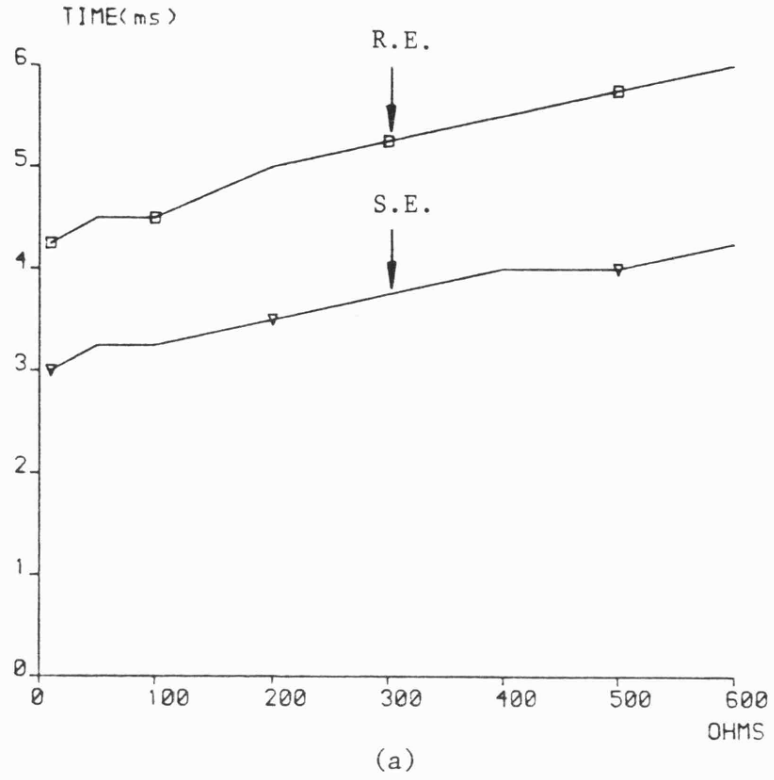

(a)

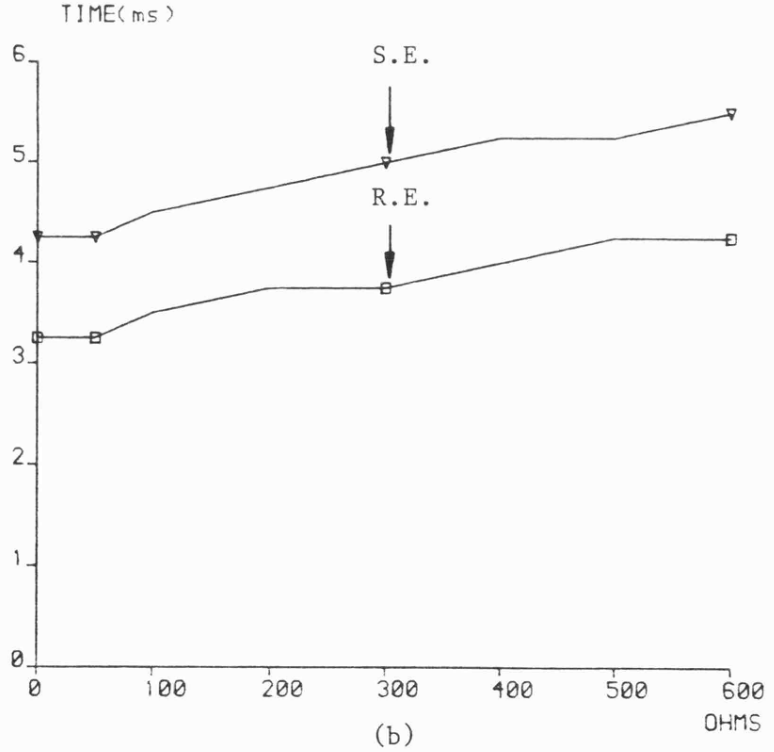

(b)

Fig 7.3 Phase selector operating time/fault resistance characteristic for single phase to ground faults

- Similar fault conditions as in Fig 7.2

(a) Distance to fault, X_F = 0km

(b) Distance to fault, X_F = 300km

sending end

receiving end

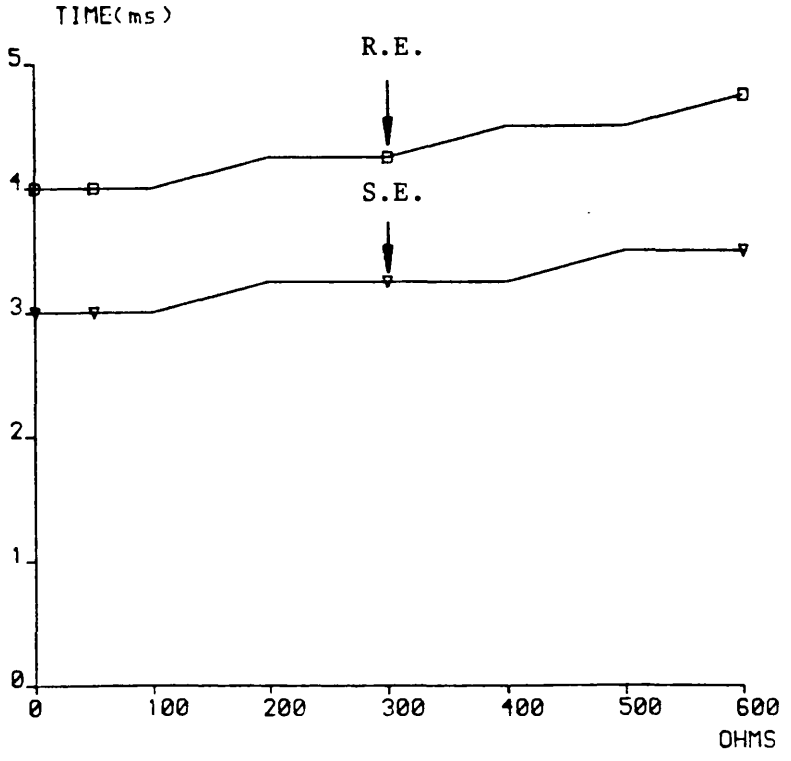

(a)

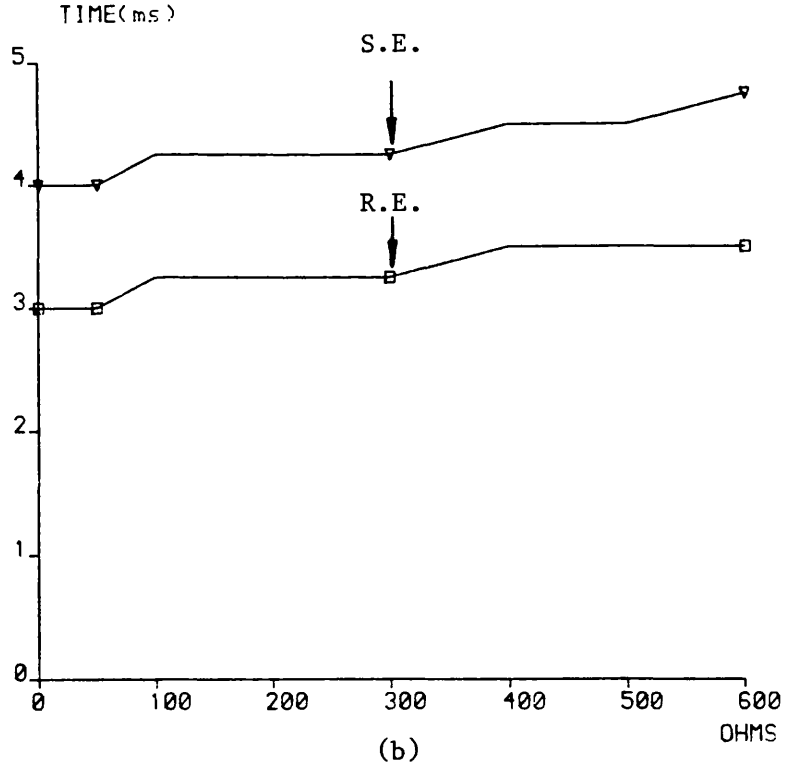

(b)

Fig 7.4 Phase selector operating time vs fault resistance characteristic curve for interphase faults

- 4 section feeder; shunt compensated; discretely transposed
- Fault type considered "a"-"b"
- Fault inception angle at zero prefault of voltage between phase "a" and "b"

(a) Fault distance, X_F = 0km

(b) Fault distance, X_F = 300km

sending end

receiving end

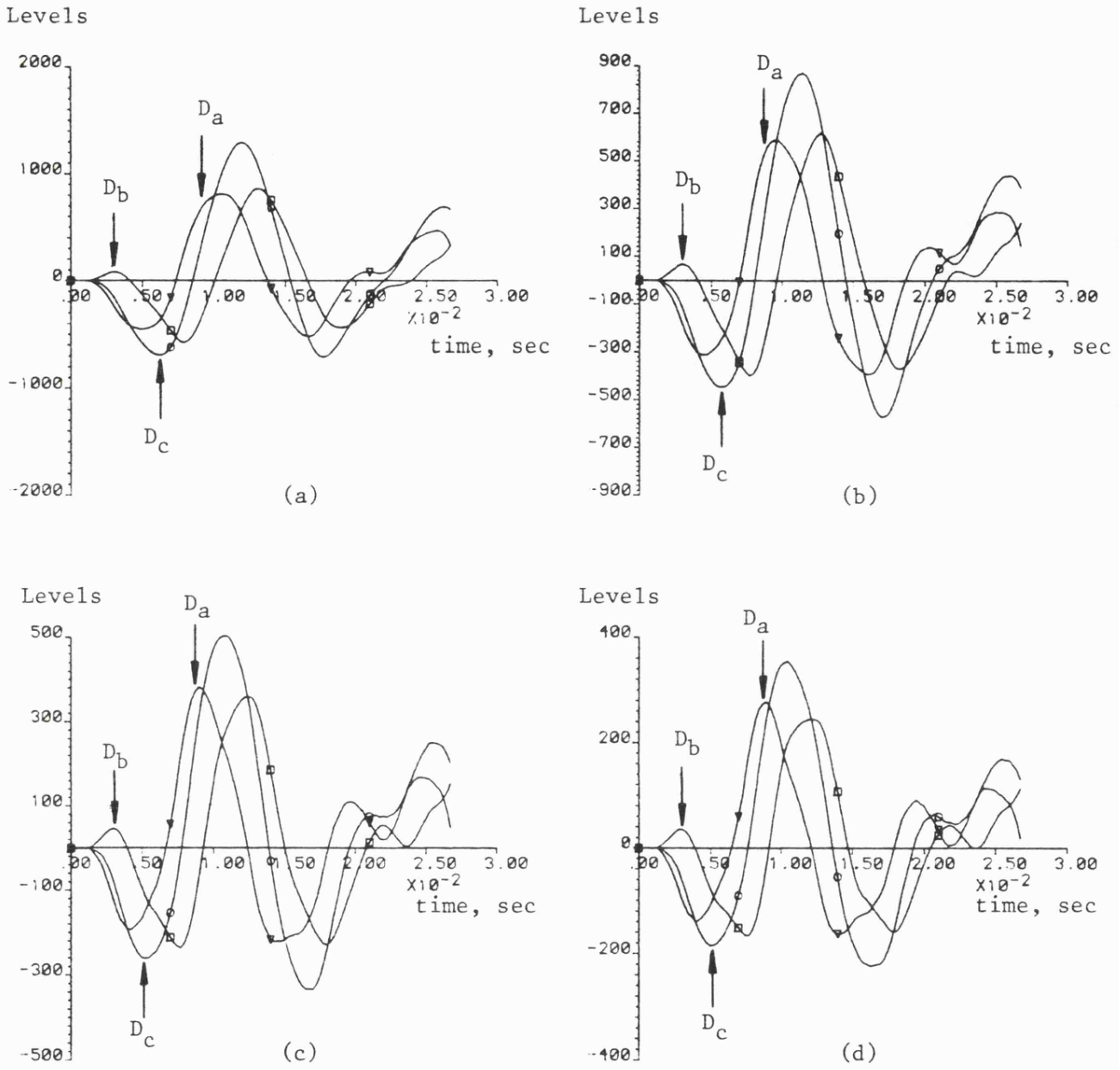

Fig 7.5 Phase to earth discriminant signal variations during double phase to earth fault conditions for different values of resistance in the fault path

- 4 section feeder; shunt compensated; discretely transposed
- Fault considered "a"-"b" to earth
- Fault inception angle at zero prefault of voltage between phases "a" and "b"
- Fault resistance varation

(a) R_F = 50Ω

(b) R_F = 100Ω

(c) R_F = 200Ω

(d) R_F = 300Ω

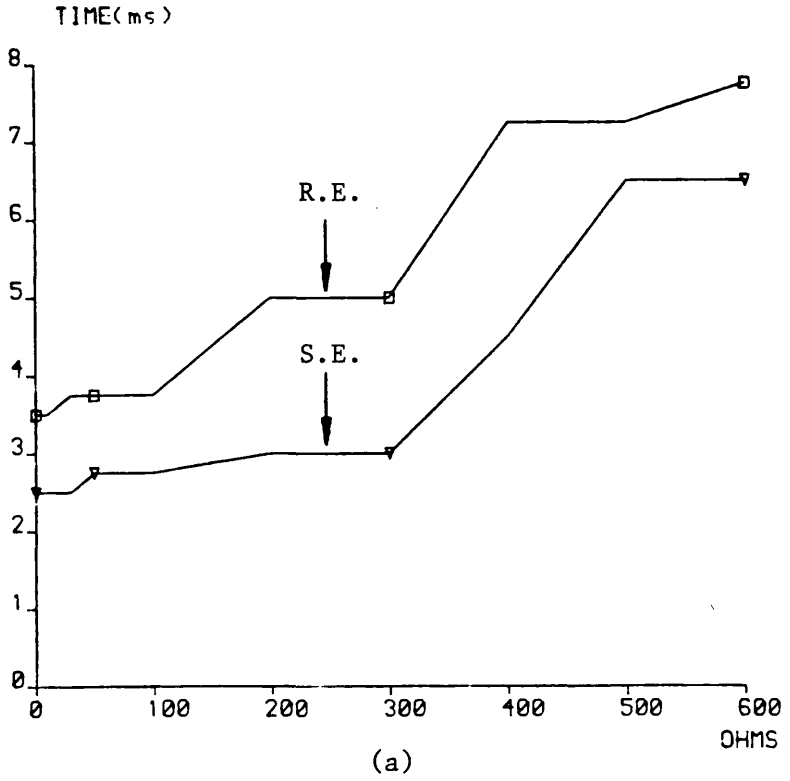

(a)

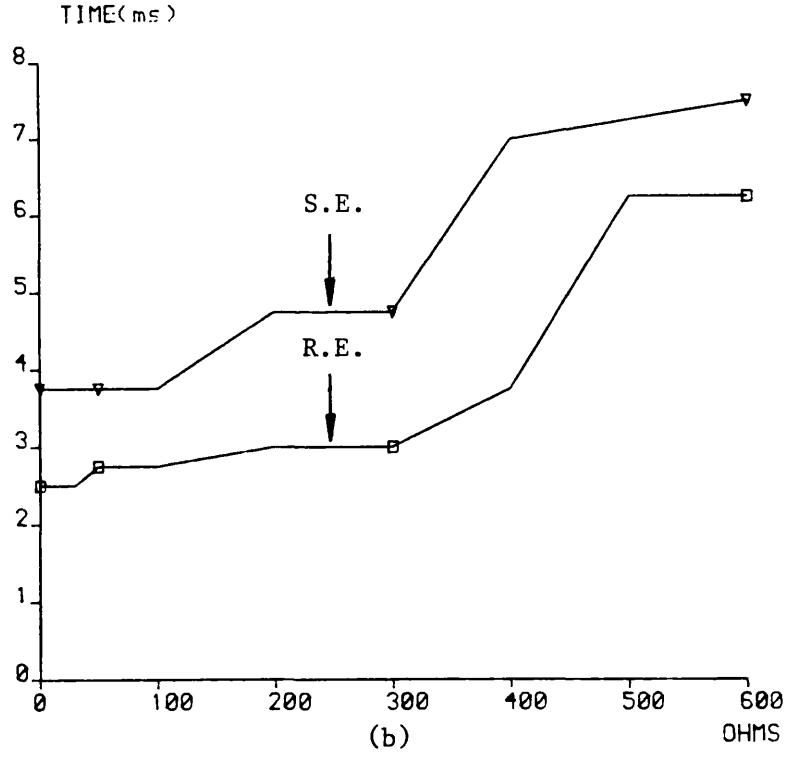

(b)

Fig 7.6 Phase selector operating time-fault resistance characteristics for selection equipment at each end, under double phase to ground fault conditions

- Similar fault conditions as in Fig 7.5

(a) Distance to fault, X_F = 0km

(b) Distance to fault, X_F = 300km

Sending end

Receiving end

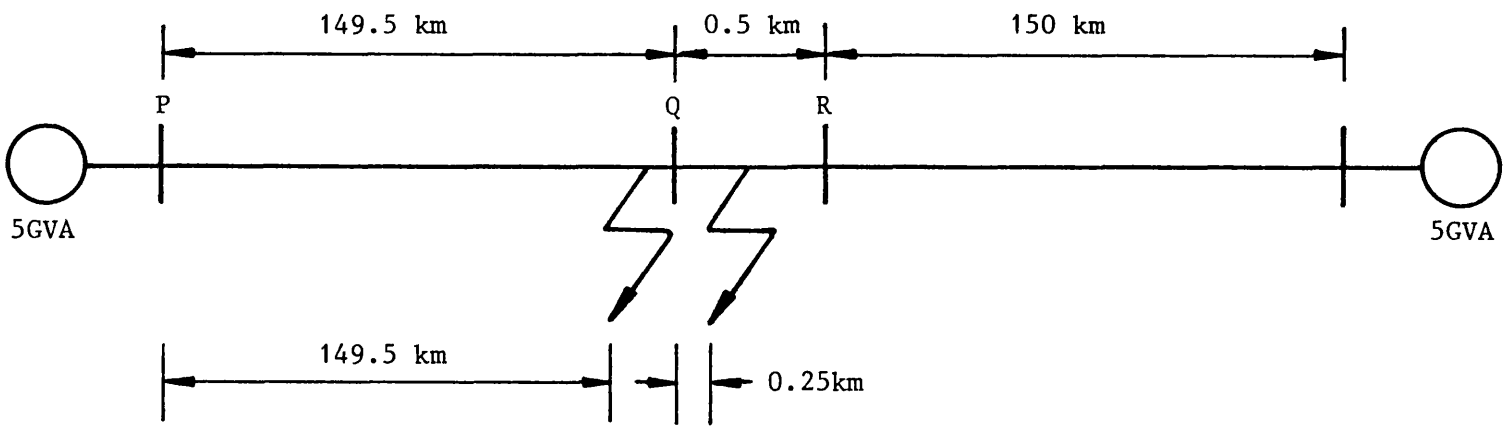

Fig 7.7 Single line representation of system model developed for studying evolving fault conditions

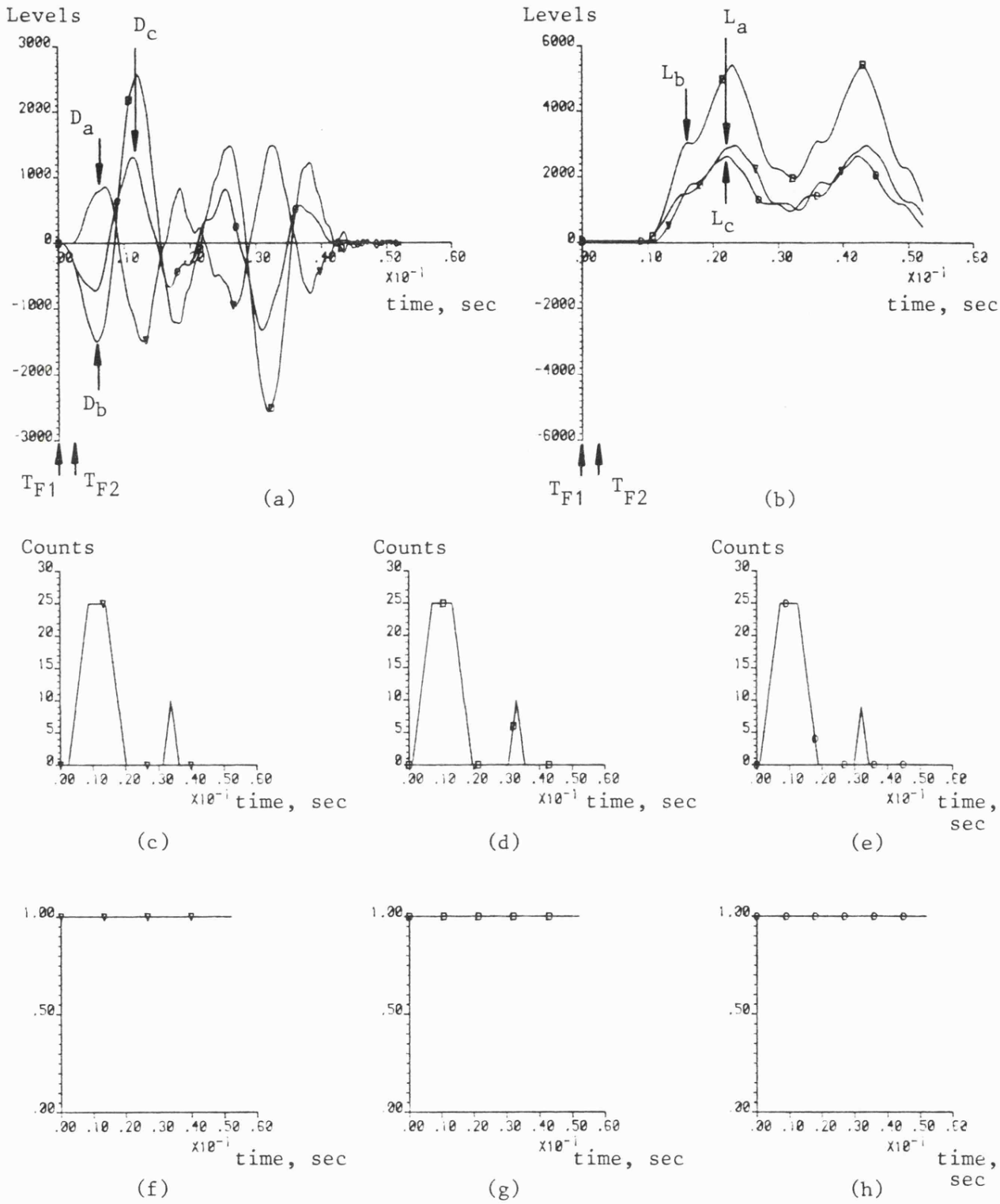

Fig 7.8 Signal responses at various stages in the phase selection process for an evolving fault condition

- Configuration considered, see Fig 7.7
- Fault type "a"-e followed by "c"-e
- Time between faults T_{F1} and T_{F2}, 1.8ms

(a) Discriminant signal behaviour (D_a, D_b, D_c)

(b) Dynamic threshold level response (L_a, L_b, L_c)

(c),(d),(e) Event counters (EC_a, EC_b, EC_c)

(f),(g),(h) Output from phase selector tripping logic (T_a,T_b,T_c)

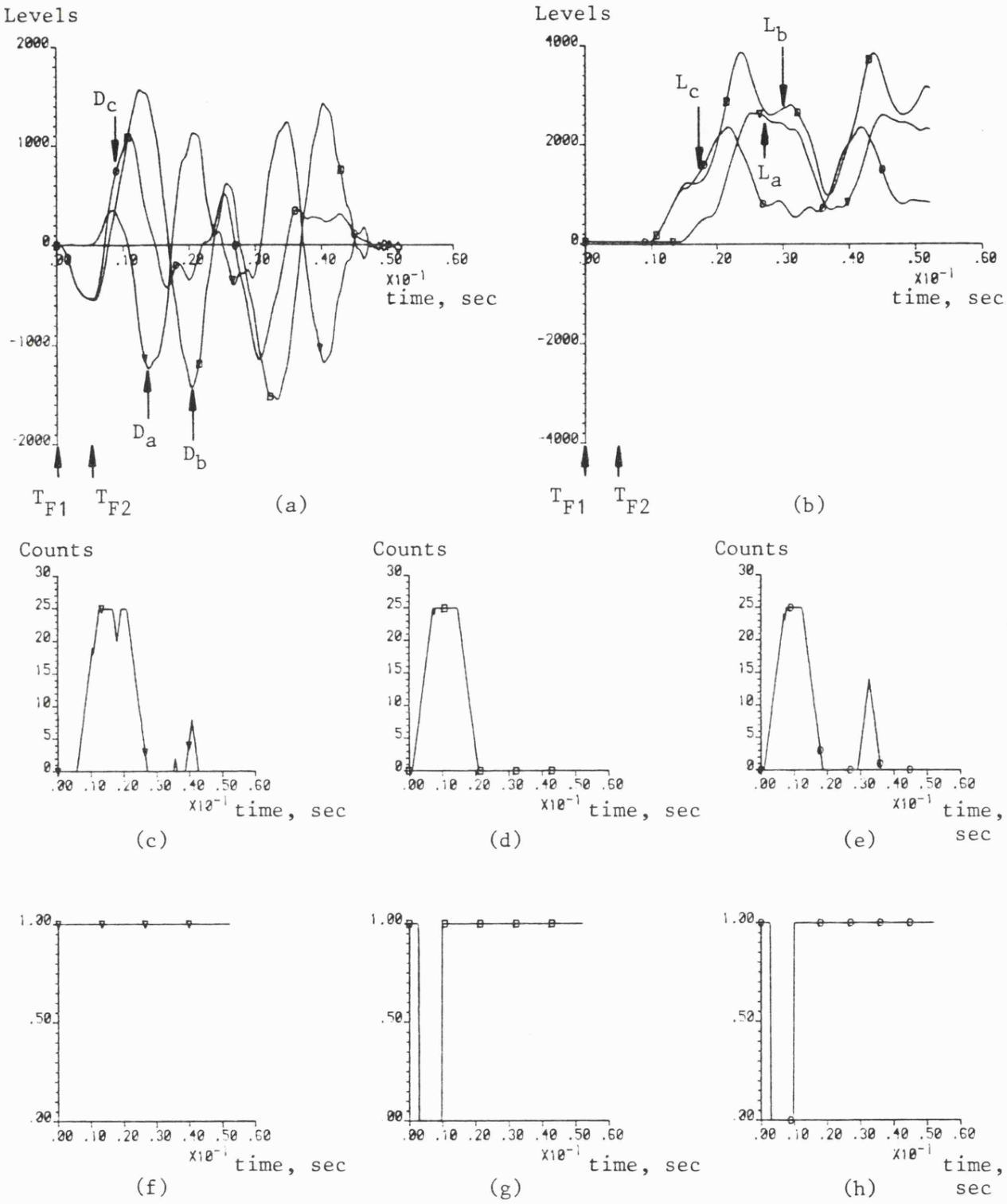

Fig 7.9 Signal responses at various stages in the phase selection process for an evolving fault condition

- Similar fault conditions as in Fig 7.8
- Time between faults, T_{F1} and T_{F2}, 5ms

(a) Discriminant signal behaviour (D_a, D_b, D_c)

(b) Dynamic threshold level response (L_a, L_b, L_c)

(c),(d),(e) Event counters (EC_a, EC_b, EC_c)

(f),(g),(h) Output from phase selector tripping logic (T_a, T_b, T_c)

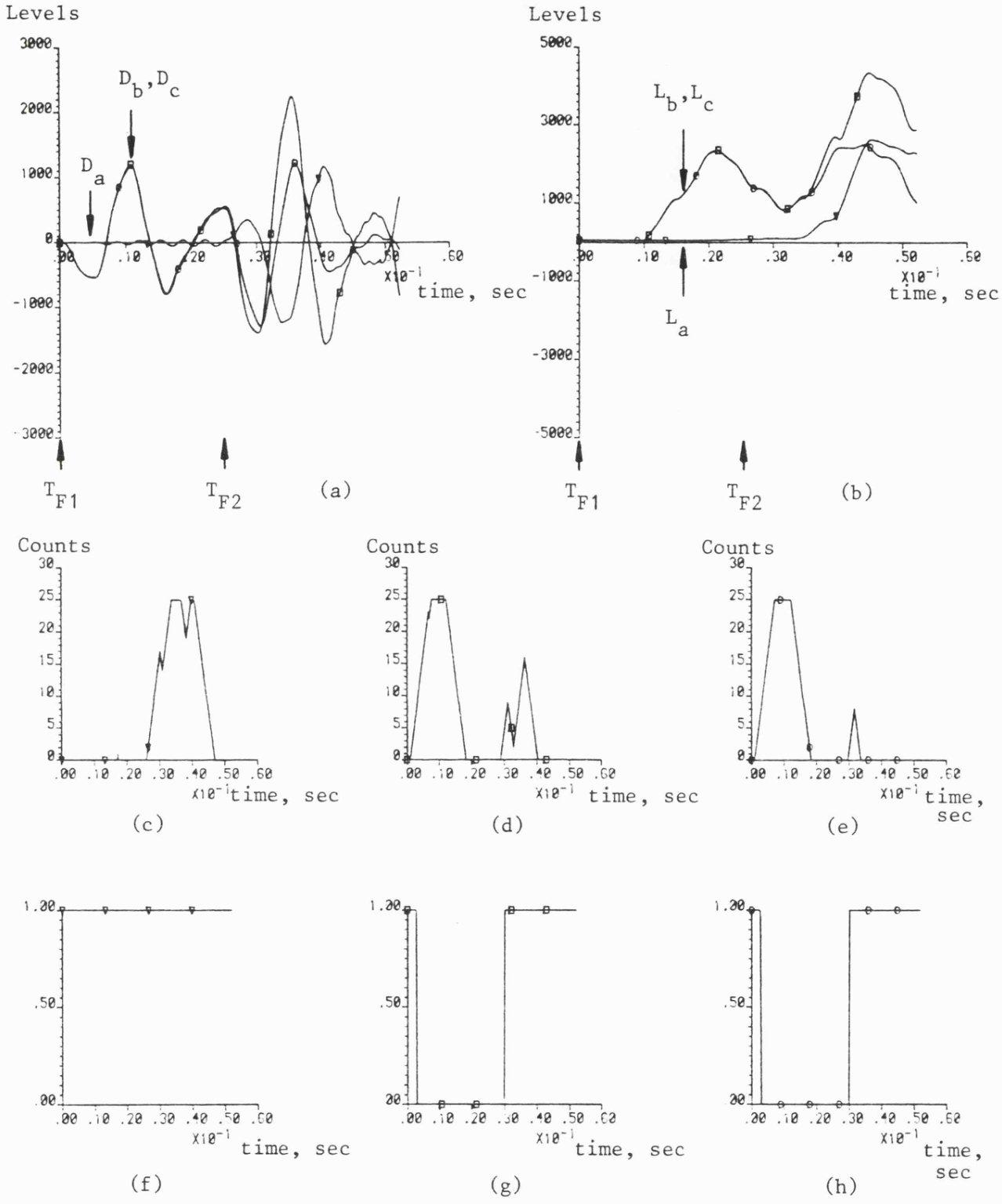

Fig 7.10 Signal responses at various stages in the phase selection process for evolving fault condition

- Similar fault conditions as in Fig 7.8
- Time between faults T_{F1} and T_{F2}, 25ms

(a) Discriminant signal behaviour (D_a,D_b,D_c)

(b) Dynamic threshold level response (L_a, L_b, L_c)

(c),(d),(e) Event counters (EC_a, EC_b, EC_c)

(f),(g),(h) Output from phase selector tripping logic (T_a, T_b, T_c)

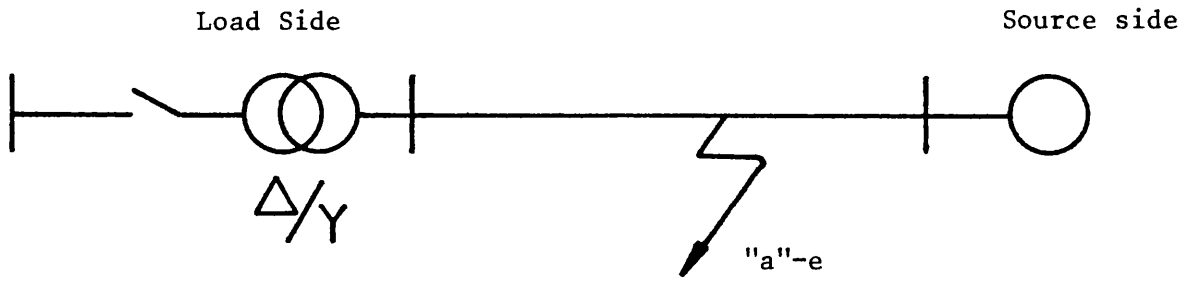

Fig 7.11 Single line representation of fault conditions with open circuit delta winding at the load side Δ/Y transformer

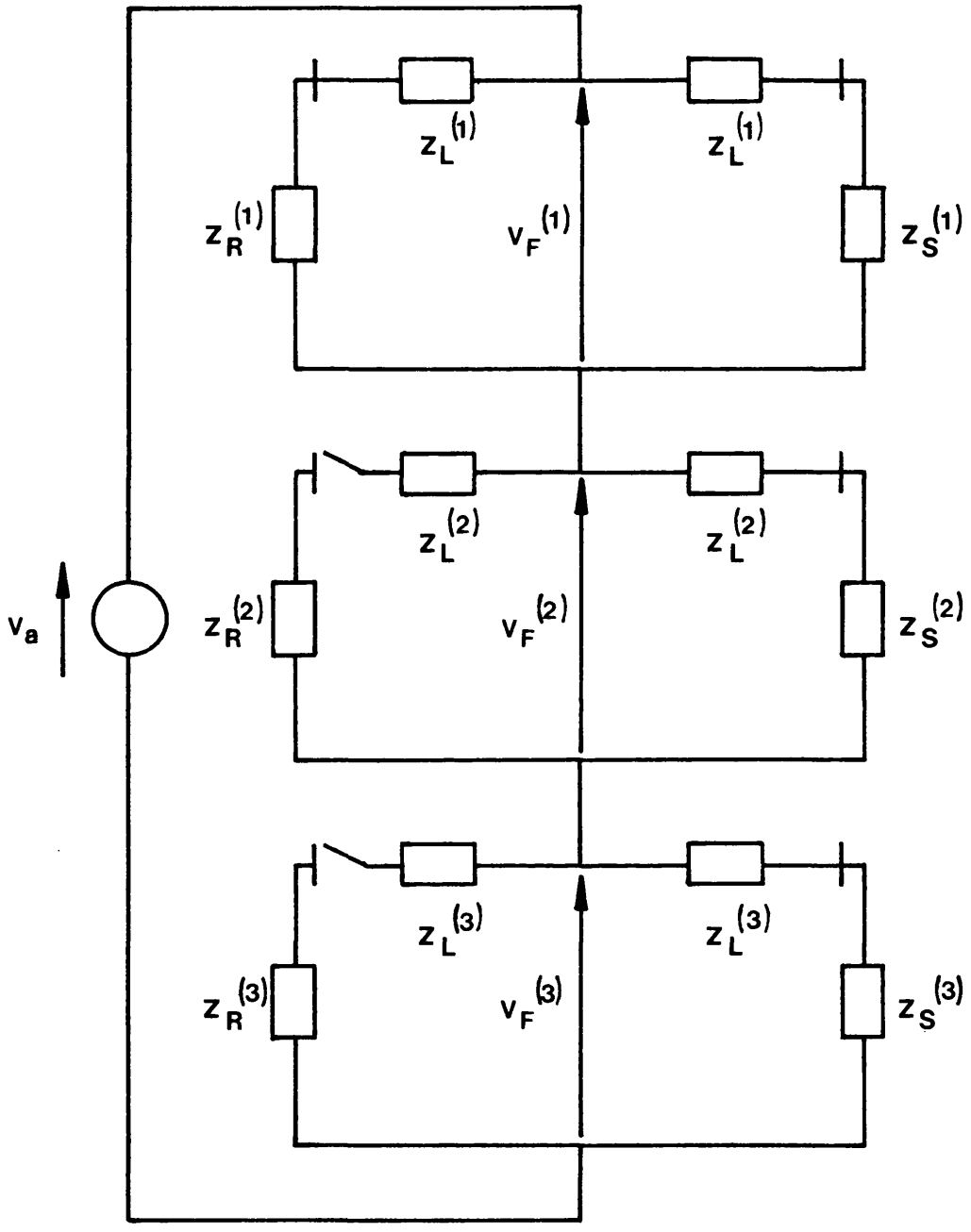

Fig 7.12 Modal network interconnection for an "a"-e fault with ZS0/ZS1 = 0 at the sending end

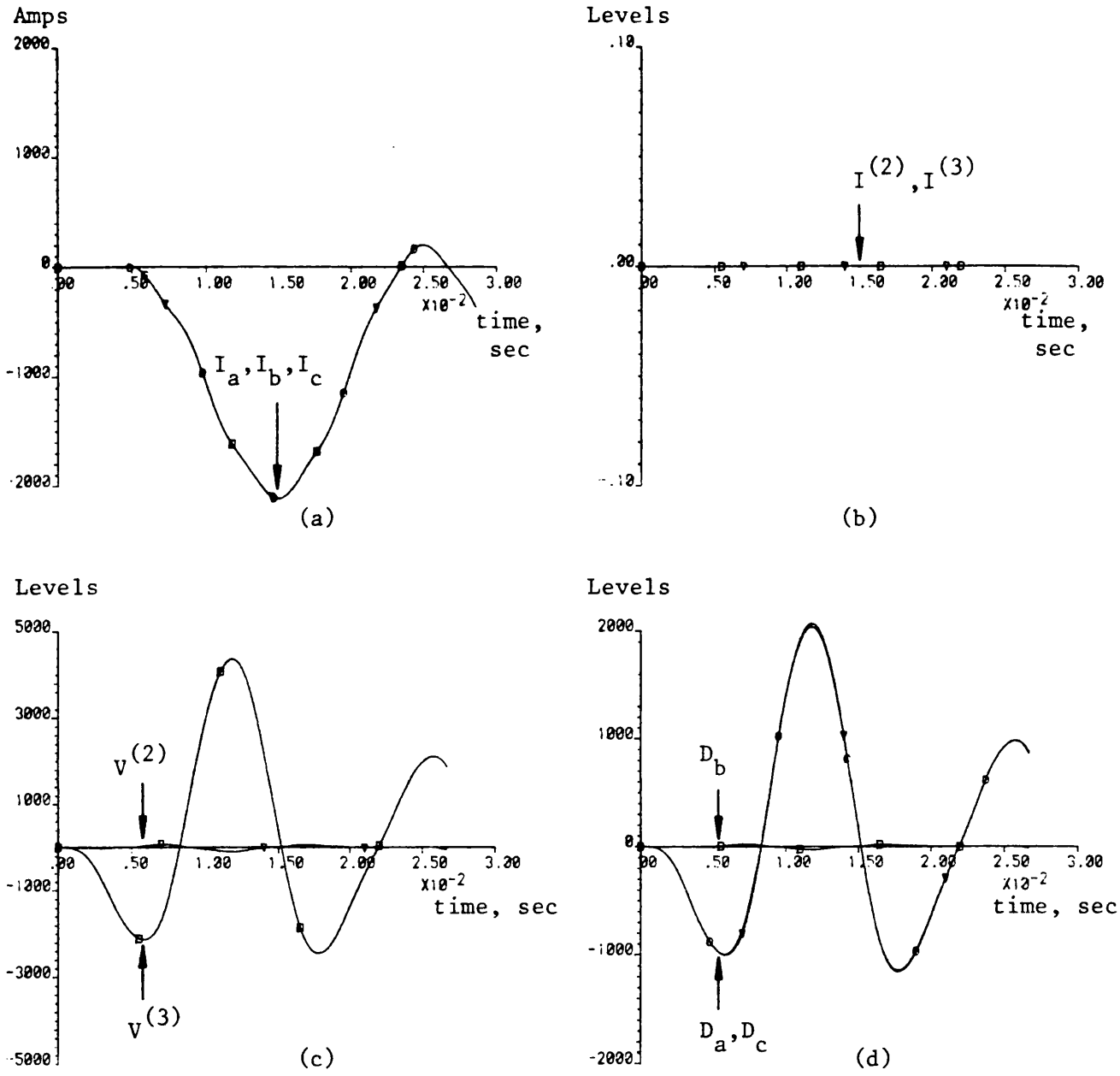

Fig 7.13 Variation of phase and modal signals at different stages of filtering within the phase selector

- Single section feeder; shunt compensated; discretely transposed
- fault type "b"-e
- fault inception angle at zero of prefault of "b"-e phase voltage
- S.E. s.c.l. = 5GVA; R.E. s.c.l. = 5GVA
- R_F = 0.5Ω; X_F = 10km; line length, L = 300km
- ZS0/ZS1 (S.E.) = 0.0; ZS0/ZS1 (R.E.) = 1.0

(a) Initial variation of line currents

(b) Digitally filtered aerial mode currents

(c) Digitally filtered aerial mode voltages

(d) Filtered discriminant signals

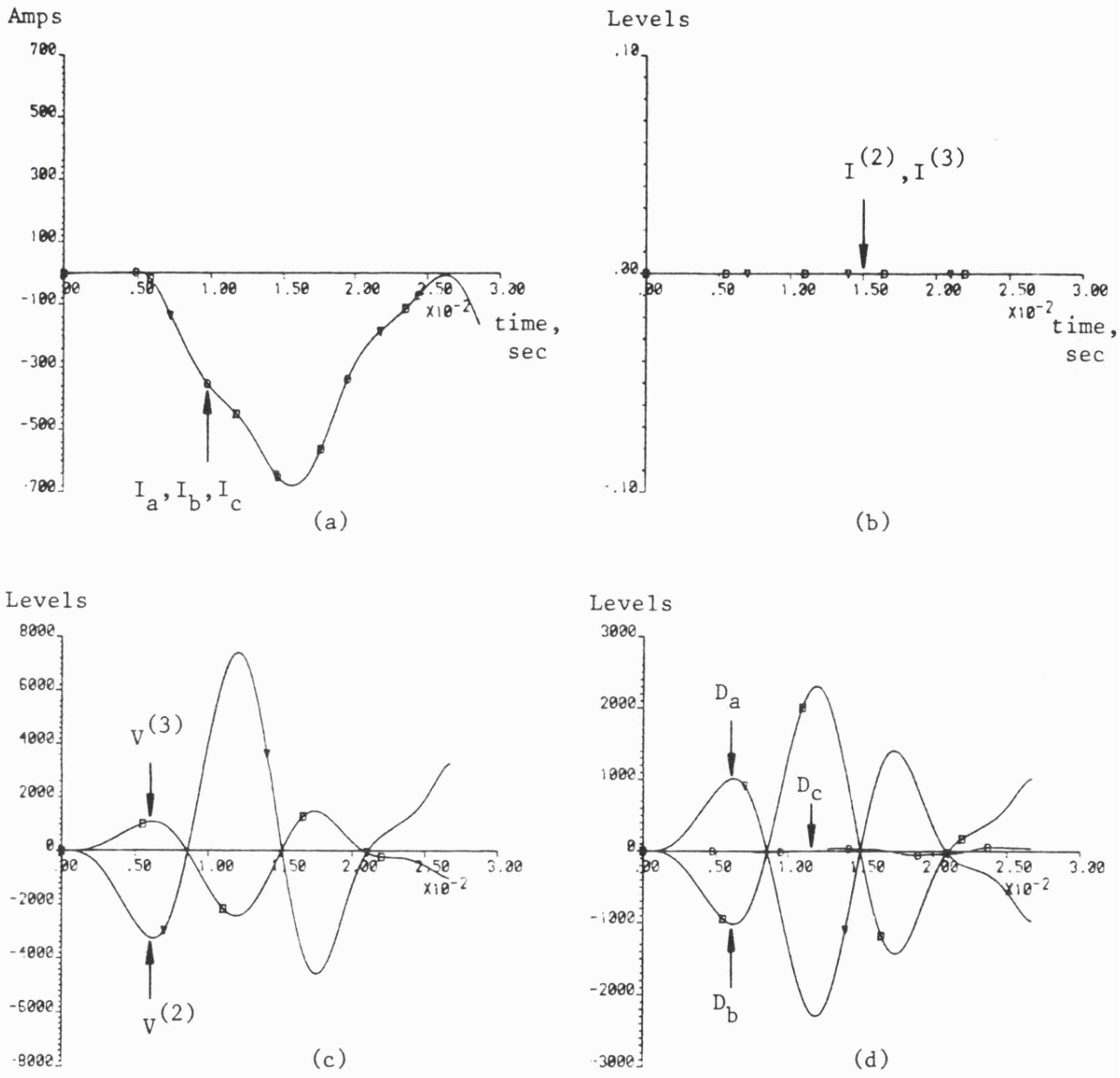

Fig 7.14 Variation of phase and modal signals at different stages of filtering process within the phase selector

- Fault type "c"-e
- Fault at zero of prefault "c"-earth phase voltage
- S.E. s.c.l. = 1GVA; R.E. s.c.l. = 1GVA
- Other fault conditions are stated in Fig 7.13.

(a) Initial variation of line currents

(b) Digitally filtered aerial mode currents

(c) Digitally filtered aerial mode voltages

(d) Filtered discriminant signals

CHAPTER EIGHT

PERFORMANCE OF THE PHASE SELECTOR SCHEME DURING SINGLE POLE AUTORECLOSURE SEQUENCES

8.1 Communication Channel Considered

The overall relaying time of any unit protection scheme is dependent upon the communication channel response time and the operatime time of the fault detection relays and associated phase selection equipment. In addition, the mode of operation in which the scheme is employed, ie. intertripping, blocking or hybrid mode, directly affects the minimum time at which fault clearance cycles can be initiated at each end[43].

There are two main methods employed to indicate a change in a locally generated tripping signal over a communication link, which are:

(a) ON-OFF keying

(b) Frequency shift keying

(a) ON-OFF keying (OOK)

As the name implies, the channel is normally operating in an off state and signals are only transmitted when the channel is switched on by a change in the decision of the local relaying equipment.

(b) Frequency shift keying (FSK)

A frequency shift channel normally carries a continuous 'TRIP' frequency signal until the relaying equipment indicates a block decision. At this instant, the frequency is shifted to a continuous 'BLOCK' signal. The condition of this type of communication channel can be monitored at all times, since a signal is always being transmitted.

With OOK, a malfunction can therefore only be detected when the channel is required to operate. In practice, OOK channels are employed mainly in blocking schemes, whereas the FSK channels are more commonly associated with tripping and hybrid schemes.

It was envisaged that a unit protection scheme comprising of directional relays and phase selectors would involve power line carrier techniques as a means of linking the two ends. Hence, the advantages and disadvantages of each type of communication signalling in conjunction with blocking, tripping and hybrid schemes in turn, are discussed below.

8.1.1 Blocking scheme

At any particular end in a two-ended blocking scheme, a local trip signal will initiate local tripping if no blocking signal is received from the other end. A delayed tripping action is used for co-ordinating the two ends, allowing for communication channel delay and differences in fault detection times of the two relays. In the absence of a blocking signal, which is possible when the communication

channel is inoperative, local tripping will then be initiated after the fixed co-ordination delay. Therefore, the loss of the communication channel would not affect tripping for internal faults, but would possibly result in overtripping for external faults, since at least one relay may indicate that a forward disturbance has occurred. A blocking scheme employing OOK signalling is therefore considered to be more dependable than secure. However, if FSK is used, all tripping is prohibited when the channel is lost, thereby reducing the dependability of the scheme but adding to the security.

8.1.2 Tripping scheme

A tripping scheme, commonly called an intertrip or permissive overreach scheme, relies for its operation upon trip signals being generated from each end. A co-ordination delay is included for reasons mentioned above and if no trip signal is received from the remote end after the local end has indicated a trip, then no action is taken. Hence, in comparison with the blocking scheme, which would still permit tripping for internal faults should the communication link fail, the tripping scheme would prevent such action being taken.

Tripping schemes including FSK signalling are therefore considered very secure in that overtripping (tripping for external faults) cannot take place during channel failure. For the very same reason, tripping for internal faults would be prohibited, which therefore makes such schemes less dependable.

8.1.3 Hybrid scheme

The hybrid scheme comprises of blocking and tripping functions and improves the overall operating performance for true tripping systems applied to systems with dissimilar infeed conditions at each end. The communication channel, normally operating in a blocking state, is keyed to a tripping state whenever the relay at one end reaches a trip decision. When both ends indicate a trip, the overall tripping times are the same as for a true tripping scheme. In cases where one end is slow to operate or does not operate at all, that is when no blocking signal is generated, any trip signal received from the remote end will be repeated or reflected back to the remote end. The effect of this is to cause faster tripping at the ends which would normally be slowest in a true tripping scheme.

A review of the above advantages of each scheme has led to the choice of a blocking scheme, employing OOK signalling for the complete unit protection scheme, including the directional relay and phase selector. This would ensure that dependable operation is maintained for the protected zone during communication channel failure. Had security been the primary requirement, FSK signalling would be a more attractive proposition, since the detection of channel loss could override all trip action.

Furthermore, an intertripping scheme offers greater security than a blocking scheme but when using PLC techniques, transmission of trip signals through faulted sections cannot be guaranteed. The CEGB requirements for the transmission of trip signals are more

restrictive than those of block signals and are subject to very stringent criteria. Therefore the overall time taken to render a trip decision is inherently longer and can be critical when using UHS protection equipment.

Having decided upon the type of communication link and associated blocking mode, a knowledge of the relevant channel delays then permits an evaluation of the performance of the overall protection scheme.

8.2 Interfacing of Phase Selector and Main Directional Comparison Scheme with Appropriate Logic for Blocking Mode Operation

The action of combining the phase selector and the main relay decisions has been mentioned in Chapter 4. This overall decision is further combined with remote end signals to form the complete protection scheme, one end of which is shown in Fig 8.1.

The communication equipment comprises of a transmitter and receiver which allows a locally generated block signal (reverse direction) to be sent to the remote end. As seen in Fig 8.1, any block signal received will prevent local tripping since this would force a logic zero on the input terminal "D" on the latch circuit. The delay Tc is dependent upon the communication channel delay Tch and the relay coordination delay Td. For PLC the minimum channel delay is typically 6ms and the coordination delay is very much a function of the line length, typically between 1ms and 2ms for long line applications. The latch reset is controlled by the main

relay scheme logic and the period after which a decision is reset is dependent upon the system application. The results presented in this chapter, however, are concerned only with the resetting of the phase selector decisions and not the overall protection scheme.

The simple interface circuit of Fig 8.1, which coordinates the decisions from the local and remote relays and the phase selector, can form an integral part of the main scheme logic mentioned above.

An assessment of the overall performance of the scheme can be gained from the detailed diagram of Figs 8.2 and 8.3, which show the signal output states at the various stages within the equipment of Fig 8.1. Two cases of "a"-earth faults are considered, one inside the protected zone and the other at a position just beyond the remote end relaying equipment. As illustrated in Fig 8.2, the in zone "a"-earth fault causes the local dwd to indicate a forward disturbance. After Tc from the forward signal going high, the latch is enabled and the input on terminal "D" is referred to the output Q. The absence of a block signal from the remote end therefore results in Q being high since the AND combination of signal "A" and "C" is also high at this instant in time. Signal Q then forms the intermediate trip T, which when ANDed with the phase selector outputs results in the overall decision T_{Fa}, to open the "a" phase pole.

As seen in Fig 8.3 the out of zone disturbance, which is in the forward direction with respect to the relaying end considered,

causes the phase selector decision to be overridden, since a block signal is received from the remote end.

In the latter case, where phase selection is made after the local forward decision, the channel delay then directly influences the action taken by the overall scheme. Should the channel delay be less than the difference between the relay and phase selector operating times, then the latched intermediate trip would render the phase selector ineffective. This is because of the fail safe or trip all three mode of the phase selector which under such circumstances would unnecessarily open all three poles for the single phase fault. An exhaustive series of tests have revealed that the decision time stagger is no more than 1ms for the worst case fault conditions. Recent advances in communication technology have produced optical fibre links capable of achieving channel delays of about 2ms, which therefore suggests that the above scheme is not only compatible with conventional links, but with the current state of the art.

8.3 Performance of Phase Selector Scheme during Autoreclosure Sequences

It is important to ensure that integrity of operation of the protective DWD and the associated phase selector equipment is maintained at all times. Thus, an evaluation of the protection responses following the initiation of the various autoreclosure sequences encountered in practice was necessary. For this purpose, a computer program developed to simulate full autoreclosure sequences, based upon the theoretical analysis discussed in ref 44

was employed. Results are presented for both single-pole and three pole autoreclosure sequences.

The number of possible autoreclosure sequences is vast and in practice the choice of dead times is often decided on the basis of transient stability considerations. For a high speed autoreclosure scheme, whether it be of the three or single-pole type, dead times in the range of 0.5 - 1 sec are encountered. However, there is a practical limit on computational observation time, which therefore restricted the actual dead time periods which could be simulated. Other approximations relevant to actual SPA equipment and conditions include:

(i) Linear fault path resistance of 0.5Ω.

(ii) One cycle, or three cycle circuit breakers.

(iii) Current interruption at a precise zero-crossing following breaker contact separation, with no simulation of pre-arcing.

(iv) Reclosure occurring at a preset time from fault inception, which therefore does not produce optimum pole reclosure from a viewpoint of minimising switching surge overvoltages.

The performance of a complete autoreclosure scheme is dependent upon the main directional relays and the phase selector equipment. As stated previously, the two independent decisions are combined to give an overall trip decision. The response of the main relay

under full autoreclosure schemes had therefore to be investigated, in order to determine the action which would be taken by the complete scheme.

Fig 8.4 presents the main relay responses for a complete autoreclosure cycle following an in zone "b" phase to ground fault. The changes in system conditions at the time instances t1 to t5 clearly affect the variation of the mode-3 relaying signals, S1 and S2. The autoreclosure cycle is broken down into the following individual events:

(1) Fault inception time, t1.

(2) Breaker interrupting time, t2 at S.E. and R.E. simultaneously.

(3) Fault break off time, t3.

(4) Breaker reclosure time (S.E.), t4.

(5) Breaker reclosure time (R.E.), t5.

The relaying equipment was situated on the line side of the breakers and as seen in Figs 8.4b and d, which display the counter action of the relays at each end, the correct forward and reverse decisions are reached for each subsequent disturbance.

Upon fault inception, each relay indicates a forward disturbance, with the counter steadily increasing until being reset after 16ms. The most common type of high speed circuit breakers employed in practical autoreclosure schemes can perform single or three pole

opening within 3 cycles. Similar breaker opening capability was considered for this particular test and approximately 60ms after fault inception, the opening of the "b" phase pole at each end, behind the relays, is seen to cause the latter to indicate a reverse disturbance. At the instant of fault break off, t3, there was insufficient change in line current at each end for the relays to render any decision, since the "b" phase was still isolated. The cycle was completed at time, t5, by the re-energisation of the "b" phase, which was again a system disturbance behind the relays. The direction of the relay count verified that the disturbances were exterior to the protected zone, but due to the lightly load conditions prevalent at the reclosure instant, a decisive count of 5 was not reached and no further action was taken by the relays.

The corresponding responses of the phase selection equipment at the sending end are shown in Fig 8.5. The discriminant signal and dynamic threshold variations, show that one variable remains relatively low throughout the observation period, this being the discriminant D_b and the associated threshold level L_b.

To illustrate the capability of the phase selector to detect successive disturbances, two resetting techniques were adopted. The three trip outputs from the decision logic, utilising a dynamic reset method, are shown in Figs 8.5(c), 8.5(d) and 8.5(e). This technique was outlined in Chapter 4 whereby the phase selector decision is held until each dynamic threshold has returned to its minimum level. For this case, the decision to open the "b" phase,

made after 2.5ms following fault inception, is held for the duration of the autoreclosure cycle. The threshold levels did not settle down at any time due to the close succession of events which therefore prevented any phase selector resetting. However, when considering resetting after a preset time following an initial decision (approx 64ms), Figs 8.5(f), 8.5(g) and 8.5(h) clearly demonstrate the ability of the phase selector to detect all subsequent disturbances on the "b" phase. The repeated selection of the "b" phase was possible despite the reduction in sensitivity due to relatively high threshold levels. It is envisaged, therefore, that the latter reset would be more suited for single pole reclosure schemes since it would still be possible for the selector to detect changes in system fault conditions during the dead time period and take appropriate action.

The forward and blocking decisions of the main relays at the sending and receiving ends respectively can then be combined with the phase selector outputs, in the manner described in the previous section. For the two selector reset schemes considered, the overall protection equipment would then correctly initiate tripping and reclosing of the "b" phase only.

The case of an interphase fault involving the "a" and "b" phases was chosen to illustrate the relay and selector performance during a 3 phase autoreclosure sequence. Fig 8.6 shows the counter action of the main relays situated at the ends of the protected zone and clearly indicates an internal disturbance. When the latter

decisions are combined with the receiving end phase selector outputs (Fig 8.7) as explained above, a correct overall decision to activate the three pole reclosure mechanism is rendered.

It has therefore been demonstrated that the new selector scheme is suitably versatile for it to form an integral part of a single pole autoreclosure scheme employing directional comparison protection relays.

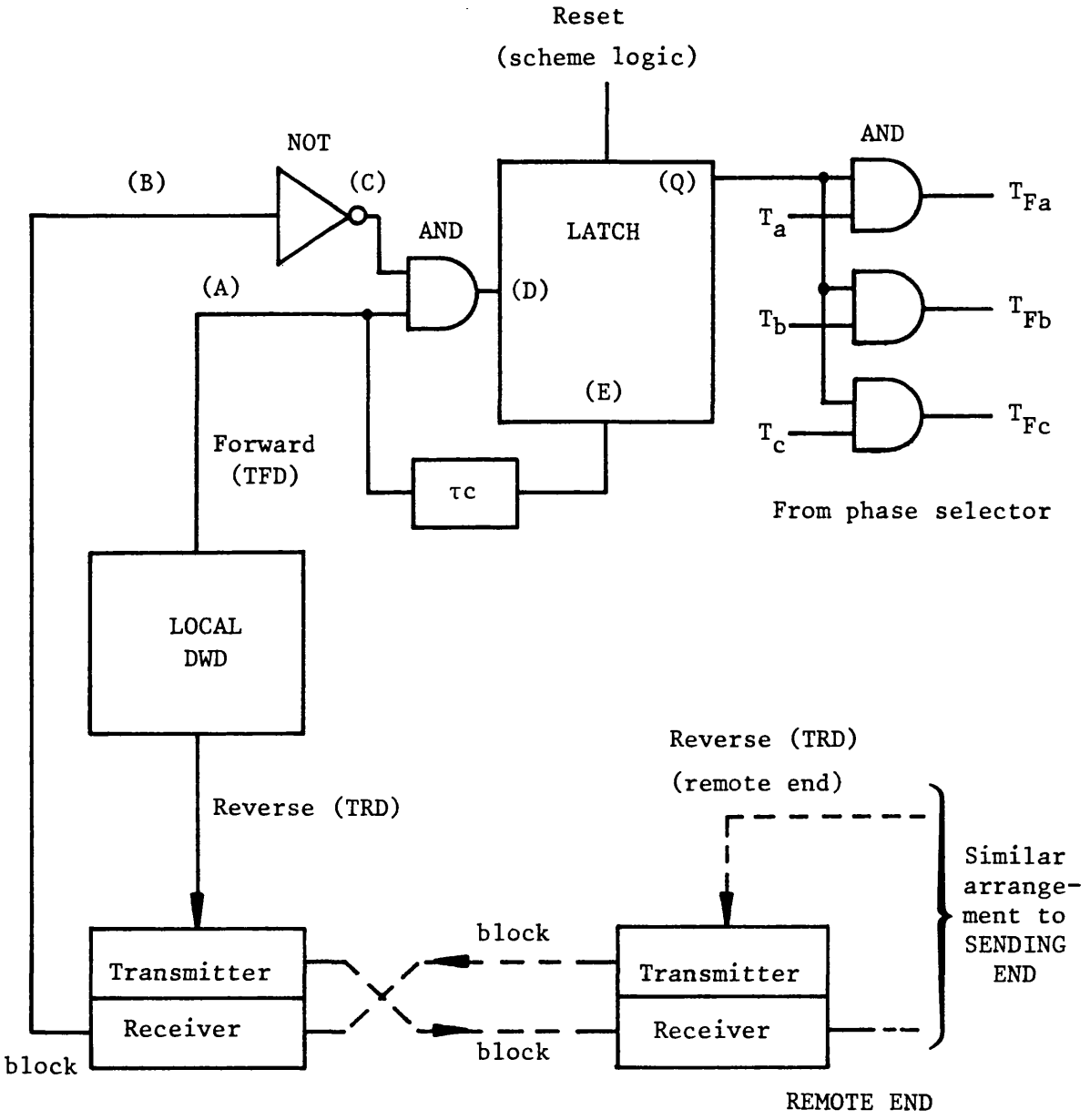

Fig 8.1 Block schematic of UHS protection

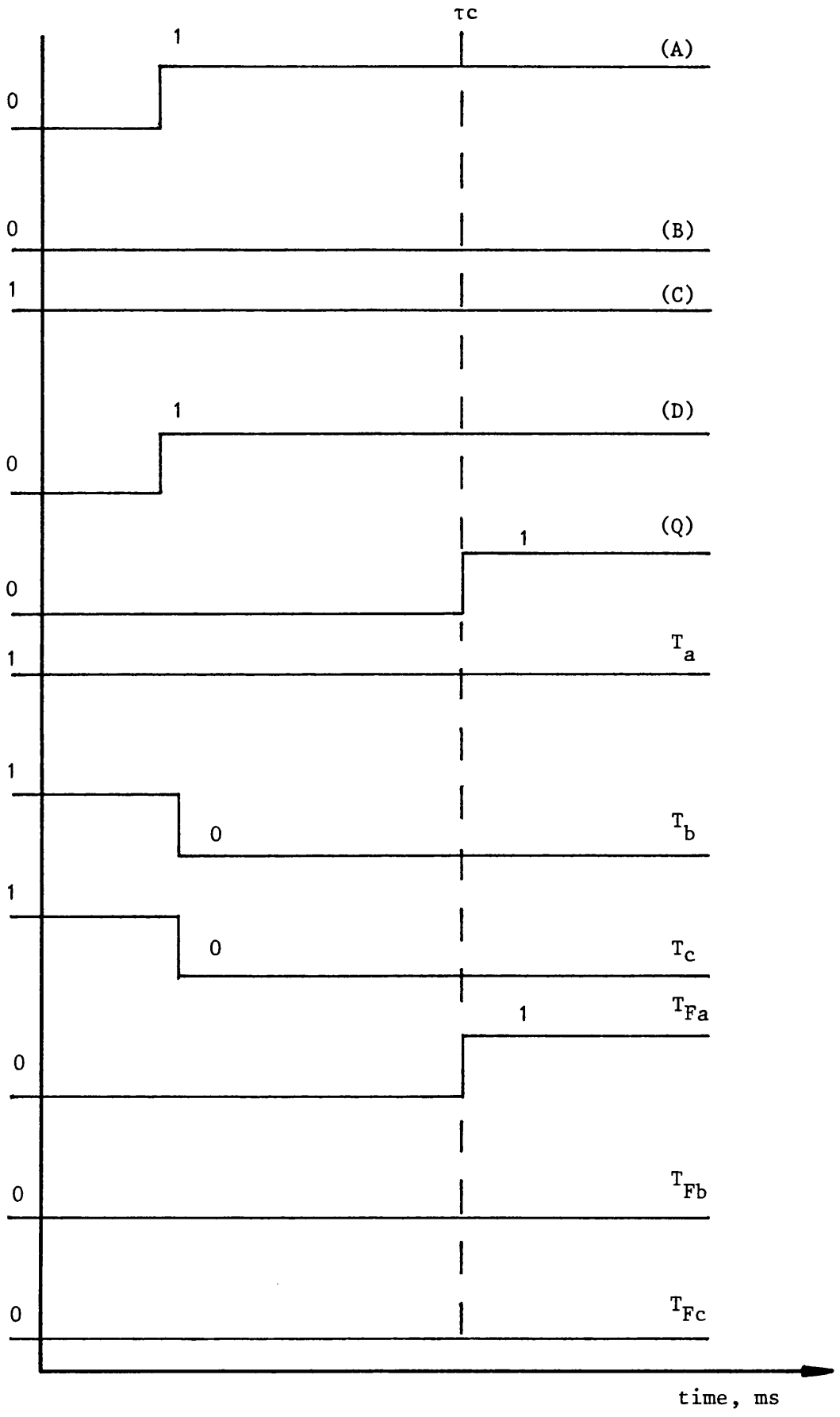

Fig 8.2 Response of the protection scheme of Fig 8.1 to an in-zone disturbance on the "a" phase

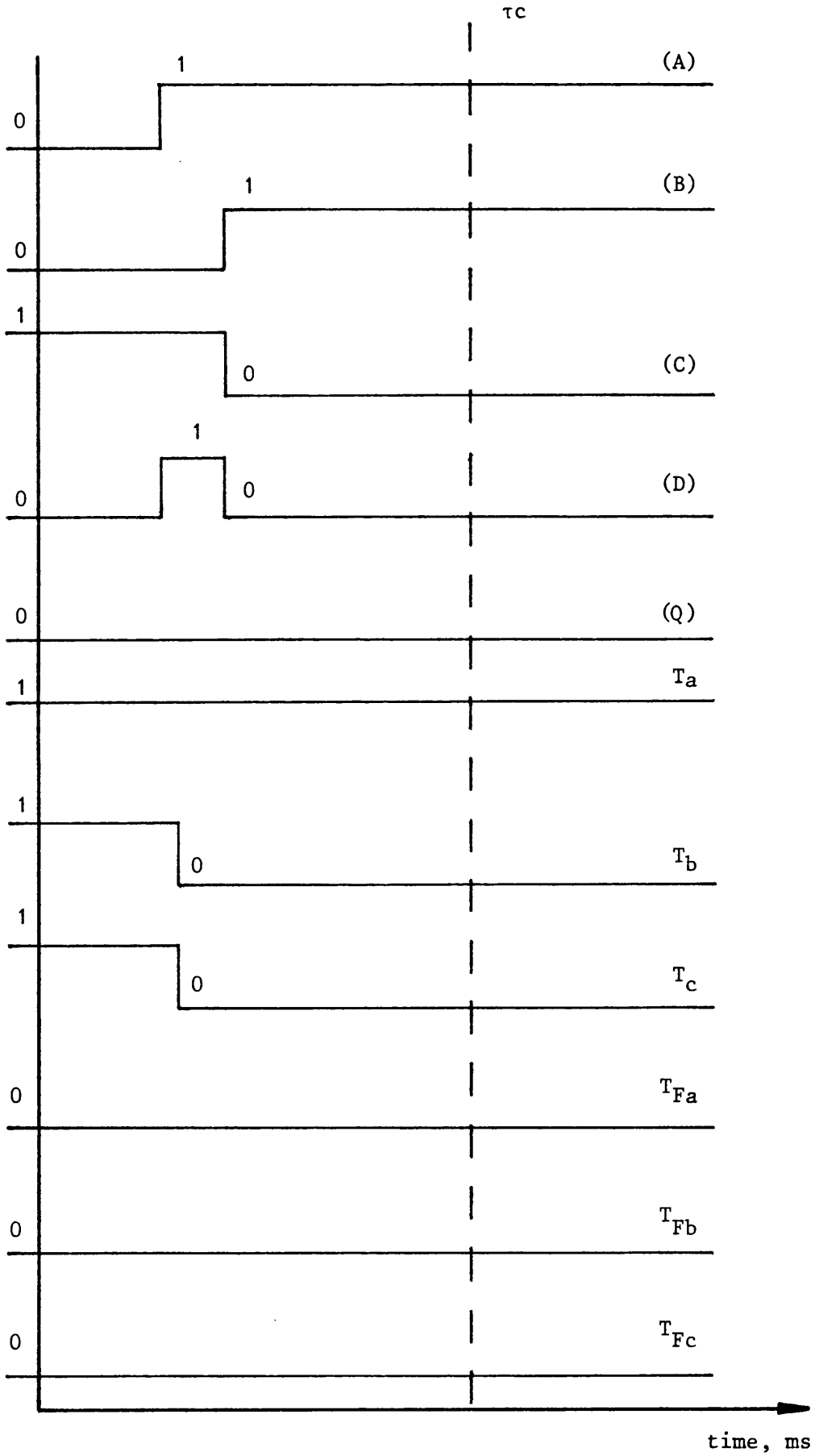

Fig 8.3 Response of the protection scheme of Fig 8.1 to an out-of-zone disturbance on the "a" phase (forward local beyond other end)

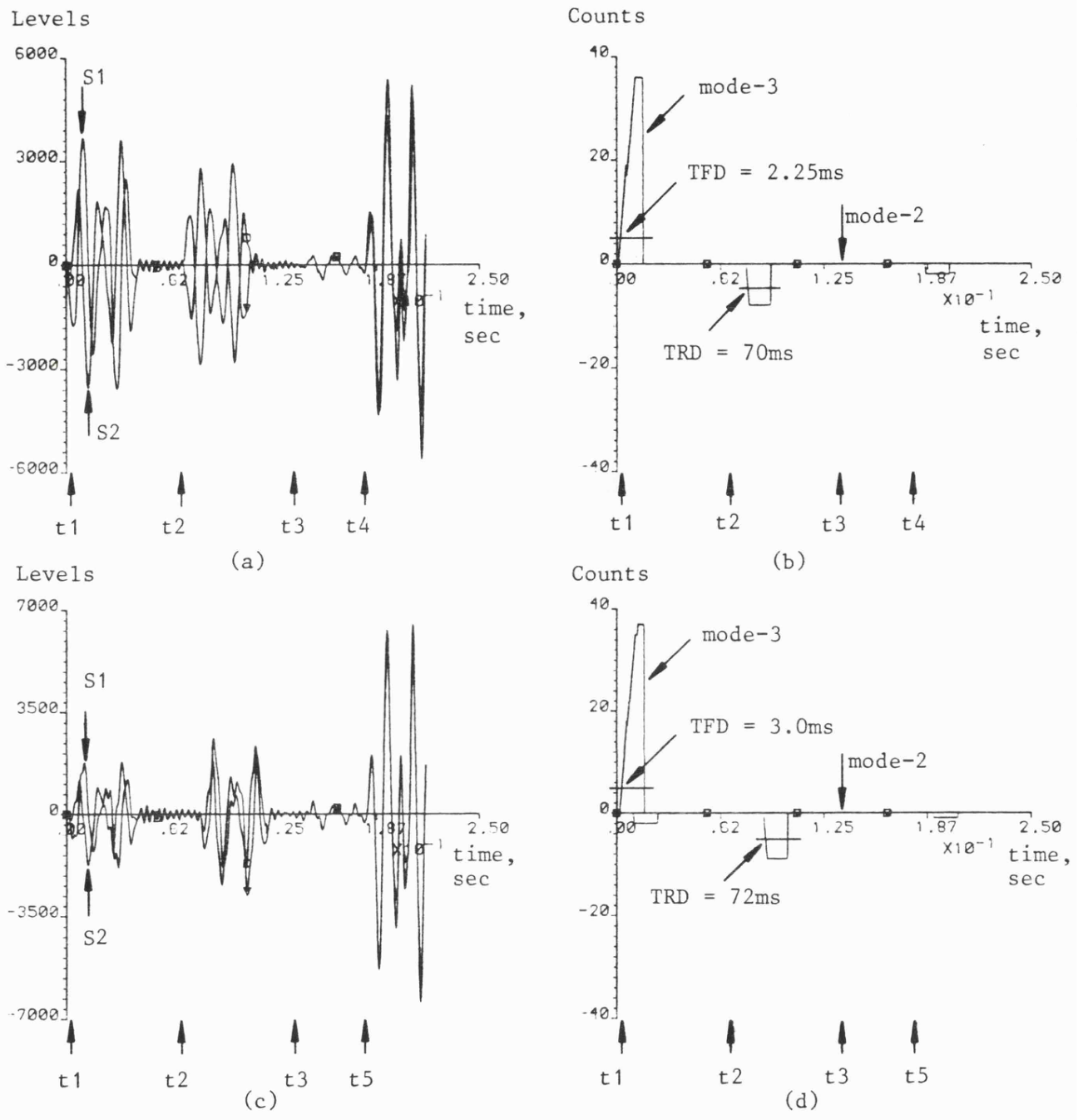

Fig 8.4 Directional wave detector response during single pole autoreclosure sequences

- Single-section feeder; X_F = 10km; line length = 300km; R_F = 0.5Ω
- Line discretely transposed and shunt compensated
- Type of fault "b"-earth fault at peak of prefault "b" phase voltage
- Sending end S.C.1 = 5GVA; receiving end S.C.2 = 5GVA
- Vs/Vr = 1/0; ZS0/ZS1 = 1.0

t1 = 5ms; t2 = 60ms after fault; t3 = 140ms after fault;

t4 = 180ms after fault; t5 = 190ms after fault;

TFD = forward decision time; TRD = reverse decision time

(a), (b) = Mode-3 signals (S1 & S2) at the sending end S and its corresponding counters decision

(c), (d) = Mode-3 signals and counters for receiving end R

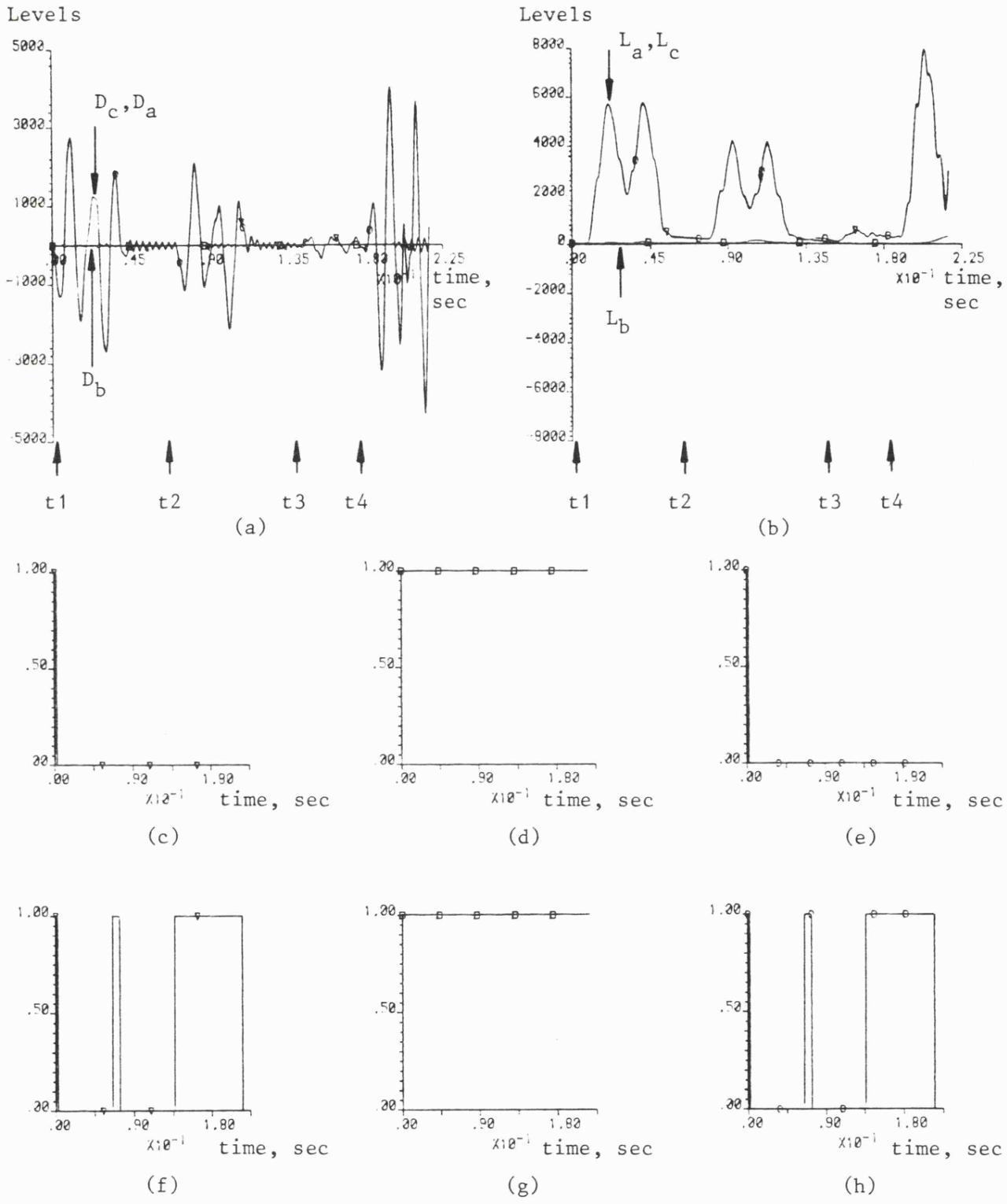

Fig 8.5 Performance of phase selector equipments at sending end S during single pole autoreclosure

- Fault conditions as stated in Fig 8.4

(a) Discriminant signal variations

(b) Dynamic threshold level responses (minimum threshold = 45 levels)

(c),(d),(e) Output from phase selector decision logic (T_a, T_b, T_c) using dynamic reset technique

(f),(g),(h) Output from phase selector decision logic (T_a, T_b, T_c) using fixed reset time

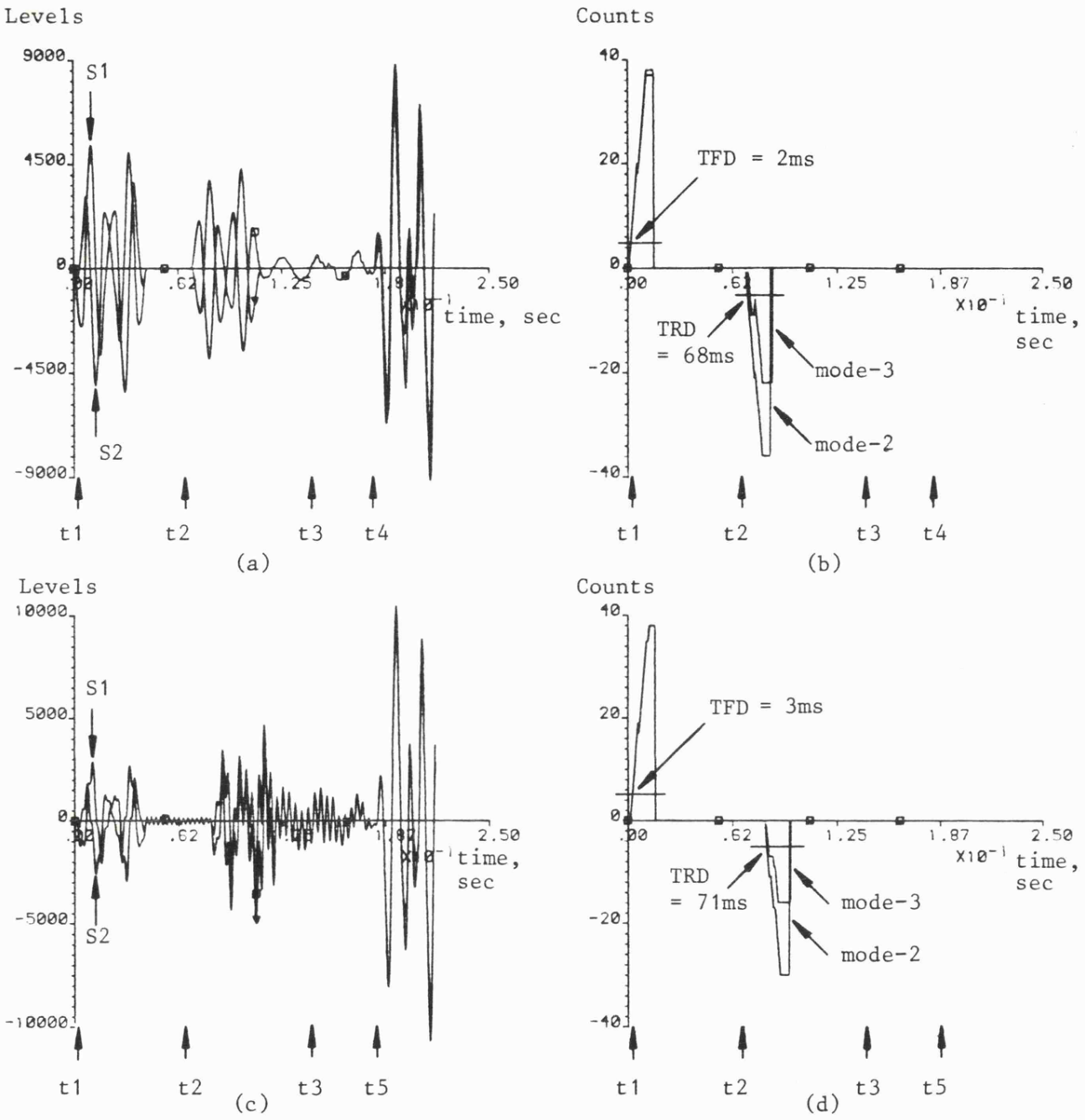

Fig 8.6 Directional wave detector response during three pole autoreclosure sequences

- Type of fault "a"-"b" fault clear of ground
- Instant of fault at peak of prefault voltage between phases "a" and "b"
- Other fault conditions are as stated in Fig 8.4

(a) Mode-3 signals (S1 & S2) at the sending end

(b) Mode-2 and Mode-3 counters at the sending end

(c) Mode-3 signals (S1 & S2) at the receiving end

(d) Mode-2 and Mode-3 counters at the receiving end

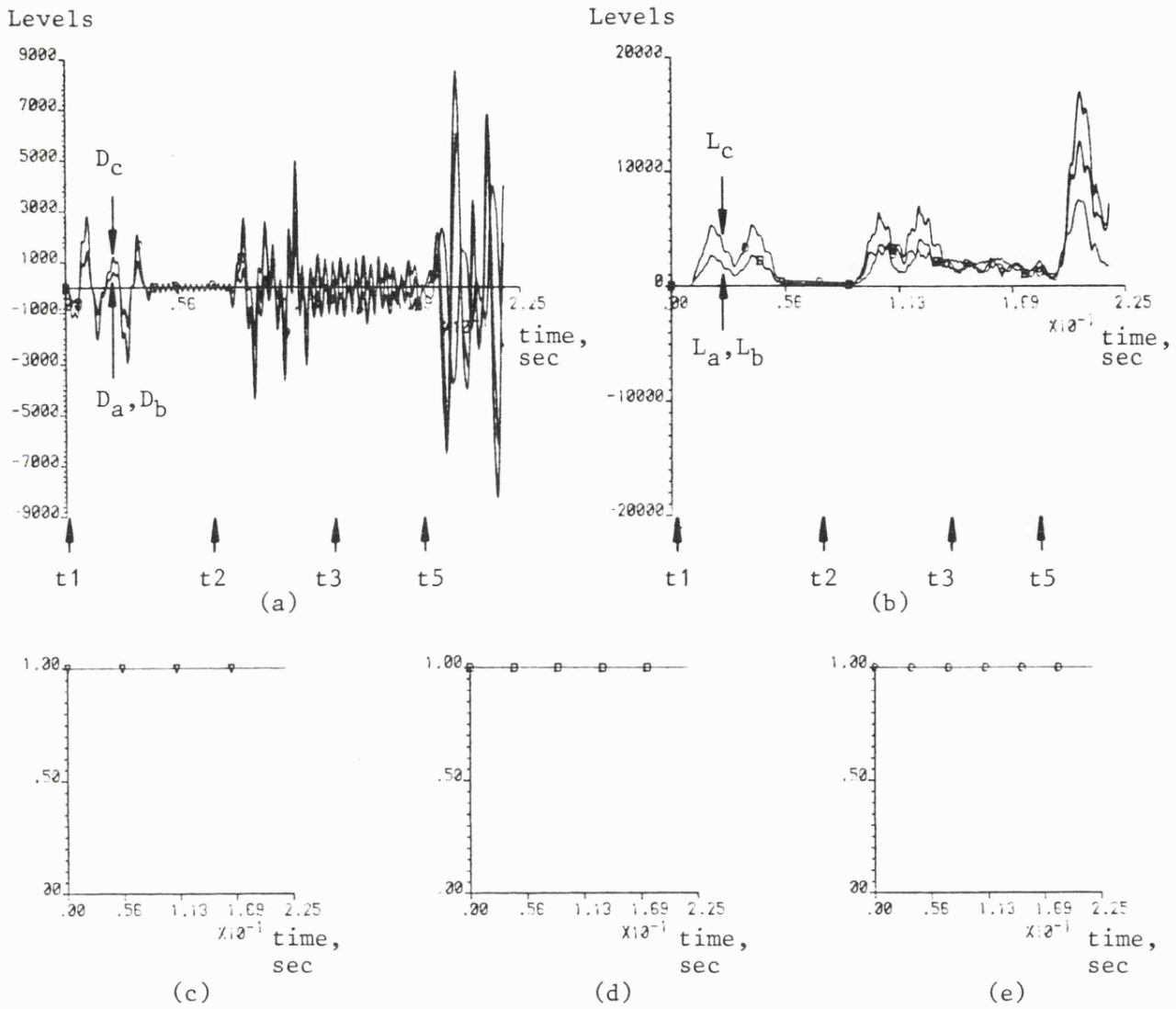

Fig 8.7 Performance of phase selector equipment at the receiving end R during three pole autoreclosure sequence

- Fault conditions are as stated in Fig 8.6

(a) Discriminant signal variations

(b) Behaviour of dynamic threshold levels (minimum threshold = 45 levels)

(c), (d), (e) Output from phase selector tripping logic (T_a, T_b, T_c) for either method of resetting

NB: Same tripping output for both dynamic and fixed rest

CHAPTER NINE

RESULTS OF PRELIMINARY FIELD TESTS

9.1 Background to Field Test Arrangement

This chapter describes the response of the phase selector when supplied with actual system data collected at Cellarhead substation in the CEGB Midlands region. The monitoring equipment was connected to a 400kV transmission line of 87km length, routed across the Pennine hills to Stocksbridge, which includes a short section of cable (approximately 1.5km). A detailed system schematic of the area in which the line is situated is given in Fig 9.1. The inclusion of a cable section within a length of transmission line increases the high frequency content of faulted system waveforms, due to the extra points of impedance discontinuity. The service history of the CEGB transmission network shows that this line has the highest incidence of recorded faults and from a prototype test point of view was therefore considered ideal. However, it should be noted that the performance must be assessed in the presence of components produced by everyday occurrences such as load current variations, remote switching operations and all other sources of disturbance. Initially, the field tests were arranged to estimate actual system noise levels for the main directional relay[45], but the readily available data provided a good opportunity to assess the basic performance of the phase selector.

9.2 Instrumentation and Data Acquisition Equipment

The equipment was contained in 1 of the 4 block-houses within the 400kV compound, and comprised the superimposed component relay, a VDU terminal, a Penny & Giles cartridge tape recorder (3.6 Mbytes storage capacity), a 3-channel slow speed chart recorder and a high speed UV recorder. The slow speed recorder running a 1"/hour monitored the relay forward and reverse signal outputs. The Penny & Giles recorder was used for monitoring system disturbances as they occurred and a self-triggering mechanism was incorporated in the main relay software which initialised a recording sequence as soon as any mode output counter reached a level of one. Any system noise resulting in no counter action was therefore deemed insignificant and was not recorded.

The relay memory was capable of storing a running window of 150ms of data, which comprised of approximately 50ms pre-triggered and 100ms post-triggered information for both modes. Once the 100ms had elapsed, the window of information was transferred to the cartridge recorder via a serial line. During the transfer period, which was 50 seconds, the relay no longer stored information but was reactivated when the transfer was complete.

At regular intervals, the tape cartridges were collected from site and converted to an easily manageable form by a PDP 11/23 mainframe computer at Bath University. The total superimposed filtered modal voltage and current signals were then processed with the phase selector to evaluate the performance of the latter with

actual system information. This technique yields exactly the same results as those which would be obtained from phase selection equipment actually installed at the site, since the selection algorithm is entirely in software form.

9.3 Field Test Results

Initially, the prototype relay and the associated monitoring equipment was powered from the substation mains supply. However, this proved unsatisfactory when the data obtained for an in-zone fault condition was analysed. The breakers which were opened to clear the fault were of the air blast type, and therefore incorporated quick starting air compressors. The latter caused large fluctuations in the supply which led to the corruption of the relevant window of in zone fault information recorded. Since then, independent battery supplies have been installed, but at the time of writing the only system data available is that for out of zone disturbances. The phase selector, however, is not a directional device, and its ability to determine whether a fault is of single phase to ground type or not can still be tested for disturbances anywhere on the system, within its sensitivity limits.

Several sets of out of zone disturbance data were processed with the output at various stages of the phase selector, for one particular case, being presented in Figs 9.2 and 9.3. From Fig 9.2 it is seen that during the pre-disturbance period the amplitude of the system noise was less than the minimum threshold level of 40. This minimum setting, established from exhaustive simulation studies,

was therefore justified by the actual system data. During the disturbance period, the waveforms show how one discriminant signal and its associated threshold level remain low, and the counter responses then indicate that the disturbance is in fact a fault involving the "a" phase and earth. There was no prior knowledge of the actual fault conditions since each set of the data was considered at random.

For completeness, the same data was applied to the main relay which indicated that the fault was behind the substation on another part of the system. Furthermore, the amplitude of the discriminant signals is only of the order of 100 quantisation levels, which suggested that the fault position was quite far away from the observation point.

The decision of the phase selector and main relay was endorsed when the CEGB operational records were consulted. An "a" phase to ground fault on the Deeside-Pentir section had been logged, with the fault being approximately 150km away from the relaying equipment.

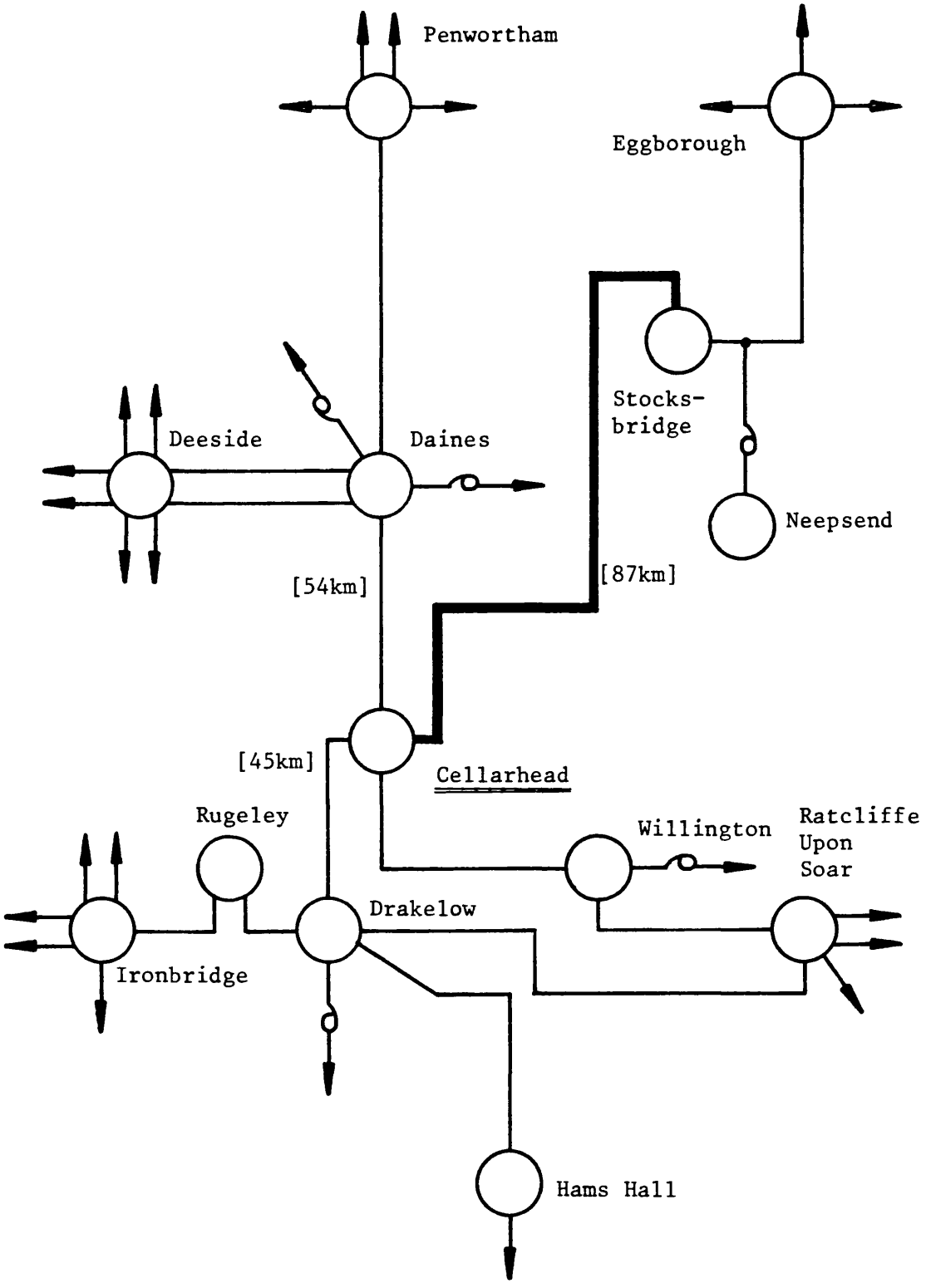

Fig 9.1 CEGB 400kV system - feeders local to Cellarhead

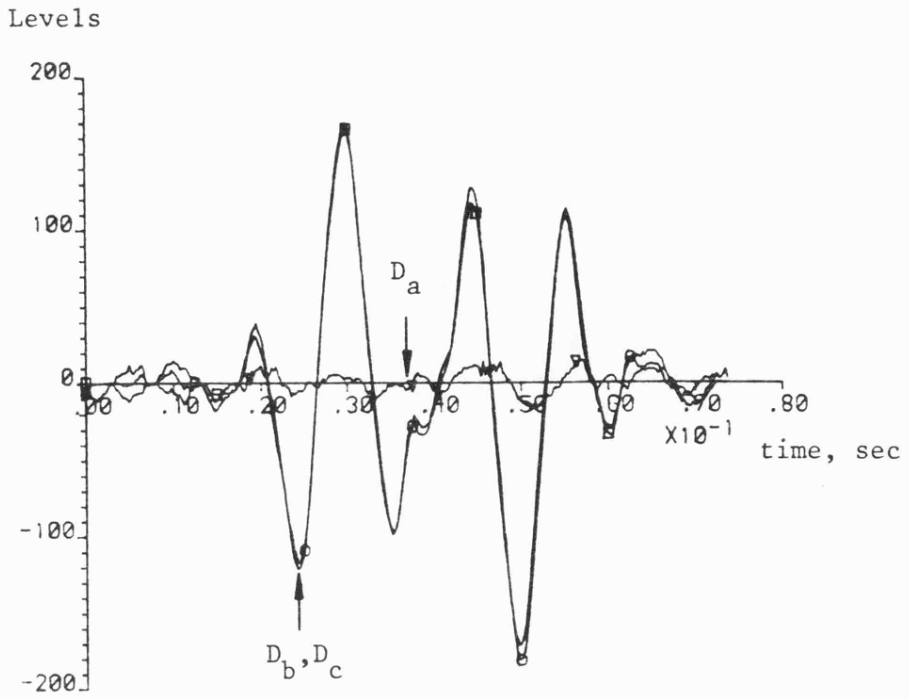

(a)

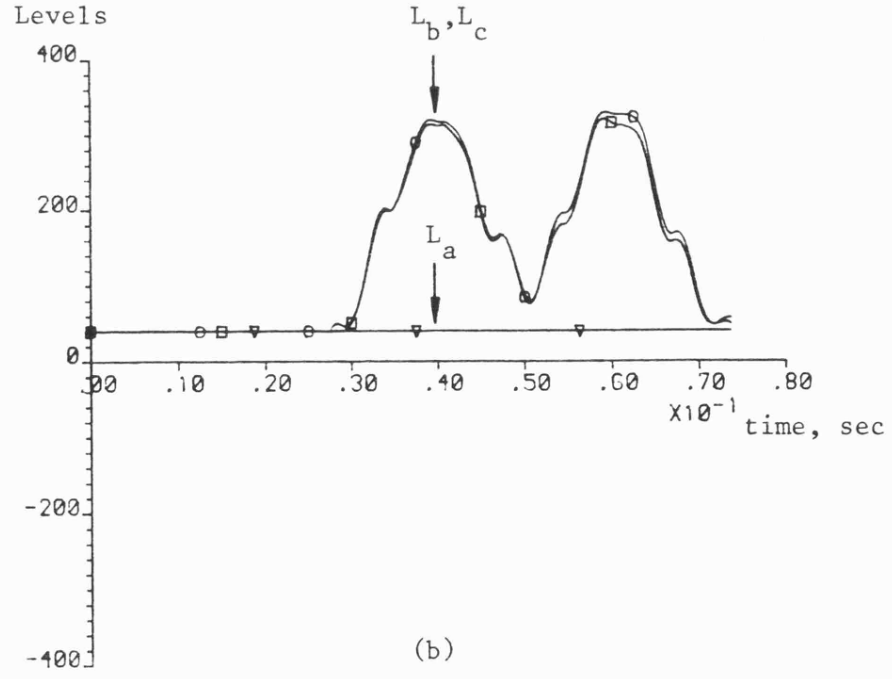

(b)

Fig 9.2 Discriminant signal and associated dynamic threshold variations derived from actual system data recorded at Cellarhead

(a) Discriminant signal variations

(b) Dynamic threshold level response (minimum threshold = 40 levels)

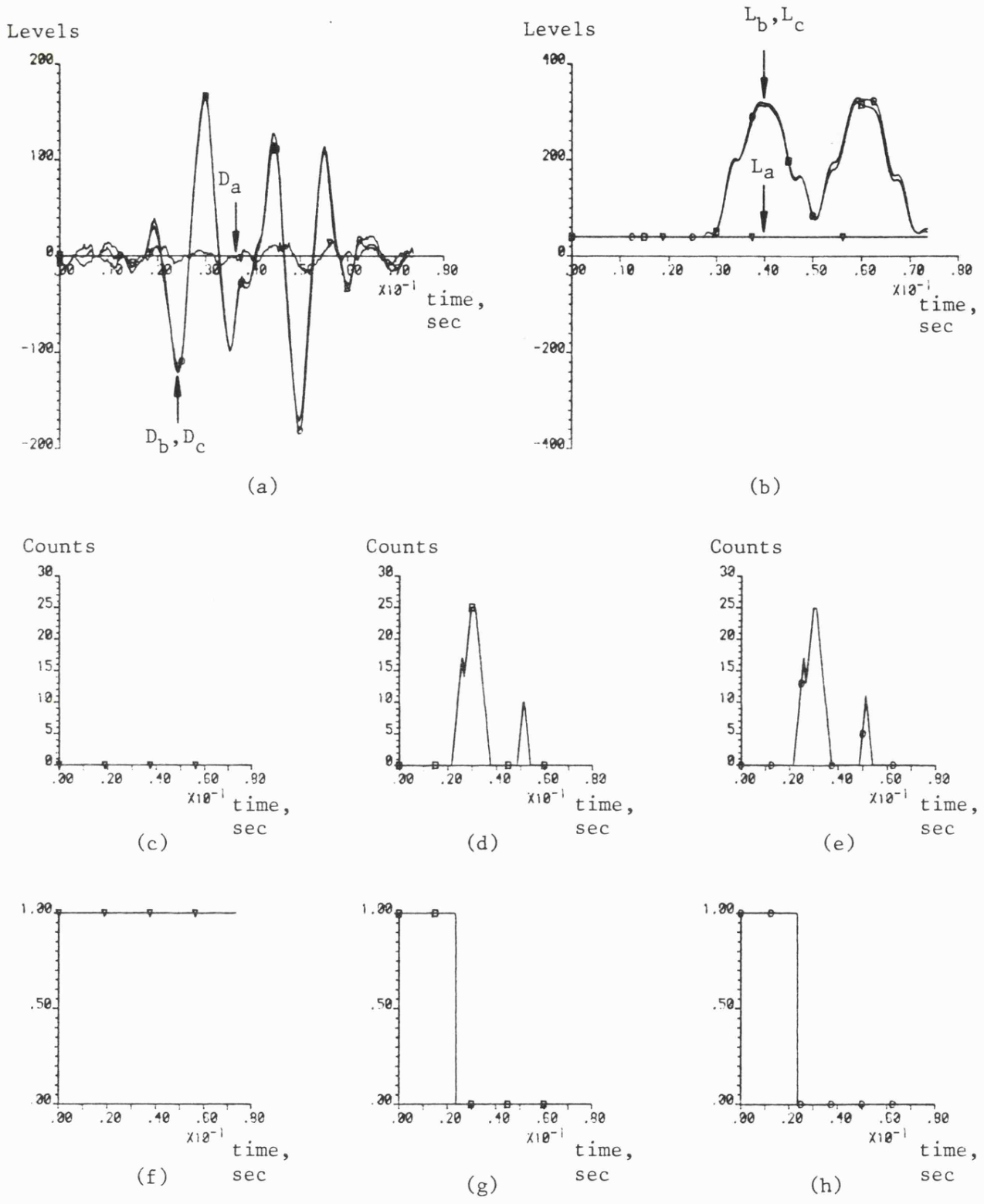

Fig 9.3 Signal variations at different output stages within the phase selector equipment when supplied with the actual system date

- Minimum threshold = 40 quantisation levels

(a) Discriminant signal variations (D_a, D_b and D_c)

(b) Dynamic threshold levels (L_a, L_b, and L_c)

(c), (d), (e) Event counters (EC_a, EC_b, EC_c)

(f), (g), (h) Output from phase selector tripping logic (T_a, T_b, T_c)

CHAPTER TEN

CONCLUSION

10.1 General Discussion

A novel technique for reliable UHS single phase selection on EHV transmission systems has been developed. Problems commonly encountered with conventional phase selection equipment have been overcome and the compatability of the proposed scheme with high technology digital protection equipment has been proven. The essential requirements of any phase selection scheme employed in single phase tripping applications have been met, together with some desirable requirements hitherto unsatisfied by existing UHS phase selection schemes. Furthermore, the theoretically developed selection technique has been verified by preliminary field test fault data.

During the early stages of the project, research was dedicated to the development of UHS phase selection equipment based upon digitally derived modal superimposed components. Subsequently, a processing algorithm suitable for implementation with digital techniques was derived. The operating principle and the performance of the new selection scheme have been described, together with problems to be solved and the effectiveness of the respective countermeasures.

The phase selector principles are partly based upon the theory of invariant propagation characteristics of the natural mode

components. During the initial fault period, the behaviour of the superimposed modal quantities is independent of the terminating source configurations behind the relaying locations. In addition, the discriminant signals are formed from a ratio of the aerial mode quantities alone, which remain unaffected and hence independent of any change in source zero-sequence conditions. The range of practical systems to which a phase selector of this type can be applied therefore include large integrated transmission networks with constantly varying source terminations.

The comparison and setting procedures are simplified by using only aerial mode components that relate to clearly definable propagation characteristics. Furthermore, the digital implementation of the selection algorithm is to some extent immune to processing errors, since each aerial mode is processed in exactly the same way. The ratio between the aerial mode components is therefore maintained, which ensures the reliability of the derived discriminant signals.

The new scheme has several distinctive features, the major one being its ability to perform correct phase selection from measurands comprising solely of voltage or current components or a combination of both. This property enhances the sensitivity characteristic of the phase selector, which therefore permits the latter to be applied to systems with a very large range of source capacities, varying between 1 and 35GVA. Moreover, the proposed scheme surpasses the performance of most conventional types of phase selectors under small signal conditions, one particular example being the case of

faults involving very high values of fault path resistance. Reliable discrimination has been maintained by the newly developed selector beyond 600Ω for single phase faults, which is a vast improvement over the absolute maximum value of 200Ω quoted for existing selectors.

Another important feature of the algorithm is that travelling wave distortion does not degrade the performance of the phase selector, since the latter can operate upon measurands comprised of a wide range of frequency components. The amount of measurand preconditioning and hence signal group delay is therefore reduced to a minimum which enhances the speed of the selection equipment. Furthermore, the high speed of operation combined with the use of superimposed components was found to reduce the susceptibility of the phase selector to primary transducer errors. Many existing phase selectors suffer under conditions of CT saturation, but the new ultra high speed scheme operates before any such non-linearity can occur. Regarding CVT errors, the superimposed quantities greatly improve the effective signal/noise ratio in the voltage channel when compared with conventional selectors measuring from the total variations produced following large sudden drops in primary system voltage. In addition, the inclusion of digital filtering within the selector further improves the transducer error rejection of the new scheme as a whole.

During the extensive testing of the new scheme, attention was paid in detail not only to the conventional fault conditions applied for performance assessment of existing phase selectors, but to many other abnormal situations. Specific examples of the latter include

faults which give rise to unusual phase current distributions and evolving fault conditions. In the former case, where for example no aerial mode current components are available for comparison, reliable phase selection is still possible. This is because of the aforementioned ability of the phase selector to operate upon aerial mode voltage components alone, which are still present despite the absence of any aerial currents. For the latter case, the continuous monitoring of the discriminant signals enhances the security of the phase selector in that the single phase trip indication could be changed if the initial fault evolved into any other type. The newly developed scheme therefore satisfies the essential requirement of phase selectors employed in single pole applications in that reliable phase re-selection is achievable.

The simulation results show the phase selector to have very good discriminative properties complemented with a very high speed of operation of typically 2 to 5ms for most fault conditions. An operating time of 2ms is the minimum figure which can be achieved by the new scheme, since the added security introduced into the decision process involves a multi-sample checking technique. When combined with the directional relay in single pole and three pole autoreclosure sequences, correct co-ordination of the relay and phase selector decisions enabled the successful opening and reclosing of the faulted phase poles. No significant delay is introduced into the decision of the protection scheme as a whole, since the difference between the phase selector and main relay operating time is at worst less than 1ms. Furthermore, any non-operation of the phase selector

does not introduce any delay into the action taken by the overall protection because of the fail-safe mode which further improves the security of the protection equipments.

Some thought was directed to producing a segregated scheme capable of indicating the relevant phase pole, which when opened would clear both single phase faults and double phase clear of ground faults. Theoretical proposals were made, and from a phase selection point of view, the new ideas appeared to be sound. However, the lack of simulation techniques to provide switched reactor arrangements for arc extinction purposes precluded any further testing of the proposed scheme during single pole autoreclosure sequences.

The new selection algorithm was exhaustively tested using the simulation programs of systems having various configurations. These include horizontal long line construction with shunt compensation (both with and without discrete transposition), and uncompensated vertical construction lines. In each case the simulation results showed the phase selector to have no performance deficiencies in terms of operating speed and reliability. The performance of the phase selector was also examined using some field test data derived from the CEGB transmission network. It was found that the selector performed satisfactorily for the fault condition considered (as confirmed by the CEGB service records), this being a single phase to ground fault. Although only one particular fault condition was considered (due to unavailability of any more practical data at that time), nevertheless the results for that study showed the validity

of the phase selection technique considered in the thesis.

As mentioned previously, the phase selector was primarily designed to complement the aforementioned directional comparison scheme in a UHS, single pole autoreclosure unit protection scheme. The selector was found to be directly compatible with the existing relay design in that the processing of the discriminant signals merely required extra software. The implementation of the new scheme as an integral part of the directional relay was therefore an attractive proposition, since this required no further modifications from a digital hardware point of view. However, this is not to say that the new phase selector could not be constructed as a stand-alone device for application with other protection schemes, in which fault type identification is of prime importance.

10.2 Future Work Proposed

The results and discussions at various stages of research, have revealed the need for extensions to the existing work to be made. These include:

(1) The testing of the protection equipment (main DWD and phase selector) during the dead time period of single pole autoreclosure sequences. In the event of a fault occurring on one or both of the healthy phases whilst the faulted phase is isolated, the behaviour of the phase selector and main relay could be investigated.

(2) The development of a software to simulate suitable reactor compensated schemes for arc extinction when only one pole is

opened to clear interphase faults. This arrangement would permit the testing of the proposed segregated scheme when employed in SPA applications.

(3) The derivation of discriminant signals to allow the reliable selection of the faulted phases in the case of double phase to ground faults. This feature would enhance the capability of the existing phase selector, whereby a segregated scheme, capable of selecting one, two or three poles as required could be achieved.

(4) The extension of the method to double circuit and multi-terminal lines.

(5) Further field testing of the phase selector equipment to endorse the preliminary findings and to assess the response to a wider range of day-to-day disturbances present on large systems.

References

(1) Haubrich, H J, Hoseman, G and Thomas, R: "Single phase auto-reclosing in ehv systems", CIGRE, Report 31-09, 1974.

(2) Kimbark, E W: "Suppression of ground fault arcs on single pole switched ehv lines by shunt reactors", IEEE Trans., 1964, PAS-83, pp.285-290.

(3) Edwards, L, Chadwick, J W, Riesh, H A and Smith, L E: "Single pole switching on TVA 7s paradise-Davidson 500kV line - design concepts and staged fault test results", IEEE Trans., 1971, PAS-90, pp.2436-2444.

(4) Groza, L, Creta, D, Opashi, D, Vreme, A and Zlatonovici, D: "The operation of large low speed hydroelectric generators under abnormal and special conditions", CIGRE, Paris, Paper 11-07, 1972.

(5) Carlsson, L, Groza, L, Cristovici, A, Necsulescu, D S and Ionescu, A L: "Single pole reclosing and ehv lines", CIGRE, Paris, Paper 31-03, 1974.

(6) Winick, K: "System protection considerations related to single pole tripping of high voltage transmission lines", Proc. of American Power Conf., 37th, Vol.37, 1975, pp.957-961.

(7) Dietsh, C: "Selection of faulty phases on power transmission lines", CIGRE, Paris, Report 325-3, pp.31-42, 1954.

(8) Gray, H: "Phase selectors - general study", GEC Measurements, Report S/PE 3000.

(9) Mathews, C A and Wilkinson, S B: "Ultra high speed relaying for transmission line protection", IEE Conf. Publication 185, pp.187-191, June 1980.

(10) Wagner, C L and Lokay, H E: "Independent pole circuit breakers improve system stability performance", Westinghouse Engineer, pp.131-137, Sept.1973.

(11) Kimbark, E W: "Charts of three quantities associated with single pole switching", IEEE PAS Trans., Vol.83, March 1964, pp.285-290.

(12) Takaqi, T, Baba, J, Uemura, K and Sakagushi, T: "Fault protection based on travelling wave theory - Part I Theory", IEEE PES Summer Meeting, A.77750-3, July 1977.

(13) Takagi, T, Miki, Y, Makino, J I, Matori, I: "Feasibility study for a current differential carrier relay system based on travelling wave theory", IEEE PES Winter Meeting, A.78 132-3, Feb.1978.

(14) Dommel, H W, Michels, J M: "Digital high speed relaying using travelling wave transients analysis", IEEE PES Winter Meeting, A 78 214-9, Jan-Feb 1978.

(15) Chamia, M and Liberman, S: "Ultra high speed relay for EHV/UHV transmission lines - development, design and application", IEEE Trans. on Power Apparatus and Systems, Vol.PAS-97, pp.2104-2116, Nov-Dec.1978.

(16) Guiliante, A T, Slatem, R R, Stranne, G and Ohlen, C: "A directional wave detector relay with enhanced application

capabilities for EHV and UHV lines", IEEE Trans. on Power Apparatus and Systems, Vol.PAS-102, No.9, Sept.1983, pp.2881-2892.

(17) Johns, A T: "New ultra high speed directional comparison technique for the protection of EHV transmission lines", IEE Proc., Vol.127, Pt.C, No.4, July 1980, pp.228-239.

(18) Johns, A T: "Discussion on ultra high speed directional comparison technique for the protection of EHV transmission lines", IEE Proc., Vol.128, Pt.C, No.3, May 1981.

(19) Report GR/B/59365/1: "Directional comparison based protection for multi-ended power transmission lines", Nov.1981.

(20) Report GR/B/59365/2: "Preliminary hardware proposals for wave directional comparison relay", Jan.1982.

(21) Report GR/B/59365/5: "Progress in the implementation of directional comparison relay", July 1982.

(22) Report GR/B/59365/7: "Decision process and effects of system frequency changes", October 1982.

(23) Report GR/B/59365/8: "Sensitivity requirements and application limits for superimposed component directional relay", Oct.1982.

(24) Report GR/B/59365/9: "Adjustment and setting facilities for superimposed component directional relay", Oct.1982.

(25) Warrington, A R, Van, C: "Graphical method for estimating the performance of distance relaying during faults and power swings", AIEE Trans., 1949, 68, pp.608-621.

(26) Zurowski, E: "New static six-unit distance relay for UHV and EHV systems", Siemens Review, 1974, (9), pp.426-429.

(27) Sharples, H D: "Phase selectors for switched distance schemes", IEE Colloquium, 1968-19.

(28) Breingan, W D, Gallen, T F, Chen, M M: "The laboratory investigation of a digital system for the protection of transmission lines", IEEE Trans., PAS, March 1979, pp.350-368.

(29) Clarke, E: "Circuit analysis of AC power systems", Vol.1, Wiley.

(30) El-Kateb, M M and Cheetham, W J: "A new approach to high speed phase selection", Electric Power Conference.

(31) Frey, W, Althammer, P: "The calculation of electromagnetic transients on lines by means of a digital computer", The Brown Boveri Review, Vol.48, No.5/6, May/June 1961, pp.344-355.

(32) Bewley, L V: "Travelling waves on transmission systems", New York, Dover Publication, 1963.

(33) Johns, A T, Aggarwal, R K: "Digital simulation of faulted EHV transmission lines with particular reference to very high speed protection", Proc.IEE, Vol.123, No.4, April 1976, pp.353-359.

(34) Wedepohl, L M: "Application of matrix methods to the solution of travelling wave phenomena in polyphase systems", Proc.IEE, 1963, 110, (12), pp.2200-2212.

(35) Johns, A T, El-Nour, M and Aggarwal, R K: "Performance of distance protection of EHV feeders utilising shunt reactor arrangements for arc suppression and voltage control", IEE Proc., Vol.127, No.5, Sept.1980, pp.304-316.

(36) Dienne, G: "Transient behaviour of instrument transformers and associated high speed and directional comparison protection", Electra No.72, pp.115-139.

(37) Wedepohl, L M and Mohamed, S E T: "Multiconductor transmission lines", Proc.IEE, 1969, 116, (9), pp.1553-1563.

(38) Galloway, R H, Shorrocks, W B and Wedepohl, L M: "Calculation of electrical parameters for short and long polyphase transmission lines", IEEE Trans. (PAS), 1964, 111, (12), pp.2051-2059.

(39) Johns, A T and Al-Rawi, A M: "Digital simulation of EHV systems under secondary arcing conditions associated with single-pole autoreclosure", IEE Proc., Vol.129, Pt.C, (2), March 1982, pp.49-58.

(40) Al-Rawi, A M: "Simulation of secondary arcs in EHV systems employing single-pole autoreclosure", PhD Thesis, University of Bath, 1981.

(41) Day, Sylvia, J, Mullinex, N and Reed, J R: "Developments in obtaining transient response using Fourier Transforms: Gibbs phenomena and Fourier integrals", Internat. J. Elect. Engng. Educ., 1965, 3, pp.501-506.

(42) Day, Sylvia, J, Mullinex, N and Reed, J R: "Developments in obtaining transient response using Fourier transforms: use of the modified Fourier transform", ibid, 1966, 4, pp.31-40.

(43) Andrichak, J G and Wilkinson, S B: "Considerations of speed, dependability and security in high speed pilot relaying schemes", presented to the Georgia Tech. Protective Relay Conf., Atlanta, Georgia, May 5-6, 1977.

(44) Johns, A T and Aggarwal, R K: "Digital simulation of fault autoreclosure sequences with particular reference to the performance evaluation of protection for EHV transmission lines", IEE Proc., Pt.C, Gen., Trans. and Distrib., 1981, 128 (4), pp.183-195.

(45) Report GR/B/59365/17: "Interim results for noise monitoring field trials", Dec.1983.

APPENDIX A1

FAULT ANALYSIS ALGORITHM

The fault analysis algorithm is derived by making use of the modal components[17], which can be used to extract classification features for the different types of fault. In general a fault on a three phase line will excite three modes of travelling waves. Even though these modes travel independently, the conditions at the fault location will be coupled. In order to analyse the modal behaviour at any point within the system, interconnected networks that are unique to each type of fault can be constructed.

The following analysis describes the construction of each particular interconnected network which enables essential fault point features to be calculated, such as reflection and refraction coefficients, and initial variations of each mode.

A1.1 Line to Ground Faults

"a"-e fault

The voltage and current changes produced by a single line to ground fault in phase "a" are obtained by connecting a voltage source:

$$V_{fFa}(t) = -\frac{\sqrt{2}}{\sqrt{3}} \cdot Vrms \cdot \sin(\omega_0 . t + \phi)h(t) \qquad \ldots (1A1)$$

and two current sources:

$$I_{fFb}(t) = 0 \qquad \ldots (2A1)$$

$$I_{fFc}(t) = 0 \qquad \ldots (3A1)$$

to the fault location F, assuming that the prefault voltage in phase "a" was:

$$V_{sFa}(t) = \frac{\sqrt{2}}{\sqrt{3}} \cdot Vrms \cdot \sin(\omega_0.t + \phi)$$

There are a number of transformation matrices [S] and [Q] which can be chosen to decompose the phase variations of the currents and voltages into modal components. If an ideally transposed single circuit line is considered, the form [Q] = [S] is given in eqn (4A1).

$$[S] = [Q] = \begin{matrix} 1 & 1 & 1 \\ 1 & 0 & -2 \\ 1 & -1 & 1 \end{matrix} \qquad \ldots (4A1)$$

The same basic transformation applies to the system currents. Now, converting to 1, 2, 3 modal components, eqns (1A1), (2A1) and (3A1) become:

$$V_{fFa}(t) = V_{fF}^{(1)}(t) + V_{fF}^{(2)}(t) + V_{fF}^{(3)}(t) \qquad \ldots (5A1)$$

$$I_{fFb}(t) = I_{fF}^{(1)}(t) - 2.I_{fF}^{(3)}(t) \qquad \ldots (6A1)$$

$$I_{fFc}(t) = 0 = I_{fF}^{(1)}(t) - I_{fF}^{(2)}(t) + I_{fF}^{(3)}(t) \qquad \ldots (7A1)$$

From eqns (6A1) and (7A1) we can deduce that:

$$I_{fF}^{(1)}(t) = 2.I_{fF}^{(3)}(t) \qquad \ldots (8A1)$$

$$3.I_{fF}^{(3)}(t) = I_{fF}^{(2)}(t) \qquad \ldots (9A1)$$

Currents and voltages at the fault location are related independently for each mode by:

$$I_{fF}^{(1)}(t) = 1/Z0^{(1)} \cdot V_{fF}^{(1)}(t)$$

$$I_{fF}^{(2)}(t) = 1/Z0^{(2)} \cdot V_{fF}^{(2)}(t) \quad \ldots (10A1)$$

$$I_{fF}^{(3)}(t) = 1/Z0^{(3)} \cdot V_{fF}^{(3)}(t)$$

until the first reflection from the fault location arrives. From eqns (5A1) and (8A1), (9A1) and (10A1) it follows that:

$$V_{fF}^{(1)}(t) = Z0^{(1)}/(Z0^{(1)} + 2.Z0^{(2)}) \cdot V_{fFa}(t) \quad \ldots (11A1)$$

$$V_{fF}^{(2)}(t) = 3/2.(Z0^{(1)}/(Z0^{(1)} + 2.Z0^{(2)})).V_{fFa}(t) \quad \ldots (12A1)$$

$$V_{fF}^{(3)}(t) = 1/2.(Z0^{(1)}/(Z0^{(1)} + 2.Z0^{(2)})).V_{fFa}(t) \quad \ldots (13A1)$$

It follows from the foregoing analysis, and from eqn (5A1), that Fig 3.2(b) represents the equivalent modal circuit for "a"-phase to earth faults. Since both aerial modes propagate at the same velocity, and the assumption of ideal transposition is taken, further simplification of the above equivalent circuit can be accomplished by replacing the series combination of mode-2 and mode-3 by a single mode, designated as mode-4. This hybrid mode must therefore have the following circuit parameters:

$$Z0^{(4)} = Z0^{(2)} + Z0^{(3)} \quad \ldots (14A1)$$

$$V^{(4)} = V^{(2)} + V^{(3)} \quad \ldots (15A1)$$

and $$I^{(4)} = I^{(2)} + I^{(3)} \quad \ldots (16A1)$$

Finally, by taking the assumption that $Z0^{(2)} = Z0^{(3)}$, $Z0^{(4)}$ then becomes:

$$Z0^{(4)} = 2Z0^{(2)} \qquad \ldots (17A1)$$

Fig 3.2(a) can then be replaced by the equivalent interconnected modal network of Fig 3.2(b).

For the purpose of lattice diagram construction, the behaviour of an incident modal wave, at the point of fault, must be investigated. The sudden application at the superimposed voltage V_{fFa} at the instant of fault inception, then causes simultaneous changes in $V_{fF}^{(1)}$ (the magnitude of which is given in eqn (11A1)) and $V_{fF}^{(4)}$ (the magnitude of which is obtained by adding eqn (12A1) and (13A1)). Subsequently, travelling waves of each mode propagate away from the fault point, but are reflected back towards the latter, from the terminating sources. The speed and magnitude of these reflected waves, which are now incident on the fault point, are subject to the transit times, source and surge impedances of each mode.

Fig 3.3(a) shows the equivalent circuit presented to a mode 4 voltage wave, magnitude $(V_i^{(4)})$, which propagates from a surge impedance ZI and is incident on the fault point F. From Fig 3.3(a), it is seen that the effective Thevenin terminating impedance at F, presented to the wave is:

$$ZT = 2Z0^{(2)} \,//\, [Z0^{(1)} \,//\, Z0^{(1)}] \qquad \ldots (18A1)$$

$$= Z0^{(1)}\, Z0^{(2)} \,/\, (2Z0^{(2)} + Z0^{(1)}/2) \qquad \ldots (19A1)$$

Now, the surge impedance $Z0^{(1)} = 2Z0^{(2)}$, hence by using Bewley refraction theory[32] the transmitted and reflected components of mode 4 voltage are calculated from:

$$V_t^{(4)} = 2ZT / (ZI + ZT) \cdot V_i^{(4)}$$

$$= V_i^{(4)} \cdot [2Z0^{(2)} / Z0^{(1)} + 1] \quad \ldots (20A1)$$

$$V_r^{(4)} = (ZT - ZI) / (ZT + ZI) \cdot V_i^{(4)}$$

$$= -V_i^{(4)} \cdot [Z0^{(1)} / 2Z0^{(2)} + 1] \quad \ldots (21A1)$$

The arrival of the incident, mode-4 wave at F therefore causes a change in the voltage $V_{fF}^{(4)}$ (Fig 3.3(a)). Because of the network interconnection, it is seen that the relationship between the mode-1 and mode-4 fault point voltage must remain as:

$$V_{fF}^{(1)} + V_{fF}^{(4)} = 0$$

or

$$V_{fF}^{(1)} = -V_{fF}^{(4)} \quad \ldots (22A1)$$

for all time after fault inception.

Hence, any change in the mode-4 voltage $V_{fF}^{(4)}$ will cause an equal and opposite change in the mode-1 circuit. This shows that even in cases of no mode-1 incident waves, transmitted and reflected components of mode-1 are initiated by the arrival of the mode-4 components. Furthermore, the two fault point voltages $V_{fF}^{(1)}$ and $V_{fF}^{(4)}$ can be considered in terms of their own transmitted and reflected component.

$$V_{fF}^{(1)} = V_t^{(1)} + V_r^{(1)} \quad \ldots (23A1)$$

and

$$V_{fF}^{(4)} = V_t^{(4)} + V_r^{(4)} \quad \ldots (24A1)$$

By considering Fig 3.3(b), which summarises the situation at F, the following modal relationships can be obtained.

At a point just beyond F:

$$V_t^{(1)} + V_t^{(4)} = 0$$

or

$$V_t^{(1)} = -V_t^{(4)} \quad \ldots (25A1)$$

and at a point just before F:

$$V_r^{(1)} + V_r^{(4)} + V_i^{(4)} = 0$$

or

$$V_r^{(1)} = -(V_r^{(4)} + V_i^{(4)}) \quad \ldots (26A1)$$

Hence, by substituting for $V_i^{(4)}$, $V_t^{(4)}$ and $V_r^{(4)}$ in (25A1) and (26A1) we obtain $V_t^{(1)}$ and $V_r^{(1)}$ as:

$$V_t^{(1)} = -V_i^{(4)} / (1 + 2Z0^{(4)} / Z0^{(1)}) \quad \ldots (27A1)$$

and

$$V_r^{(1)} = -V_i^{(4)} / (1 + 2Z0^{(4)} / Z0^{(1)}) \quad \ldots (28A1)$$

Similarly, it can be shown that an incident wave of modal voltage at F will not only produce mode-1 reflected and transmitted components, but will also give rise to mode-4 components, as shown in Fig 3.3(c).

A similar analysis can be carried out for the other phase to earth faults, the corresponding interconnected networks being shown in Fig 3.4 and 3.5.

"b"-e fault

The fault point currents in all but the "b"-phase are zero, and with this constraint, it follows:

$$I_{fF}^{(1)}(t) = 1/3\ I_{fFb}(t)$$

$$I_{fF}^{(2)}(t) = 0 \qquad \ldots (29A1)$$

$$I_{fF}^{(3)}(t) = -1/3\ I_{fFb}(t)$$

The superimposed fault point voltage $V_{fFb}(t)$ can be expressed in terms of the modal component voltage at fault point, and it follows that the voltage $V_{fFb}(t)$ is given by:

$$V_{fFb}(t) = V_{fF}^{(1)}(t) - 2V_{fF}^{(3)}(t) \qquad \ldots (30A1)$$

Using the above constraints, Fig 3.4 represents the modal interconnection circuit for "b"-earth faults. The mode 2 circuit does not exist for this fault, because of the assumption of ideal transposition the sound phase voltages are equal.

"c"-e fault

Fig 3.5 represents the equivalent circuit for "c"-earth faults. The superimposed fault point voltage $V_{fFc}(t)$ is given by:

$$V_{fFc}(t) = V_{fF}^{(1)}(t) - V_{fF}^{(2)}(t) + V_{fF}^{(3)}(t) \qquad \ldots (31A1)$$

The fault point currents in all but the "c"-phase are zero, from which:

$$I_{fF}^{(1)}(t) = 1/3\ I_{fFc}(t)$$

$$I_{fF}^{(2)}(t) = -1/2\ I_{fFc}(t) \qquad \ldots (32A1)$$

$$I_{fF}^{(3)}(t) = 1/6\ I_{fFc}(t)$$

From the foregoing we can see the similarity between this type of earth fault and the "a"-e fault, the only difference being in this case the reverse polarity of the mode-2 voltage and current quantities.

A1.2 Phase to Phase to Earth Fault

As with the phase to earth situation, modal interconnected networks can be derived for the 3 types of phase to phase to earth fault.

"b"-"c"-e fault

The voltage and current changes produced by a line to line fault from phase "b" to "c" with solid connection to ground are obtained by connecting two voltage sources:

$$V_{fFb}(t) = -\sqrt{2}Vrms\ /\sqrt{3}\ \sin(\omega_o t + \phi - 120)\ h(t) \qquad \ldots (33A1)$$

$$V_{fFc}(t) = -\sqrt{2}Vrms\ /\sqrt{3}\ \sin(\omega_o t + \phi + 120)\ h(t) \qquad \ldots (34A1)$$

and one current source:

$$I_{fFa}(t) = 0 \qquad \ldots (35A1)$$

to the fault location F, assuming that the prefault voltage in phase "a" was:

$$V_{sFa}(t) = \sqrt{2}\ Vrms\ /\ \sqrt{3}\ \sin(\omega_o t + \phi) \quad \ldots (36A1)$$

Converting to modal components, eqns (33A1), (34A1) and (35A1) become:

$$V_{fFb}(t) = V_{fF}^{(1)}(t) - 2V_{fF}^{(3)}(t) \quad \ldots (37A1)$$

$$V_{fFc}(t) = V_{fF}^{(1)}(t) - V_{fF}^{(2)}(t) + V_{fF}^{(3)}(t) \quad \ldots (38A1)$$

and

$$I_{fFa}(t) = 0$$

$$= I_{fF}^{(1)}(t) + I_{fF}^{(2)}(t) + I_{fF}^{(3)}(t) \quad \ldots (39A1)$$

Again, currents and voltages at the fault location are related independently for each mode by eqn (10A1), until the first reflection from the fault location arrives. From eqns (37A1), (38A1) and (39A1), it follows that:

$$V_{fF}^{(1)}(t) = Z0^{(1)}/(2Z0^{(1)} + Z0^{(2)}).(V_{fFb}(t) + V_{fFc}(t)) \quad \ldots (40A1)$$

$$V_{fF}^{(2)}(t) = V_{fFb}(t).[(Z0^{(1)} - Z0^{(2)})/(4Z0^{(1)} + 2Z0^{(2)})]$$

$$- V_{fFc}(t).[(Z0^{(1)} + 2Z0^{(2)})/(4Z0^{(1)} + 2Z0^{(2)})] \quad \ldots (41A1)$$

$$V_{fF}^{(3)}(t) = V_{fFc}(t).[(Z0^{(1)})/(4Z0^{(1)} + 2Z0^{(2)})]$$

$$- V_{fFb}(t).[(Z0^{(1)} + Z0^{(2)})/(4Z0^{(1)} + 2Z0^{(2)})] \quad \ldots (42A1)$$

The modal components $I_{fF}^{(2)}$, $I_{fF}^{(3)}$ are associated with a common propagation characteristic and can be replaced by an equivalent mode-4 current $I_{fF}^{(4)}$ and eqn (39A1) becomes:

$$I_{fF}^{(1)}(t) = -I_{fF}^{(4)}(t) \qquad \ldots (43A1)$$

Likewise, the superimposed fault point voltage can be expressed in terms of the mode-4 voltage:

$$(V_{fFb}(t) + V_{fFc}(t)) = 2V_{fF}^{(1)}(t) - V_{fF}^{(2)}(t) - V_{fF}^{(3)}(t)$$

$$= 2V_{fF}^{(1)}(t) - V_{fF}^{(4)})t) \qquad \ldots (44A1)$$

It follows from eqns (43A1) and (44A1) that Fig 3.6 represents the equivalent circuit for "b"-"c" to earth fault.

An analysis similar to that presented for phase to earth fault to determine the reflection and refraction coefficients at the fault point reveals that for "b"-"c"-earth fault the terminating impedance assuming an incident wave of mode-1 voltage, $V_i^{(1)}$, arriving at the fault will have the form:

$$ZT = 2Z0^{(1)} // (Z0^{(2)} // Z0^{(2)})$$

$$= 2Z0^{(1)} . Z0^{(2)} / (4Z0^{(1)} + Z0^{(2)}) \qquad \ldots (45A1)$$

and

$$ZI = 2Z0^{(1)} \qquad \ldots (46A1)$$

By substituting the values of both terminating and incident impedance found from the equivalent circuit shown in Fig 3.6(a), in eqn (47A1), the transmitted voltage of mode-1 will have the form:

$$V_t^{(1)} = 2[ZT/(ZT + ZI)] . V_i^{(1)} \qquad \ldots (47A1)$$

$$= V_i^{(1)} / [1 + 2Z0^{(1)}/Z0^{(2)}]$$

Similarly, the reflected component $V_r^{(1)}$ can be evaluated by substituting the above corresponding values of ZT and ZI in eqn (48A1) and will be given by:

$$V_r^{(1)} = [(ZT - ZI) / (ZT + ZI)] \cdot V_i^{(1)}$$
$$= -2V_i^{(1)} / (Z0^{(2)}/Z0^{(1)} + 2) \quad \ldots (48A1)$$

The mode-4 reflected and transmitted voltage component at the fault point due to the incidence of mode-1 wave voltage component can be obtained by referring to Fig 3.7(a). It can be seen that just after the arrival of $V_i^{(1)}$ we have:

$$V_t^{(4)} = 2V_t^{(1)} \quad \ldots (49A1)$$

and just before the arrival of $V_i^{(1)}$:

$$V_r^{(4)} = 2V_i^{(1)} + 2V_r^{(1)} \quad \ldots (50A1)$$

Substituting for $V_t^{(1)}$ and $V_r^{(1)}$ found above, eqns (49A1) and (50A1) become:

$$V_t^{(4)} = 2V_i^{(1)} / (1 + 2Z0^{(1)}/Z0^{(2)}) \quad \ldots (51A1)$$

$$V_r^{(4)} = 2V_i^{(1)} / (1 + 2Z0^{(1)}/Z0^{(2)}) \quad \ldots (52A1)$$

The reflection and refraction behaviour at the point of fault due to the inception of mode-1 voltage component is as shown in Fig 3.7(a). A similar analysis can be carried out to study the effects of a mode-4 voltage wave arriving at the fault point, the result of which is depicted in Fig 3.7(b).

The remaining types of line to line to ground fault can be studied in a similar manner after deriving an appropriate modal network interconnection for each particular type.

"a"-"b"-e fault

The fault point current for the "c"-phase is zero, and with this constraint the modal currents at the fault point are given by:

$$I_{fF}^{(1)}(t) = 1/3\ (I_{fFa}(t) + I_{fFb}(t)) \quad \ldots (53A1)$$

$$I_{fF}^{(2)}(t) = 1/2\ I_{fFa}(t) \quad \ldots (54A1)$$

$$I_{fF}^{(3)}(t) = 1/6\ I_{fFa}(t) - 1/3\ I_{fFb}(t) \quad \ldots (55A1)$$

Hence,

$$I_{fF}^{(1)}(t) = I_{fF}^{(2)}(t) - I_{fF}^{(3)}(t) \quad \ldots (56A1)$$

and the superimposed fault point voltage $(V_{fFa}(t) + V_{fFb}(t))$ can be expressed in terms of modal voltage as:

$$V_{fFa}(t) + V_{fFb}(t) = 2V_{fF}^{(1)}(t) + V_{fF}^{(2)}(t) - V_{fF}^{(3)}(t) \quad \ldots (57A1)$$

The aerial modal components are associated by common propagation characteristics and can be represented by an equivalent mode-4, such that eqn (56A1) and (57A1) can take the form:

$$I_{fF}^{(1)}(t) = -I_{fF}^{(4)}(t) \quad \ldots (58A1)$$

and

$$V_{fFa}(t) + V_{fFb}(t) = 2V_{fF}^{(1)}(t) + V_{fF}^{(4)}(t) \quad \ldots (59A1)$$

Fig 3.8 represents the equivalent interconnected modal component circuits for "a"-"b"-earth faults, this being very similar to the

"c"-"b"-e case due to the structure of the transformation used.

"a"-"c"-e fault

The modal currents at the fault point, with the constraint of a "b"-phase current equal to zero, are as given by eqns (60A1 - 62A1).

$$I_{fF}^{(1)}(t) = 1/3\ (I_{fFa}(t) + I_{fFc}(t)) \quad \ldots (60A1)$$

$$I_{fF}^{(2)}(t) = 1/2\ (I_{fFa}(t) - I_{fFc}(t)) \quad \ldots (61A1)$$

$$I_{fF}^{(3)}(t) = 1/6\ (I_{fFa}(t) + I_{fFc}(t)) \quad \ldots (62A1)$$

Hence,

$$I_{fF}^{(1)}(t) = 2I_{fF}^{(3)}(t) \quad \ldots (63A1)$$

The following voltage relationships can be used to obtain the superimposed voltage at the fault point:

$$V_{fFa}(t) + V_{fFc}(t) = 2(V_{fF}^{(1)}(t) + V_{fF}^{(3)}(t)) \quad \ldots (64A1)$$

and

$$V_{fFa}(t) - V_{fFc}(t) = 2V_{fF}^{(2)}(t) \quad \ldots (65A1)$$

From the foregoing we can conclude that the mode-2 modal circuit is separately connected and has a reflection coefficient at the fault point of -1, since, due to the transformation, the unfaulted phase is not included in the mode-2 combination. Therefore, to represent such a fault we need two different modal interconnected circuits, one which comprise a combination of mode-1 and mode-3, and another comprising of mode-2 only as shown in Fig 3.9.

A1.3 Phase to Phase Fault Without Ground Connection

"b"-"c" fault

The voltage and current changes produced by a line to line fault clear of ground from phase "b" to "c" are similar to that obtained for the "b" to "c" to ground fault condition. The phase currents at the fault point are related to their modal currents by:

$$I_{fFa}(t) = 0 = I_{fF}^{(1)}(t) + I_{fF}^{(2)}(t) + I_{fF}^{(3)}(t) \quad \ldots (66A1)$$

$$I_{fFb}(t) = I_{fF}^{(1)}(t) - 2I_{fF}^{(3)}(t) \quad \ldots (67A1)$$

$$I_{fFc}(t) = I_{fF}^{(1)}(t) - I_{fF}^{(2)}(t) + I_{fF}^{(3)}(t) \quad \ldots (68A1)$$

It is important to note that the superimposed current at the fault location for phase "b" and "c" are equal and opposite.

$$I_{fFb}(t) = -I_{fFc}(t) \quad \ldots (69A1)$$

By combining eqns (67A1) and (69A1) it follows that:

$$I_{fF}^{(3)}(t) = -I_{fF}^{(2)}(t) \quad \ldots (70A1)$$

$$I_{fF}^{(1)}(t) = 0 \quad \ldots (71A1)$$

The modal currents and voltages at the fault location, until the first reflection arrives, are related independently for each mode by the relationships shown in eqn (10A1). Therefore,

$$V_{fF}^{(1)}(t) = 0 \quad \ldots (72A1)$$

$$V_{fF}^{(2)}(t) = -V_{fF}^{(3)}(t) \quad \ldots (73A1)$$

Combining eqns (36A1), (37A1), (72A1) and (73A1), we obtain:

$$V_{fF}^{(1)}(t) = 0 \qquad \ldots (74A1)$$

$$V_{fF}^{(2)}(t) = (V_{fFb}(t) - V_{fFc}(t))/4 \; . \; h(t) \qquad \ldots (75A1)$$

$$V_{fF}^{(3)}(t) = -(V_{fFb}(t) - V_{fFc}(t))/4. \; h(t) \qquad \ldots (76A1)$$

The interconnected modal network circuits shown in Fig 3.10(a) represent the case for "b"-"c" fault clear of ground. In this case, it turns out that the incident modal voltage component is reflected at the fault point with polarity reversal, as shown in Fig 3.10(b).

The same basic technique can be extended to any type of pure interphase fault, Fig 3.11(a) and Fig 3.12(a) showing the equivalent modal interconnection circuits for ("a"-"c") and ("a"-"b") fault respectively. The corresponding reflection and transmission coefficients for each fault are then obtained from Fig 3.11(b) and 3.12(b).

A1.4 Three Phase Fault

"a"-"b"-"c" fault

The summation of the superimposed voltages and currents at the fault point are equal to zero.

$$V_{fFa}(t) + V_{fFb}(t) + V_{fFc}(t) = 0 \qquad \ldots (77A1)$$

and

$$I_{fFa}(t) + I_{fFb}(t) + I_{fFc}(t) = 0 \qquad \ldots (78A1)$$

Therefore:

$$V_{fF}^{(1)}(t) = 0 \quad \text{and} \quad I_{fF}^{(1)}(t) = 0 \qquad \ldots (79A1)$$

$$V_{fF}^{(2)}(t) = 1/2\ (V_{fFa}(t) - V_{fFc}(t)) \quad \ldots (80A1)$$

$$V_{fF}^{(3)}(t) = 1/3\ (1/2V_{fFa}(t) - V_{fFb}(t) + 1/2V_{fFc}(t)) \quad \ldots (81A1)$$

Combining eqns (77A1) and (81A1) we obtain:

$$V_{fF}^{(3)}(t) = 1/2\ (V_{fFa}(t) + V_{fFc}(t)) \quad \ldots (82A1)$$

Eqns (80A1) and (82A1) lead to the conclusion that each aerial mode has a separate connected network as shown in Fig 3.13; therefore the mode 2 and mode 3 components are totally reflected at the fault point. This balanced fault condition does not initiate earth mode components.

The values of $V_{fF}^{(1)}(t)$, $V_{fF}^{(2)}(t)$ and $V_{fF}^{(3)}(t)$ for all types of fault are listed in Table 3.3.

Table 3.4 gives the values of the modal voltage components at the fault point for all different types of fault, assuming that the earth mode surge impedance ($Z0^{(1)}$) is equal to twice the aerial mode ($Z0^{(2)}$).

APPENDIX A2

PHASE SELECTOR SETTING PROCEDURE

The particular application under study is described in detail in Chapter 5 and the relevant variables for calculating the hardware gain factors are as follows:

Minimum threshold level	=	45 quantisation levels
Maximum source capacity	=	35 GVA
Maximum line loading	=	1660MW
Voltage regulation	=	1.05
System line voltage, V_L	=	500kV
Line Length, L	=	300km
p.p.s. line impedance	=	0.29 ohms/km
Aerial mode surge impedance	=	270 ohms (see Chapter 5) (primary)
	=	270 x (110/500.10^3) x (1200)
	=	71 ohms (secondary)

A2.1 Current Interface Gain Ki

From equation (4.10),

$$Ki = 10/(2 \times \sqrt{2} \times Ic)$$

where Ic is the rms value of the secondary phase current which would just cause clipping. Ic is calculated as the maximum through 3 phase fault current. I_F, plus the maximum expected load current, I_L.

Then,

$$Ic = I_F + I_L/2 \quad \ldots \text{(A2.1)}$$

and

$$I_F = V_{phase}/(ZL1 + ZS1) \quad \ldots \text{(A2.2)}$$

where

ZL1 = line p.p.s. impedance

= .29 x line length

= 0.29 x 300

= 87 ohms

ZS1 = source PPS impedance

= $(500\ 10^3)2/35\ 10^9$

= 7.1 ohms

Hence,

$I_F = 500/\sqrt{3}\ /\ (87 + 7.1)$

= 3067 amps (primary)

or I_F = 2.55 amps (secondary)

Now,

$$\text{Power} = \sqrt{3}\ V_L\ I_L \cos\Theta \quad \ldots \text{(A2.3)}$$

and, taking a typical power factor of 0.8:

$I_L = 1660 \times 10^6\ /\ (\sqrt{3} \times 500 \times 10^3 \times 0.8)$

= 2396 amps (primary)

= 2 amps (secondary)

Hence,

Ic = 2.55 + 1.0 = 3.55 amps

This figure is the exact current that would cause clipping, but in practice a factor of safety is introduced and hence a more suitable value for this particular application is I_c = 6 amps. This gives:

$$Ki = 10 / (2 \times \sqrt{2} \times 6) = 0.589$$

A2.2 Voltage Gain, Kv2

From a knowledge of Ki and Kv, the second voltage Kv2 is calculated from equation (4.14):

$$Kv2 / 2^n = Ki / (Kv \cdot Ro)$$
$$= 0.589 / 0.0557 \times 71$$
$$= 0.15$$

and to ensure $0.5 < Kv2 < 1$, $2^n = 4$

Hence,

$$Kv2 = 0.15 \times 4$$
$$= 0.6$$

A2.3 Filter gain Kf

The digital filter gain Kf is a frequency dependent parameter. The overall 50Hz gain can be calculated as:

$$K_{overall} = kintegral^2 \times kdiff \quad \ldots (A2.3)$$

where:

kintegral is the intermediate gain at the output of each integration stage and is obtained by substituting in eqn (A2.4).

$$K_{integral} = (\sin(m+1)\theta / \sin\theta) \quad \ldots (A2.4)$$

where $\theta = \omega\tau/2$, and τ = 0.25ms and m = number of stages (m=6).

Hence, $k_{integral} = 6.9$.

The gain k_{diff} is the output gain of the two differencing stages:

$$k_{diff} = 4 \sin^2(10\omega\tau) \quad \ldots \text{(A2.5)}$$

$$= 2$$

By substituting the differencing and integral gains in equation (A2.3) we obtain:

$$k_f = 95.6/8 = 11.95 \quad \ldots \text{(A2.6)}$$

It must be noted that the overall gain calculated above assumes the gain of the superimposed component extraction circuit, K_X, to be unity.